Øyvind Brandvoll

Chemical Looping Combustion

Fuel conversion with inherent CO2 capture

Trondheim, January 2005

Doctoral thesis for the degree of doktor ingeniør

Norwegian University of Science and Technology
Faculty of Engineering Science and Technology
Department of Energy and Process Engineering

NTNU

Acknowledgements

First and foremost, thoughts of sincere gratitude and respect goes to my supervisor; Professor Olav Bolland at the Department of Energy and Process Engineering, NTNU, Norway. Your crystal-clear logic, constructive criticism and practical point of view have made a profound impact on my own approach towards mathematical modeling and process engineering. I appreciate your academic professionalism which was extended to personal support and sympathy during a difficult period of the project. This helped make it bearable.

I am indebted to the highly professional staff at SINTEF Materials and Chemistry, Oslo, Norway, for the use of their high-end experimental equipment. Without your cooperation, expertise and goodwill, the experimental sessions described herein would not have been as productive as they turned out to be. In random order these individuals include; Kari-Anne Andreassen for her technical expertise and practical skills; Richard Blom for his insights and good spirits; Anja Olafsen for her constructive criticism and thoroughness; Ivar M. Dahl for his barrage of new ideas and suggestions, Yngve Larring for interesting insights into the world of perovskites, Jesper Bennetsen for assistance on the GC and for overhauling the rig and finally French exchange student Nikolas for assistance during the final session.

My co-supervisor, Professor Leiv Kolbeinsen at the Department of Materials Technology, NTNU, Norway, receives a great deal of thanks for his support and suggestions on the experimental sections of this thesis. I also would like to thank laboratory technician Jan Båtnes for his assistance during initial experiments.

My esteemed colleague Rehan Naqvi receives my heartfelt gratitude for his fresh ideas and friendship. MSc. students Niklas Olsen and Kaare Helle receive thanks for interesting projects and for bearing over with my impatience.

Last, but by no means least; my thanks go to the Norwegian Research Council for the funding that made this project possible.

Trondheim 26 January 2005

Abstract

Chemical looping combustion (CLC) is a new concept for fuel energy conversion with CO_2 capture. In CLC, fuel combustion is split into separate reduction and oxidation processes, in which a solid carrier is reduced and oxidized, respectively. The carrier is continuously recirculated between the two vessels, and hence direct contact between air and fuel is avoided. As a result, a stoichiometric amount of oxygen is transferred to the fuel by a regenerable solid intermediate, and CLC is thus a variant of oxy-fuel combustion. In principle, pure CO_2 can be obtained from the reduction exhaust by condensation of the produced water vapor. The thermodynamic potential and feasibility of CLC has been studied by means of process simulations and experimental studies of oxygen carriers. Process simulations have focused on parameter sensitivity studies of CLC implemented in 3 power cycles; CLC-Combined Cycle, CLC-Humid Air Turbine and CLC-Integrated Steam Generation. Simulations indicate that overall fuel conversion ratio, oxidation temperature and operating pressure are among the most important process parameters in CLC. A promising thermodynamic potential of CLC has been found, with efficiencies comparable to, - or better than existing technologies for CO_2 capture. The proposed oxygen carrier nickel oxide on nickel spinel (NiONiAl) has been studied in reduction with hydrogen, methane and methane/steam as well as oxidation with dry air. It has been found that at atmospheric pressure and temperatures above 600°C, solid reduction with dry methane occurs with overall fuel conversion of 92%. Steam methane reforming is observed along with methane cracking as side reactions, yielding an overall selectivity of 90% with regard to solid reduction. If steam is added to the reactant fuel, coking can be avoided. A methodology for long term investigation of solid chemical activity in a batch reactor is proposed. The method is based on time variables for oxidation. The results for NiONiAl do not rule out CLC as a viable alternative for CO_2 capture, but long term durability studies along with realistic testing of the carrier in a continuous rig is needed to firmly conclude. For comparative purposes a perovskite was synthesized and tested in CLC, under similar conditions as NiONiAl. The results indicate that in a moving bed CLC application, perovskites have inherent disadvantages as compared to simpler compounds, by virtue of low relative oxygen content.

Symbols and abbreviations

Latin symbols

A_i	Bed area	[m^2]
C	Reactant concentration	[vol. %]
Cp_i	Specific heat capacity	[$kJmol^{-1}K^{-1}$]
d_p	Particle diameter	[m]
e_i^n	Specific exergy, *n* refers to chemical or physical exergy	[kJ kg^{-1}]
$\dot{e}_i^n$	Specific exergy flux	[kW]
$\dot{E}_i^n$	Exergy flux	[kW]
G	Gibbs free energy	[kJ mol^{-1}]
h	Specific enthalpy	[kJ mol^{-1}]
h_b	Bed height	[m]
H_i	Relative humidity	-
ΔH^0	Standard enthalpy of formation	[kJ mol^{-1}]
I_i	Intensity	-
K	Equilibrium constant	-
L	Length	[m]
m	Mass	[kg]
m_b	Bed mass	[g]
$\dot{m}_i$	Mass flux	[kg s^{-1}]
Mw	Molar mass	[g mol^{-1}]
n	Number of moles	[mol]
$\dot{n}_i$	Molar flux	[mol s^{-1}]
N	Stoichiometric factor	
P_i	Pressure	[bar]
$\dot{Q}_i$	Heat flux	[W]
R	Universal gas constant (0.082)	[dm^3 atm K^{-1} mol^{-1}]
R_0	Oxygen ratio	
s	Specific entropy	[J K^{-1} mol^{-1}]
S	Selectivity	
S_R	Reforming selectivity	
ΔS^0	Standard entropy of formation	[J K^{-1} mol^{-1}]
t	Time	[s]
T	Temperature	[K] & [°C]
u_0	Superficial velocity	[m s^{-1}]
u_{mf}	Minimum fluidization velocity	[m s^{-1}]

Latin symbols (continued)

$\dot{V}$	Volumetric flowrate	[m^3 s^{-1}]
$\dot{w}$	Specific work	[kJ kg^{-1}]
$\widetilde{w}_i$	Reversible, isothermal compression work	[W]
$\dot{W}$	Work	[W]
X	Degree of oxidation	
y_i	Molar fraction	
$y_{S,i}$	Solid molar fraction	

Greek symbols

α	Oxygen carrying potential	
β	Oxygen carrier overall composition	
δ	Stoichiometric number of mobile oxygen equivalents	
ε	Void fraction	
ϕ	Reactant conversion	
λ	Air ratio	
η	Efficiency	
ν	Specific volume	[m^3 kg^{-1}]
ρ	Density	[kg m^{-3}]
σ_S	Sphericity	
τ	Time	[s]
μ	Viscosity of gas	[kg m^{-1} s^{-1}]

Abbreviations

Ar	Archimedes number (dimensionless)
ASU	Air Separation Unit
BPR	Back-Pressure Regulator
CF	Coolant Fraction
CFB	Circulating Fluidized Bed
CLC	Chemical Looping Combustion
CSTR	Continuously Stirred Reactor
DFR	Direct Fuel Reduction
EUD	Energy Utilization Diagrams
FB	Fixed Bed
FLB	Fluidized Bed

Abbreviations (continued)

FR	Fluidization Regime
GC	Gas Chromatograph
GT	Gas Turbine
HE	Heat Exchanger
HPLC	High Pressure Liquid Chromatography
HRSG	Heat Recovery Steam Generator
LHV	Lower Heating Value
MFC	Mass Flow Controller
MS	Mass Spectrometry
NDIR	Non-Dispersive Infra Red analysis
NG	Natural Gas
NiONiAl	Nickel oxide on nickel spinel
NiNiAl	Nickel on nickel spinel (reduced form of NiONiAl)
PCDC	Pre-Combustion De-Carbonization
PMA	Para-Magnetic Analysis
POX	Partial Oxidation
PR	Pressure Ratio
Re	Reynolds number (dimensionless)
RV	Relief Valve
SEM	Scanning Electron Microscopy
SMR	Steam Methane Reforming
SOFC	Solid Oxide Fuel Cell
SRK	Soave-Redlich-Kwong (equation of state)
TC	ThermoCouple
TCD	Thermal Conductivity Detector
TET	Turbine Exit Temperature
TGA	Thermo Gravimetric Analysis
TIT	Turbine Inlet Temperature
TOS	Time On Stream
TPR	Temperature Programmed Reduction
XRD	X-Ray Diffraction
YSZ	Yttrium Stabilized Zirconia

Table of contents

1 INTRODUCTION

Svante Arrhenius hypothesized already in 1896 that an increase in the concentration of carbon dioxide, as a result of ever increasing combustion of fossil fuels, would result in a temperature increase. In the following the rationale of this doctoral thesis will be presented along with a technological overview of current research into the field of CO_2 capture.

1.1 The greenhouse effect

The earth receives approximately 1368 W/m^2 of radiation energy at the outer surface of the atmosphere, (Pleym et al., 1992). If this energy is distributed evenly across the spherical outer shell of the atmosphere, the atmosphere and the surface absorb 236 W/m^2. To maintain the energy balance the earth and its atmosphere should emit 236 W/m^2 of long-wave radiation. The mean surface temperature of the earth, however, is 15 °C (288 K) which corresponds to a black body emitting 390 W/m^2. The atmosphere thus reduces the long-wavelength radiation by 390-236= 154 W/m^2. The energy balance is shown simplified in Figure 1:

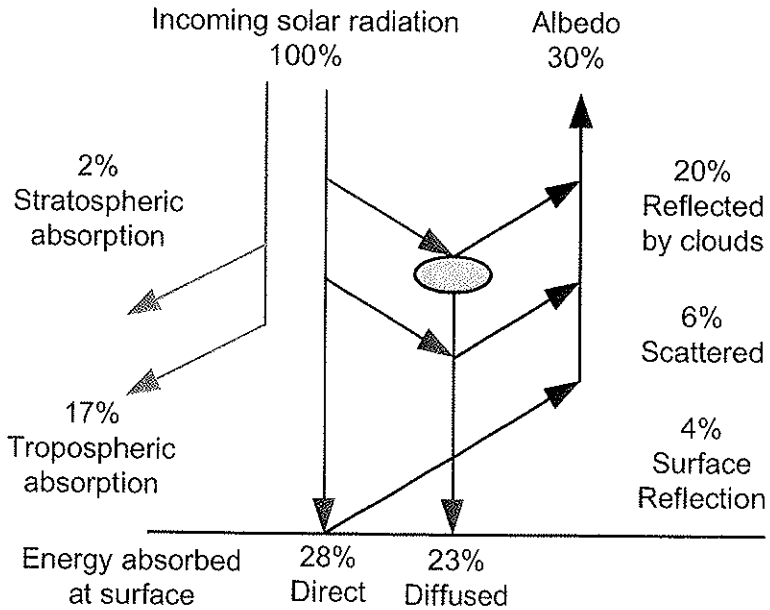

Figure 1 Global shortwave radiation cascade (source: Physical Geography website, physicalgography.net)

It is this energy "surplus" that is generally referred to as the *natural* greenhouse effect. If the earth had no atmosphere, the temperature would be -19°C, corresponding to 236 W/m^2 of emitted long-wavelength energy (heat). The natural greenhouse effect, caused mainly by carbon dioxide and water vapor, is a prerequisite for liquid water and life on the planet. Simply put, the greenhouse effect can be explained as follows: Energy rich short-wave radiation passes relatively unimpeded through the atmosphere, but reflected thermal long-wave radiation is absorbed by a number of gas species. These gases are commonly referred to as *GreenHouse Gases* (GHGs), of which the most important are listed in Table 1.

Table 1 Most important greenhouse gases (source: CDIAC, Carbon Dioxide Information Analysis center website (http://cdiac.esd.ornl.gov))

GHG	Concentration 1750	Concentration Present
Carbon dioxide	280 ppm	373.2 ppm
Methane	730 ppb	1843 ppm
Nitrous Oxide	270 ppb	318 ppb
Chlorofluorocarbons (CFC)	0	~1000 ppt
Ozone	25	34

The numerical values for the concentration of individual species vary depending on source and measurement location. The largest variation is found for methane, which has a reported 6% difference between mid-latitude northern hemisphere (1843 ppb) and mid-latitude southern hemisphere (1729 ppb). H_2O, CO_2 and clouds contribute to 90% of the greenhouse effect, while O_3, CH_4 and N_2O makes up for the remaining 10 %. The present value for total concentration of chlorofluorocarbons is the sum of several related species with a similar potential for global warming.

Carbon dioxide is by far the most important GHG by virtue of its high abundance and the remainder of this introduction will address the issue of CO_2-induced global climate change and technologies for CO_2 capture.

1.2 Man-made greenhouse effect and global climate change

In order to determine the impact of a possible climate change, it is necessary to develop a set of interwoven models:

1 Socio-economic models to predict future fossil fuel consumption and emissions of climate gases. These models depend upon a vast array of factors where technological development, economic growth predictions and predictions on environmental concern and awareness are perhaps the most important.

2 Atmospheric models that reliably and invariably predicts how gas-emissions affect the net concentration of relevant gas-species. Such models require detailed knowledge about natural phenomena related to the distribution of carbon dioxide in oceans and biosphere and how industrial and agricultural activities affect the levels of methane, nitrogen oxides and other GHGs in the atmosphere.

3 "Climate-models", i.e. coupled ocean-atmosphere models to determine the response of the climate system (temperatures, cloud cover, humidity and precipitation patterns) to changes in the average chemical composition of the atmosphere.

Predictions from climate models generally get the most attention and predictions of; say +5°C, in worst case scenarios, are quickly relayed by the media. Since the 1980s attempts have been made to simulate the impact of an increased amount of CO_2 on the earth's climate using complex numerical methods. These climate models have been constantly refined as processing power has increased, and natural feedback-mechanisms are better understood. Additionally, the climate models will contain uncertainties related to both the socio-economical models and the atmospheric models which provide critical input parameters, and the resulting predictions on global temperature are not better than e.g. predictions on future economic growth in the third world.

It is evident that climate models are still inherently flawed and contain computational uncertainties. It can, however, be argued that the potentially negative consequences of global temperature increase are so severe that even uncertain evidence of such a process taking place must be regarded with much attention.

Burning of fossil fuels (oil, coal & natural gas) extracted from the earths' crust, inevitably releases carbon to the atmosphere that otherwise would be locked in place indefinitely. As previously mentioned, this release of carbon, and consequent increase in the concentration of carbon dioxide might disturb the energy balance of the earth, due to its infrared absorption properties and lead to an overall increase in the average global surface temperature. The level of CO_2 in the atmosphere has been documented to increase by about 60 ppm during the period (1958-2002) according to Figure 2. Measurements of the surface temperatures over the last century has documented that there has been an increase of about 0.6 K (Figure 3).

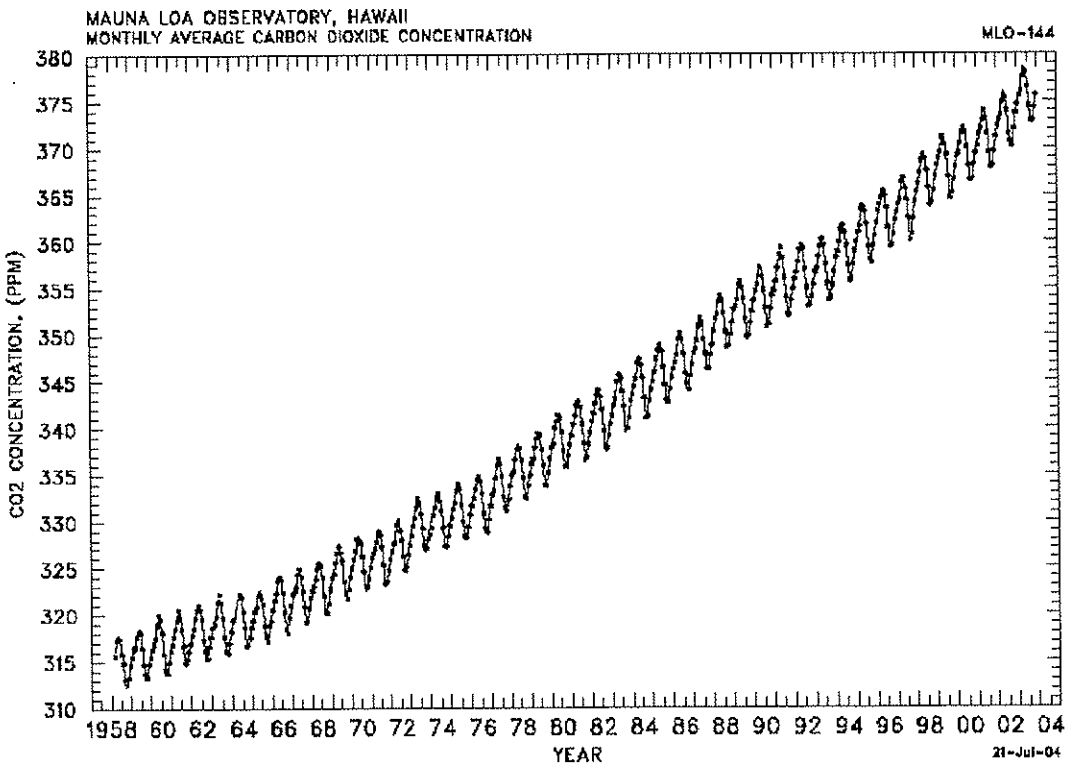

Figure 2 CO_2-concentration measured at Mauna Loa, (source: CICERO Policy note 1998:3)

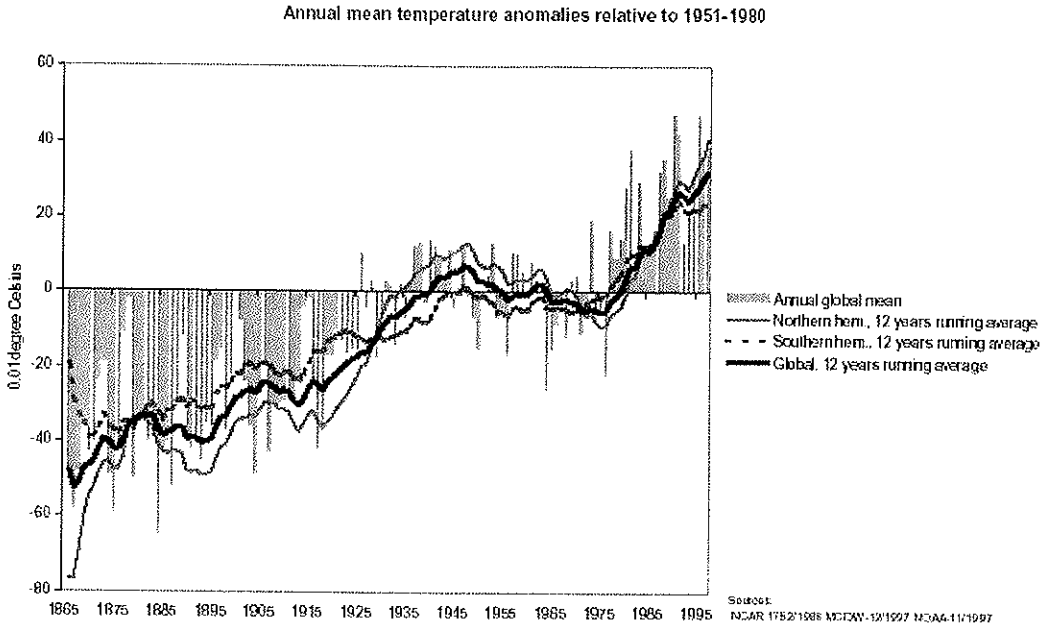

Figure 3 Global temperature development (source: CICERO Policy note 1998:3)

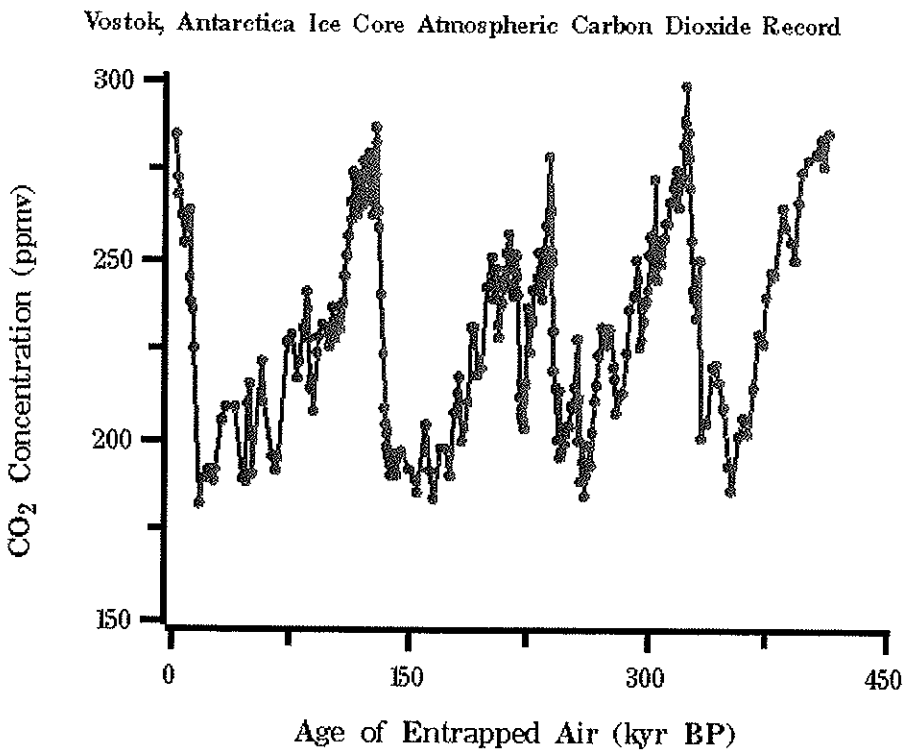

Source: Jean–Marc Barnola et al.

Figure 4 CO_2-variations over the last 40000 years, based on ice-core samples from Vostok research station, Antarctica (source: Trends online website, http://cdiac.esd.ornl.gov)

Whether or not the temperature increase is related to the observed increase in CO_2 concentration, and even if the latter increase is related to human activities, is still a matter of debate. The vast majority of scientists have overruled skeptics who have claimed that other, natural mechanisms, such as variations in solar radiation and cosmic radiation, could also explain the documented temperature rise over the past 100 years. The absorption properties of CO_2 provide a sound and logical explanation for this concurrence. There is, however, a small community of scientists who argue that the rise in carbon dioxide levels is a combined result of lower solubility of CO_2 in the earth's oceans because of temperature increase caused by normal climate-variations. A complicating factor that supports large scale natural variations is that CO_2-levels have a historical record of variation, as can be seen in Figure 4, evidently without human influence.

Based on pre-emptive principles and the fact that the consequences of global warming are potentially devastating, there is a broad consensus that measures must be taken to preferably reduce the emissions of climate gases, or at least freeze emissions to what has been defined as an "acceptable" level.

1.3 Confronting the problem

The evidence of temperature increase and the logical relation between CO_2 concentration and IR-absorption provides a strong incentive to initiate research into the field of energy production with sequestration of the produced CO_2. There are two fundamental approaches to control the concentration of CO_2 in the atmosphere: reducing emissions related to human activities or by increasing the amount of carbon stored in organic matter. There are other natural carbon sinks such as carbonates in ocean sediments but these processes are not easily manipulated.

Reduction of the carbon emissions can be achieved by two principal means: 1) Converting less fossil fuel by combustion, or 2) Capturing the carbon produced in fossil fuel combustion, and storing the carbon dioxide in a long term deposit rather than releasing it to the atmosphere. Based on an ever increasing energy demand, the lack of a viable alternative energy source, and the relative high abundance of fossil fuels on earth, alternative 1 is not a realistic approach to reducing carbon emissions, at least not in the short-term. Reduction of CO_2 emissions by sequestration is the only remaining option. The most significant decision regarding this issue took place at the famous

"Kyoto Conference" in 1997. The protocol from this conference obliged participating countries to reduce their GHG emissions to the level of 1990. The protocol is very ambitious but has been seriously compromised by the reluctance of the US to sign the protocol. The main argument on their part was that full implementation of the protocol would be enormously costly and unfair as the full burden of reducing CO_2 emissions was placed on the developed countries. It has also been argued that the protocol is primarily a political agreement of good will, and does not solve the problem of global warming caused by CO_2 emissions, -if such a problem indeed exists.

The basis for the protocol was a complex system of emission-allocations and the possibility of trading emission allocations between countries. The collapse of the Soviet Union in 1989-91 and the subsequent economic decline put some countries (e.g. Russia and Ukraine) in a position where emissions were *less* than those in 1990 at the time the protocol was negotiated and signed. Countries with such "emission-surpluses" could trade their emission allocations with other countries to balance their negative carbon-balances as compared to 1990. The net CO_2 emission would thus remain at the 1990-level. Ironically this was the main reason Russia initially withdrew its support for the protocol, due to severe limitations on the possibilities for economic growth if such emission permits were sold. Quite unexpectedly, Russia has recently ratified the protocol, thus surpassing the limit of 55% of the industrialized countries necessary to put the agreement into effect.

Due to the high abundance of carbon-based fuels still available, development of novel technologies for energy production with CO_2 capture, or adopting new capture technologies to already existing processes is at present he best option to achieve a significant reduction in carbon emissions.

1.4 CO_2 capture technologies

It is beyond the scope of this thesis to give a thorough, in-depth survey of current CO_2 capture technologies. A brief overview of the main options will be presented to give an impression of the basic strategies involved. Three main approaches to CO_2 capture from combustion of fossil fuels or biomass can be distinguished: post-combustion CO_2 capture, pre-combustion CO_2 capture and stoichiometric combustion of fuel with pure oxygen as oxidant (oxy-fuel).

1.4.1 Post-combustion separation of CO_2

Capture of CO_2 from flue gases produced by combustion processes is referred to as post-combustion capture. Post-combustion methods can be classified as follows:

Absorption
CO_2 is removed from flue gas by selective absorption in a liquid phase, either by exploiting solubility differences (physical solvent process) or by chemical interaction with the solvent.

Adsorption
CO_2 is removed by adsorption onto a solid medium, (molecular sieves or activated carbon) and subsequently removed by pressure swing operation (PSA) or temperature swing operation (TSA).

Membrane separation (with absorption)
Used primarily to remove CO_2 from natural gas, as flue gas CO_2 concentration is to low to provide sufficient driving force (concentration difference across a permeable membrane). Membrane separation can be coupled with absorption, the membrane then acts as a permeable barrier between gas/liquid phases.

Regenerable solid solvent
Flue gas is put in contact with a (alkali or earth alkali) metal oxide that reacts to form carbonates. Regeneration of solids in a different reactor facilitates the release of CO_2 in a controllable way.

At present, economic and technical considerations are clearly in favor of amine absorption, and pending political incentives the technology could in principle be applied in large-scale plants. Absorption processes are by far the most mature technology and hence only these will be discussed in more detail.

The fundamental principle of amine absorption is transfer of specific gas components to a liquid phase where they are selectively soluble or captured by chemical interactions between solvent and solute. An example of the latter is selective amine absorption which is the current "state of the art" in CO_2 separation by absorption.

The process is based on the interaction between an aqueous (basic) amine and a CO_2 containing flue gas. The acidic nature of CO_2 leads to the formation of

a loosely bonded acid-base complex which is not thermally stable, and subsequent heating of the solvent will lead to a release (stripping) of CO_2, and regeneration of the solvent. The absorption process is susceptible to clogging of the reactor by particulate matter and solvent-detrimental acidic components (SO_x, NO_x) that form thermally stable amine complexes. Pre-treatment of the flue gas is therefore required. Flue gases from coal-fired power plants typically have flue gas CO_2-concentration in the range of 12-15%, while natural-gas fired boiler exhausts contain about 8% CO_2 by volume. In natural gas fired combined cycles the concentration of CO_2 is even lower (3-4%), due to the large excess of air used in gas turbines. A schematic of an absorption process for removal of CO_2 from flue gas is shown in Figure 5.

The solubility of gas components in a liquid is temperature dependent and heating the solvent after CO_2 saturation in the absorber (generally to around 100-140°C) leads to a release of gas components in a subsequent stripper. The most important current drawback of the technology is the energy penalty associated with the need to recirculate and heat a large amount of solvent. There are also a number of other hurdles to be overcome, such as long term amine stability, improved pre-absorption treatment of flue gas to remove solvent-detrimental components and the development of new solvents with improved CO_2 selectivity and capacity.

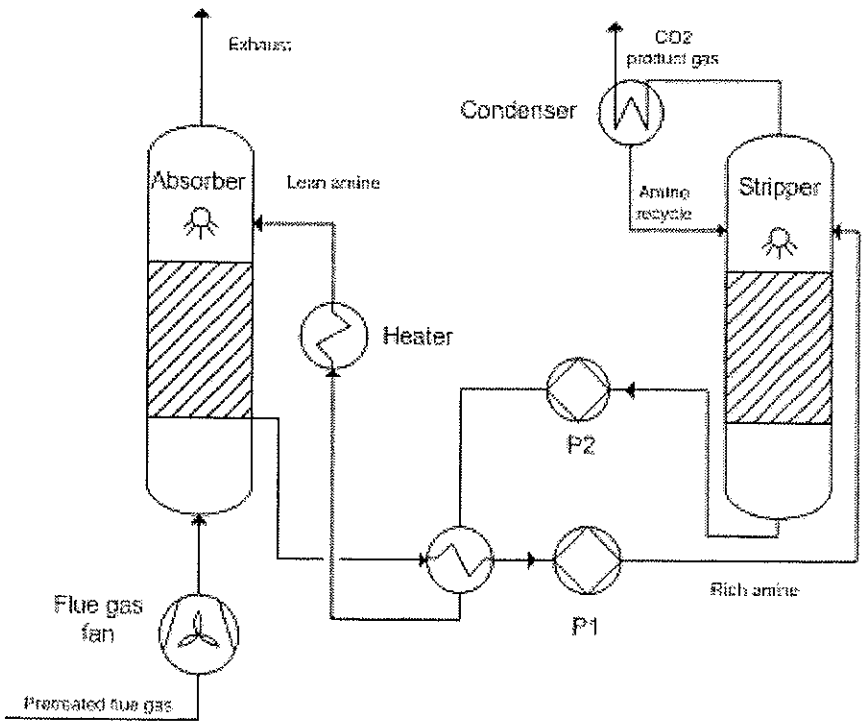

Figure 5 Schematic of amine absorption process

1.4.2 Pre-combustion decarbonisation (PCDC)

The PCDC-concept involves converting the fuel into hydrogen and CO_2 followed by CO_2-capture by PSA or physical solvent processes prior to combustion. Generally, PCDC will involve a syngas production stage with subsequent conversion of the remaining CO to CO_2 (water gas-shift). There are four main approaches to syngas production as indicated in Figure 6:

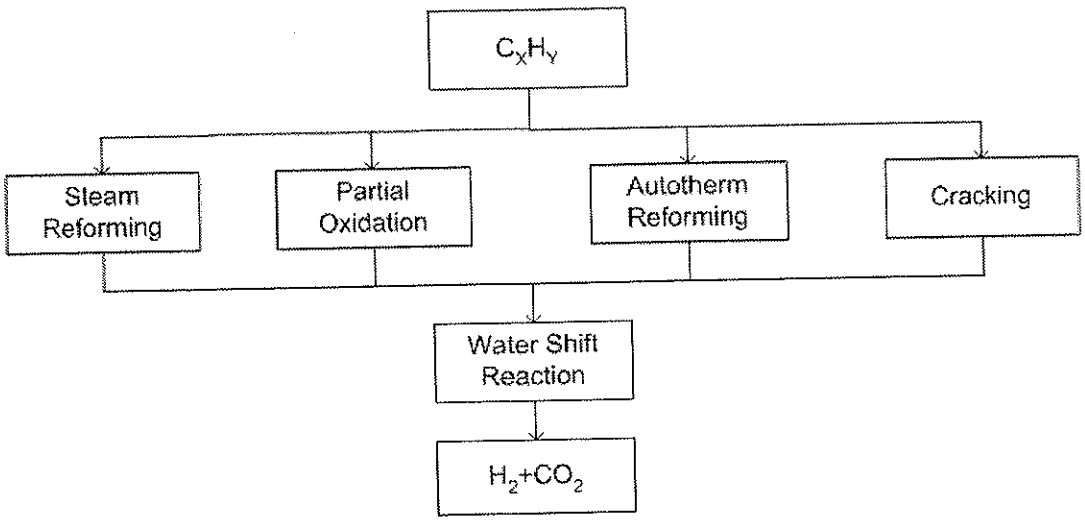

Figure 6 PCDC pathway overview

Steam reforming is a commercially important, and mature industrial process, and can be formulated as follows for a light weight hydrocarbon with a low tendency of coke formation:

$$C_XH_Y + xH_2O \Leftrightarrow xCO + (x + {}^{y}/_{2})H_2 \qquad , \Delta H^0_f >> 0 \qquad (1.1)$$

When the process involves converting natural gas it is referred to as steam-methane reforming (SMR). SMR is a highly endothermic catalytic process, and is carried out in reaction tubes at 800-900°C. Part of the natural gas (secondary fuel) is burned outside the reaction tubes to supply the necessary heat of reaction.

Partial oxidation, on the other hand, is an exothermal process taking place at 1250-1400°C. Fuel is oxidized to CO and hydrogen by supplying pure oxygen:

$$C_XH_Y + {}^{x}/_{2}O_2 \Leftrightarrow xCO + {}^{y}/_{2}H_2 \qquad , \Delta H^0_f < 0 \qquad (1.2)$$

The need for a cryogenic air separation unit (ASU) for oxygen production, leads to high investment costs and energy demands, but this is compensated by the higher reforming efficiency and the elimination of nitrogen from the syngas greatly reduces the cost associated with the subsequent separation of CO_2.

Auto-thermal reforming is carried out at 950-1050°C and can be viewed as a combination of steam reforming and partial oxidation, as both processes take place within different sections of the reactor. Secondary fuel is not required since fuel is first partially oxidized by air or oxygen in a POX burner. SMR is carried out in a downstream catalytic reactor by the introduction of steam.

Thermal cracking, or methane pyrolysis, is the decomposition of methane to hydrogen and carbon:

$$CH_4(g) \Leftrightarrow C(s) + 2H_2(g) \qquad \Delta H^0_f > 0 \qquad (1.3)$$

In this way, fuel is converted endothermally to carbon and hydrogen, potentially yielding a clean product gas free of oxides. The chemical energy associated with carbon oxidation is not released, and consequently only 60% of the heating value of methane may (theoretically) be utilized by later combustion of the hydrogen. Several methods employing the principle of pyrolysis are under development, including thermal catalytic, thermal non-catalytic and plasma cracking. The latter represents a promising option for hydrogen production in which a plasma arc supplies the necessary heat of reaction and has been investigated by Kvaerner in the 'Carbon Black' process.

In all pre-combustion capture process schemes, the final step is cooling of the reforming gas and conversion of carbon monoxide to CO_2 and yet more hydrogen by the so-called water gas-shift reaction:

$$CO + H_2O \Leftrightarrow CO_2 + H_2 \qquad , \Delta H^0_f > 0 \qquad (1.4)$$

To yield a carbon-free fuel for combustion, the CO_2 is separated by PSA or (previously) by physical absorption processes. By virtue of the higher partial pressures of CO_2 in the syngas, pre-combustion separation can be carried out with relative ease as compared to post-combustion of CO_2 in atmospheric flue gases.

1.4.3 Stoichiometric combustion of fuel with pure oxygen

Due to dilution by inert nitrogen and the use of excess combustion air, the partial pressure of CO_2 in flue gases is in the range of 0.03-0.15 bar. Using concentrated O_2 instead of air as oxidizer yields a flue gas consisting of only CO_2 and water vapor:

$$CH_4 + 2O_2 \Leftrightarrow CO_2 + 2H_2O \qquad , \Delta H^0_f << 0 \qquad (1.5)$$

This would allow for the use of simpler post-combustion separation techniques such as condensation, with significantly reduced energy and capital costs. However, the stoichiometric combustion of fuel will lead to combustion temperatures well in excess of current material specifications. The issue can be resolved either by recycling flue gases or injecting water to moderate combustion temperature which is utilized in the following three cycles.

Indirect heating (O_2/CO_2 recycling)
Combustion temperature is moderated by recycling of flue gas and heat is transferred from an oxy-fuel process to a separate fluid which is used for process heating or in a Rankine steam cycle. Method is sensitive to fouling (reduced heat transfer) and requires the design of high temperature-tolerant boilers.

Direct heating - Brayton cycle (O2/CO2 recycling)
Flue gas is recycled, compressed and the resulting CO_2-rich fluid is subsequently expanded in a gas turbine. Remaining heat in exhaust is utilized in a Rankine steam cycle (see Figure 7). Proposed variants of this principle include MATIANT cycle (Mathieu 2003), AZEP-cycle (Griffin 2002), Graz-cycle (Heitmer 2003). Main technical obstacle is the complete redesign of turbo machinery components and combustor, compatible with a CO_2-rich working fluid.

Direct heating – Rankine cycle (O_2/H_2O recycling)
Combustion temperature is regulated by direct injection of water, and the resulting fluid is expanded in turbines followed by condensation of water. Example cycle is that proposed by Clean Air Systems (CES) (Anderson et al. 2003). The main technical obstacle is the design of high-temperature (TIT=1300°C) steam turbines.

The use of pure O_2 invariably implies the use of an *Air Separation Unit* (ASU) using cryogenic, membrane or adsorption principles and herein lays the main energy penalty and investment costs associated with oxy-fuel combustion.

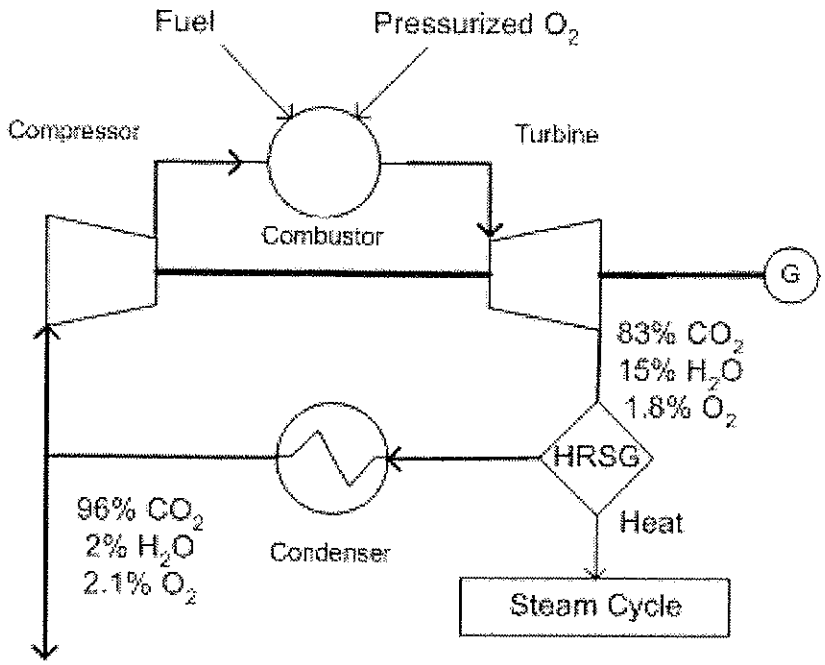

Figure 7 Schematic of direct heating Brayton cycle oxy-fuel process combined with a steam cycle

1.5 Thesis rationale and structure

Power generating cycles with CO_2 capture has become a highly prioritized area of research due to the potentially adverse effects of global climate change. *Chemical Looping Combustion* (CLC) was proposed by Richter & Knoche (1983) as an innovative method for power production with CO_2 capture involving the indirect conversion of fuel by introducing a reactive solid intermediate and splitting the combustion of fuel into two separate processes. A solid oxygen carrier is recirculated between the two vessels, alternately being reduced (looses oxygen) and oxidized (accepts oxygen).

In effect, fuel is combusted with a stoichiometric amount of oxygen, and hence CLC is classified as a variant of oxy-fuel combustion. Relatively little work (as compared to other CO_2-capture processes) has been carried out since the time of introduction, and hence CLC is far from being a mature

technology. The rationale for the thesis is to investigate if CLC has the potential to become a viable alternative to the methods discussed in chapter 1.4.

This has been done by focusing on two main areas of interest:

1 Cycle analyses to explore the efficiency potential of CLC.

2 Experimental studies of oxygen carriers using hydrogen and methane as fuel in fluidized reactors. The work has focused on fuel conversion rates at different reactor temperatures and oxygen carrier durability.

Specific contributions to the field are discussed in context.

Chapter 2 is an introduction to the concept of CLC and the existing literature on the topic as well as theoretical considerations. Chapter 3 is a summary of the cycle heat and mass balance simulations that have been carried out. The experimental work on oxygen carriers is covered in chapters 4 & 5, which deals with methodology and results, respectively. Conclusions and recommendations for further work can be found in chapters 6 & 7 respectively.

Also included are four scientific publications that have been produced during the period of work.

1.5.1 List of papers

Paper I: Brandvoll Ø., Bolland O., Vestøl S., **2001**, *"Chemical Looping Combustion- Fuel Energy Conversion with inherent CO_2 capture"*, paper published in the proceedings of The International Conference Power Generation And Sustainable Development, Liege, Belgium, 8-9 October

Paper II Brandvoll Ø., Bolland O., **2004**, *"Inherent CO_2 Capture Using Chemical Looping Combustion in a Natural Gas Fired Power Cycle"*, Journal of Engineering for Gas Turbines and Power, vol. 126, p. 316-321

Paper III Brandvoll Ø., Kolbeinsen L., Olsen N., Bolland O., **2003**, *"Chemical Looping Combustion - Reduction of NiO:$NiAl_2O_4$*

with hydrogen", Chemical Engineering Transactions, vol. 3, p. 105-110

Paper IV Naqvi R., Bolland O., Brandvoll O., Helle K., **2004**,*"Chemical Looping Combustion, Analysis of natural gas fired power cycle with inherent CO_2 capture"*, Paper presented at ASME Turbo Expo 2004, 14-17 June, Vienna, Austria

Paper I is a parameter variation study of chemical looping implemented in a humid air turbine cycle. The work was based on previous work by MSc. student Sondre Vestøl, NTNU, and included development and encoding of a mathematical model of the process in *Matlab Mathworks 6.0*. Temperature and pressure at various locations in the process were varied and the most important impacts on cycle efficiency were found.

Paper II is an elaborated and extended version of Paper I, including a fundamental comparative exergy analysis of chemical looping combustion and a conventional combustion process.

Paper III is an experimental study of the potential oxygen carrier nickel oxide on nickel spinel (NiONiAl). Nickel oxide is reduced with hydrogen to form water vapor. By measuring the rate of water production, strong indications of mass transfer limitations where found. The bulk of the experimental work was carried out by MSc. student Niklas Olsen, NTNU, while the author supervised the experimental work, compiled and analyzed the results for publication.

Paper IV is a study of chemical looping combustion implemented in two cycles: a combined GT-Steam cycle and an atmospheric Rankine type process. The model is based on the work from Paper I and the work firstly included encoding the model for CLC in FORTRAN, and embedding of the model in *Simsci ProVision PRO*/II process simulation software. PhD student Rehan Naqvi carried out the fine tuning and actual number crunching and the author contributed to the final paper by virtue of a continuous process of results discussion and computational problem solving.

2 CHEMICAL LOOPING COMBUSTION

In the following, the principles, literature and theory related to CLC will be discussed.

2.1 Introduction

The idea of chemical looping combustion (CLC) is to separate combustion products from excess air, by splitting conventional combustion into separate reduction and oxidation reactions. The reactions take place in separate vessels and oxygen is transferred from the air to the fuel by means of a reactive solid intermediate. This "oxygen carrier" can in principle be any oxide of a transition metal with the ability to release oxygen under reducing conditions (fuel) and be rapidly regenerated in contact with an oxygen rich atmosphere (air). Abbreviations "Me" and "MeO" will be used as general terms for reduced and oxygenated carrier, respectively, while a carbonaceous fuel (C_nH_{2m}) and air are used as gaseous reactants.

In the reduction vessel, fuel is converted to carbon dioxide and water in a gas-solid reaction with the oxygen-rich oxygen carrier:

$$C_nH_{2m} + (2n+m)MeO \Leftrightarrow nCO_2 + mH_2O + (2n+m)Me \qquad (2.1)$$

The oxygen carrier is then transported to another vessel in which it is regenerated in contact with air:

$$Me + \tfrac{1}{2}O_2 \Leftrightarrow MeO \qquad (2.2)$$

Transportation of the regenerated oxygen carrier to the reduction vessel thus completes one "loop". The reduction reaction is, with some exceptions, endothermic while the oxidation is exothermic to such an extent that the net heat of reaction equals that of combustion of the fuel with a stoichiometric amount of oxygen:

$$\sum \Delta H^0 = \Delta H^0_{Red} + 2 \cdot \Delta H^0_{Ox} = \Delta H^0_{Comb} \qquad (2.3)$$

Balancing and addition of Eq. (2.1) and (2.2) eliminates the oxygen carrier species and yields the net reaction:

$$C_nH_{2m} + \frac{(2n+m)}{2}O_2 \Leftrightarrow nCO_2 + mH_2O \qquad (2.4)$$

The basic principle of CLC can be recognized in Figure 8:

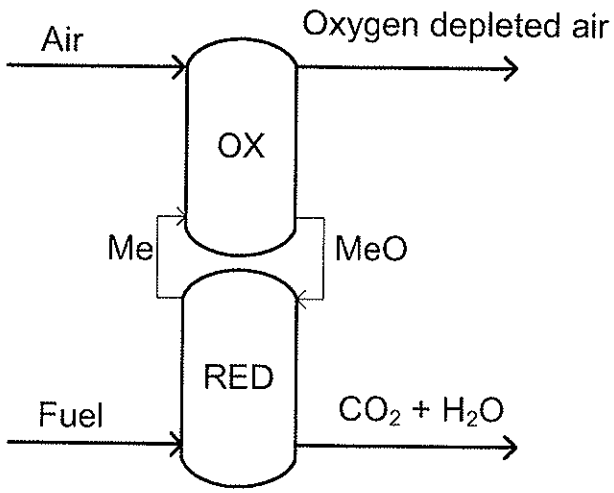

Figure 8 CLC principle with oxidation (OX) and reduction (RED) reaction vessels

The power producing potential of CLC lies within the hot exhaust gas from the oxidation reactor. Since fuel is converted with a stoichiometric amount of oxygen, and direct contact between fuel and combustion air is avoided, chemical looping combustion can be classified as an oxy-fuel process with inherent separation of CO_2 from the nitrogen and excess air of the combustion air.

2.2 *Literature*

The literature directly related to chemical looping is still sparse but growing at an increasing rate. The papers can be classified according to the following categories:

Oxygen carrier development
Experimental work to determine reaction rates, fuel conversion and selectivity, and durability characteristics of potential oxygen carriers. Development of a methodology for comparable screening of potential oxygen carriers is the first logical step and hence the bulk of the literature on CLC concerns this area.

Reactor system development
Experimental work to find and test reactor system designs suitable for application in CLC and study of operational aspects of long term operation. The latter includes, among others, oxygen carrier deactivation, agglomeration and mechanical breakdown; solids transportation; gas-solid separation equipment and determination of optimal process parameters in large scale operation (Temperature and Pressure).

Thermodynamic cycle analysis
CLC is modeled and implemented in power cycles to investigate its power producing potential and important process parameters with regard to cycle efficiency. Simulations of this type is highly dependent on sensible assumptions regarding oxygen carrier and reactor system performance, and the cycle in which CLC is implemented must be selected so that conventional cycles are comparable.

2.2.1 Oxygen carrier development

Experimental work related to finding suitable materials for CLC accounts for the bulk of the papers as finding suitable materials is a prerequisite for further development of the concept. The table includes some details on materials (col. 3) and method (col. 4) as well as the main topics of each study (col. 5). The oxygen carrier(s) used are listed with the reactive component and inert binder, while reactant gases are given with reducing/oxidizing gases. A similar survey focusing on the oxygen carriers and reaction rates with experimental details is given by Lyngfelt et al. (2001).

Table 2 Oxygen carrier development, in chronological order (Part I)

Authors	Year	Carriers Reactant gases	Reactor type and analysis	Topic/results
Ishida, Jin	1994a	Pure NiO, NiO, Fe_2O_3 on YSZ, Fe_2O_3 on Al_2O_3 H_2/Air	TGA	Effect of inert binder, composition and reaction temperature
Ishida, Jin	1996	NiO, NiO/YSZ, H_2/Air	TGA	Zero NO_X emissions, comparative study of NiO and NiO/YSZ
Ishida, Jin, Okamoto	1996	NiO/YSZ, H_2/Air	TGA	Preparation methods, effect of cycling, gas composition and temperature
Hatanaka, Matsuda, Hatano	1997	NiO CH_4/Air	FB GC-TCD	Reduction and oxidation kinetics of pure Ni/NiO, carbon deposition in a small fixed bed
Ishida, Jin, Okamoto	1997	NiO/YSZ, NiO/Al_2O_3, Fe_2O_3/YSZ, H_2/Air	TGA	Iron-particles unsuitable due to crust formation, carbon formation can be controlled by addition of water vapor
Ishida, Jin, Okamoto	1998a	NiO, Fe_2O_3 on YSZ, Al_2O_3, TiO_2 CH_4/H_2O	TGA	Effect of material on reduction rate, effect of composition, H_2O/CO_2 on carbon deposition, model for carbon deposition developed
Jin, Okamoto, Ishida	1998b	NiO, CoO, Fe_2O_3 on YSZ, CoO-NiO on YSZ CH_4/Air, H_2/Air	TGA	Reactivity of single oxide and double oxide, regenerability of materials (with H_2) , carbon deposition
Ishida, Jin	1999	NiO, CoO-NiO, CoO, Fe_2O_3 on YSZ, Al_2O_3, TiO_2 CH_4/Air, H_2/Air	TGA	Summary of earlier results

Table 3 Oxygen carrier development, in chronological order (Part II)

Authors	Year	Carriers Reactant gases	Reactor type and analysis	Topic/results
Jin, Okamoto, Ishida	1999	NiO, CoO, Fe_2O_3 on Al_2O_3, TiO_2, MgO and NiO on $NiAl_2O_4$ CH_4/H_2O and Air	TGA	Effect of solid reactant and binder on reactivity, suppression of carbon deposition, pressure increase reduces necessary reaction temperature
Jin, Ishida	2001	Pure NiO, NiO on YSZ, $NiAl_2O_4$, H_2/Air	TGA, FB, GC-MS	Effect of pressure and investigation of regenerability, potential of $NiO/NiAl_2O_4$ pointed out
Ishida, Jin	2001	Pure NiO, NiO, CoO, Fe_2O_3 on YSZ, Al_2O_3, TiO_2, MgO H_2/Air, CH_4/H_2O/Air	TGA	Summary of earlier results (effect of solid reactant and binder on reactivity, carbon deposition, regenerability) Effect of pressure and use of simulated gasified coal
Mattisson, Lyngfelt, Cho	2001	α-Fe_2O_3 CH_4/Air	NDIR+PMA FB	Impact of bed mass and reaction time, effect of cycling on reduction/oxidation. Proposals for reactor design
Ryu et al.	2001	NiO/Bentonite CH_4 (5%) in Ar/Air	TGA	Effect of particle composition on rate, unreacted shrinking core model
Ishida, Yamamoto, Ohba	2002	$NiO/NiAl_2O_4$ H_2/Ar	TGA & FLB-GC	Circulation characteristics, circulation rates, solid conversion rates, particle durability
Copeland et al.	2002	'Iron based sorbents' and NiO/Al_2O_3, Simulated syngas/Air	TGA+FLB Not cited	Effect of cycling on rates, estimation of carrier attrition. Testing in pilot scale fluidized bed

Table 4 Oxygen carrier development, in chronological order (Part III)

Authors	Year	Carriers Reactant gases	Reactor type and analysis	Topic/results
Jin, Ishida	2002	NiO on $NiAl_2O_4$, CoO-NiO on YSZ CH_4/H_2O/Air	GC-MS FB	Effect of material, temperature and pressure on reduction rates. Carbon deposition.
Brandvoll et al.	2003	NiO on $NiAl_2O_4$, H_2/Air	FLB+FIB Gravimetric	Effect of particle size, temperature, composition on reaction rates. Rate limiting mechanism
Mattisson, Järdnäs, Lyngfelt	2003	Cu, Co, Mn, Ni on Al_2O_3 10%CH_4, 5% CO_2, 10% H_2O 10% O_2	TGA	Effect of material, temperature and cycling on reaction rates, estimation of mechanical properties, application of design criteria
Villa R. et al	2003	Ni-Al-O and Ni-Mg-Al-O mixed oxides H_2, CH4/Air	TPR+MS	Materials synthesis and characterization (XRD), H_2-TPR pulse experiments
Adanez et al.	2004	240 combinations of oxides/supports CH_4/H_2O/Air	TGA	Effect of composition and binder/active component on reactivity and crush strength.
Cho, Mattisson, Lyngfelt	2004	CuO, Fe_2O_3, Mn_3O_4, NiO on Al_2O_3 $CH_4/H_2O/5\%O_2$ in Ar	FLB NDIR-GC	Effect of solid reactant and cycling on reaction rates, agglomeration characteristics, physical characterization
Diego et al.	2004	CuO on Al_2O_3, SiO_2, TiO_2, ZrO_2 and sepiolite CH_4, H_2 or CO, H_2 Air	TGA	Effect of solid binder and gross composition, gas concentration

Table 5 Oxygen carrier development, in chronological order (Part IV)

Authors	Year	Carriers Reactant gases	Reactor type and analysis	Topic/results
Jin, Ishida	2004	NiO on $NiAl_2O_4$ and CoO-NiO on YSZ Simulated goal gasification syngas	FB GC-MS	Comparative study of two carriers, NiO on $NiAl_2O_4$ found to be superior, coal gas found more suitable than NG
Mattisson, Johansson, Lyngfelt	2004	Fe_2O_3 on Al_2O_3, ZrO_2, TiO_2, $MgAl_2O_4$ $CH_4/H_2O/5\%\ O_2$	FB NDIR	Carrier synthesis and comparative study of reaction rates at 950°C, study of agglomeration characteristics

As can be seen from Tables 2-5, the main contribution to the development of oxygen carriers for CLC has come from a Japanese research group at the Tokyo Institute of technology, headed by Masaru Ishida. The research effort started in the mid nineties and initial experiments by Ishida & Jin (1994b) studied the reactivity of pure nickel oxide (NiO) and particles of NiO and iron (III) oxide (Fe_2O_3) mixed with yttrium stabilized zirconia (YSZ). The study concluded that particles of pure NiO were unsuitable due to the formation of dense layers of elementary metal after a few cycles of reduction and oxidation. This effectively hindered the diffusion of reactants to the particle interior and also led to a loss of mechanical stability. Particles containing a mixture of metal oxide and an inert binder, such as YSZ or alumina improved reaction rates, regenerability (i.e. consistency of reaction rates after repeated red/ox cycles) and mechanical durability.

In a later study by Jin et al. (1999), the reactivity of NiO, CoO and Fe_2O_3 were investigated on different supports (Al_2O_3, TiO_2 and MgO). It was found that NiO supported on alumina produced nickel-aluminate ($NiAl_2O_4$) at high temperatures. $NiAl_2O_4$ belongs to a class of compounds more generally referred to as *spinels*, and the 'new' binder showed excellent reaction rates and durability in combination with NiO. A variety of binders have been tested, but none with significantly better results than those achieved using nickel-aluminate. Based on these results, nickel oxide supported on nickel-aluminate was selected as a reference material and starting point in the experimental work of this thesis.

The well known problem of carbon deposition in carbonaceous fuels at high temperature and low oxygen partial pressures was investigated by Ishida et al. (1998b). It was found that a steam-carbon ratio (S/C) of 2 was needed to effectively suppress carbon formation in the reduction.

The second largest contribution to the experimental data on oxygen carriers comes from a research group at Chalmers (Sweden) headed by Anders Lyngfelt. Early studies (Mattisson et al. (2001)) focused on iron oxide (Fe_2O_3, hematite) due to low price and promising results. However it seems that this group recently has also shifted its focus towards metal oxides on alumina and other supports.

In later years, other groups have also made contributions to the accumulated experimental data on oxygen carriers, most notably that of Copeland and co-workers. The Sorbent Energy Transfer System (SETS) proposed by this group and CLC are identical in every respect, with the important difference that SETS exploits the fact that both reduction and oxidation reactions for CuO are exothermic. A mixture of oxides (Fe_2O_3 –CuO) supported on alumina is thus selected to yield an oxygen carrier where both reactions are exothermic, with some significant implications for reactor design and cycle efficiency.

Although the research community involved in oxygen carrier development for CLC is still limited, the prospects of finding suitable materials for large scale and long term realistic testing have become significantly brighter during recent years. The number of publications pr. year is seen to rise, and the bulk of the papers have been produced during the last 3 years. The majority of the publications involve experiments using thermogravimetric methods, but there is a clear trend towards more realistic experimental set-ups using fixed and fluidized beds.

2.2.2 Reactor system literature

In contrast to oxygen carrier development, experimental data on reactor systems suitable for CLC are virtually non-existent. The paper by Johansson et al. (2003) provides experimental data for a cold, scaled model of two interconnected fluidized beds. Gas leakages are simulated by tracking helium and air within the reactors. It was shown that although controllable by means of steam injection, gas leakage between different components of the reactor system, might be a significant problem. The nature of CLC demands that gas leaks be kept at a minimum. It was also demonstrated that solids circulation

is relatively easily controllable. The first experimental data on continuous CLC are given by Ishida et al. (2002). For short term operation (<300 minutes) conversions of 100- and 70% were found for reduction and oxidation respectively.

Table 6 Literature related to reactor system design

Authors	Year	Topic Materials	Results
Lyngfelt, Leckner, Mattisson.	2001	General discussion of concept	Literature survey on oxygen carriers, reactor design equations, cycle considerations
Ishida, Yamamoto, Ohba	2002	Circulation of solids NiO on $NiAl_2O_4$, H_2/Air	100% hydrogen conversion and 70% air conversion found for continuous operation with circulation.
Johansson et al.	2003	Gas leakage measurements in interconnected fluidized beds, scaled cold model Sand, He/Air	Reactor leaks are in the area of 2-15% of reactor inlet flowrates. Gas leakage can be controlled by using steam.
Lyngfelt et al.	2004	10 kW pilot plant operation Nickel based carrier, NG/Air	First operational CLC-prototype, fuel conversion of 99.5% achieved, gas leakages not detectable, no deactivation observed, small attrition rates indicate long particle lifetime

The publication by Lyngfelt et al (2004) in the above table, represents a major breakthrough in the development of CLC. This is the first demonstration of all the aspects of CLC and the results that have been published so far must be said to be highly promising. This provides a strong incentive to continue development of CLC.

By virtue of its well documented suitability as a gas-solid reaction system (Levenspiel & Kunii 1994), the concept of interconnected fluidized beds as the reactor system of choice is assumed in virtually all publications on CLC. There are, however, some alternatives of which two will be discussed in the following sections.

2.2.2.1 Metallurgical Conversion of Natural Gas

Originally introduced by Kolbeinsen et al. (2000, 2001) in a series of unpublished internal notes as an alternative way to produce syngas, metallurgical conversion of natural gas bears a close resemblance to CLC. In this process, carbon is transferred to a melt of iron that circulates between two interconnected reactors as outlined in Figure 9.

The central component is a dual-vessel reactor in which molten iron circulates between a carburizer and decarburizer. Methane will dissociate to hydrogen gas and carbon dissolved in the liquid iron. Simultaneously, introduced oxygen will readily react with dissolved carbon and form carbon monoxide gas. The net reaction is partial oxidation of methane to syngas:

$$CH_4(g) + \tfrac{1}{2}O_2(g) \Leftrightarrow CO(g) + 2H_2(g) \qquad (2.5)$$

Methane is cracked to carbon and hydrogen upon contact with molten iron:

$$CH_4(g) \Leftrightarrow \underline{C} + 2H_2(g) \qquad (2.6)$$

The underscore in Eq. 2.6 denotes that carbon is dissolved in the liquid iron. In the temperature interval from 1153°C (iron-graphite eutectic temperature) to 1600°C the saturation limit for carbon in liquid iron is 4.3 to 5.6 %wt. The oxygen entering the bath may partly dissolve as elemental oxygen, but will mainly react with the iron to form liquid ferrous oxide:

$$Fe(l) + \tfrac{1}{2}O_2(g) \Leftrightarrow FeO(l) \qquad (2.7)$$

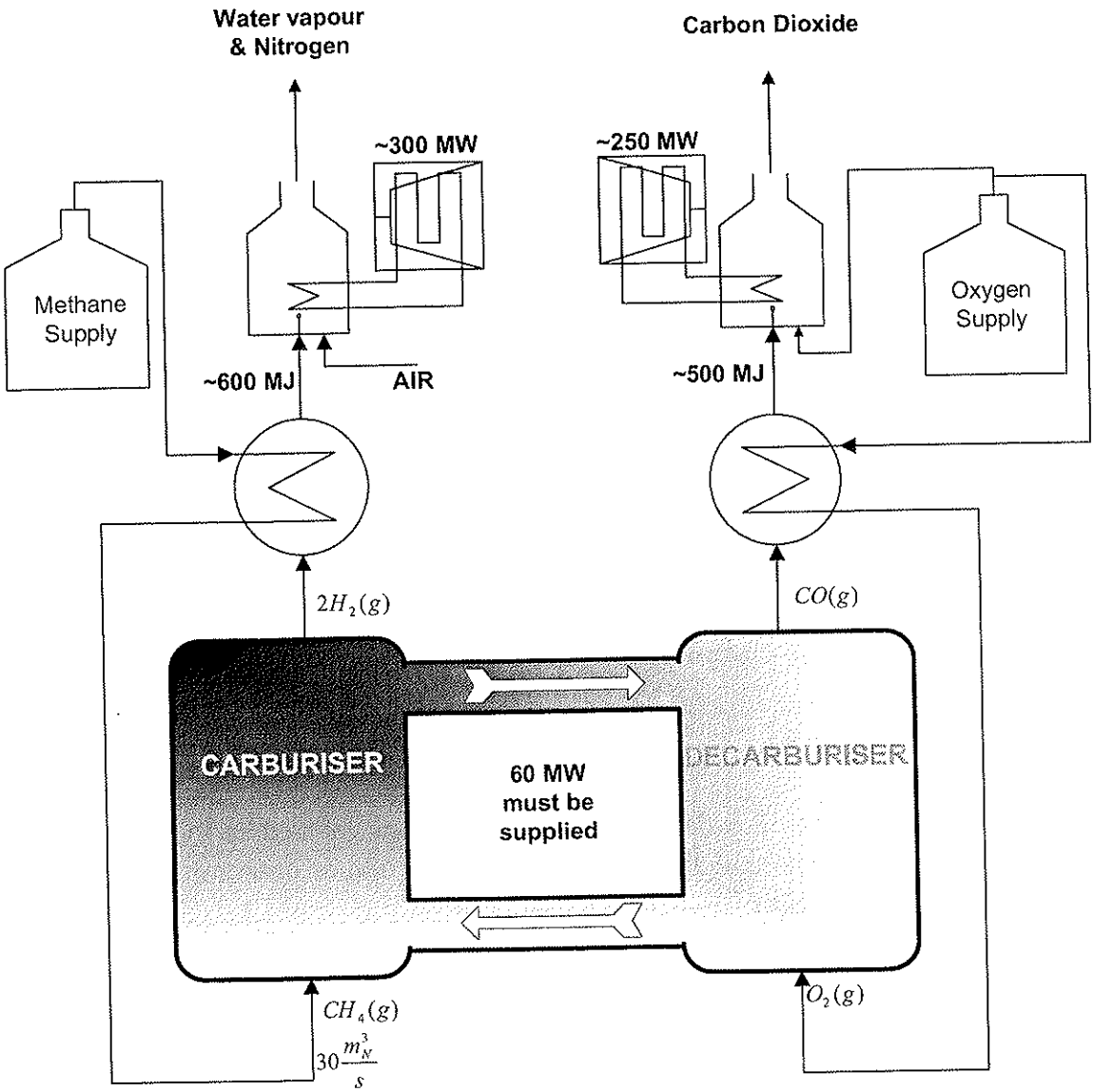

Figure 9 Metallurgical Conversion of Natural Gas (reproduced with permission)

The generated FeO can in turn react with the dissolved carbon according to:

$$\underline{C} + FeO(l) \Leftrightarrow CO(g) + Fe(l) \qquad (2.8)$$

A summation of Eq. (2.6), (2.7), and (2.8) gives the net reaction (2.5).

For the processing of 30 Nm^3/s CH_4, 60 MW needs to be supplied by induction in the iron melt. This is because the net sum of reactions (2.7) and (2.8 is exothermic, but reaction (2.6) is endothermic to such a degree that the process has an energy deficiency of about 2 MJ/m^3 CH_4. The process also has the apparent disadvantage of producing a 'split' synthesis gas with one stream containing hydrogen and the other carbon monoxide. This implicates

the use of a dual GT-cycle to combust product gases, increasing capital cost and cycle complexity. Other uncertainties include adverse effects of bubble formation and refractory wear. Initial studies including experimental work, thermodynamic process analysis and simulations of fluid flow patterns in the reactor have been carried out by Bergstrøm (2003). The investigations had some promising results, e.g. flow can be controlled by buoyancy differences within different sections of the melt, but have not been publicized at the present time. Work on this process has not been continued due to general lack of interest and funding.

2.2.2.2 Rotary chemical looping

A variant of chemical looping combustion resembling the 'CO_2 wheel' proposed by Shimomura (2003) for absorption of CO_2 by formation of lithium carbonate, suggests that the oxygen carrier be immobilized in a rotary reactor that is subjected to fuel and air in separated compartments.

The concept is currently subjected to considerable research by e.g. Alstom (Jukkola et al. 2003). It has not been a major consideration in this thesis, however, and only a brief description of the principles involved will be given. The cylindrical reactor is comparable to a fixed bed and will need to be divided into channels running the length of the vessel in order to prevent gas mixing within the cylinder. The channels are then filled with oxygen carrier material in a porous form that allows gas to flow through the cylinder without excessive pressure losses. A stationary gas-handling system will be required at both ends of the reactor, to feed reactants and inert gas (for purging of air and fuel respectively) and effluent gases respectively.

The reactor itself will rotate (either continuously or in discrete steps) with respect to the gas handling system, and this can potentially lead to problems associated with gas leaks.

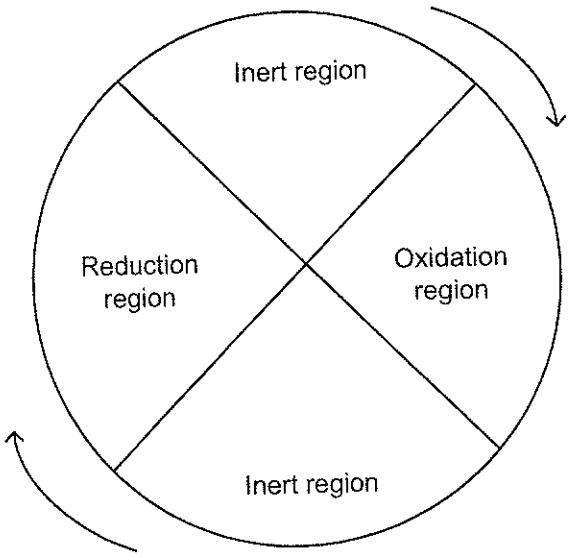

Figure 10 Rotary reactor schematic

The same chemistry as that for conventional CLC outlined in section 2.3.2 will apply, and effluent gases will in principle consist of a stream rich in CO_2 and a stream of oxygen depleted air. The carrier is reduced with fuel/steam in the reduction region whereas hot air regenerates the carrier in the oxidation region. Oxygen depleted air might be used as fluid in the inert regions.

2.2.3 Cycle analysis literature

Thermodynamic analysis of the energy producing potential of CLC is essential in all phases of CLC research & development. Firstly, the goal is to establish a theoretical basis for the potential of the process, and secondly to investigate the characteristics of CLC implemented in already existing power cycles. The lack of real experimental data on long term operation of continuous CLC systems is problematic as simulations become prone to errors, unrealistic and idealized with regard to the potential drawbacks of CLC. Using experimental results on oxygen carriers to establish sound assumptions such simulations can provide 'benchmarks' for further carrier development, i.e. minimum requirements on reaction rates and reactor temperatures to yield acceptable efficiencies.

Two main topics of investigation can be recognized from Table 7 and Table 8; cycle analyses that have mainly focused on comparative studies of different variants of CLC, and secondly, exergy analyses of CLC and conventional combustion processes.

Table 7 Literature related to cycle analysis (Part I)

Authors	Year	Carrier Fuel/oxidizer	Cycles Topics	Topics and results
Richter, Knoche	1983	Generalized	Concept introduction and thermodynamic analysis of CLC potential	Increased exergetic efficiency as compared to conventional combustion.
Ishida et al.	1987	NiO Saturated CH_4/Air	CLC-GT Brayton cycle Exergy analysis	CLC-GT: 50.2% eff. (LHV), preheating of reactants necessary for reduced exergy losses.
Harvey, Richter	1994	Fe_2O_3/FeO CH_4	CLC-SOFC with reforming of fuel	Highest theoretical eff. 78.4% (LHV), with losses projected 69% thermal eff.
Ishida, Jin	1994b	NiO CH_4/Air	CLC-HAT Cycle calculation & exergy analysis with energy utilization diagrams (EUDs)	CLC-HAT: 55.1% eff. (LHV), exergy losses reduced in CLC
Anheden, Svedberg	1998	NiO, Fe_2O_3 CH_4/Air and simulated coal gasification syngas	CLC-GT Brayton cycles compared to conventional GT cycle. Exergy analysis	Net power efficiencies: NiO CLC-GT: 44.9%, Fe_2O_3 CLC-GT: 48.72%, conv. comb. GT: 45.19%. Reduced exergy losses in CLC-GT processes.
Jin, Ishida	1998	NiO, Fe_2O_3 CH_4/Air and simulated coal gasification syngas	CLC-GT	Efficiencies for CLC-GT cycles similar or higher than conventional GT cycles. Exergy losses are lower in CLC-GT.

Table 8 Literature related to cycle analysis (Part II)

Authors	Year	Carrier Fuel/oxidizer	Cycles Topics	Topics and results
Brandvoll, Bolland	2004	NiO on YSZ Methane/ humid air	CLC-HAT Parameter variation, exergy analysis	CLC-HAT optimum eff. 55.9%, ≈ 52% with CO_2 separation, and recompression
Naqvi et al	2004	NiO on $NiAl_2O_4$ Natural gas/Air	CLC-CC and CLC-ISG compared to conventional processes, fuel conversion and exhaust recirculation	CLC-CC optimum eff.: 52.3% (PR=18), CLC-ISG eff. 42.8%, 41% with CO2 recompression. 0.5%-point loss in eff, for each %-point decrease in fuel conversion.

Generally, all simulations of CLC show very promising results as efficiencies are similar or higher than conventional combustion systems with the added benefit of full or partial CO_2 capture. As noted, all CLC cycle analyses have inherent uncertainties associated to them by virtue of the lack of reliable data for long term operation. Nonetheless, the potential of CLC has been found to be promising when applied to a number of cycles, including simple GT cycles, combined cycles, humid air turbine cycles and even with integrated coal gasification. Important requirements on reactor temperatures and pressures have also been revealed, providing goals for materials development. Furthermore all exergy analyses performed on the CLC concept, show reduced losses as compared to conventional combustion.

2.3 Oxygen carriers

Three main criteria that potential oxygen carriers must meet in order to be applicable in CLC can be stated:

- The reduction and oxidation reaction rates must be sufficient, over time, to ensure high conversion of fuel and rapid regeneration of oxide
- The mechanical properties of the carrier particles must be such that material breakdown and sintering/agglomeration is minimized

- Carrier particles should also be economically and environmentally sound to manufacture

The requirements on mechanical strength and chemical activity are generally contradictory, as a rigid, dense particle with high crush strength will lack the porosity necessary for complete conversion of the particle. This poses maybe the greatest single challenge in CLC development.

2.3.1 Oxygen carrier characterization

In order to describe different oxygen carriers on a comparable basis, a mathematical framework for quantifying oxygen carrier capacity has been developed. The literature concludes that the addition of an inert supporting material is necessary, and hence the overall composition, β, of an oxygen carrier particle is given as the mass fraction of active component, m_{Rx}, to total mass, m_{Tot}, when the active component is in the oxidized state:

$$\beta = \frac{m_{Rx}}{m_{Tot}} \tag{2.9}$$

Most of the literature on oxygen carriers concerns batch-experiments using gravimetric measurements to follow the course of oxidation and reduction reactions. A useful parameter when dealing with oxygen carriers in this context is the degree of oxidation, X_i, which is defined as:

$$X_i = \frac{m_i - m_R}{m_O - m_R} \tag{2.10}$$

In Eq. 2.10, m_i refers to the instantaneous mass of the oxygen carrier particle(s), while m_R and m_O refers to the mass of the fully reduced and oxidized sample respectively. The degree of oxidation is also useful when carrying out mass-balances in cycle analyses. In experiments where the sample is fluidized, the weight of the oxygen carrier within the reactor is not easily monitored, and in such situations the degree of oxidation throughout the course of the reaction must be estimated indirectly by measuring one or several of the reaction products (Brandvoll et al. 2003).

In experiments where concentrations of effluent species are quantified, it is more convenient to use molar quantities. Hence, the molar fraction of active component (i) is defined as the ratio of actual to initial amount:

$$y_i = \frac{n_i}{n_i^0} \tag{2.11}$$

The *oxygen carrying potential*, α, is defined as the mass fraction of mobile oxygen equivalents to the total mass of solids:

$$\alpha = \frac{\text{Mass of mobile oxygen equivalents}}{\text{Total mass of solids}} = \frac{m_{Oxygen}}{m_{Tot}} \tag{2.12}$$

The mass of mobile oxygen equivalents is an intrinsic property of oxygen carriers and is calculated from the following stoichiometric relationship:

$$m_{Oxygen} = \frac{m_{Rx}}{Mw(Rx)} \cdot \delta \cdot Mw(Oxygen) \tag{2.13}$$

where δ is the stoichiometric number of mobile oxygen equivalents in the active compound. For the conversion:

$$Me_nO_m \Leftrightarrow nMe + {}^{m}/_{2}\, O_2 \tag{2.14}$$

δ is defined as:

$$\delta = \frac{m}{n} \tag{2.15}$$

Combining the definition of overall composition for a fully oxidized carrier (Eq. 2.9) with Eq. 2.12 & 2.13 yields a useful expression for the determination of α based on the molar mass of the oxygen carrying compound (Mw(Rx)), molar mass of an oxygen equivalent (Mw(Oxygen) (i.e. 16.0 g/mol), overall composition (β) and stoichiometric number of mobile oxygen equivalents (δ):

$$\alpha = \beta \cdot \delta \cdot \frac{Mw(Oxygen)}{Mw(Rx)} \tag{2.16}$$

The oxygen ratio, R_0, proposed by Lyngfelt et al (2001) is defined as the mass fraction of transferable oxygen in the carrier in its fully oxidized state:

$$R_0 = \frac{m_O - m_R}{m_O} \qquad (2.17)$$

R_0 and α express the same intrinsic quantity.

For a thorough comparison of oxygen carrier materials on the basis of experimental findings, the reader is referred to Lyngfelt et al. (2001). Based on the literature cited earlier, the most promising candidate materials for use in CLC are NiO, CuO, CoO and Fe_2O_3 (converted to Fe_3O_4 (magnetite)). Based on findings by Cho et al. (2004), other conversions of iron-based materials are not considered. A comparison of the standard heats of reaction and the theoretical oxygen carrying capacity of the above mentioned oxides is given in Table 9. To make oxygen capacities comparable, all carriers are assumed to be mixed with an inert support (β=0.60). Thermodynamic data from CRC Handbook 57th ed. (1976) are used throughout.

Table 9 Standard enthalpies of reaction and oxygen carrying potential of selected oxygen carrying species

Conversion	**ΔH^0_{Red} [kJ/mol CH_4]**	**ΔH^0_{Ox} [kJ/mol O_2]**	**Mw(Rx) [g/mol]**	**α**	**δ[1]**
$NiO - Ni + 1/2\ O_2$	175.0	-488.7	74.7	0.129	1
$CoO - Co + 1/2\ O_2$	155.0	-478.7	74.93	0.128	1
$CuO - Cu + 1/2\ O_2$	-181.4	-310.5	79.54	0.121	1
$3Fe_2O_3 - 2Fe_3O_4 + 1/2\ O_2$	126.5	-464.4	159.7	0.02	0.33

In Table 9 oxidation enthalpies are calculated from standard heats of formation of the oxygen carrying species and reduction enthalpies are inferred from the net reaction (combustion of methane with 2 oxygen equivalents, Eq. 2.18).

$$\Delta H^0_{Red} = -802.3\ \text{kJ/(mol } CH_4) - 2 \cdot \Delta H^0_{Ox} \qquad (2.18)$$

Iron based carriers have an advantage as the raw materials are relatively cheap but it might be argued that the multiple states of oxidation (FeO-Fe_3O_4-

[1] Theoretical values, in practice full reduction is not feasible

Fe_2O_3) makes the oxidation somewhat difficult to control with regard to the actual composition of the carrier at any given time. Furthermore, the oxygen capacity (α) is significantly lower than for the other oxides under consideration. This is because 3 equivalents of Fe_2O_3 are required in order to deliver 1 oxygen equivalent (i.e. δ=0.33), and due to a much lower molecular weight ratio as compared to NiO, CoO and CuO, which are found to have similar oxygen capacities (0.121-0.123). Even if pure Fe_2O_3 is used as oxygen carrier (β=1) the oxygen capacity is still small (α=0.033) and this illustrates the main disadvantage of Fe_2O_3. In order to transfer a given amount of oxygen in the fuel reactor, a significantly larger total solid influx of Fe_2O_3 is required than for Ni, Co and Cu. It should be emphasized that this comparison is of oxygen carrying potential, and does not take into account the actual kinetics that can be achieved with the different materials.

The heats of reaction are similar for all oxides under consideration except CuO, in which both reduction and oxidation reactions are exothermic. This is thought to be an advantage as the heat balances of both reactors are supported by a negative heat of reaction. On the other hand, it might be argued that oxygen carriers with a slightly endothermic reduction are preferable, because this implies that the oxidation will be exothermic to a higher degree than the net combustion of fuel. Consequently, the thermal potential can be retrieved from *one* process stream (oxidation air exhaust) and not split equally between a small (by comparison) CO_2-rich stream and oxygen depleted air. The thermal potential of the former is more difficult to extract than that of the oxygen depleted air due to lack of suitable turbomachinery. At present, it is also unclear if copper based oxides are suitable in high temperature CLC operation, due to a reported tendency towards sintering (Cho et al. 2004). A recent publication by Garcia-Labiano et al. (2004) reports no such sintering tendency, however and it seems that more research on copper oxides is required.

2.3.1.1 Perovskites as oxygen carriers

In search of candidates to be employed as oxygen carriers, an interesting class of compounds is the *perovskites*. This class of oxides includes a wide variety of compounds with composition and crystal structure similar to the mineral Perovskite, $CaTiO_3$.

Ideal perovskites have the general formula ABO_3. A is normally an alkali, alkaline earth or rare earth metal, and the smaller B atom is an element in the transition series or in the main groups III, IV or V. The most interesting

property of perovskites in this context is the ability of the structure to accommodate an oxygen deficiency without major structural change (Olafsen, 1999):

$$ABO_3(s) \Leftrightarrow ABO_{3-\delta}(s) + \frac{\delta}{2}O_2(g) \qquad (2.19)$$

Perovskites are easily re-oxidized by air at elevated temperatures and the mobility of oxygen is expressed with the parameter δ. For ideal perovskites ($ABO_{3-\delta}$) δ is generally in the area $\{0<\delta<0.5\}$. The experimental work related to perovskites, have focused on determining δ at different temperatures to determine and compare the oxygen carrying potential of the perovskite and relate this to what has been found for NiONiAl.

A weakness of such systems is that the temperature stability generally is low. For example perovskites of the general type $La_nCo_nO_{3n-1}$ are known to undergo decomposition at temperatures above 650°C:

$$LaCoO_{3-\delta} \rightarrow La_{m+1}CmO_{3m+1} + La_2O_3 + Co \qquad (2.20)$$

To increase the temperature stability, elements such as Sr and Fe can be added to the structure resulting in compounds with general formula $La_xSr_{1-x}Co_{1-y}Fe_yO_{3-\delta}$.

In chapter 5, a perovskite with x=y=0.8; $La_xSr_{1-x}Co_yFe_{1-y}O_{3-\delta}$ has been tested in a chemical looping context.

2.4 Chemical reactions of CLC

Thermo-chemical data from Barrow (1988) is used throughout this section for calculation of standard heats of reaction at 298K, 1 atm. To exemplify, nickel oxide/nickel is used as carrier in the following.

2.4.1 Oxidation

In oxidation, elementary nickel embedded in the spinel matrix is converted exothermically to Nickel oxide (ΔH^0=-488.7 kJ/mol O_2).

$$2Ni(s) + O_2(g) \Leftrightarrow 2NiO(s) \qquad (2.21)$$

Previous experimental investigations (see literature section) indicate that oxidation of NiO is rapid at elevated temperatures. Carrier re-oxidation is crucial to CLC feasibility, as it represents the source of thermal energy within the reactor system. Results on the oxidation of nickel oxide with dry air, is covered in chapter 5.5.

2.4.2 Reduction

It can be distinguished between two sets of reactions involved in the reduction of NiONiAl with methane; *Direct Fuel Reduction (DFR)* and *reforming reactions*.

DFR using methane and nickel oxide (ΔH^0=175.0 kJ/mol CH_4), can be formulated as follows:

$$4NiO(s) + CH_4(g) \Leftrightarrow 4Ni(s) + CO_2(g) + 2H_2O(g) \qquad (2.22)$$

Multiplication of Eq. (2.21) by 2 and subtraction of Eq. 2.22 gives the net reaction for the combustion of methane (ΔH^0= -801.3 kJ/mol CH_4):

$$CH_4(g) + 2O_2(g) \Leftrightarrow CO_2(g) + 2H_2O(g) \qquad (2.23)$$

Coking is a possible complication whenever carbonaceous fuels are exposed to high temperatures and reducing conditions. The presence of elementary nickel generated by DFR, poses additional problems by virtue of its tendency to catalyze the formation of coke (Lødeng et al., 2000). In order to suppress coke formation, studies by Ishida et al. (1998b) indicate that addition of steam, can effectively suppress coke formation on NiONiAl.

In the presence of water vapor, however, methane is converted to carbon monoxide, carbon dioxide, carbon and hydrogen by a complex set of reactions commonly known as reforming reactions. The literature associated with experimental studies of methane reforming is vast, and it is far beyond the scope of this thesis to give a thorough discussion of the topic. A brief overview of the reactions that are likely to be encountered is given in Table 10:

Table 10 Methane reforming reactions

	Reaction	ΔH^0_{298} [kJ/mol]
Reforming reactions (strongly endothermic)	$CH_4(g) + H_2O(g) \Leftrightarrow CO(g) + 3H_2(g)$	206.1
	$CH_4(g) + CO_2(g) \Leftrightarrow 2CO(g) + 2H_2(g)$	247.3
Water shift reaction (weakly exothermic)	$CO(g) + H_2O(g) \Leftrightarrow CO_2(g) + H_2(g)$	-41.1
Methane decomposition	$CH_4(g) \Leftrightarrow C(s) + 2H_2(g)$	74.8
Boudouard reaction	$2CO(g) \Leftrightarrow C(s) + CO_2(g)$	-172.5
	$CO(g) + H_2(g) \Leftrightarrow C(s) + H_2O(g)$	-131.3

In addition to the reactions in the above table there are numerous mechanisms of minor importance that will not be considered. A complete listing of reforming reactions and equilibrium constants is given by Hou et al. (2001).

DFR and reforming reactions involved in the reduction of NiO is covered in chapter 5.

The hydrogen produced in SMR is a complicating factor as it might participate in reduction of nickel oxide ($\Delta H^0 = 2.5$ kJ/mol H_2):

$$NiO(s) + H_2(g) \Leftrightarrow Ni(s) + H_2O(g) \qquad (2.24)$$

Hydrogen reduction of NiO is covered in Paper III, and section 5.1.

2.4.3 Reduction and oxidation in a fluidized bed

Consider the differential segment of a fluidized bed (Figure 11). Solid particles (A) are suspended by an upward flow of gaseous reactant (B) and converted to solid product (C) and gaseous products (D+E). The reaction thus resembles a typical example of reduction:

$$aA(s) + bB(g) \rightarrow cC(s) + dD(g) + eE(g) \tag{2.25}$$

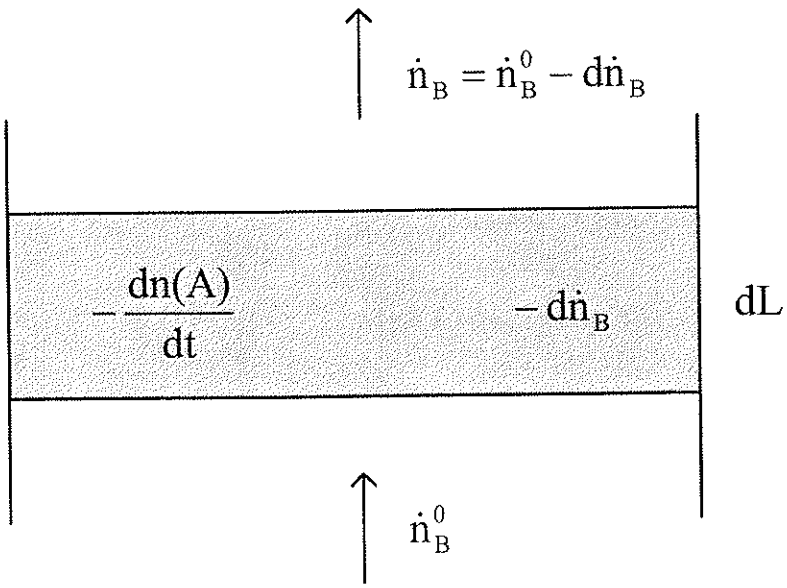

Figure 11 Differential segment of fluidized bed

Based on the stoichiometry of Eq. 2.25, a molar balance across the segment of differential height dL can be formulated with regard to solid reactant (A) as:

$$a \cdot \begin{pmatrix} \text{mol A} \\ \text{converted} \end{pmatrix} = d \cdot \begin{pmatrix} \text{mol D} \\ \text{produced} \end{pmatrix} \tag{2.26}$$

Per time unit, this can be expressed in terms of molar flux of D:

$$-\frac{dn_A}{dt} = \frac{d}{a} \cdot d\dot{n}_D \tag{2.27a}$$

Differentiating the definition of y_A (dn_A/dy) yields:

$$dn_A = n_A^0 \cdot dy_A \tag{2.28}$$

The conversion of solid can be expressed in terms of molar composition

From reaction stoichiometry it is clear that:

$$d\dot{n}_D = \frac{b}{d}\left(\dot{n}_B^0 - \dot{n}_B\right) \tag{2.29}$$

The molar balance with regard to solid conversion now becomes:

$$-dy_A = \frac{b}{a}\cdot\frac{1}{n_A^0}\cdot\left(\dot{n}_B^0 - \dot{n}_B\right)\cdot dt \tag{2.27b}$$

Reactant conversion (ϕ) is defined as:

$$\phi_i(t) = \frac{\text{mol reactant converted at time t}}{\text{mol reactant fed}} \tag{2.30}$$

or equivalently:

$$\phi_B(t) = \frac{\left(\dot{n}_B^0 - \dot{n}_B\right)}{\dot{n}_B^0} \Rightarrow \phi_B(t)\cdot\dot{n}_B^0 = \left(\dot{n}_B^0 - \dot{n}_B\right) \tag{2.31}$$

Substitution of Eq. 2.31 into Eq. 2.27b yields:

$$\int_{y^0}^{y(t)} -dy_A = \frac{b}{a}\cdot\frac{1}{n_A^0}\cdot\dot{n}_B^0\cdot\int_{\tau^0}^{\tau}\phi_B(t)\cdot dt \tag{2.27c}$$

Integration of the left-hand side with the above boundary conditions then gives:

$$y_A(t) = y_A^0 - \frac{1}{n_A^0}\frac{b}{a}\dot{n}_B^0\cdot\int_{\tau 0}^{\tau 1}\phi_B(t)\cdot dt \tag{2.27d}$$

For the particular case of reduction of NiO with CH_4, a=1, b=1/4, d=1/4. With condensation and separation of water vapor, the number of gaseous components is unchanged through the reactor. Conversion can now be expressed in terms of partial pressure when d/b is unity:

$$y_{NiO}(t) = y^0_{NiO} - \frac{4}{n^0_{NiO}} \frac{p^0_{CH4} \dot{V}^0}{RT^0} \cdot \int_{\tau 0}^{\tau 1} \phi_B(t)\, dt \qquad (2.27e)$$

Overall reactant conversion can now be expressed in terms of product gas composition:

$$\phi_B(t) = \frac{y_{CO2}(t)}{y^0_{CH4}} \qquad (2.32)$$

For a fully oxidized carrier the initial amount of active component is given as:

$$n^0_i = \frac{m_{Tot} \cdot \beta}{Mw(Rx)} \qquad (2.33)$$

where β is the overall composition of the carrier.

A similar expression can be derived for reoxidation with air:

$$NiO(s) + \tfrac{1}{2} O_2(g) \rightarrow NiO(s)$$

$$y_A(t) = y^0_A + \frac{2}{n^0_{O2}} \frac{p^0_{O2} \dot{V}^0}{RT^0} \cdot \int_{\tau 0}^{\tau 1} \phi_{O2}(t)\, dt \qquad (2.34)$$

For oxidation, conversion is defined as:

$$\phi_{O2}(t) = 1 - \frac{p_{O2}(t)}{p^0_{O2}} \qquad (2.35)$$

2.4.3.1 Experimental strategies

Reforming reactions are here considered as competing (and unwanted) reactions, as the primary goal of CLC is to produce a stream consisting of pure CO_2 and H_2O. Based on the set of chemical reactions involved in CLC, the main goals of the experimental section can be summarized as follows:

1 Determination of reactant conversion in oxidation and reduction with dry air and hydrogen respectively
2 Determination of CO_2 gas yield in reduction with methane
3 Determination of the relative importance of DFR and reforming reactions from exhaust gas partial pressures
4 Determination of solid conversion rates in reduction with methane/steam

Reactant conversions (ϕ_i) in reduction/oxidation using hydrogen/air are deduced from on-line MS analysis of residual reactant concentrations (pH_2 & pO2) in reduction and oxidation exhausts respectively.

$$\phi_i = 1 - \frac{p_i}{p_i^0} \qquad (2.36)$$

The relative importance of DFR and reforming reactions can be deduced qualitatively from the ratios of product gases during reduction. Conclusions can then be inferred from the stoichiometric coefficients of the relevant reactions and the literature on reforming. DFR and SMR are both endothermic to a similar extent, but it is expected that DFR will take precedence as it is thermodynamically favorable by virtue of its positive standard entropy (ΔS^0=397.0 J mol^{-1} K^{-1}) as compared to SMR (ΔS^0=-160.2 J mol^{-1} K^{-1}).

Coking during reduction can be deduced by the presence of carbon dioxide in exhaust gases upon re-oxidation, as coke is irreversibly converted to carbon dioxide (ΔH^0=- 393,5 kJ/mol O_2):

$$C(s) + O_2(g) \Leftrightarrow CO_2(g) \qquad (2.37)$$

Point 4 is difficult to address directly as hydrogen reduction (Eq. 2.24) might convert significant amounts of nickel oxide. Water is condensed and direct measurement of this mechanism is not possible. As will be shown in experimental sections, solid conversions in reduction with methane can only be determined under the assumption that reduction of NiO is dominated by DFR.

2.5 *Reactor system rationale*

Along with a solid material that has the ability to reversibly accept and donate oxygen, a gas-solid reactor system capable of high mass and heat transfer are one of the cornerstones of CLC. The configuration of the reactor system must be selected to meet several critical demands:

- Gas-Solid mass transfer must be high to ensure high conversion of the fuel and sufficient reaction rate in the oxidation reactor.

- Reduction is in many cases (Table 9) endothermic and the gas-solid heat transfer must be adequate to transfer the necessary heat of reaction from the hot, oxygen carrier entering the reduction vessel.

- Significant amounts of solids needs to be transported between reactors with minimal gas leakage and energy requirements.

The reduction reactor should ideally have a very high fuel conversion and selectivity towards CO_2 to ensure a reasonably pure exhaust stream. In the oxidation reactor, on the other hand, a high conversion of the oxygen supplied in the air is not required (or even desired). The rate of oxidation must be sufficiently large to transfer heat to large amounts of air for power production while keeping reactor volumes practical. Additionally, a significant amount of solids needs to be transported between the reactors avoiding excessive mechanical stresses on the oxygen carrier and with minimal energy penalty.

Consequently, CLC has some unique characteristics that separate it from other existing processes, but also many similarities that allow it to use technology from already existing industrial processes. The solids circulation closely resembles that employed in fluid catalytic cracking (FCC) of major commercial importance, with the exception that solids are actually converted in CLC. Generally fluidized beds offer many tempting advantages for an application such as CLC. Among the most important are the excellent gas-solid heat/mass-transfer characteristics and the liquid-like behavior of fluidized materials simplifies handling and transportation of large amounts of solids as compared to other reactor systems. Furthermore, solids within the reactors represent a thermal reservoir that resists rapid temperature changes, avoiding rapid changes in temperature, and allowing for stabile operation.

Bubbling fluidized beds offer high gas conversion rates and are suitable for large-scale operations with a variety of solids. Heat exchange is also highly efficient and reactor temperature is controllable by means of solids recirculation rates. On the downside, such reactors may experience problems associated with the erosion of pipes and immersed objects possibly accompanied by high particle attrition rates. Moreover, deep beds generally have high pressure drops, leading to large power consumption.

'Fast fluidized beds' with pneumatic transport of solids are suitable for fast reactions and fine solids. The co-current nature of the reactor allows for high solids conversion. Pressure drops are generally low and dependent on particle size, with large particles giving the greatest pressure drop. By virtue of the high local velocities within a transport reactor erosion and particle attrition can be a significant problem. Finally, heat exchange is not as good as for bubbling beds but heat transport to and from the reactor can be facilitated with circulation of solids.

A combination of two fluidized beds operating in different flow regimes can provide a working solution, with a configuration like that outlined in Figure 12.

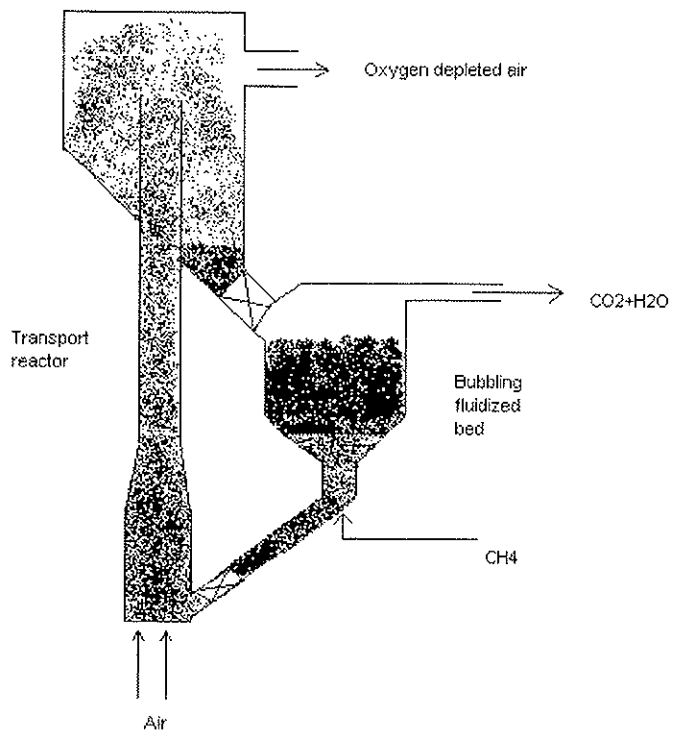

Figure 12 Schematic of reactor system without gas/solid separation equipment.

The oxidation reactor is a transport-reactor where solid material is lifted by the rapid flowing oxidation air to a buffer-tank before being transferred in a controlled way to the reduction vessel. Particular material (fines) must be removed by means of a cyclone or similar equipment. Recovered material could then be processed and regenerated for continued use in the process. Material is transported from the reduction reactor by gravity. The two reactors are separated by a system of valves providing a steady and controllable flow of oxygen carrier with a minimum of gas leakage. Recent studies of gas leakage between reactors by Johansson et al. (2003) indicate that this problem can be controlled by relatively simple means.

2.5.1 Reactor design equations

In the following the heat and mass balance equations of CLC will be given according to the reactor system schematic in Figure 13:

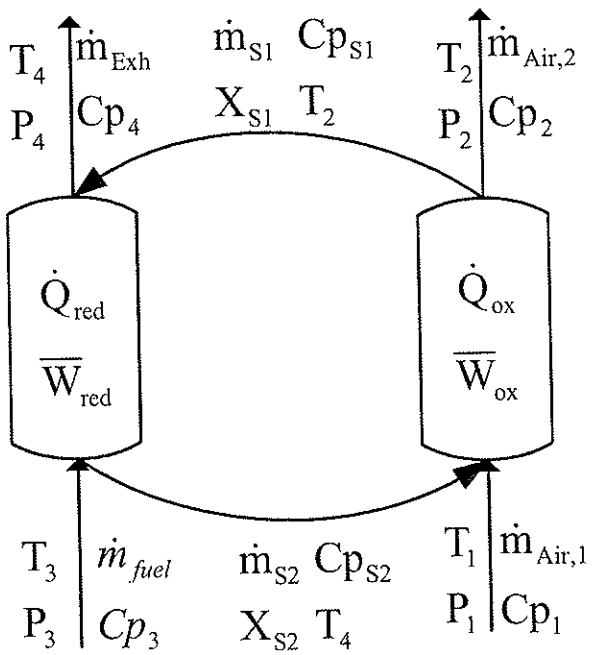

Figure 13 Dual reactor schematic

Based on the co-current nature of transport reactors, it is a relatively safe assumption that solids exiting the oxidation reactor ($\dot{m}_{S1}$) are in thermal equilibrium with the oxygen-depleted air that carries the material out of the reactor. With this assumption, $T_{S1}=T_2$. If adiabatic conditions are assumed, the oxidation reactor heat balance can be written as follows:

$$\dot{m}_{Air,1}Cp_1\Delta T_1 + \dot{m}_{S2}Cp_{S2}\Delta T_2 + \dot{Q}_{ox} = \dot{m}_{Air,2}Cp_2\Delta T_2 + \dot{m}_{S1}Cp_{S1}\Delta T_2 \qquad (2.38)$$

Heat of reaction is related to the molar enthalpy change and the amount of air that is consumed in the reactor:

$$\dot{Q}_{ox} = -\Delta H(ox)\cdot\frac{\left(\dot{m}_{Air,1} - \dot{m}_{Air,2}\right)}{Mw(O_2)} \qquad (2.39)$$

It is equally safe to assume that the temperature in the reduction reactor will be essentially constant throughout the bed volume, and the reduction heat balance then becomes:

$$\dot{m}_{fuel}Cp_3\Delta T_3 + \dot{m}_{S1}Cp_{S1}\Delta T_2 + \dot{Q}_{red} = \dot{m}_{Exh,4}Cp_4\Delta T_4 + \dot{m}_{S2}Cp_{S2}\Delta T_2 \qquad (2.40)$$

Introducing the fuel conversion factor, ϕ, and assuming that reforming reactions can be neglected, the heat of reaction is given by:

$$\dot{Q}_{Red} = -\Delta H_{Red}\cdot\frac{\dot{m}_{fuel}}{Mw(Fuel)}\cdot\phi \qquad (2.41)$$

The fuel conversion factor is defined as the ratio of reacting moles of fuel to total moles of fuel fed:

$$\phi = \frac{\dot{n}_{Fuel,rx}}{\dot{n}_{Fuel}} \qquad (2.42)$$

For a given fuel feed rate the O_2 consumption is given by:

$$\dot{m}_{O_2} = N\cdot\phi\cdot\dot{m}_{Fuel}\frac{Mw(O_2)}{Mw(Fuel)} \qquad (2.43)$$

The amount of air needed is dependent on the conversion of oxygen that can be achieved, i.e. on the fraction of oxygen in oxygen that is transferred in the oxidation reactor is expressed by the air ratio, as described by Lyngfelt et al (2001):

$$\lambda = \frac{0.21\left(1 - y_{O_2,E}\right)}{0.21 - y_{O_2,E}} \qquad (2.44)$$

The mass flow rate of air can then be expressed in terms of fuel consumption:

$$\dot{m}_{Air,1} = \frac{\lambda}{0.233} \cdot N \cdot \varphi \cdot \dot{m}_{Fuel} \frac{Mw(O_2)}{Mw(Fuel)} \tag{2.45}$$

The superficial gas velocity in the oxidation and reduction reactors can now be expressed in terms of reactor geometry and volumetric flow rate of air and fuel respectively, and compensating for expansion due to temperature increase:

$$(u_0)_{Ox} = \frac{\dot{V}_{Air,in}}{A_{Ox}} \cdot \frac{T_{Ox}}{T_0} = \frac{\dot{m}_{Air,in} \cdot \nu_{Air}}{A_{Ox}} \cdot \frac{T_{Ox}}{T_0} \tag{2.46}$$

$$(u_0)_{Red} = \frac{\dot{V}_{Fuel}}{A_{Red}} \cdot \frac{T_{Red}}{T_0} = \frac{\dot{m}_{Fuel} \cdot \nu_{Fuel}}{A_{Red}} \cdot \frac{T_{Red}}{T_0} \tag{2.47}$$

The total mass of oxygen carrier within each reactor can be calculated from bed volume and average particle density and correcting for the bed voidage in the current fluidization regime. The average bed mass for reduction and oxidation reactors then become:

$$m_{b,Red} = (A \cdot h_b (1 - \varepsilon_b) \rho_S)_{Red} \tag{2.48}$$

And similarly for oxidation:

$$m_{b,Ox} = (A \cdot h_b (1 - \varepsilon_b) \rho_S)_{Ox} \tag{2.49}$$

Using data from Kunii & Levenspiel (1991) it can be estimated that bubbling fluidized beds generally have a voidage [$0.50 < \varepsilon_{b,Red} < 0.55$] while a transport reactor with a high solid flow has a voidage in the region [$0.2 < \varepsilon_{b,ox} < 0.1$]

Average solids residence times can be estimated as the ratio of total bed mass to solids influx:

$$\tau_r = \frac{m_{b,R}}{\dot{m}_{S1}} = \frac{A_b h_b (1 - \varepsilon_b) \rho_S}{\dot{m}_{S1}} \tag{2.50}$$

2.5.2 Fluidization properties

The superficial fluid velocity at minimum fluidization conditions is referred to as the minimum fluidization velocity, u_{mf}. At this velocity the bed is kept suspended by the fluid up-flow and the solid suspension takes on fluid-like behavior. This can be observed visually as the upper level of the bed at this point remains horizontal even when the bed is tilted with regard to the vertical plane. The precise onset of full fluidization for a given set of gas-solid properties is generally determined experimentally from pressure-drop versus velocity diagrams.

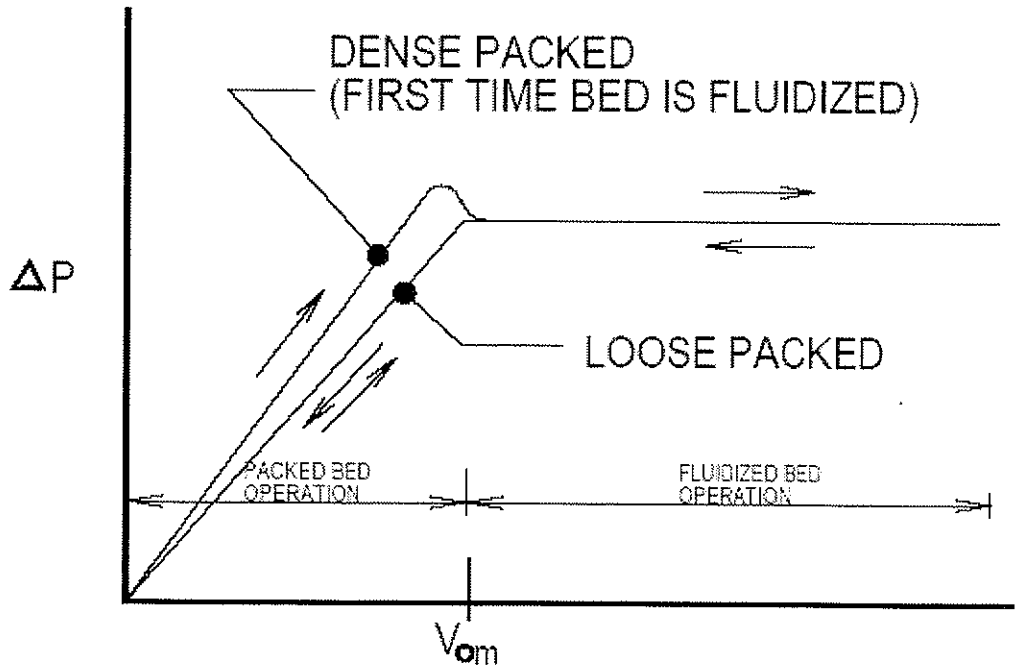

Figure 14 Pressure-drop versus velocity diagram (source: University of Akron website, http://www.ecgf.uakron.edu)

The numerical value of u_{mf} can be estimated analytically from a force balance:

$$\begin{pmatrix} \text{drag force by} \\ \text{upward moving gas} \end{pmatrix} = \begin{pmatrix} \text{weight of} \\ \text{particles} \end{pmatrix}$$

Or

$$\begin{pmatrix}\text{pressure drop}\\ \text{across bed}\end{pmatrix}\cdot\begin{pmatrix}\text{cross - sectional}\\ \text{area of tube}\end{pmatrix}=\begin{pmatrix}\text{volume}\\ \text{of bed}\end{pmatrix}\cdot\begin{pmatrix}\text{fraction}\\ \text{consisting}\\ \text{solids}\end{pmatrix}\cdot\begin{pmatrix}\text{specific}\\ \text{weight}\\ \text{of solids}\end{pmatrix}$$

It can be shown (Kunii & Levenspiel, 1991) that the pressure drop for minimum fluidizing conditions is given by:

$$\frac{\Delta p_b}{L_{mf}} = (1-\varepsilon_{mf})\cdot(\rho_s-\rho_f)g \qquad (2.51)$$

By introducing Eq. 2.52 into the frictional pressure drop correlation for a packed bed (Ergun equation) the following square in Reynolds particle number at minimum fluidizing conditions is obtained:

$$\frac{1.75}{\varepsilon_{mf}^3 * \sigma_s}\mathrm{Re}_{mf}^2 + \frac{150(1-\varepsilon_{mf})}{\varepsilon_{mf}^3\sigma_s^2}\mathrm{Re}_{mf} - \mathrm{Ar} = 0 \qquad (2.52)$$

or equivalently:

$$A\mathrm{Re}_{mf}^2 + B\mathrm{Re}_{mf} - \mathrm{Ar} = 0 \qquad (2.53)$$

where

$$A = \frac{1.75}{\varepsilon_{mf}^3\sigma_s} \text{ and } B = \frac{150(1-\varepsilon_{mf})}{\varepsilon_{mf}^3\sigma_s^2}$$

Analytical determination of u_{mf} firstly involves estimation of the dimensionless Archimedes[2] number (Ar) for a particle suspended by a fluid:

$$\mathrm{Ar} = \frac{d_p^3\rho_g(\rho_s-\rho_f)g}{\mu^2} \qquad (2.54)$$

Solving Eq. 2.53 with regard to Re_{mf} then allows for the determination of u_{mf} from:

---

[2] Referred to as the Galileo number by some authors

$$u_{mf} = \frac{Re_{mf}\mu_f}{d_p\rho_f} \tag{2.55}$$

The fluidization regime (FR) at a given fluid velocity can be expressed in qualitative terms by the ratio of actual superficial velocity and minimum fluidization velocity:

$$FR \propto \left(\frac{u_0}{u_{mf}}\right)_T \tag{2.56}$$

3 CLC IN POWER CYCLES

3.1 Introduction

Steady-state simulations of power cycles with chemical looping combustion were carried out in order to identify efficiency potential and parameter sensitivity. Parameter variations related to the CLC-unit provides estimates of the relative importance of these, and increase the general understanding of the concept. Additionally, such investigations will provide target values for the experimental work related to oxygen carrier development and reactor design, as well as design criteria for future large-scale applications of CLC. Target values for oxygen carrier performance include requirements on difference in degree of oxidation (ΔX), temperature and pressure sensitivity, solids transportation rates and fuel conversion.

3.2 Power cycles

The dual reactor system of CLC was modeled and implemented in 3 power cycles, and the characteristics of these cycles will be presented here. The integration of CLC into processes using standard gas turbines and bottoming cycles has very tempting advantages. The direct use of a dual reactor system replacing the traditional combustor and an external air separation unit means a potential of a reduction of costs and energy penalty as compared to traditional oxy-fuel combustion methods. In all cycles, the oxidation reactor is assumed to be the riser of a circulating fluidized bed, while the reduction reactor is a bubbling fluidized bed for Computational assumptions are given in Appendix A. To date, no high-temperature (i.e. over 1000°C) experimental data on nickel-based carriers exists. It was chosen to go beyond the temperature reported from experimental work, and 1200°C was set as the upper temperature limit.

The following cycles have been evaluated:

1 Chemical looping combustion in a Humid Air Turbine process (CLC-HAT)
2 Chemical looping combustion in a Combined Cycle (CLC-CC)

3 Chemical looping combustion in an indirect heating cycle with Internal Steam Generation (CLC-ISG)

3.2.1 CLC-Humid Air Turbine

The cycle is outlined in Figure 15, showing the variables that have been varied around the CLC reactors.

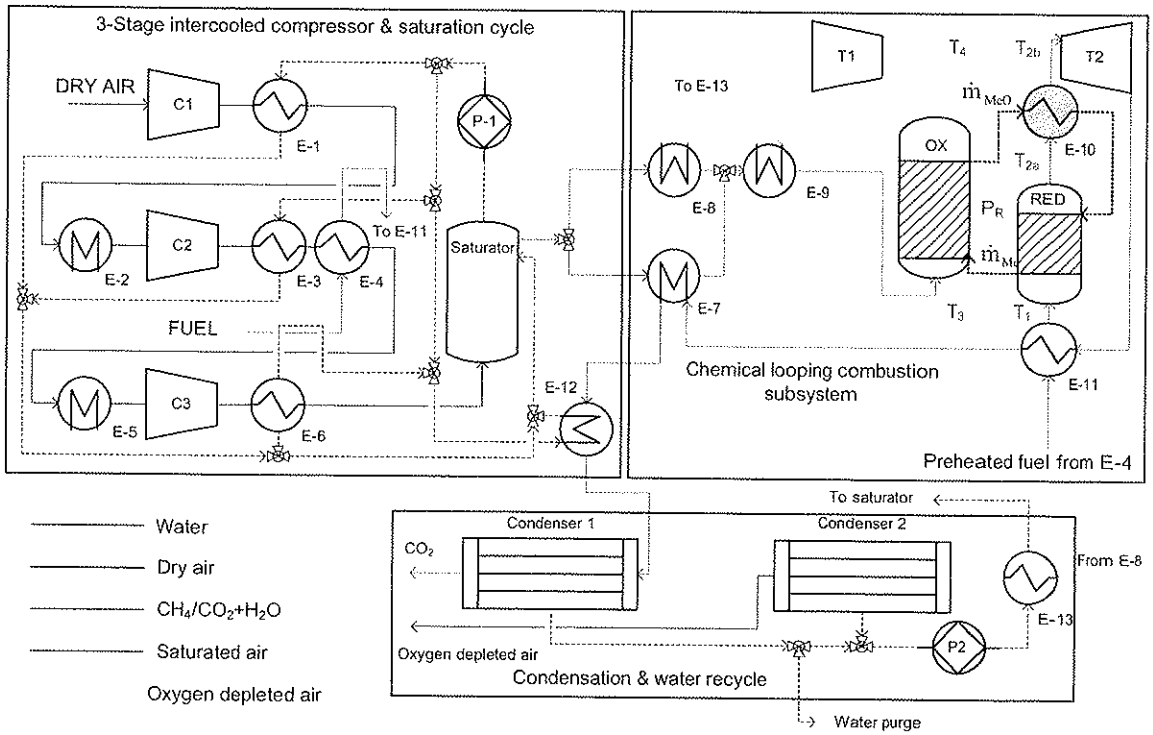

Figure 15 CLC-HAT cycle schematic

Cycle description

The process may be divided into three sub-systems as shown in Figure 15. These include a 3-stage intercooled compressor and saturation cycle, the chemical looping reactors and a water condensation/separation cycle. Ambient air is compressed in a three-stage intercooled compressor train (C1 to 3) and saturated with steam in a saturator. The water used for saturation of the air represents a major heat absorbent in the cycle. The cold water stream leaving the saturator is therefore split and used to lower the air temperature at each stage of the compressor. Additionally, cooling water (15°C) is used in E-2 & E-3 to further lower the temperature of the compressed air at intermediate stages. After being saturated with steam, the air enters the oxidation reactor where the temperature increases rapidly as oxygen reacts exothermically with the reduced form (Me) of the metal oxide. Thermal

energy is converted to work in T1 and the hot exhaust recuperated with inlet oxidation air in heat exchangers E-5 and E-9. Steam is condensed in Condenser 1, and the water is recycled back to the saturator after being heated with the hot oxidation air. Air with a reduced content of oxygen leaves the cycle after E-8. Fuel (methane) is preheated in E-4 & E-11 and assumed to be converted quantitatively to CO_2 (66%) and H_2O (33%) in the reduction reactor. Reduction is endothermic for nickel-based carriers. The sensible heat of the metal oxide (MeO) provides the necessary heat of reaction to avoid major temperature drop in the reduction reactor. The reduction exhaust consisting of CO_2 and water vapor is heated in gas-solid heat exchanger E-10 before expansion in CO_2-turbine T2. In the original publications (Paper I & II), water is removed by condensation and pure CO_2 leaves the cycle at atmospheric pressure. In order to make efficiencies of CLC-HAT comparable to those of CLC-CC and CLC-ISG, the energy penalty associated with CO_2 recompression is also considered in the results section. Fuel consumption and reactor pressure are fixed variables in this cycle analysis. Initial pressure variations suggested an optimum reactor pressure of 20 bar as discussed in the results section. The cycle is further analyzed by varying temperatures at various positions in the CLC-subsystem.

3.2.2 CLC-Combined Cycle

The cycle is outlined in Figure 16 and is a combined cycle where the conventional combustor of the gas turbine is replaced by a CLC-reactor unit, and with the addition of a CO_2 recompression train.

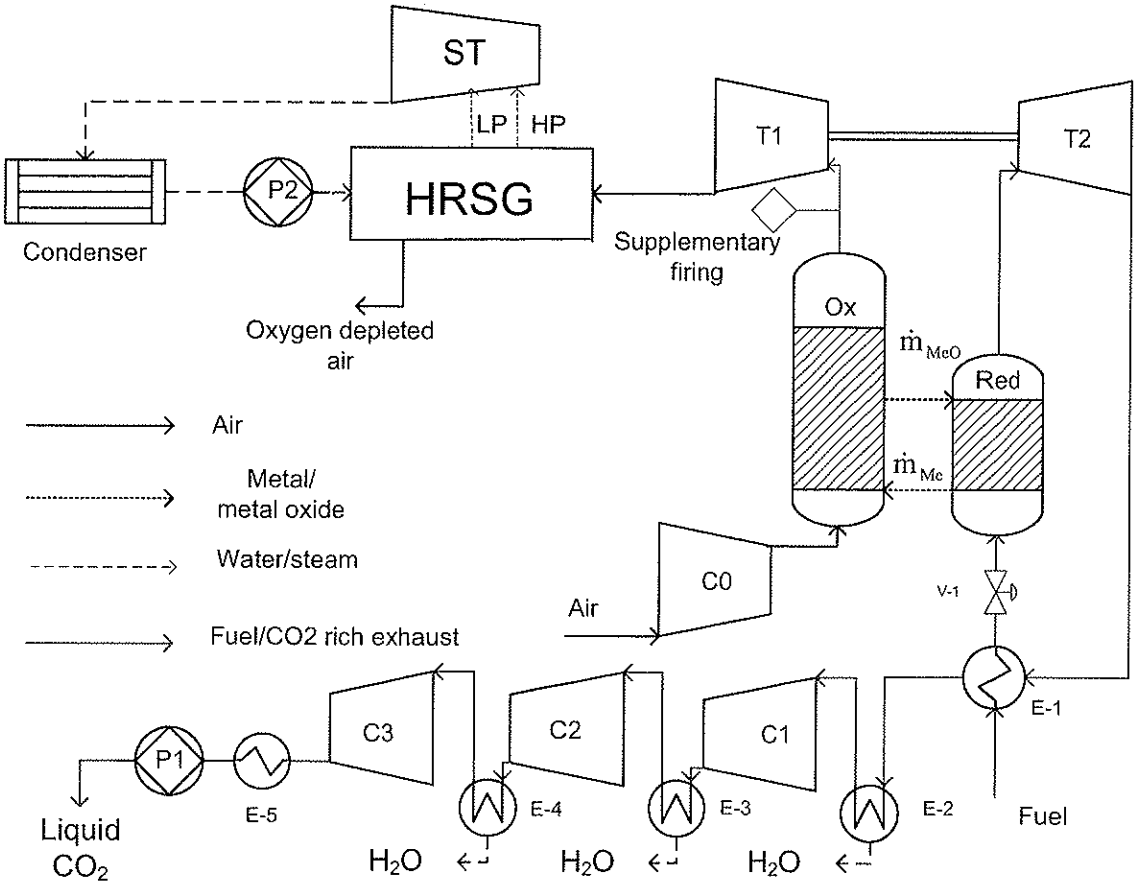

Figure 16 Schematic of CLC-Combined Cycle

Cycle description

Ambient air is compressed to the relevant pressure without any further preheating before entering the oxidation reactor. The hot oxidation exhaust is expanded in gas turbine T1 before entering a dual pressure heat recovery steam cycle. The impact of supplementary firing was also investigated. Supplementary firing is necessary for high pressure ratios and low TITs to meet the requirements of the HRSG on live steam temperature. Fuel (natural gas) is supplied at 50 bar and preheated by heat exchange (E-1) with the exhaust gases from T2. Pressure is reduced (V-1) before the fuel enters the reduction reactor. Exhaust gases containing CO_2/H_2O and small amounts of unconverted natural gas (dependent on fuel conversion ratio, ϕ) are expanded in turbine T2. Turbines 1 & 2 are assumed to be on the same shaft. The exhaust gas (CO_2 + H_2O) is cooled (E-2) before recompression (C1 – C2) with intercoolers including water condensation (E-3 & E-4). A final compression (C3) and cooling stage (E-5) provides dense CO_2 at 80 bar delivered by pump (P2) ready for storage or other uses. The steam cycle is calculated in *GT-Pro (Thermoflow, Inc.),* by exporting stream data (mass flow, temperature, composition).

Various aspects of CLC were investigated in this study. The cycle was analyzed by varying pressure ratio while maintaining turbine (T1) inlet temperature. Secondly, turbine cooling energy penalty was estimated by bypassing a fraction of the oxidation air for this purpose. A model proposed by Bolland and Stadaas (1993) was used to estimate mixing losses (Figure 17) and is elaborated more in section Cooling of the CO_2 turbine was not considered as the working fluid does not allow for conventional air cooling techniques. Furthermore, the CO_2 turbine contributes only 10% of net output.

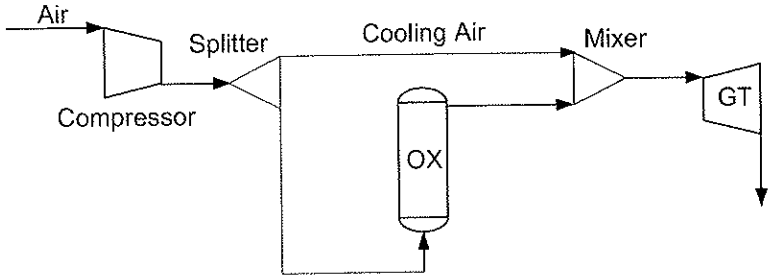

Figure 17 Turbine cooling principle (from Naqvi et al. 2004)

The problem of carbon formation in the fuel reactor is well documented in several studies on oxygen carriers (section 2.2.1), and is best resolved by recirculating some of the CO_2/H_2O-rich exhaust from the fuel reactor. Exhaust was therefore recirculated so that the steam/carbon ratio was 2, by the addition of a splitter and a light duty compressor to compensate for pressure losses (Figure 18).

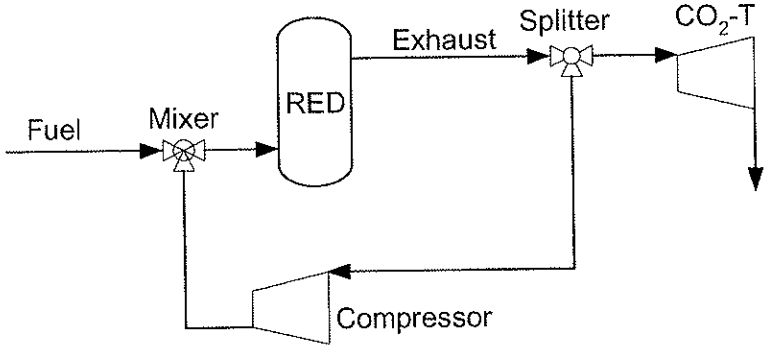

Figure 18 Reduction exhaust recirculation principle (from Naqvi et al. 2004)

Furthermore, starting points for supplementary firing, - i.e. minimum turbine inlet temperatures at which supplementary firing becomes necessary for operation of the HRSG -, were estimated. Finally the effect of less-than 100% fuel conversion ratio was investigated for the case of TIT=1200°C and PR=18 bar.

3.2.3 CLC-Integrated Steam Generation

An alternative way to utilize the heat generated in the oxidation reactor, is to employ the CLC-combustion system in an atmospheric oxidation/reduction process with internal steam generation (CLC-ISG). Steam is generated and reheated in heat exchangers embedded in the fluidized bed, and the cycle resembles an indirect heating, Rankine–type process. As mentioned with regard to supplementary firing, there are still many questions regarding the high temperature durability of oxygen carriers. Material constraints (sintering and agglomeration of the carrier) might limit oxidation reactor temperature to below 1000°C, and CLC-ISG might, in that case, be the best immediate alternative to employ CLC in power production. Internal heat exchange and steam production in fluidized beds is highly efficient with regard to heat transfer and well proven on industrial scales (Kunii and Levenspiel, 1991). The cycle is outlined in Figure 19.

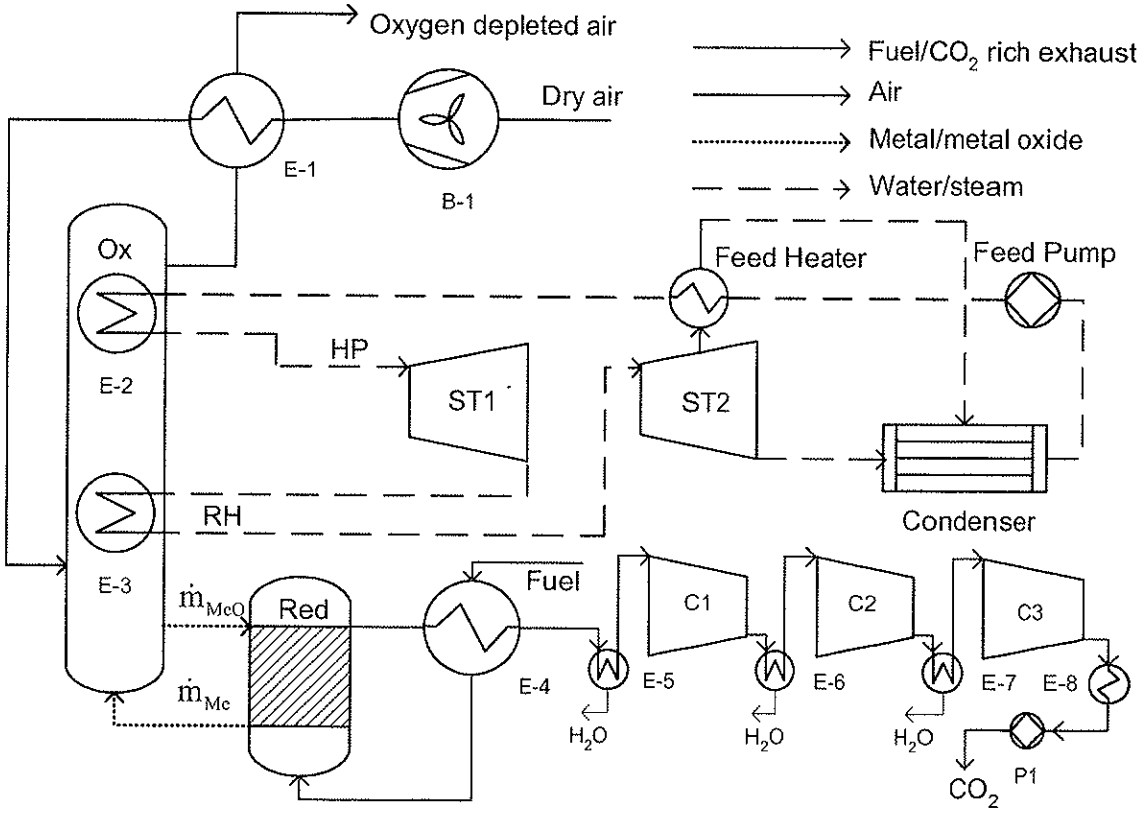

Figure 19 Schematic of CLC with internal steam generation

Cycle description

Oxidation air is compressed in a blower (B-1) to overcome reactor pressure losses, and preheated with hot exhaust gases from the oxidation reactor in

heat exchanger E-1. The oxidation reactor is equipped with internal heat exchangers (E2 & E-3) providing HP & RH steam for steam turbines ST1 & ST2, respectively. Fuel enters the reduction reactor at slightly higher than atmospheric pressure after recuperation with reduction exhaust gases (E-4). The same CO_2 separation and recompression train as that in CLC-CC is used.

3.3 Modeling aspects

The modeling of the dual reactor system is based on heat and mass balances. Nickel oxide is used as active oxygen carrier in all cycles, but with different inert stabilizers. The HAT-cycle employs NiO:YZT (3:2) (by mass), while the combined and atmospheric cycles uses NiO:$NiAl_2O_4$ (3:2) (by mass). This leads to differences in heat capacity and solid mass flow rates, but has little impact on overall cycle efficiency as the assumptions regarding the chemical conversion characteristics of the active component are similar.

3.3.1 Oxidation reactor balance equations

In the following, parameter indexes are assigned according to Figure 20. Both reactors are assumed to be at equilibrium. For simplicity, indexes "Me" and "MeO" are used for solid streams leaving the reduction and oxidation reactors respectively even if the degree of oxidation of the oxygen carrier is not 0.0 and 1.0, respectively. Nickel oxide/nickel is the active component in all simulations.

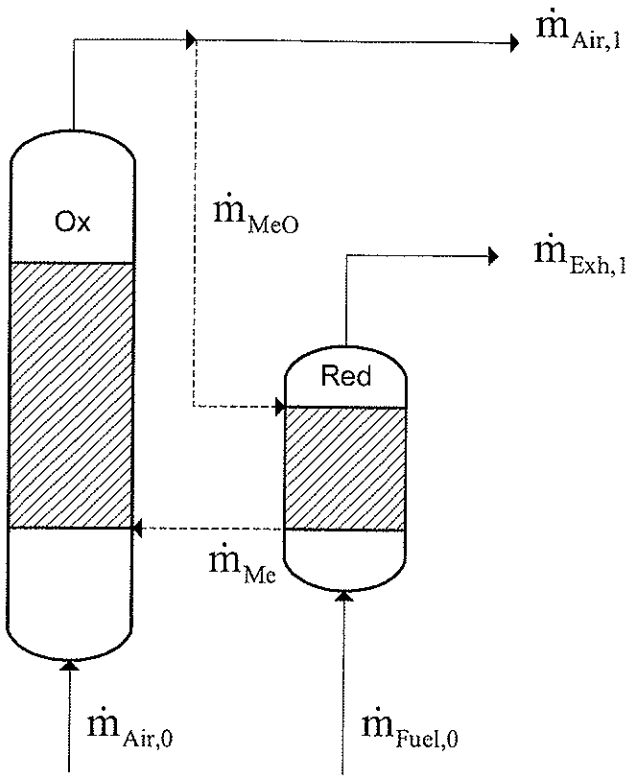

Figure 20 CLC reactor system schematic with indexes

The basis for all CLC simulations has been the amount of fuel converted in the reduction reactor. With given fuel flow, the amount of oxygen converted is found from reaction stoichiometry, and the heat balance for the air reactor can be solved. The sum of the sensible heat of the streams entering and leaving the oxidation reactor must equal the sum of the heat of reaction and the heat-loss.

The heat balance for the oxidation reactor can be formulated as follows:

$$\dot{Q}_{Air,0} + \dot{Q}_{Me} + \dot{Q}_{Rx} = \dot{Q}_{Air,1} + \dot{Q}_{MeO} + \dot{Q}_{HL} \qquad (3.1)$$

Where the sensible heat of streams is estimated from:

$$\dot{Q}_i = \dot{m}_i \cdot Cp_i \cdot \Delta T \qquad (3.2)$$

The heat of reaction is calculated on a molar basis at a standard reference condition, in this case 15°C and 1 bar:

$$\dot{Q}_{Rx} = (\dot{m} \cdot \Delta H_f^0)_{O_2} + \left(\dot{m} \cdot \Delta H_f^0\right)_{Ni} - \left(\dot{m} \cdot \Delta H_f^0\right)_{NiO} \qquad (3.3)$$

The standard enthalpy of formation for the nickel/nickel oxide system that has been used throughout in simulations is ΔH_{ox}= -977 kJ/mol Ni.

The heat-loss in the oxidation reaction is estimated as 1% of the total sensible heat leaving the reactor:

$$\dot{Q}_{HL} = \frac{\left(\dot{Q}_{Air,1} + \dot{Q}_{MeO}\right)}{100} \tag{3.4}$$

The amount of oxygen that is removed from the air is transferred to the oxygen carrier:

$$\dot{m}_{Air,0} + \dot{m}_{Me} = \dot{m}_{Air,1} + \dot{m}_{MeO} \tag{3.5}$$

or equivalently:

$$\dot{m}_{Air,0} - \dot{m}_{Air,1} = \dot{m}_{MeO} - \dot{m}_{Me} = \Delta\dot{m}_{O,RX} \tag{3.6}$$

3.3.2 Reduction reactor balance equations

Heat and mass balances for the fuel conversion in the reduction reactor are very similar to those of the air reactor, but using fuel and CO_2/H_2O instead:

$$\dot{Q}_{Fuel,0} + \dot{Q}_{MeO} + \dot{Q}_{Rx} = \dot{Q}_{Fuel,1} + \dot{Q}_{Me} + \dot{Q}_{HL} \tag{3.7}$$

where:

$$\dot{Q}_{Red} = \left(\dot{m}\cdot\Delta H_f^0\right)_{Fuel} + \left(\dot{m}\cdot\Delta H_f^0\right)_{NiO} - \left(\dot{m}\cdot\Delta H_f^0\right)_{Ni} - \left(\dot{m}\cdot\Delta H_f^0\right)_{E} \tag{3.8}$$

The standard heat of reduction for the nickel/nickel oxide is ΔH_{red}= 175 kJ/mol.

Heat loss is estimated in the same manner as for the oxidation reactor:

$$\dot{Q}_{HL} = \frac{\left(\dot{Q}_{Fuel,0} + \dot{Q}_{Me}\right)}{100} \tag{3.9}$$

The mass balance over the reduction reactor is:

$$\dot{m}_{Fuel,0} + \dot{m}_{MeO} = \dot{m}_{E,1} + \dot{m}_{Me} \qquad (3.10)$$

The molar balances used for calculating CLC-CC with incomplete fuel conversion are given in Figure 21:

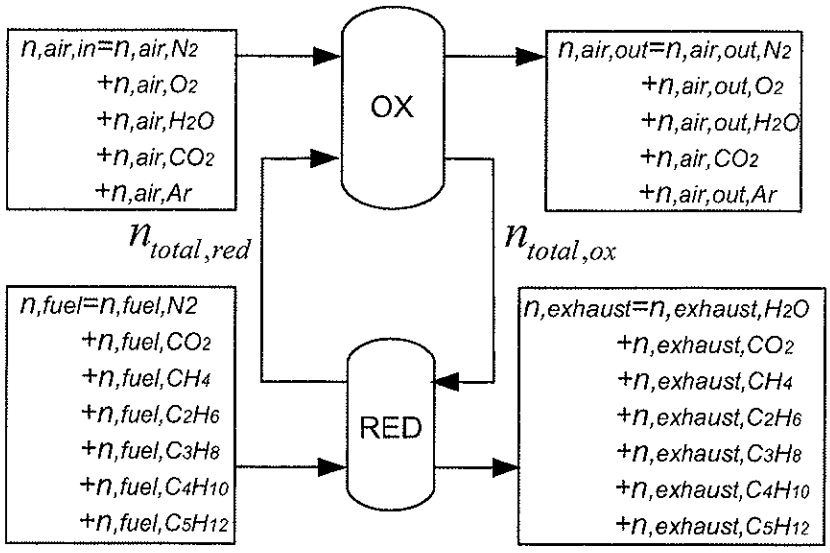

Figure 21 Molar balances for incomplete fuel conversion

3.3.3 Unit operations

In the following the mathematical framework for calculating unit operations are presented.

Compressors/turbines

The HAT-cycle implements a three stage intercooled compression cycle where the outlet temperature is calculated using the standard compressor equation:

$$\frac{T_1}{T_0} = \left(\frac{P_1}{P_0}\right)^{\frac{R}{C_p \eta_c}} \qquad (3.11)$$

Each compressor is calculated individually and in sequence by recalling scripts that return output values and assign new variables. Required compressor work is calculated from a mass balance over each compressor:

$$\dot{W}_C = \dot{m} \cdot Cp \cdot (T_1 - T_0) \tag{3.12}$$

Similarly, the two turbines are calculated using the standard equation:

$$\frac{T_1}{T_0} = \left(\frac{P_1}{P_0}\right)^{\frac{R\eta_T}{C_p}} \tag{3.13}$$

Potential turbine output is calculated from a mass balance:

$$\dot{W}_T = \dot{m} \cdot Cp \cdot (T_0 - T_1) \tag{3.14}$$

Turbine cooling was not considered in the calculations on CLC-HAT. In CLC-CC, however, turbine cooling was a major consideration. The principle is outlined in Figure 17 and involves bleeding off a fraction of the compressed air to be used as turbine coolant (film cooling). Since total mass flow is higher at compressor inlet than at turbine outlet (due to O_2 consumption in oxidation), coolant fraction (CF) was estimated as a percentage of turbine exhaust:

$$\dot{m}_{coolant} = CF \cdot \dot{m}_{exhaust} \tag{3.15}$$

Figure 22 shows coolant fraction (CF) as a function of turbine inlet temperature (TIT) and pressure ratio (PR).

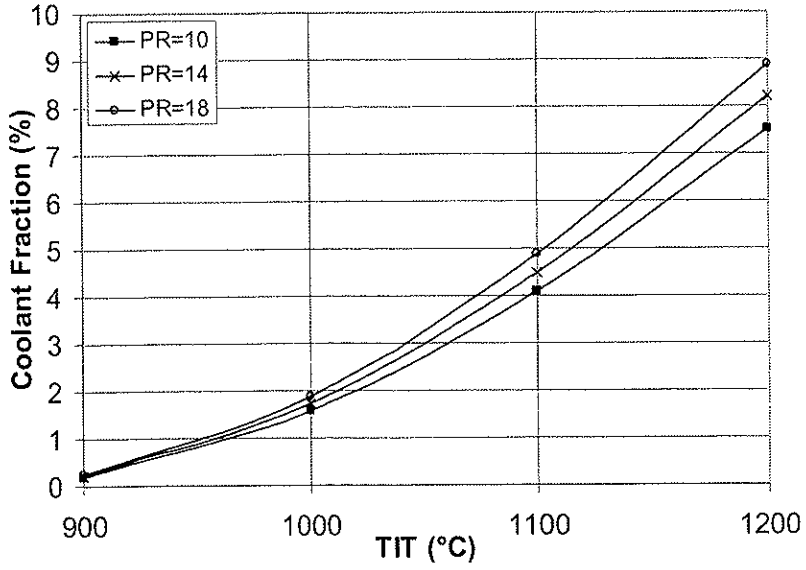

Figure 22 Coolant fraction (CF) as % of turbine exhaust flowrate

Pumps
Two pumps are required to circulate water in the HAT-cycle. Power requirements are estimated from:

$$\dot{W} \approx \frac{\dot{m} \cdot \nu_S \cdot (P_1 - P_0)}{\eta_P} \qquad (3.16)$$

where ν_S is the specific volume of the fluid at the actual saturation pressure and temperature.

Heat exchangers
All heat exchangers are calculated using a mass-balance for hot (H) and cold (C) sides:

$$\dot{m}_H \cdot Cp_H \cdot (T_{H,1} - T_{H,0}) = \dot{m}_C \cdot Cp_C \cdot (T_{C,0} - T_{C,1}) \qquad (3.17)$$

The humid air turbine process has gas-solid heat exchanger highlighted with grey shading in Figure 15, is used to optimize power generation in the CO_2 turbine, and is calculated in the same manner using the solid and gas streams entering the unit.

3.3.4 Model implementation

The mathematical framework provided in sections 3.3.1-3.3.3 for calculating heat and mass balances in chemical looping reactors and unit operations, is implemented in *Mathworks Matlab 6.0* (CLC-HAT) and FORTRAN/PRO/II for combined cycle and ISG calculations, respectively. The combined cycle model was later transferred and implemented in gPROMS® (Model builder 2.3.3) for further development. In the Matlab model, computational assumptions and global variable designations are organized in individual databases, whereas unit operations and CLC reactors are modeled in individual subroutines. These functions return the desired unknown variables using relevant input data. The main script contains the lines of code that recall computational data, functions for unit operations and reactors as necessary and logical structure (e.g. iterative loops) required to compute all unknown properties in the process. The complete model for the CLC-humid air turbine consists of a total of 20 scripts including 2 datasets with computational assumptions and global variable designations. In HAT-cycle calculations, unit operations are calculated by manually added subroutines,

while this task is performed by in-built software routines in PRO/II and gPROMS.

3.4 Exergy analysis

The potential of a chemical conversion to produce useful mechanical work is expressed by the *Gibbs function*:

$$dG \equiv dH - TdS \tag{3.18}$$

Integration of Eq. 3.18 yields:

$$G - G^0 = H - H^0 - T(S - S^0) \tag{3.19}$$

The change in the free energy of a system ($G-G^0$) at constant temperature is thus equal to the change in enthalpy minus the product of absolute temperature and entropy change. The Gibbs free energy can also be expressed in terms of the equilibrium constant K:

$$dG = -RTlnK \tag{3.20}$$

The laws of thermodynamics state that the maximum mechanical energy that can be drawn from a reaction occurring at a fixed temperature and pressure is obtained when the process is balanced and reversible, i.e. when entropy production is at a minimum (Kotas, 1995). In thermodynamic cycle analyses ΔG for a chemical conversion is commonly referred to as exergy. As noted in chapter 2, Richter and Knoche (1983) showed that exergy losses in chemical looping are inherently lower in CLC compared to conventional combustion by virtue of splitting the red/ox process of fuel combustion into separate reactions with a solid intermediate. In the latter process, fuel is oxidized by air at a temperature limited by gas turbine and combustor specifications. Taking methane as an example, the adiabatic flame temperature as reported by Griffiths and Barnard (1995) for stoichiometric combustion of methane with air is 2222 K when reactants are at 20°C and 1 atm. Current state-of-the art combustors for power generation cycles operate at temperatures well below this, around 1200-1400°C (Saravanamuttoo, 2001). Combustion at this temperature is far from equilibrium and highly irreversible. In the following,

the exergy balance used to compare exergy destruction rates in CLC and conventional combustors will be developed.

In Figure 23 a control volume is shown with streams entering and leaving containing a total exergy $\dot{e}_0^{TOT}$ and $\dot{e}_i^{TOT}$, respectively. Additionally, exergy can be exchanged with the surroundings by mechanical work ($\dot{W}$) and heat transfer ($\dot{E}_Q$):

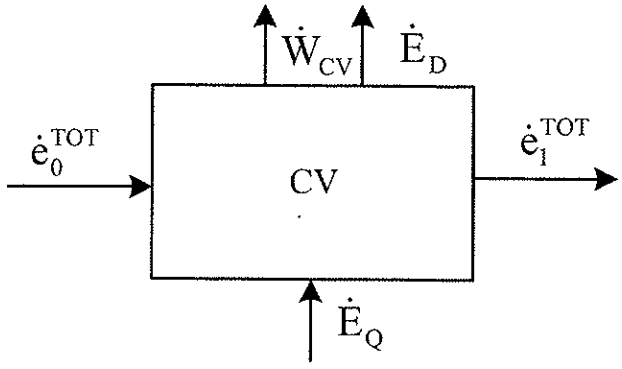

Figure 23 Schematic of general control volume with exergy terms

The rate of exergy destruction ($\dot{E}_D$) within the control volume can be found from the following general exergy-balance:

$$\sum_{cv}\dot{E}_Q + \sum_{i}\dot{m}_i e_i - \dot{W}_{cv} - \sum_{e}\dot{m}_e e_e = \dot{E}_D \qquad (3.21)$$

The first term expresses exergy destruction associated with heat transfer between the control volume and the thermal surroundings. For a given heat rate, $\dot{Q}_r$, this can be expressed as:

$$\sum_{cv}\dot{E}_Q = \sum_{cv}\dot{Q}_r \cdot \left(1 - \frac{T^0}{T}\right) \qquad (3.22)$$

If adiabatic conditions are assumed (i.e. $\dot{Q}_r = 0$) this term can be neglected.

The work equivalent ($\dot{W}$) of a given form of energy is defined as a measure of its exergy. However, since the control volumes (Figure 23) do not include turbo-machinery, exergy destruction due to work generation can also be disregarded.

The rate of exergy destruction, for this particular case, equals the difference in total exergy in the streams entering and leaving the control volumes. Assuming that mechanical exergy (kinetic + potential) is negligible, the total exergy of a stream can be separated into physical (P) and chemical exergy (CH).

Physical exergy can be defined as the maximum amount of work obtainable when the stream of substance is brought from its initial state to the environmental state defined by P^0 and T^0 by physical processes involving only thermal interaction with the environment. The physical exergy (e^P) of a stream at temperature T and pressure P, with relation to the environmental state, is identical to the Gibbs function:

$$e^P = \left(h - h^0\right) - T^0\left(s - s^0\right) \tag{3.23}$$

Chemical exergy is defined as the maximum amount of work obtainable when the substance under consideration is brought from the environmental state to the dead state by processes involving heat transfer and exchange of substances only with the environment. From the concept of reversibility it follows that chemical exergy also can be defined as the minimum amount of work necessary to synthesize and deliver the substance under consideration in the environmental state. Furthermore, chemical exergy must be related to the exergy of reference substances. Chemical exergies of reference substances is calculated from an imaginary process in which a substance *i* is expanded from the environmental state P^0 to the partial pressure of the component in the atmosphere P^{00}. For an ideal gas this is given by:

$$e_i^{ch} = RT^0 \ln \frac{P^0}{P^{00}} \tag{3.24}$$

When considering individual components in mixtures the exergy of each component is given as the necessary work for reversible and isothermal compression of each component from the environmental pressure P^0 to partial pressure P_i:

$$\sum_i \left[\tilde{w}_{xi}\right]_{REV} = RT \sum_i y_i \ln y_i \tag{3.25}$$

where y_i is the molar fraction of component *i*. The total chemical exergy is then given as the sum of reference exergy and the chemical exergy (or

potential) of the mix of components in the stream as compared to that in the ambient surroundings:

$$e^{CH} = \sum_i y_i e_i^{CH} + RT \sum_i y_i \ln y_i \qquad (3.26)$$

Relevant reference exergies have been tabulated by Barin (1995). Exergy destruction rate can now be expressed by a simplified exergy balance as the sum of inlet and outlet exergies:

$$\dot{E}_D = \sum_{INLET} \left(e^P - e^{CH}\right) - \sum_{OUTLET} \left(e^P - e^{CH}\right) \qquad (3.27)$$

The control volumes under consideration are given in Figure 24:

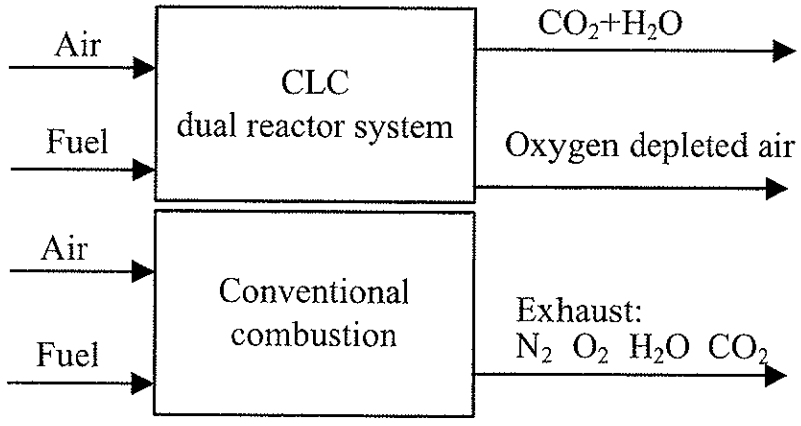

Figure 24 Comparison of conventional combustion and chemical looping combustion

The exergetic efficiency (η_{ex}) of the combustion process can now be expressed in terms of exergy destruction rate and the total fuel exergy content ($\dot{E}_F$):

$$\eta_{ex} = 1 - \frac{\dot{E}_D}{\dot{E}_F} \qquad (3.28)$$

3.5 *Efficiency definitions*

Combined cycle efficiency is given by:

$$\eta_{NET}^{CC} = \frac{\left(\dot{W}_{GT} + \dot{W}_{CO2-T} + \dot{W}_{ST} - \dot{W}_{C0} - \dot{W}_{P2}\right)\cdot \eta_{m+g+aux} - \dot{W}_{CO2-COMP}}{\dot{m}_{FUEL}\cdot LHV} \quad (3.29)$$

where:

$$\dot{W}_{CO2-COMP} = \dot{W}_{C1} + \dot{W}_{C2} + \dot{W}_{C3} + \dot{W}_{P1} \quad (3.30)$$

Specific work is defined as:

$$\dot{w} = \frac{\left(\dot{W}_{GT} + \dot{W}_{CO2-T} + \dot{W}_{ST} - \dot{W}_{C0} - \dot{W}_{P2}\right)\cdot \eta_{m+g+aux} - \dot{W}_{CO2-COMP}}{\dot{m}_{Air}} \quad (3.31)$$

$\eta_{m+g+aux}$ is a cumulative term accounting for mechanical losses and losses in generators and auxiliary power consumption and has a numerical value of 0.966 in all calculations.

The atmospheric-pressure cycle is defined similarly, using the same term for CO_2 recompression (Eq. 3.30):

$$\eta_{NET}^{ISG} = \frac{\left(\dot{W}_{ST1} + \dot{W}_{ST2} - \dot{W}_{C1} - \dot{W}_{P2}\right)\cdot \eta_{m+g+aux} - \dot{W}_{CO2-COMP}}{\dot{m}_{FUEL}\cdot LHV} \quad (3.32)$$

It should be noted that the energy penalty associated with CO_2 recompression is found to be 1.13 MW/ (kg fuel converted) for the CLC-CC, and slightly lower in CLC-ISG (1.09 MW/ (kg fuel converted). This is because of a slightly lower compressor inlet temperature in the ISG cycle.

In CLC-HAT cycle analyses, efficiency was originally calculated as gross, total efficiency:

$$\eta_{TOT} = \frac{\left(\dot{W}_{T1} + \dot{W}_{T2} - \dot{W}_{C,TOT} - \dot{W}_{P1} - \dot{W}_{P2}\right)}{\dot{m}_{FUEL}\cdot LHV} \quad (3.33)$$

where:

$$\dot{W}_{C,TOT} = \sum_{Ci=1}^{3} \dot{W}_{Ci} \tag{3.34}$$

In order to make results from HAT-cycle calculations comparable to those of the combined- and atmospheric cycles, corrected values for efficiency (as compared to the results in Paper I & II) are calculated from:

$$\eta_{NET}^{HAT} = \frac{\left(\dot{W}_{T1} + \dot{W}_{T2} - \sum_{1}^{3} \dot{W}_{Ci} - \dot{W}_{P1} - \dot{W}_{P2} \right) \cdot \eta_{m+g+aux} - \dot{W}_{CO2-COMP}}{\dot{m}_{FUEL} \cdot LHV} \tag{3.35a}$$

CO_2 recompression is estimated using the same recompression train as in CC and ISG calculations, and the energy penalty was estimated to 0.3836 MW/ (kg CO_2). The formula for recalculation of efficiencies then becomes:

$$\eta_{NET}^{HAT} = \frac{\left(\eta_{TOT}^{HAT} \cdot LHV \cdot \dot{m}_{Fuel} \cdot \eta_{m+g+aux} - \dot{W}_{CO2-COMP} \cdot \dot{m}_{CO2} \right)}{LHV \cdot \dot{m}_{Fuel}} \tag{3.35b}$$

3.6 Thermodynamic basis

Two different approaches for Cp-calculation have been adopted when modeling the CLC-reactors. In calculations on the HAT-cycle, cp-values for individual components (including solids) are estimated by interpolating tabulated data in Barin (1995). Multi-component streams are calculated by first assigning values to individual components (*i*) by interpolation of tabulated data and then estimating an overall value (Cp_{MIX}) by mass-averaging:

$$Cp_{MIX} = \frac{\sum_{i} \left(\dot{m}_i Cp_i \right)}{\sum_{i} \dot{m}_i} \tag{3.36}$$

In combined cycle and internal steam generation calculations, cp-values for non-solid streams are calculated using a polynomial:

$$Cp_i = \left(\alpha_i + \beta_i T + \gamma_i T^2 + \delta_i T^3 + \varepsilon_i T^4\right) \cdot R \qquad (3.37)$$

Heat capacity of the inert binder ($NiAl_2O_4$) was estimated by interpolation of tabulated data in Barin (1995) while heat capacity of Nickel/nickel oxide was calculated by:

$$Cp_i = \left(a_i + b_i T^{-3} + c_i T^6 + d_i T^{-6}\right) \qquad (3.38)$$

In calculations of the CLC-CC and CLC-ISG cycles, the Soave-Redlich-Kwong (SRK) equation of state was selected and used throughout. This is probably the most reliable and widely applicable equation of state currently available. More details about the SRK and properties for components of natural gas are given in Appendix A.

3.7 Results and discussion

The original results for the CLC-HAT and CLC-CC & CLC-ISG cycles are given in detail in papers I/II & IV, respectively.

As mentioned, efficiencies in HAT-calculations have been recalculated to include recompression losses. The corrected efficiencies as well as the original results are presented for CLC-HAT to illustrate the energy penalty associated with CO_2-recompression.

Following publication of paper IV, the model for CLC-CC was implemented in gPROMS, as this was believed to be a more flexible tool, facilitating further development of the CLC reactor model. During the process of implementation, some flaws in the original design of the CLC-CC and -ISG models were fortunately discovered. Consequently, the simulations on CLC-CC have been repeated in gPROMS, and the results thereof will be presented in the following, along with the revised efficiencies of CLC-ISG. As will be shown, efficiency differences between the original and new simulations are small.

3.7.1 CLC-CC

The cycle was analyzed by varying oxidation outlet temperature (TIT) over a range of pressure ratios (PR).

In Figure 25 specific work versus net efficiency is plotted for un-cooled (dashed lines) and cooled (solid lines) turbines. The cooling penalty as a %-points reduction in overall efficiency corresponds to the difference between curves for the same TIT. The computational assumptions for the gas turbine are selected so that the performance is similar to that of a modern 'F-class' machine. In the curves, PR increases from right (10) to left (20) by an increment of 2.

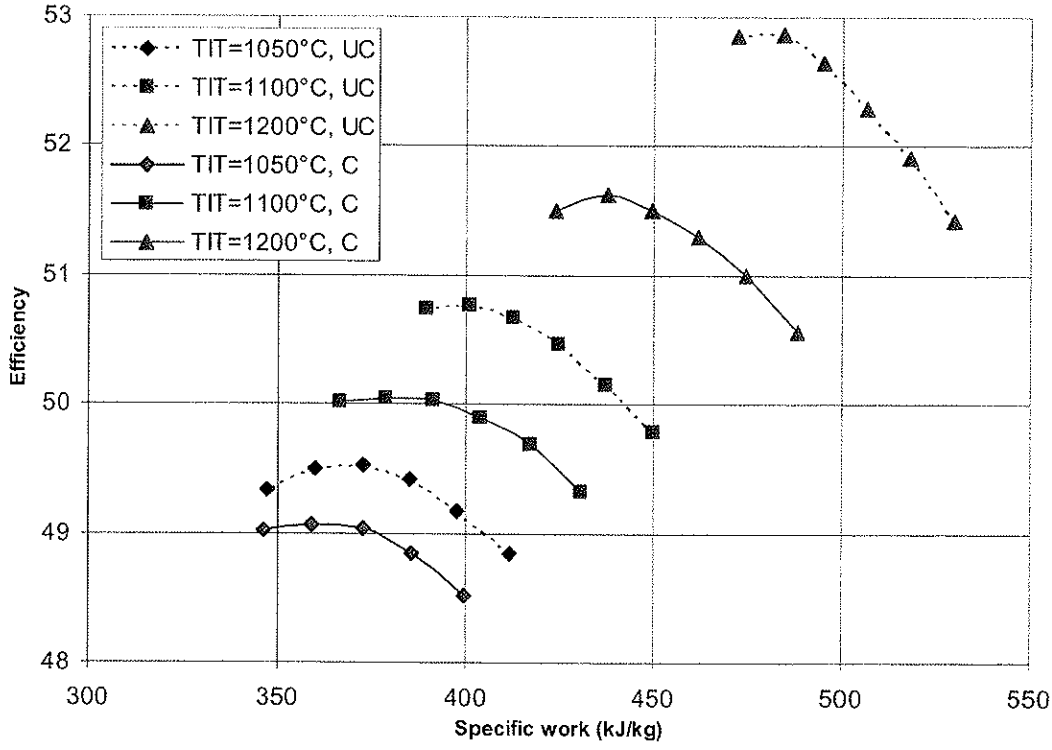

Figure 25 Results summary for cooled (C) and un-cooled (UC) turbines, PR increases (10-20) from right to left within each series

3 primary aspects of Figure 25 should be emphasized; TIT versus specific work, PR versus efficiency (at a given TIT) and effect of cooling as a function of TIT and specific work. Additionally, starting points for supplementary firing and estimation of solid mass fluxes are discussed.

3.7.1.1 Turbine inlet temperature

Firstly, it can be seen that airflow is inversely related to TIT, i.e. required airflow decreases with increasing TIT. The relation between airflow and TIT can be explained by the oxy-fuel nature of CLC. Excluding (for the time being) the possibility of supplementary firing, there are two principal ways to increase TIT when fuel consumption is fixed. Either by supplying additional heat by means of increasing the reactor inlet temperature or by reducing the air flow rate. In case of the latter, the same heat of reaction is distributed to a smaller volume of fluid with a consequent increase in temperature. Hence, the maximum specific work is found for TIT=1200°C and PR=10.

3.7.1.2 Pressure ratio

Increasing the pressure ratio for a given TIT reduces specific work and results in a minor, but significant, increase in efficiency. Efficiency can be seen to reach a maximum within the range of PR for a given TIT. The observed pressure versus efficiency relationship can be explained by considering the heat balance of the oxidation reactor. Oxidation air enters the oxidation reactor without heat exchange, i.e. oxidation inlet temperature is dependent on pressure ratio. To maintain the desired TIT at high PR, additional air needs to be supplied (as was discussed in the previous paragraph). Hence the highest specific work is found at the lowest pressure ratios.

The other main factors to be considered are required compressor work and air/steam turbine output. At the maximum efficiency, the increase in turbine output is balanced by the increase in necessary compressor work. Increasing PR beyond this point consequently leads to a *decrease* in net efficiency. Within each series (TIT= 1050, 1100, 1200°C) of pressure ratios, the maximum efficiency can be seen to move towards lower PR for lower values of TIT. Consequently, a maximum efficiency is reached at PR=16 at 1050°C while the corresponding PR 18 for 1100 and 1200'C, respectively, indicating that there is less to be gained by increasing pressure at low TIT than at high TIT. This conclusion makes sense, as turbine output is affected by TIT, but necessary compressor work is not.

3.7.1.3 Turbine cooling

Thirdly, the energy penalty associated with turbine cooling can be estimated as a reduction in net efficiency, by subtracting corresponding dashed and solid lines in Figure 25. At 1050°C, the reduction in efficiency is approx.

0.5%-points while the corresponding values for TIT=1100°C and 1200°C are 0.7% and 1.4%-points, respectively. Cooling penalty is not only related to TIT, however, and a slightly higher energy penalty (in %-points) is observed at the high-end of the pressure ratio scale. Recollecting Figure 18, this result seems reasonable as the coolant fraction is dependent on both PR and TIT.

A summary of the findings for un-cooled and cooled turbine (General Electric 93519FA) at PR=18 is given in Table 11.

Table 11 Summary of findings for un-cooled and cooled turbine, PR=18

	Un-cooled turbine			Cooled turbine		
TIT [°C]	1050	1100	1200	1050	1100	1200
Airflow at compressor exit [kg/s]	960	884	761	988	923	823
Coolant flow [kg/s]	0	0	0	28	39	62
POWER TERMS [MW]						
Fuel input (LHV)	697.5	697.5	697.5	697.5	697.5	697.5
Air turbine	634.3	604.2	554.7	644.7	618.7	578.0
CO2-turbine	45.5	47.8	52.4	45.5	47.8	52.4
Compressor	-407.6	-375.2	-323.1	-419.4	-391.9	-349.6
Steam Turbine	98	102	110	96	99.3	104.2
Losses	-9.2	-9.3	-9.4	-9.2	-9.3	-9.4
CO2-Comp.	-15.6	-15.6	-15.6	-15.6	-15.6	-15.6
Net Power	345.6	354.0	369.0	342.0	349.0	360.0
Net Efficiency [%]	49.5	50.8	52.9	49.0	50.0	51.6

3.7.1.4 Incomplete fuel conversion and exhaust recirculation

As a secondary analysis, the impact of fuel conversion and exhaust recirculation on net efficiency was estimated. As can be seen in Table 12, a 5% drop in fuel conversion gives 3.0%-points reduction in cycle efficiency. The effect of fuel reactor exhaust recirculation on net cycle efficiency was found to be negligible.

Table 12 Effect of incomplete fuel conversion on efficiency for TIT=1200°C, PR=18 bar, un-cooled turbine

ϕ	1	0.99	0.98	0.97	0.96	0.95
η_{NET}	52.9	52.3	51.7	51.1	50.5	49.9

Both findings can be explained by the splitting of reactions that characterize CLC. The bulk of the generated power principally originates from the heat of reaction associated with the regeneration of nickel oxide. Hence, changes in the chemical performance of the reduction reactor lead to a reduced production of nickel, and a significant impact on efficiency is observed. Recirculation of exhaust necessitates the use of a light duty compressor to compensate for pressure losses. The energy consumption of this component is negligible when compared to the power terms associated with the oxidation.

3.7.1.5 Supplementary firing

At high pressure ratios and low TIT, turbine exit temperature (TET) is found to be insufficient for production of superheated steam. Under such conditions supplementary firing becomes necessary. Since the present work is intended to investigate a zero-emission plant, it is relevant to establish an operating range of TIT in which supplementary firing can be avoided. Estimated minimum values for TIT to avoid supplementary firing in the range of pressure ratios investigated, are given in Table 13.

Table 13 Supplementary firing starting points, cooled turbine, TIT refers to oxidation reactor outlet temperature

PR	10	12	14	16	18	20
TIT [°C]	912	956	998	1030	1060	1090

This is an important result for the development of carrier materials, as it provides a benchmark-value for carrier temperature tolerance. The study indicates that the oxidation reactor needs to be operated at temperatures above 1060°C to avoid supplementary firing in a combined cycle, at the base-case operating pressure of 18 bar.

3.7.1.6 Solid streams

The required mass flow of solids is an important parameter as the transportation of solids represents one of the practical challenges of a dual-vessel moving bed.

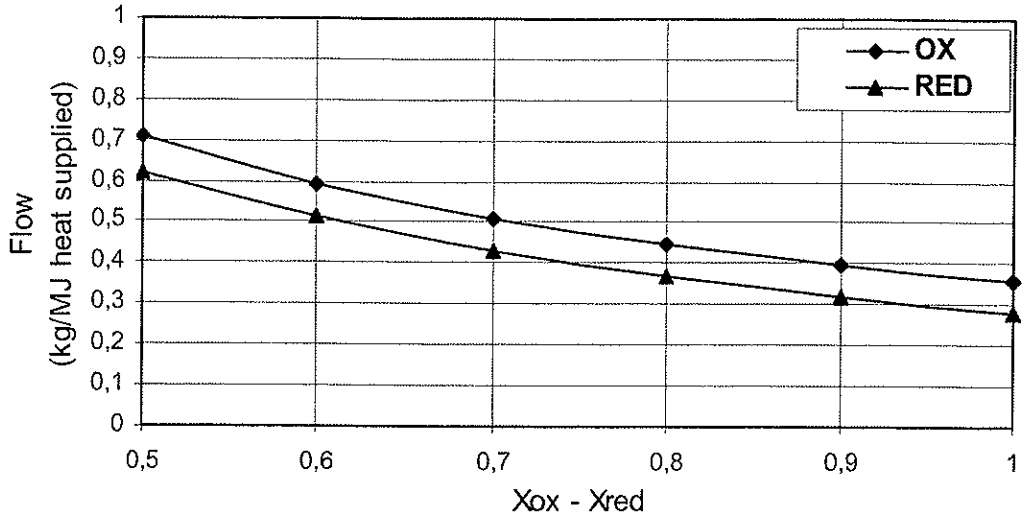

Figure 26 Specific solid flow versus difference in solid conversion

Solid fluxes are largely dependent on the oxygen carrying capacity of the recirculating solid. Mass flowrates are found to be acceptable for a moving bed application. For further elaboration on solid fluxes estimated from experimental data it is referred to section 5.3.5.

As will be showed in subsequent sections, the results of the CLC-CC study confirms the main results of the humid air turbine study and further underscores the importance of developing temperature tolerant materials capable of near 100% fuel conversion. Oxidation reactor exit temperature should ideally be close to 1200°C and 18-20 bar seems to be a reasonable operating pressure, with respect to efficiency. Furthermore, the results are very promising, as they indicate a cycle efficiency of approximately 52%, including CO_2 capture and recompression as well as turbine cooling.

3.7.2 CLC-HAT

Figure 15 shows the process with parameters that have been varied (highlighted in red), while key results are given in Table 14.

Parameters:

T_1 Fuel inlet temperature
T_{2a} Reduction exhaust temperature
T_{2b} Turbine 2 inlet temperature
T_3 Air inlet temperature
T_4 Turbine 2 inlet temperature
P_R Reactor inlet pressure

Table 14 CLC-HAT simulation overview

CASES	PARAMETERS T_3 [°C]	T_1 [°C]	T_4 [°C]	T_{2a} [°C]	T_{2b} [°C]	P_R [Bar]	η_{TOT} η_{NET}
1	400-520	465	1200	560	900	20	50.2-55.3 46.4-51.3
2	522-519	375-465	1200	548	900	20	55.2-55.3 51.2-51.3
3	349-519	465	900-1200	257	900	20	45.1-55.3 41.5-51.3
4	519-527	681	1200	485-560	900-1200	20	55.3-55.9 51.4-51.9
5	519	465	1200	224-1067	900	20	55.4-54.0 51.4-50.0
6	633-505	549	1200	573	900	10-20	54.6-55.3 50.6-51.3
Base case	**520**	**465**	**1200**	**560**	**900**	**20**	**55.3** **51.3**

In the above table, η_{TOT} is calculated by Eq. 3.35a whereas η_{NET} is calculated from Eq. 3.35b. From the column of calculated efficiencies, it can be seen that the incorporation of intrinsic losses and CO_2 recompression comes with an energy penalty corresponding to 4%-points reduction in efficiency.

3.7.2.1 Reactor pressure (P_R)

An interesting difference in behavior is seen when analyzing different pressure ratios in CLC-HAT as compared to CLC-CC. In the latter, oxidation inlet temperature is equal to compressor exit temperature and hence dependent on PR. In CLC-HAT, oxidation inlet temperature is not directly

related to compressor pressure ratio, due to subsequent heat exchange after the compressor. Hence in CLC-HAT, the full oxy-fuel nature of CLC can be seen. In order to supply the same amount of oxygen with decreased pressure (and air density) an *increase* in airflow rate is required, assuming that conversion rates are unchanged. Reduced pressure invariably leads to reduced power generation in both turbines, along with a reduction in required compressor work. The effects of reduced pressure, increased air flow rate and fluid density tend to cancel each other, and hence there is only a slight increase in compressor work whilst turbine output (W_{T1}) remains constant over the pressure range. Net efficiency increases, however, due to an increased contribution from the CO_2-turbine (W_{T2}) which contributes more to the efficiency as a result of higher pressure ratio, regardless of air flow rate.

In accordance with the discussion above, reactor outlet pressure has been found to have a small but significant effect on η_{NET}. The overall picture is similar to that observed in CLC-CC, but for different reasons. Overall efficiency as a function of pressure is presented in Figure 27:

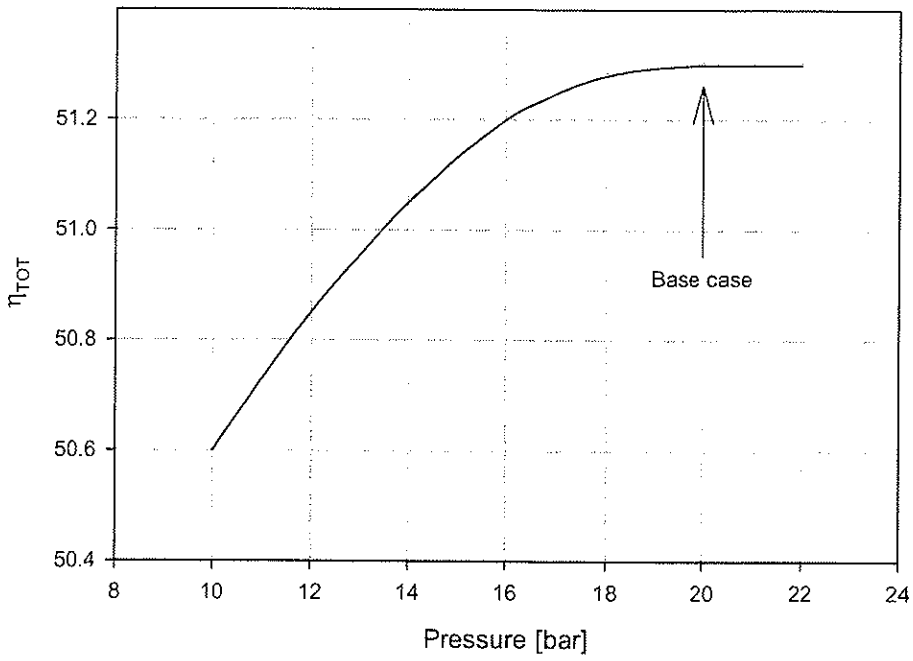

Figure 27 Pressure vs. efficiency chart for CLC-HAT (TIT=1200°)

The total efficiency is seen to rise slightly for pressures up to 18-20 bar; - beyond this point the increase in compressor work exceeds the increase in work of turbine 2. A pressure of 20 bar was therefore selected as the operating pressure for this cycle analysis.

3.7.2.2 Oxidation reactor inlet/outlet temperature

It has been found that oxidation reactor inlet (T_3) and outlet (T_4) temperatures have the biggest impact on cycle efficiency as indicated in Figure 28:

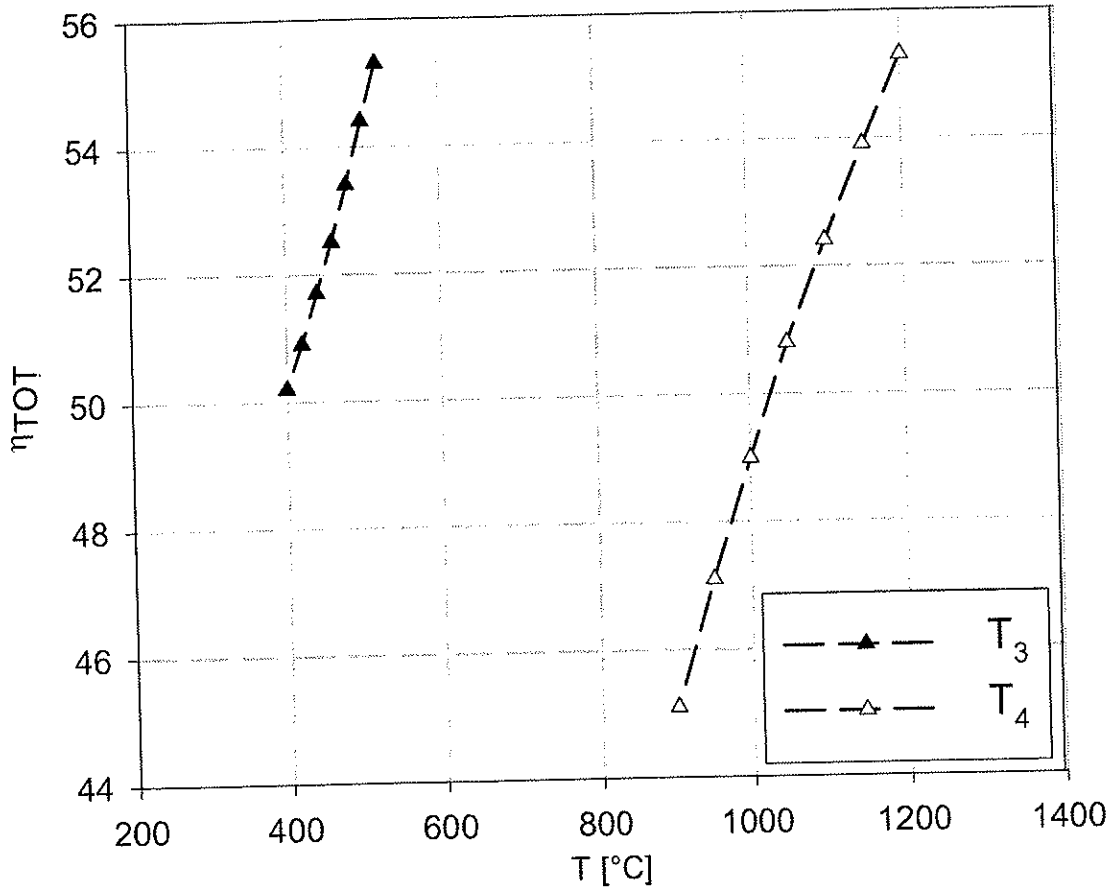

Figure 28 Impact of oxidation reactor inlet and outlet temperature on efficiency

The effect of oxidation reactor inlet/outlet conditions on efficiency can be explained by considering the individual terms of the efficiency definition. The effect of increasing T_4 from 900°C (1) to 1200°C (2) on air flow rate and turbine/compressor work, respectively, is shown in Figure 29.

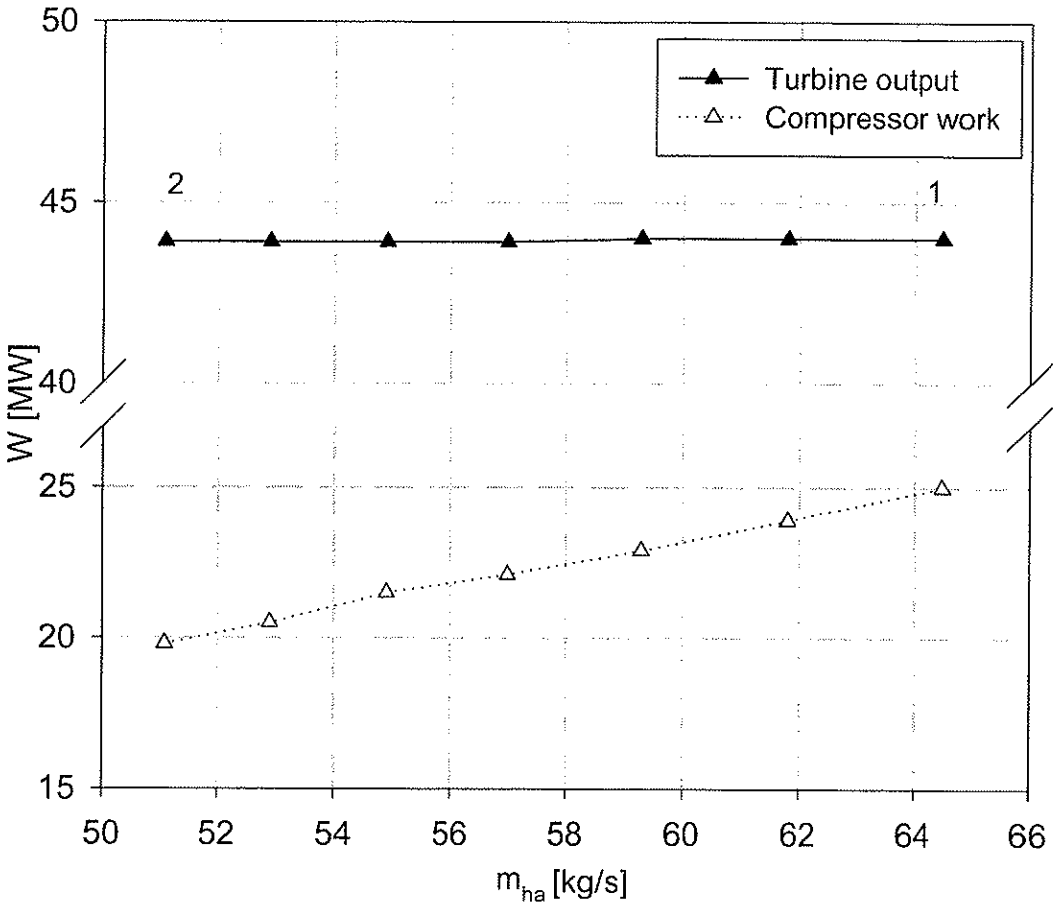

Figure 29 Effect of oxidation outlet temperature (T_4) on air flow rate and compressor/turbine duties when T_4 increases from 900-1200°C (1 → 2)

Reactor volumes and residence times are of course dependent on air flow rate and will vary accordingly for each case. It is thus observed that air flow rate, for a given fuel flow rate, is the controlling factor with regard to overall cycle efficiency. As can be seen in Figure 29, required compressor work decreases with decreasing air flow rate. In the turbine, an increase in TIT cancels the effect of reduced flow and turbine output remains essentially constant ($\dot{W}_{T1} \approx 44\,\mathrm{MW}$). As a result overall efficiency increases with approximately 10%-points over the temperature range [$900 < T_4 < 1200$°C].

A similar mechanism is observed for variations in air reactor inlet temperature, when outlet temperature is fixed. Increasing the inlet temperature is possible by increasing the air flow rate. Outlet temperature is maintained due to the increased amount of sensible heat entering the oxidation reactor at higher temperatures. As a consequence a proportionally bigger increase in turbine output than compressor work is seen. The effect is

smaller than for oxidation reactor outlet temperature T_4, and a 5%-point increase in net efficiency is observed over the temperature range [$400 < T_3 < 520°C$].

The effects of the remainder of the parameters on net efficiency are relatively smaller and are discussed in detail in Paper II.

3.7.2.3 Exergy analysis

The results of a calculation of exergy destruction rates in chemical looping combustion and a comparable conventional combustor, using the mathematical framework outlined in chapter 3.3 are presented in Figure 30 & Table 15. The calculation is derived from the humid air turbine study, and hence saturated air is used. A conventional combustor and the chemical looping combustor are fed the same reactants and the exergies of the streams entering and leaving the control volume is calculated.

Table 15 Exergy analysis summary

		$\dot{E}_{Fuel}$ [kW]	$\dot{E}_{Air}$ [kW]	$\dot{E}_{Exh1}$ [kW]	$\dot{E}_{Exh2}$ [kW]	$\dot{E}_{D}$ [kW]	η_{Ex} [%]
$\dot{E}_i^{CLC}$	$\sum e^{P} + e^{CH}$	53,679	29,290	10,562	60,613	11,789	78,03
$\dot{E}_i^{C}$	$\sum e^{P} + e^{CH}$	53,679	29,198	-	69,803	13,074	75,6
$\Delta\dot{E}_i$	$(\dot{E}^{TOT})_{CLC} - (\dot{E}^{TOT})_{C}$	0	+101	+10,562	-9,190	-1,250	+2,4

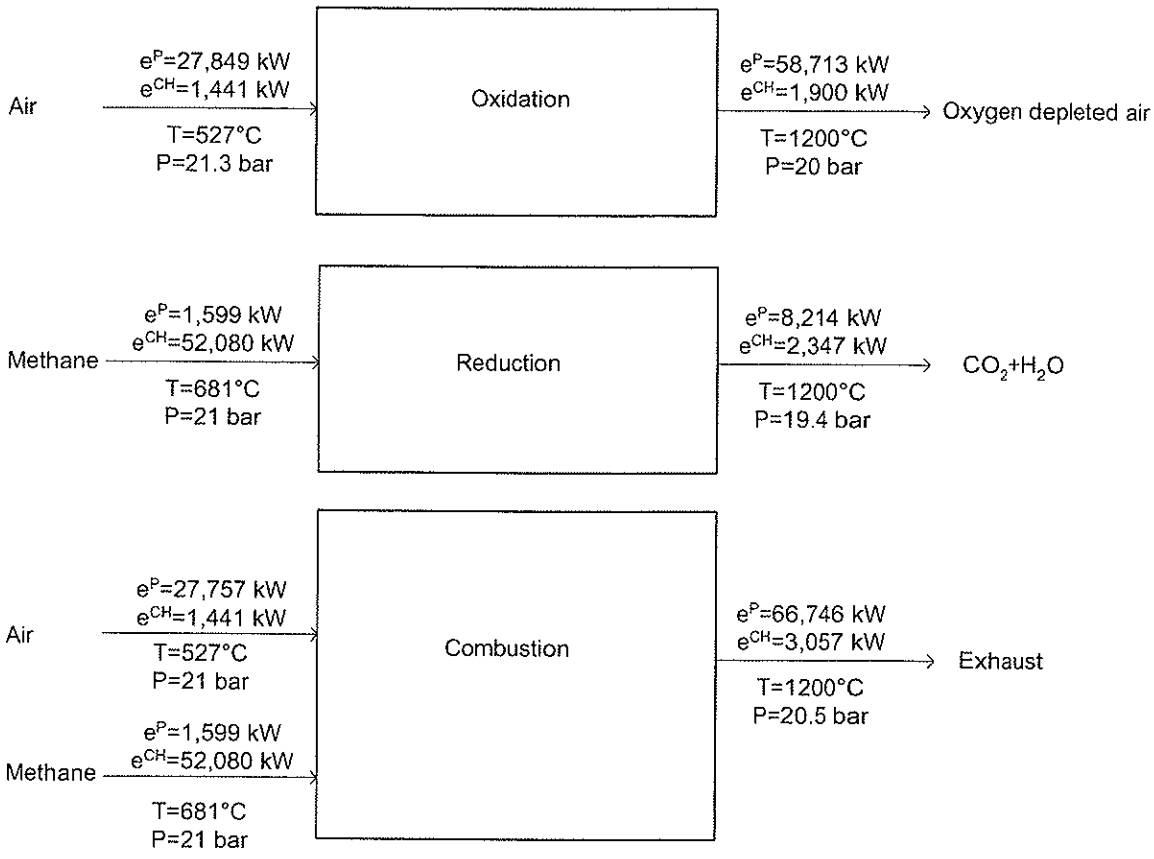

Figure 30 Exergy analysis of CLC vs. conventional combustion, e^P=physical exergy, e^{CH}=chemical exergy

In Table 15, exergetic efficiency is calculated according to Eq. 3.28. Exhaust 1 and 2 corresponds to exhausts from fuel and air reactors, respectively.

It has been found that the reaction splitting and inherent separation of CO_2 and H_2O from the excess combustion air gives a 2.4%-points improvement in exergetic efficiency in CLC as compared to conventional combustion where exhaust gases are mixed. This difference in exergy destruction rate is closely related to the minimum theoretical work required for separation of the mentioned components from an exhaust gas, and can be found as the total exergy in the CO_2/H_2O stream. It might be argued that this exergetic potential will not be easily converted to useful work, because of the additional intrinsic losses associated with gas-solid reactors. However, the exergy analysis shows the principal difference in losses between conventional combustion and chemical looping combustion.

The study of CLC implemented in a humid air turbine cycle indicates that CLC has a promising thermodynamic potential. A maximum efficiency of 55.9% has been found, not including intrinsic losses and CO_2 recompression.

Inclusion of intrinsic losses and CO_2 recompression, the cycle efficiency is 51.3%. The study indicates that fuel reactor temperature is of relatively less importance, at least from a thermodynamic point of view, while oxidation temperature is of vital importance to the overall cycle efficiency. Reactor pressure has also been shown to be a significant factor. The study thus clearly emphasizes the importance of developing materials that can withstand operational pressures of around 20 bars, and in particular high operating temperatures, such as 1200°C.

By means of a stream exergy balance calculation, the theoretical rate of exergy destruction in the chemical conversion process of fuel to heat in a CLC has been shown to be lower by 2.4%-points as compared to that of a conventional combustor.

3.7.3 CLC-ISG

The base case cycle-calculation for CLC-ISG is summarized in Table 16.

Table 16 CLC-ISG cycle analysis summary, $\dot{W}_{ST1}$ = total steam turbine output, $\dot{W}_{Aux}$ = blower and pump power consumption, $\dot{W}_{CO2\text{-}comp}$ = CO_2 recompression energy penalty, η_{Net} = net electrical efficiency

$\dot{m}_{Fuel}$ [kg/s]	T_{Ox} [°C]	$\dot{W}_{ST}$ [MW]	$\dot{W}_{Aux}$ [MW]	$\dot{W}_{CO2\text{-}comp}$ [MW]	η_{Net} [%]
15.0	850°C	315.5	3.6	16.42	40.4

Assuming an isothermal mixing temperature of 850°C in the oxidation reactor and employing internal dual pressure level internal steam generation, a cycle efficiency of 40.4% has been found for a plant with net out put > 300 MW. Condensation of water and CO_2 recompression comes with an energy penalty corresponding to 2.7%-points reduction in cycle efficiency.

3.8 *Conclusions from cycle analyses*

From the simulations described thus far a number of conclusions can be drawn with regard to CLC. Base cases are summarized in Table 17:

Table 17 Cycle analysis summary of base cases, PR= pressure ratio, T_{R1} = reduction inlet temperature, T_{R2}= reduction exhaust temperature, T_{OX}=oxidation outlet temperature, ΔX= oxygen carrier conversion difference, η_{NET}=net electrical efficiency

Cycle	Fuel	Carrier	$\dot{m}_{Fuel}$	PR	T_{OX}	ΔX	η_{NET}
CLC-HAT	CH_4	NiO:YZT	1.0	20	1200	0.7	51.3
CLC-CC (cooled)	NG	NiO on $NiAl_2O_4$	15.0	18	1200	0.7	51.6
CLC-ISG	NG	NiO on $NiAl_2O_4$	15.0	1	850	0.7	40.4

Cycle pressure ratio has been fount to have a small but significant effect on overall cycle efficiency. A maximum efficiency is found at 18-20 bar for TIT=1200°C, with optimum PR decreasing with decreasing TIT.

The power producing potential of CLC mainly lies within the hot oxygen depleted air exiting the oxidation reactor. Changes in the terms of the oxidation heat balance thus have the biggest impact on net efficiency in CLC-cycles. Important parameters are oxidation inlet and outlet temperatures and mass flow of air.

CLC-ISG is among the most realistic, short-term implementations of the concept and shows promising thermodynamic potential. An optimum theoretical electrical efficiency of 40.4% has been estimated, including CO_2-capture and recompression. By comparison, conventional coal-fired steam cycles (without CO_2 handling) have efficiencies approaching 41%, while cogeneration plants may approach 48% efficiency. Considering that current post-combustion CO_2-capture technologies have stipulated energy-penalties of 5-10%-points, CLC-ISG is an interesting alternative, pending experimental studies verifying the long term durability of oxygen carriers under realistic conditions.

A conventional combined cycle, implementing a CLC dual-vessel combustion unit, has been found to have an optimum efficiency of 51.6%. This is a highly promising and realistic result, since it includes CO_2 handling and turbine cooling. Existing NG-fired state-of-the-art combined cycles have

efficiencies in the range 56-58%. Hence, inclusion of CO_2-capture and recompression costs corresponding to 5-10%-points reduction in efficiency in existing technologies makes CLC-CC a very promising alternative.

The HAT-concept is an interesting technology for energy/heat production. In effect, CLC-HAT is a variant of CLC-CC, since the former employs steam-saturated air as the working medium. Implemented with a CLC combustor, the results are hence similar to CLC-CC, with an optimum electrical efficiency of 51.3%, including CO_2-capture and recompression, but not including turbine cooling. CLC-HAT and CLC-CC both appear to be highly promising alternatives for implementation of CLC in existing technologies.

It should be kept in mind, however, that estimations of efficiencies for CLC-cycles are associated with some inherent degree of uncertainty. Uncertainties are predominantly associated with assumptions regarding the long-term durability and chemical performance of the oxygen carrier, for which experimental data are unavailable at the moment.

It can be concluded that cycle analyses are only as good as the assumptions that have been made. With the present assumptions a highly promising potential of CLC has been revealed, that should give incentive to further experimental studies providing realistic data, reducing the uncertainty of simulations.

4 EXPERIMENTAL SET-UP

In the following, the equipment, methods and materials used in the experimental studies of the present work will be presented.

4.1 Introduction

Preliminary studies of the reactivity and durability of the nickel oxide-nickel spinel oxygen carrier (henceforth referred to as NiONiAl for simplicity) in reduction/oxidation trials with hydrogen/air were performed at the Department of Materials Technology at NTNU during the spring of 2002. The experimental set-up used in these experiments is referred to as Rig I. The results of the study are presented in Paper III. This paper was presented at the 6th Italian Conference on Chemical and Process Engineering (ICheaP-6) (Brandvoll et al. 2003). The study was limited to indirect measurements of solid conversion and deduction of probable rate limiting mechanisms during *reduction* by a gravimetric method.

The initial experiments left many questions unanswered and a cooperative project with SINTEF Materials and Chemistry in Oslo, Norway, was initiated. The team at SINTEF had earlier designed and manufactured a fluidized bed reactor, designed to operate at pressures up to 11 bar for use in a parallel project on chemical looping combustion. The experimental set-up with reactor and auxiliaries is referred to as Rig II. The overall objective of the work can be summed up in the following topics:

- Determination of exhaust gas concentrations during reduction and oxidation
- Solid conversion rates in reduction and oxidation
- Impact of temperature on conversion rates
- Impact of pressure on conversion rates
- Extent of coking and reforming reactions when using methane as fuel
- Further investigation of the durability of the NiONiAl carrier
- Comparison with other candidate oxygen carriers

4.2 *Rig I*

The experimental details and results of this study are presented in detail in Paper III. The experiments were limited to the reduction reaction using hydrogen as fuel, and focused on determining rate limiting mechanisms, impact of temperature and oxygen carrier composition on reaction rates, as well as the durability of the material upon repeated red/ox cycling. Since the rig is described in detail elsewhere, only an overview of the set-up and some additional comments on the analytical principle will be discussed here.

The experimental setup is shown schematically in Figure 31 and consists of three main sections:

1 Gas supply with mass flow controllers (MFCs) and MFC controller unit
2 Furnace with fluidized bed reactor
3 Analytical equipment with absorption vessel, moisture sensor (not shown), suction device and computer-logged electronic weight

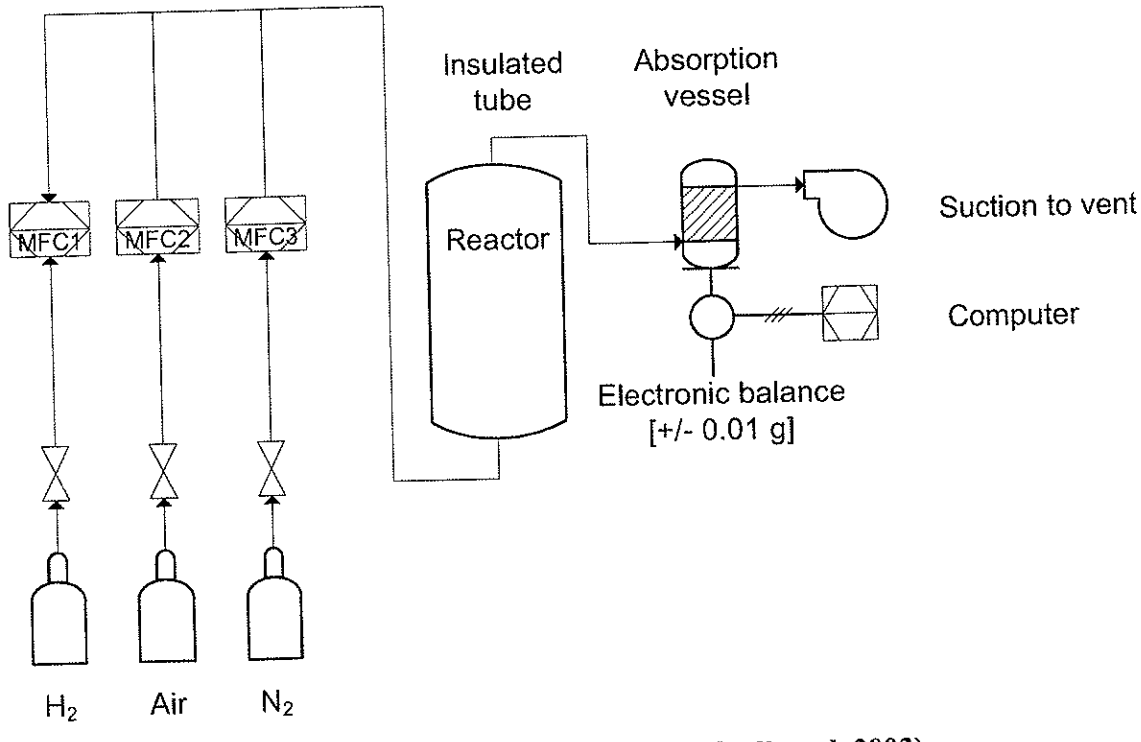

Figure 31 Rig-I, schematic representation (from Brandvoll et al. 2003)

Due to limited instrumentation at the time, an idea to capture produced water vapor in dry silica and monitor the increase in weight as a function of time

was developed. This turned out to be cumbersome, but functioning method. Problems mostly stemmed from the sensitivity of the weight towards vibrations in the rig and the weight support itself. Careful adjustments and stabilization of the entire set up provided a configuration that gave reproducible and reasonable results. The configuration of the absorption flask was most critical for stable measurements and a more detailed picture of the vessel can be seen in Figure 32:

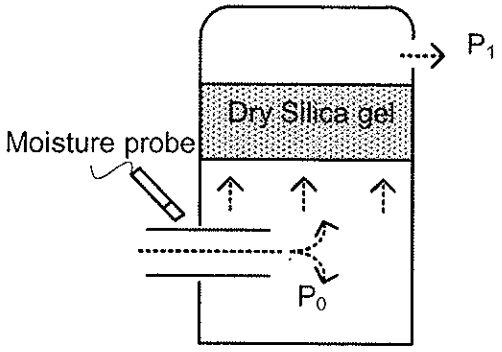

Figure 32 Absorption vessel detail ($P_1<P_0$)

A problem caused by the high initial rate of reaction was impulse-effects in the absorption vessel. The gas passing through the absorption vessel rapidly changes from nitrogen to a mixture of water vapor and unconverted hydrogen. This gave erratic readouts during the most critical part of the experiment, i.e. the initial phase when most of the water is produced. A small suction device was mounted at the flask exit (i.e. $P_1<P_0$), and this proved to be a working solution as the time dependent flow characteristics through the absorption vessel became more stable. Furthermore, the exhaust tube entering the absorption vessel could not be in direct contact with the absorption vessel due to excessive transfer of vibrations to the electronic weight. A peripheral clearance of app. 1 mm turned out to give satisfactory results without loss of exhaust gases as detected by the moisture probe.

From the gravimetric data obtained on the rate of water production, it was possible to indirectly infer details on the mass transfer limitations of the reduction as well as solid conversion rates.

4.3 Rig II

The basic structure of the rig with Mass Flow Controllers, gas pipelines, fittings, valves and pressure indicators, and furnace was installed by SINTEF-personnel. The reactor assembly was manufactured in the workshop at SINTEF, and had undergone some initial functional tests. Preparatory work included minor pipeline adjustments, leak tests under pressure, calibration of MFCs and cold experiments for determination of flow regime. The next step was integration of the rig with analytical instruments (mass spectrometer and later gas chromatograph) and fine-tuning of the effluent handling system. Starting with relatively simple experiments using hydrogen/air, the rig was gradually expanded with additional components to allow for experiments using dry methane and methane/steam mixtures as reducing agents.

The NiONiAl oxygen carrier has been the main focus of the present work. For comparative purposes a series of experiments with hydrogen/air and methane/air were also conducted using a perovskite synthesized by the SINTEF team. The experimental details of individual experiments are presented in context in chapter 5.

4.3.1 Rig schematic

As mentioned, the rig has undergone a gradual increase in complexity as the experiments progressed. The final layout is shown schematically in Figure 33. A more detailed schematic of the reactor assembly and its specifications is given in Appendix B along with specifications of individual rig components.

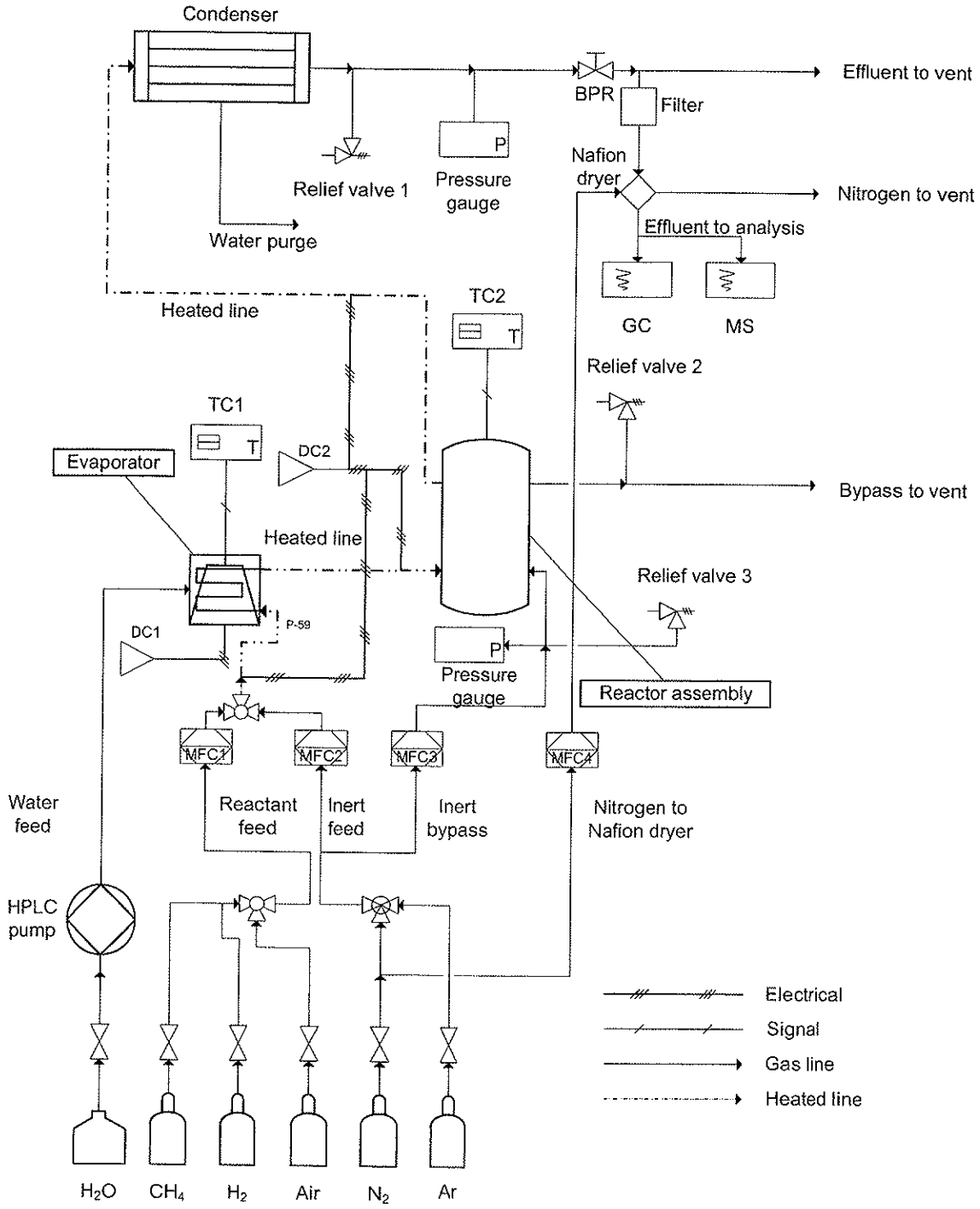

Figure 33 Rig-II, schematic representation

The main elements of the rig can be recognized:

- Gas/liquid feed system
- Evaporator with power source and temperature monitoring
- Reactor assembly
- Effluent handling system

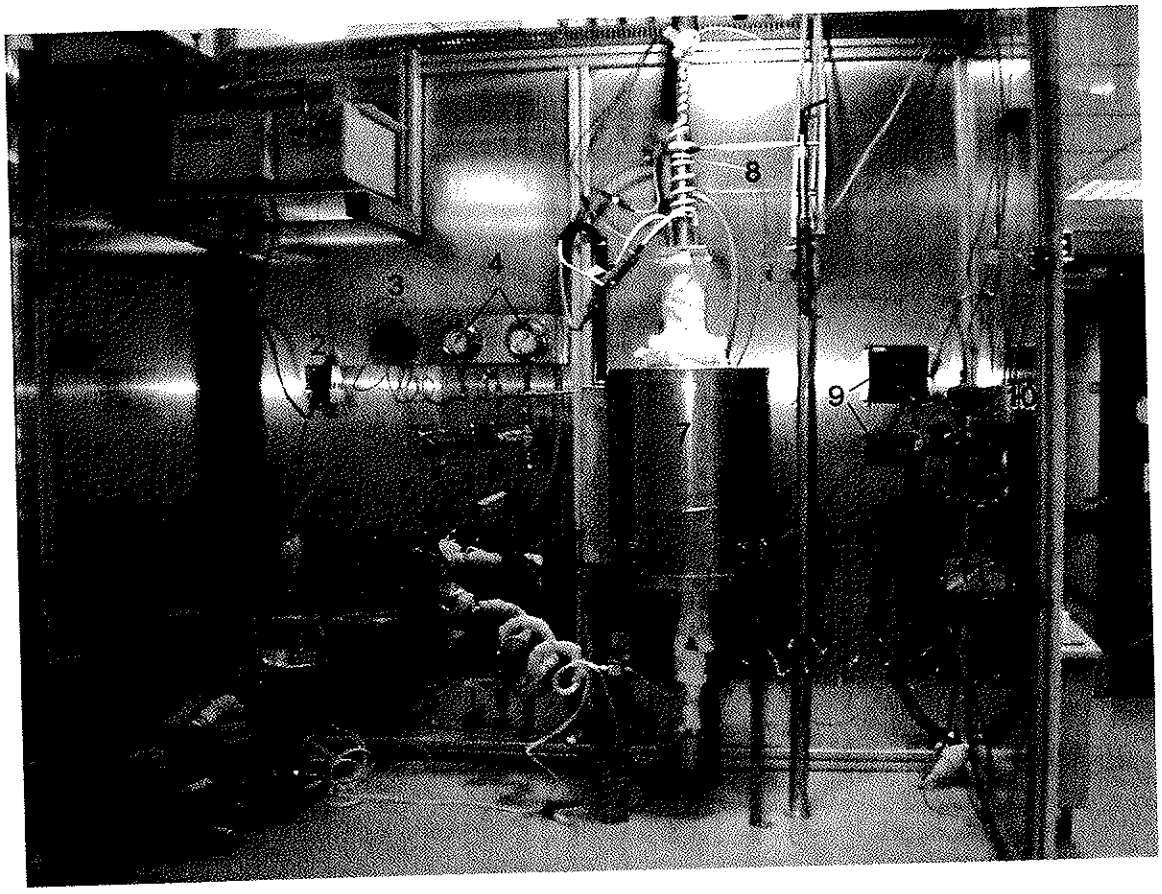

Figure 34 Rig-II with main components

Table 18 Legend

No.	Description
1	HPLC-derived pump
2	MFC4
3	BPR
4	PIs
5	Evaporator
6	TC1
7	Furnace
8	Reactor
9	Reactor TC readout
10	Main supply valve
11	MFC1-3
12	Main feed line
13	DC1, DC2
14	Water supply

4.3.2 Rig description

Gas/liquid feed system
The four individual MFCs were employed as follows:

MFC1	Hydrogen, methane, air, nitrogen feed
MFC2	Nitrogen feed
MFC3	Nitrogen to bypass (145 mln/min)
MFC4	Nitrogen to nafion dryer (60 mln/min)

Reactant gases were primarily fed by MFC1, while MFC2 was used to supply nitrogen in experiments with diluted reactants. Reactant gases are supplied to MFC1 via a 5-way ball valve allowing inert gas to be intermittently passed through the MFC as well as the reactor volume when switching between potentially explosive reactants. In this way, remaining air or combustibles within the MFC is flushed out prior to each experiment, avoiding 'plugs' of unwanted reactants in the initial phase of reduction/oxidation, respectively. MFC3 and MFC4 were used to supply 145 mln/min and 60 mln/min nitrogen to the reactor metal-quartz interspace and nafion dryer, respectively. MFC calibration data at atmospheric pressure and ambient temperature (298K) are given in Appendix D. In experiments involving methane/steam, deionized water was fed to the evaporator by a HPLC pump. Pump-readout (in ml/min) was compared to actual delivery by collecting and weighing the water delivered over a period of time. It was found that no calibration was necessary.

Evaporator
The evaporator was manufactured by SINTEF and consists principally of a thermally insulated vessel with water inlet and gas inlet/outlet piping, a heating element, and a thermocouple (TC1). Evaporator temperature is of critical importance, as temperatures above 95°C leads to excessive boiling and pressure fluctuations (as observed in MS readout) with consequently unstable flow. A water feed rate of 0.4 ml/min was used in all experiments involving steam, and for this water feed rate it was found that a voltage of 60-70 Volts gave desired evaporator temperatures (85-94°C). Power is supplied by variable DC-source 1 (DC1). The reactant gas pipes entering and leaving the evaporator are heated using resistance threads and thermally insulated to eliminate water condensation. Power to resistance threads are supplied by variable DC source 2 (DC2).

Reactor assembly

The reactor assembly is described in detail in appendix B. It is designed to be operated at pressures up to 11 bar, and hence the quartz reactor interior is physically connected to the metal-quartz interspace to equalize pressure. As a safety measure, the rig is fitted with pressure gauges and relief valves both up- and downstream of the reactor itself, allowing for the release of pressure in case of clogging of the pipes by entrained material. Nitrogen (≈145 mln/min) was fed through the bypass line, acting as a 'masking' gas to avoid diffusion of product gases to the metal-quartz interspace. Some nitrogen from the bypass flow mixes with the effluent exhaust, thus complicating CO-detection (see section 4.4.1). By keeping the inert flow constant, it is assumed that any error arising from bypass nitrogen in effluent will be systematic.

The reactor assembly (steel casing and inner quartz reactor) is mounted in a furnace equipped with a dedicated programmable temperature controller and power source (DC3). The longitudinal temperature profile of the furnace was determined in advance by SINTEF personnel allowing the reactor to be placed optimally to give bed-temperatures as close as possibly to the furnace set-point. Main inlet and exhaust tubes were fitted with heating elements (resistance threads) and thermally insulated to avoid condensation of water prior to the water condenser. Condensation in the pipes could potentially lead to (temporary) partial or full obstruction of the inlet/exhaust lines and unstable flow characteristics. Power to the resistance threads was supplied by DC-source 2, with a setting of 100 Volts. Bed temperature is measured ≈2 cm above the sinter with thermocouple (TC2)

Effluent handling system

The (heated) exhaust-line enters a water-cooled condenser that removes the bulk of the moisture from the effluent gas. Since the mass spectrometer and gas chromatographs are highly sensitive to excessive moisture levels, the portion of the exhaust gas that is to be analyzed is passed through a sodium-fluoride (NaF) drying coil prior to analysis. The 'nafion'-dryer consists of two concentric tubes in which nitrogen (60 mln/min) and exhaust gases (max 25 mln/min) flow counter-current in the outer shell and inner tube respectively. The inner tube is filled with NaF- particles that absorb moisture down to ppb levels. The absorbed moisture diffuses to the outer shell and is continuously removed. A t-piece with a septum (for GC-sampling) and a connection point for the MS sampling line is mounted at the end of the nafion-dryer. The remainder of the effluent gas is vented.

4.3.3 Flow regime determination

As a preliminary, but highly important experiment, the required gas flow to achieve bubbling fluidization of a representative bed of NiONiAl [0.2> d_p < 0.09 mm] was determined. According to Kuuni & Levenspiel (1993) the minimum fluidization velocity is defined as the superficial velocity when an increase in gas velocity no longer gives a corresponding increase in pressure drop across the bed. Lack of equipment for accurate pressure measurements at the time led to a modified experimental set-up in which the *bed voidage* was measured. When bed voidage (and hence bed volume) becomes independent of volumetric flowrate of gas, it was assumed that full bubbling fluidized behavior is achieved.

The experiment was performed at ambient temperature and pressure by mounting the quartz reactor vertically in a stand, filling the reactor with the appropriate amount of material, passing nitrogen through the bed and measuring the height of the bed as a function of nitrogen flowrate. Gas was fed to the reactor using a Bronkhorst MFC for nitrogen (0-2000 ml/min) and a flexible silicon tube mounted on the main reactant feed line. Since the quartz reactor is transparent, direct measurement of bed height vs. flowrate with a ruler and qualitative observation of bed behavior is possible.

The obtained curve for bed expansion versus flowrate is given in Figure 35. During initial stages (up to ≈400 ml/min) a significant tendency towards 'channeling' was observed. Channeling occurs when the pressure drop across the gas distributor (sinter) is not sufficient to distribute the fluid across the entire cross section of the bed. In effect, the upward-flowing fluid is forced into discrete 'columns' around the circumference of the reactor. The result is poor gas-solid contact and consequently poor results. The onset of fluidized behavior can be visually observed as a marked improvement in bulk gas-solid contact, and by gently tilting the reactor and observing that the top of the bed remains horizontal. Onset of fluidized behavior was observed at a flowrate of ≈500 mln/min. A gradual expansion of the bed as a result of increased bubble fraction was observed until ≈800 mln/min. Beyond this point the height of the bed remains constant but bubble diameter and velocity increases. At 1500 mln/min solids are expelled ≈2-3 cm above the bed by 'exploding bubbles'. At higher flowrates (>1500 ml/min) 'slugs' are observed and flow regime gradually changes towards transport-regime conditions.

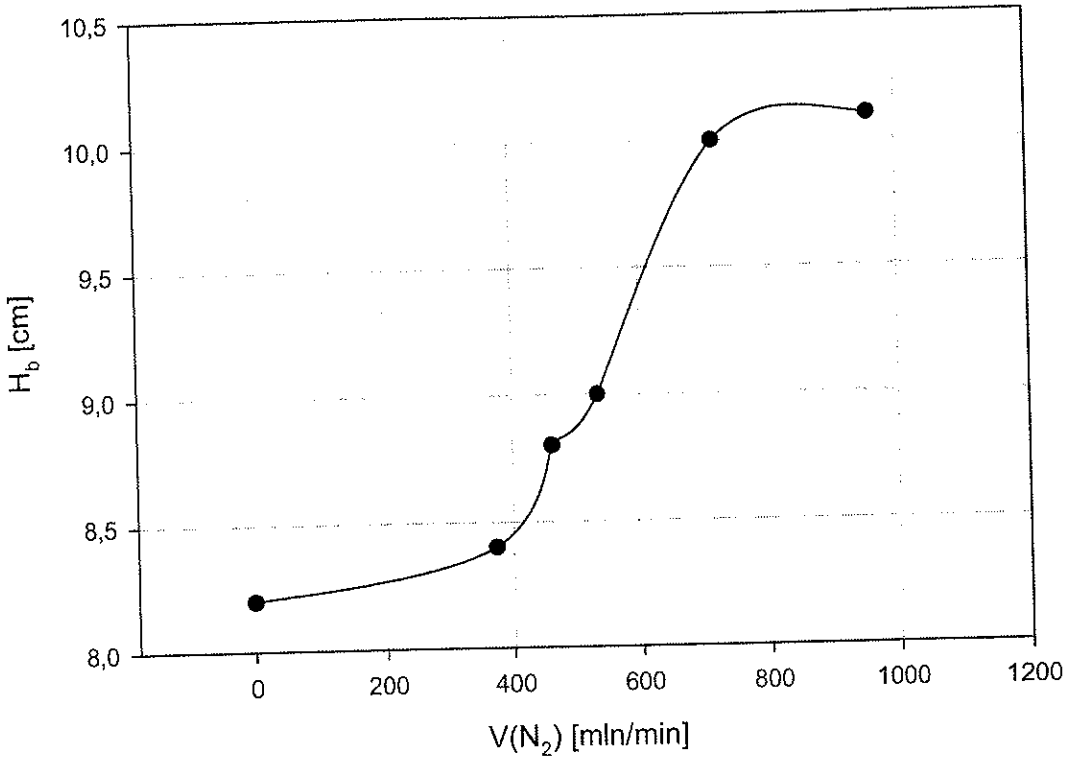

Figure 35 Bed height versus volumetric flowrate using N_2 at ambient conditions, NiONiAl (60%), d_p = [0.2-0.09] mm, bed mass=21.3 g

The reactor freeboard with a 10 cm bed is approximately 30 cm, and thus material entrainment was not observed visually.

Deciding on a reasonable flow rate to use in experiments at elevated temperature using other fluidizing gases than nitrogen (e.g. hydrogen, methane, methane/steam and air), with the additional complication of chemical reaction changing the total number of gaseous components, is a complex issue that is difficult to address accurately in the laboratory. Hydrogen and methane will be poorer fluidizing media than nitrogen (due to lower density), but rapid heating and consequent expansion of the fluid as it passes through the bed will possibly counteract this. In hydrogen reduction, the number of gaseous components remains constant while it decreases (by 1) and increases (by 2) in oxidation/reduction with air/methane, respectively. The major concern was to avoid channeling, as this was believed to have the most adverse effects on the results. As a consequence it was decided that a

flow of **400-500 mln/min** would be sufficient to ensure bubbling fluidization at elevated temperature.

On the other hand, a large amount of entrained solids is also highly undesirable due to possible clogging of the effluent pipelines as well as significant changes in the amount of solid reactant present in the bed. Clogging of the pipes has not been observed in any experiment and draining of the water condenser (where entrained solids will be collected) have confirmed that entrainment of solids at flowrates of 500 mln/min is limited to an insignificant amount of fines.

Considering that the inner diameter of the quartz-reactor is 20 mm while the bed height is approximately 10 cm, the bed has a height/diameter ratio of 5. Visual observation of reactor flow patterns in the reactor at fully developed bubbling fluidization and measurements of bed temperature during oxidation both indicate that solid mixing is far from perfect with this geometry.

4.3.4 Experiments at elevated pressure

Initial experiments at 5 and 10 bar showed that reactor operation at elevated pressure did not work well with analytical equipment operating at atmospheric pressure.

Firstly, information about time dependent changes in the effluent make-up is lost when effluent is expanded in the BPR prior to analysis. Operating the reactor at elevated pressure wile performing analysis at ambient pressure has the same apparent effect as increasing the total reactor volume. At elevated pressure, a larger number of gas molecules are confined within the same volume, and the subsequent expansion corresponds to a time delay yielding an effluent related to the average composition within the reactor at that specific time. This is an artifact related to pressure change, and it must be assumed that time dependent changes are equally rapid at elevated pressure.

Secondly, maintaining the superficial velocity necessary to fluidize the bed at, say, 5 bar requires a 5-fold increase in MFC output, as compared to experiments at atmospheric pressure. MFCs deliver the same mass flow of gas, within the pressure range for which the MFC can be used, in this case 1-20 bar.

For studies of CLC at elevated pressure, analytical equipment suitable for analysis of effluent at the actual pressure, e.g. IR spectrometry using a transparent gas-cell, should be applied.

4.4 Instrumentation

It is referred to Appendix C for the technical specifications of the mass spectrometer and Agilent 'micro-GC'.

4.4.1 Mass Spectrometer

General remarks
In the present work, it has been experimentally confirmed that measurements of effluent gas species using MS are generally of a qualitative nature. The exception was experiments using hydrogen/air as reactants, as this yields effluent gas consisting solely of un-reacted reactant and inert. Attempts were made to calibrate the MS for the relevant species by analyzing and recording intensity values for known concentrations. It was found, however, that calculated concentrations were obviously incorrect, particularly during initial stages of reduction with methane, when effluent is rich in CO_2. Hence, measured intensity values for gas species in a stream are not absolute but dependent on overall gas composition. It is speculated that this is caused by a combination of instrumental drift and changes in the physical flow characteristics of the effluent. MS is a powerful tool nonetheless, as it provides continuous monitoring of effluent species with a minimum amount of manual interaction required. Reaction time-frames for a given set of operating conditions (reactant flowrate and bed mass) can be established as well as a general impression of species concentration during the course of reaction.

Sampling and analytical principle
The mass spectrometer extracts approximately 2 mln/min of effluent through a heated capillary. The sample gas-stream then enters an ionization chamber (operated at 10^{-6}-10^{-5} torr, i.e.≈ 10^{-9}- 10^{-8} bar) in which it is bombarded at right angles by an electron beam emitted from a hot filament. The positively charged ions formed are focused and accelerated by a weak and strong electrostatic field, respectively, before being separated (filtered) and detected. There are several principles in current use for mass filtration (Silverstein et

al. 1991). The instrument at hand employs a 'quadropole mass filter', which represents the current 'state-of-the-art' in mass-filtration technology. The ions are here introduced parallel to 4 voltage-carrying rods (the quadropole) as indicated in Figure 36.

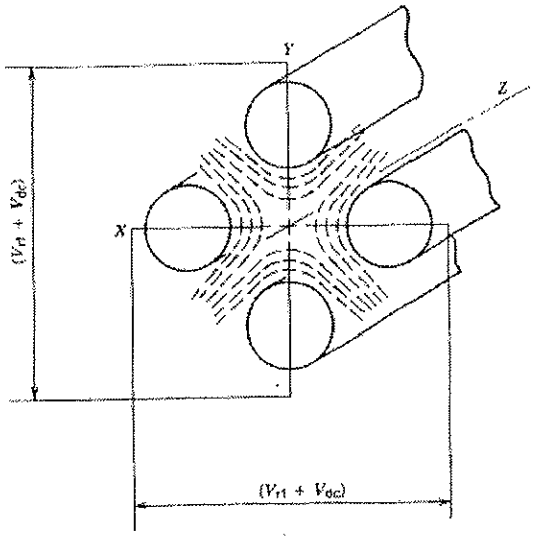

Figure 36 Quadropole mass filter schematic (from Silverstein et al., 1991)

Ions travel with constant velocity in the z-direction, but by applying a direct current voltage (V_{dc}) and a radio frequency voltage (V_{rf}) to the poles, complex oscillations occur in the x- and y-directions. There exists a 'stable oscillation', -dependent on ion mass/charge ratio- , which allows a particular ion to traverse the length of the filter without striking the rods. It is possible to perform a 'mass-scanning' by varying the direct current and radio frequency voltages so that only the desired ions are detected at any given time.

The filtered ions are then passed through collector-slits and detected by means of an electron multiplier.

Data from the MS are obtained as excel-compatible datasheets containing intensity measurements of the relevant species with timestamps according to the internal clock of the instrument. Timestamp values can be easily converted to minutes/seconds in post-analysis data treatment.

The relevant species encountered in the present work, and their characteristic ionic masses, are listed in Table 19.

Table 19 Relevant gas species and their ionic masses

Species	Primary mass $M^+(1)$ [g/mol]	Secondary mass $M^+(2)$ [g/mol]
CO_2	44	28
Ar	40	
O_2	32	
CO	28	
N_2	28	
H_2O	18	
CH_4	14	
H_2	4	

There are two complicating factors when monitoring CO-intensity. Firstly, nitrogen (from the metal-quartz interspace, or fed as inert reactant) has a primary mass that corresponds to that of CO (M^+=28). This would potentially mask CO produced during reduction with methane or from oxidation of carbon formed during reduction. Consequently, argon was used as bypass-gas in some methane-reduction experiments to avoid this complication.

Secondly, CO_2 interferes with the analysis of CO as it may defragment to CO^+ upon ionization by releasing an oxygen radical:

$$CO_2 \xrightarrow{e^-} CO^+ + O \qquad (4.1)$$

This problem could be resolved by calibrating the MS by introducing known amounts of CO and CO_2, and then eliminating the signal arising from CO_2 defragmentation. This was not carried out, however, since it was decided that Gas Chromatography was required for the accurate quantification of gas species.

As discussed, quantification of individual species was limited to experiments involving hydrogen and air. Under such conditions, assuming linearity, fractional conversion in reduction and oxidation can be expressed in terms of signal intensities:

$$\phi = 1 - \frac{I_i}{I_i^0} \qquad (4.2)$$

Where I_i is the time dependent intensity of species i, I_i^0 is the stable intensity readout when reaction is complete. I^0 is thus the reference intensity for each individual experiment.

4.4.2 Gas Chromatograph analysis and sampling

General remarks

Two different GCs have been used in the present work for quantification of individual effluent species: GC1: Agilent 'micro-GC', GC2: Agilent conventional GC. The difference between the two is principally physical size, and sampling procedure. Both instruments allow for automated sampling and analysis of effluent gas with 2-3 minute sample-intervals. However, based on the reaction time-frame obtained with qualitative MS, it was concluded that *manual sampling* using syringes to collect and store effluent gas for subsequent analysis, was required to obtain the desired number of individual data-points. In experiments using methane/steam GC1 was used while a GC2 was used for experiments using dry methane. In the former, 20 ml syringes were used for sampling, whereas 5 ml was used for the latter. The sampling and quantification procedures are otherwise similar for the two instruments, and differences are discussed in context.

Analytical principle

It is beyond the scope of this thesis to give a thorough discussion of gas chromatography, but a brief introduction to the principles involved is relevant. In gas chromatography, a gaseous sample containing a mixture of species is introduced into a stream of carrier gas (mobile phase) and fed through a column that is coated internally with a 'stationary phase'. The stationary phase is generally either hydrophilic (polar) or hydrophobic (un-polar) and, -dependent on analyte-properties -, gas components will have different *affinities* for the stationary phase and mobile phase, respectively. During the passage through the column, species will distribute themselves in the mobile- or stationary phase to a different degree and be separated by virtue of distribution equilibrium.

Components emerge (are eluted) from the column separately at a column- and species-specific *retention time* and are detected. The GCs used in the present work both employ Thermal Conductivity Detectors (TCDs). This detector can (simplified) be described as two heated filaments over which pure carrier gas and carrier gas with separated components passes,

respectively. The primary signal of the detector is the difference in electrical resistance between that of the reference filament (in thermal equilibrium with carrier gas) and that of a sample filament subject to carrier gas with eluted components. Pure carrier gas produces a background signal (baseline) while the presence of separated components changes the thermal conductivity of the fluid passing the sample-filament. The resulting change in filament temperature (and electric resistance) is observed as a peak in the chromatogram (detector signal versus time) of which the *area* is proportional to the concentration of the specific component. Integration of the peaks and deduction of concentration (in volumetric %) is carried out automatically by dedicated analytical software at the end of each analytical run. Both instruments in use were pre-calibrated by SINTEF personnel for the relevant gas species and concentration ranges encountered.

The principle of thermal conductivity gives the TCD virtually universal applicability and this together with the non-destructive nature of the TCD detector are its main advantages. The main drawback is limited sensitivity (10^{-6}g) as compared to more recently developed detectors, such as the Flame Ionization Detector (FID), Alkali-Flame Ionization Detector (AFID) and Electron Affinity Detector (EAD). The sensitivity of the TCD detector is still sufficient (by far) for the analyses at hand, in which concentrations are measured in volumetric % rather than the minute concentrations that are frequently encountered in organic trace analyses.

Sampling

Samples for analysis in the gas chromatograph are collected manually by use of standard-issue syringe (20 & 5 ml), needle (0.9 mm inner diameter) and a septum mounted on the effluent line exiting the nafion dryer.

The sampling involves a significant amount of manual interaction as compared to online MS, and a typical experimental run with GC quantification consists of:

- Switching the 5-way supply valve to feed reactant gases while starting digital timer
- Mounting clean syringe with needle in septum mounted on effluent line
- Collecting samples and noting elapsed reaction time
- Analysis of samples on GC in succession when reaction has been completed

Since product gases can be rich in hydrogen, which is known to rapidly diffuse, it was necessary to determine if storage of samples in syringes in the time span from sampling to analysis could have a significant effect on gas concentrations. Several parallels where extracted from a standard gas (AGA), stored and analyzed at different times. No time-dependent decay could be detected in samples stored for up to 30 minutes.

Sample analysis

Sample injection is carried out in a slightly different way for the two instruments that have been used.

A) GC1

When the analytical program is initiated there is a 10 sec initialization period before a sampling-pump within the GC starts to collect sample gas. During this period approximately 5 ml of the sample is flushed through the injection assembly (Figure 37) to exclude the possibility of contamination of the sample with air or remaining analyte from prior experiments. The sampling period was adjusted to 15 seconds to allow for smooth and controllable injection. It should be noted that only a small fraction (0.5 ml) of the sample is actually drawn into the GC, the remainder passing to ventilation. An element of timing and precision is involved in the injection procedure, as the remaining contents of the syringe (≈15 ml) should be injected within the 15 second sampling window. The possibility of human error was present, as premature emptying of the syringe would draw ambient air into the GC through the ventilation outlet during the final seconds of the sampling period. A 30 cm coil of 1.0 mm (inner diameter) tubing was therefore fitted on the ventilation outlet to minimize the risk of air contamination.

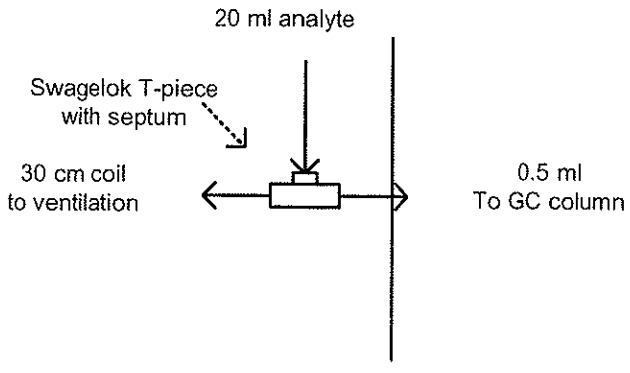

Figure 37 GC sampler schematic

B) GC2

Sample injection on the conventional GC is considerably simplified by the fact that the sampling pump can be disconnected. This allows for the direct injection of sample into the internal loop without risk of drawing in ambient air. When the syringe has been emptied into the loop, the analytical software is initiated. Pre-programmed valves within the instrument then handles the actual sample injection. As a result, less sample volume (5 mln) was required and consequently a higher sampling frequency was achieved.

4.4.2.1 Quantification

The analytical software calculates absolute % volumetric concentrations of CH_4, CO_2, CO, H_2, N_2, and O_2 from calibration data. The sum of all species is within 100 +/- 5% in all experiments.

In reduction with methane, inert nitrogen is present in significant amounts, either fed as inert along with methane, or from the bypass-flow in the metal-quartz interspace. Small amounts (<4%) of oxygen is also observed, as a result of contamination with air in the sampling and injection procedures.

The concentration of relevant effluent species, excluding inert feed and bypass nitrogen, are found by normalizing the raw-data. This is done by subtracting nitrogen and oxygen concentrations from the total sum of species, and dividing the relevant species concentration to the normalized sum of species. When switching between gas mixtures, there is a period of 30-40 seconds (depending on total flowrate) in which normalization cannot accurately be performed, since the total reactor volume must be replaced before effluent composition can be related to the feed.

4.5 Synthesis of oxygen carriers

In the following, the procedures used for synthesis of oxygen carriers will be discussed. In the case of NiONiAl, a molar balance consideration necessary to find the required precursor amounts to yield the desired gross composition (β) is given.

4.5.1 Nickel oxide on nickel-spinel

The oxygen carrier is synthesized from commercially available chemicals, by a dissolution, evaporation and calcination procedure broadly outlined by Ishida et al. (1999). All chemicals are 'off-the-shelf' and readily available in most laboratories and have an acceptable cost, at least for small scale production (<100g final product). For large scale production of this carrier, other sources of nickel and aluminum should be considered.

The solid precursors are *pro analysi* (p.a.) aluminum nitrate enneahydrate (ANE) (Al $(NO_3)_3$*$9H_2O$) and nickel nitrate hexahydrate (NNH) (Ni $(NO_3)_2$*$6H_2O$).The precursors are dissolved in aqueous 2-propanol, followed by removal of the bulk of the solvent by gentle evaporation. A sticky black/greenish residue forms and is subsequently dried overnight at 150°C. The dry solid is transferred to a high temperature furnace, and calcined 3 hrs at 1200 C. The remaining solid 'cake' has low porosity and is crushed and sieved to yield the finished carrier.

The method has been performed repeatedly for varying compositions and total yields, and has been found to be highly reproducible with regard to material yield.

4.5.2 Perovskite ($La_xSr_{1-x}Co_yFe_{1-y}O_3$)

The $La_{0.8}Sr_{0.2}Co_{0.2}Fe_{0.8}O_{3-\delta}$ sample used for chemical looping experiments was synthesized on the basis of a complexation method (citric acid method). Starting materials were La_2O_3 (Aldrich, 99.99 %), $Sr(NO_3)_2$ (Merck, p.a.), $Co(CH_3COO)_2 \cdot 4H_2O$ (Fluka, p.a.), $Fe(NO_3)_3 \cdot 9H_2O$ (Merck, p.a.), citric acid monohydrate $C_3H_4(OH)(COOH)_3 \cdot H_2O$ (Fluka, p.a.) and HNO_3 (min. 65% for analysis, Riedel-de Haën). La_2O_3 was annealed at 1000°C for 12 h and cooled to ambient temperature under dry conditions prior to use.

La_2O_3 was dissolved in diluted HNO_3 under stirring conditions before adding Fe $(NO_3)_3 \cdot 9H_2O$ to the solution. $Sr(NO_3)_2$ and $Co(CH_3COO)_2$ was dissolved in small amounts of water in a separate beaker. The two cation solutions were mixed before the citric acid was added in excess to the solution and melted. Prolonged heating was carried out in order to boil off water and nitrous gas species. The obtained material was then dried at 180°C over night before calcining at 450°C for 16 h under flowing air. The obtained powder was then cold pressed to pellets and heated at 1000°C for 16 h in air before cooling it

slowly to room temperature. The obtained product was then crushed, cold pressed, and annealed at 1000°C for 16 h under flowing air. The last procedure was carried out three times. The product was confirmed by means of powder X-ray diffraction to be phase pure.

The perovskite sample was made in two batches, obtaining a total amount of ca. 40 g.

5 RESULTS AND DISCUSSION

The experimental results section can broadly be divided between results for 60% nickel oxide on nickel spinel (NiONiAl), and those of $La_{0.8}Sr_{0.2}Co_{0.2}Fe_{0.8}O_{3-\delta}$.

The former has undergone reduction with hydrogen, methane/steam and dry methane as well as re-oxidation using air and air/steam. The main focus is on experiments with dry methane, as this most closely resembles the conditions of an operational CLC-plant.

In experiments with the perovskite, the focus has been on determination of the stoichiometric coefficient, δ, in reduction/oxidation with methane/steam and air, respectively, at various temperatures.

5.1 Reduction of NiONiAl with hydrogen

As mentioned in the previous chapter, reduction of NiONiAl with hydrogen has been investigated by two methods; gravimetric by absorption of produced water vapor and analysis of dry effluent using Mass Spectrometry-.

5.1.1 Gravimetric method

The results from this study are presented in detail in Paper III.

5.1.2 Online MS analysis

In order to functionally test the SINTEF-rig and confirm the results of Paper III, a series of experiments with hydrogen/air using MS was performed. Analytical data from MS is generally qualitative when dealing with gas mixtures of varying composition. In the case of reduction using hydrogen, however, hydrogen specific quantification is possible as the exhaust gas reaching the instrument will only consist of hydrogen diluted by nitrogen. This gas mixture can be replicated well in calibration, and hence the instrument readouts correspond excellently to calibrated values. Direct quantification of hydrogen in the exhaust is thus possible by relating

measured intensity to calibration correlations using predefined concentrations of H_2 in N_2.

To determine the importance of temperature and feed hydrogen concentration a series of experiments where performed on a batch of NiONiAl (60%), [0.2, > d_p > 0.02] mm, m_b^0= 18.02 g.

Table 20 Hydrogen reduction overview

Exp #	T [°C]	C^0 [%]	V (H_2) [mln/min]	V (N_2) [mln/min]	V (N_2) bypass
1	600	25	100	300	145
2	600	50	200	200	145
3	600	75	300	100	145
4	600	100	400	100	145
5	700	25	100	300	145
6	700	50	200	200	145
7	700	75	300	100	145
8	700	100	400	100	145
9	800	25	100	300	145
10	800	50	200	200	145
11	800	75	300	100	145
12	800	100	400	100	145

In reduction with hydrogen, water vapor is removed prior to analysis, and accordingly there are no gaseous *products* to be measured. Conversion can then be expressed in terms of measured intensity of remaining reactant, as discussed in the chapter 4. For each experiment, conversion is related to the observed reference intensity. Figure 38 is representative and shows the conversion of hydrogen at 700 °C and 25% hydrogen in nitrogen feed.

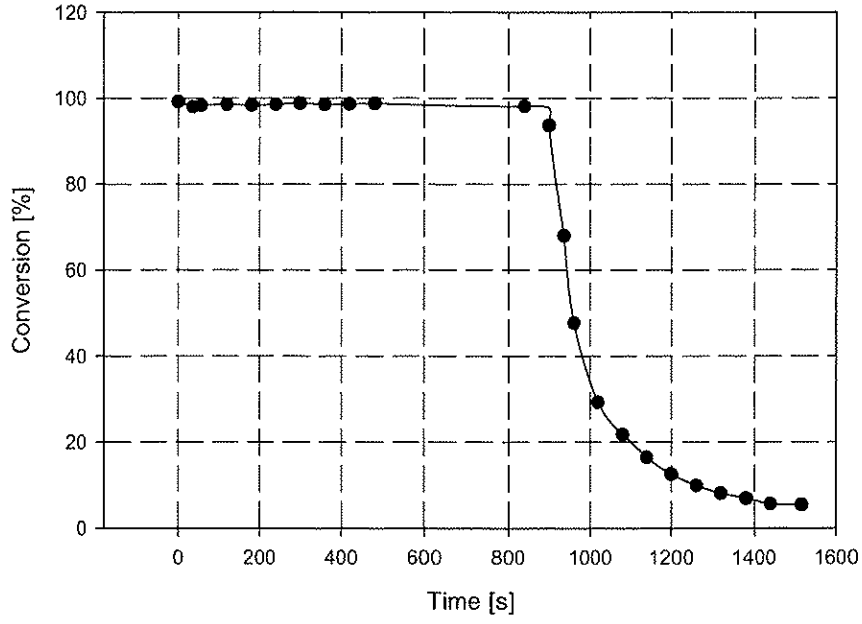

Figure 38 Hydrogen conversion at 700°C, 1 atm, 25% H_2 feed

It has been found that hydrogen conversion in reduction of NiONiAl is 95-100% for temperatures in the range 600-800°C, independent of reactant H_2-concentration (25, 50, 75 and 100%).

Paper III deals with porous particles in the size range 400-2600μm, thus significantly bigger than those in the present work (90-200 μm). The results are comparable to those obtained with the smallest cut-size in Paper III, indicating that hydrogen-reduction is virtually quantitative and limited by mass transfer mechanisms rather that chemical reaction, at temperatures above 600°C.

Reduction of NiONiAl with hydrogen is of limited interest, since a potential CLC-application is expected to utilize carbonaceous fuels directly. The remainder of the results section concerns experiments involving methane.

5.2 *Reduction of NiONiAl with methane/steam*

In order to address the questions outlined in chapter 2, regarding reforming side-reactions during reduction of NiONiAl with methane/steam, a series of experiments where carried out with GC quantification of effluent gas species.

5.2.1 Objective and overview

Experiments were carried out with a fresh batch of NiONiAl (60%, [0.2, > d_p > 0.02] mm , m_b^0=20.1 g, methane/steam (S/C=2).

The result of the 2nd cycle of reduction/oxidation is shown in Figure 39.

The curve shows clearly the mechanisms involved in batch-reduction of NiONiAl using methane/steam:

- Initial stage with direct fuel reduction (DFR)
- Transitional stage
- Reforming stage, dominated by steam methane reforming (SMR)

5.2.2 Effluent concentration profile

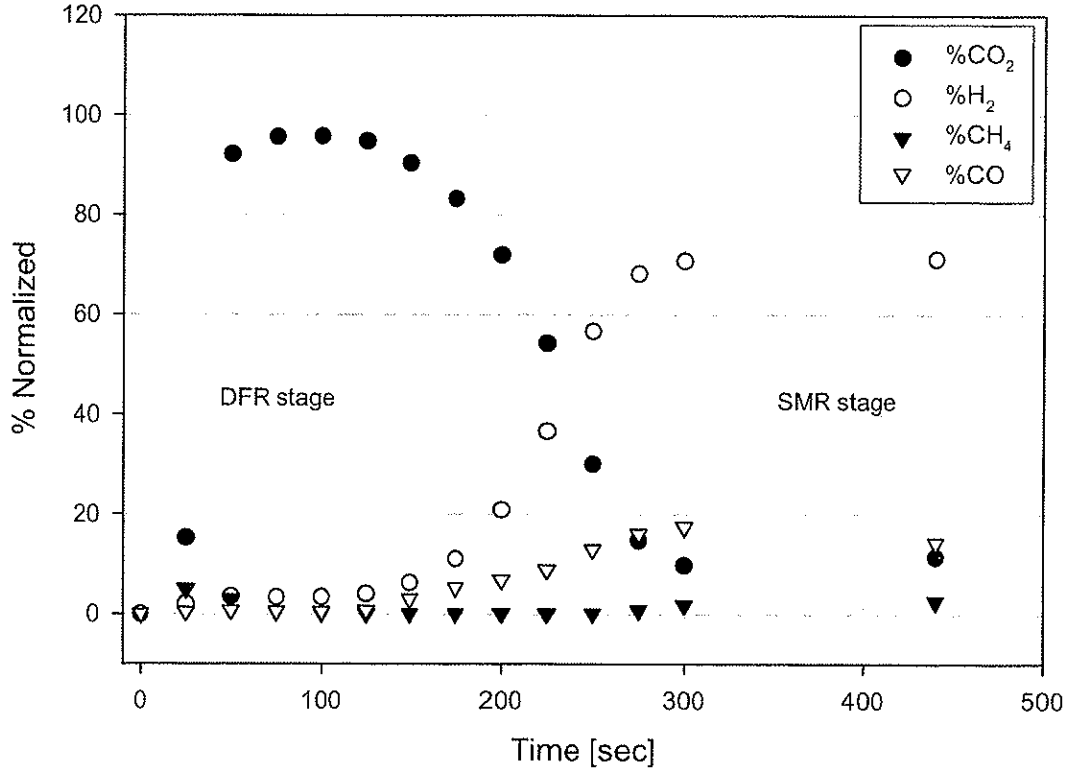

Figure 39 Reduction of NiONiAl with methane/steam (S/C)=2, T=800°C, 2nd cycle

In the above figure, it can be seen that effluent levels of carbon dioxide are relatively stable around 95% initially. Apart from a 'peak' at 15 s elapsed time, methane concentration remains low (<0.5%) during the period of DFR, increasing to an equilibrium concentration of 2.5% during the reforming stage.

Effluent concentrations on a dry basis during the reforming phase are 11.4% CO_2, 71.2% H_2, 2.6% CH_4, and 14.3% CO. These values correspond closely to thermodynamically calculated equilibrium composition for steam methane reforming of methane/steam, S/C=2, at 1 atm, 800°C over a commercial nickel catalyst (Personal reference: Ivar M. Dahl).

For this cycle it is concluded that the selectivity towards DFR is sufficient to allow for operation within an operational window before SMR becomes the dominating reaction. The gradual shift towards SMR equilibrium conditions (after 300 seconds) begins at around 150 seconds (with a flow rate of 250 mln/min methane).

However, indications of changes in material properties as a result of repeated reduction/oxidation cycles, can be seen by comparing Figure 39 with the results obtained in the 14th reduction cycle of this specific batch of NiONiAl:

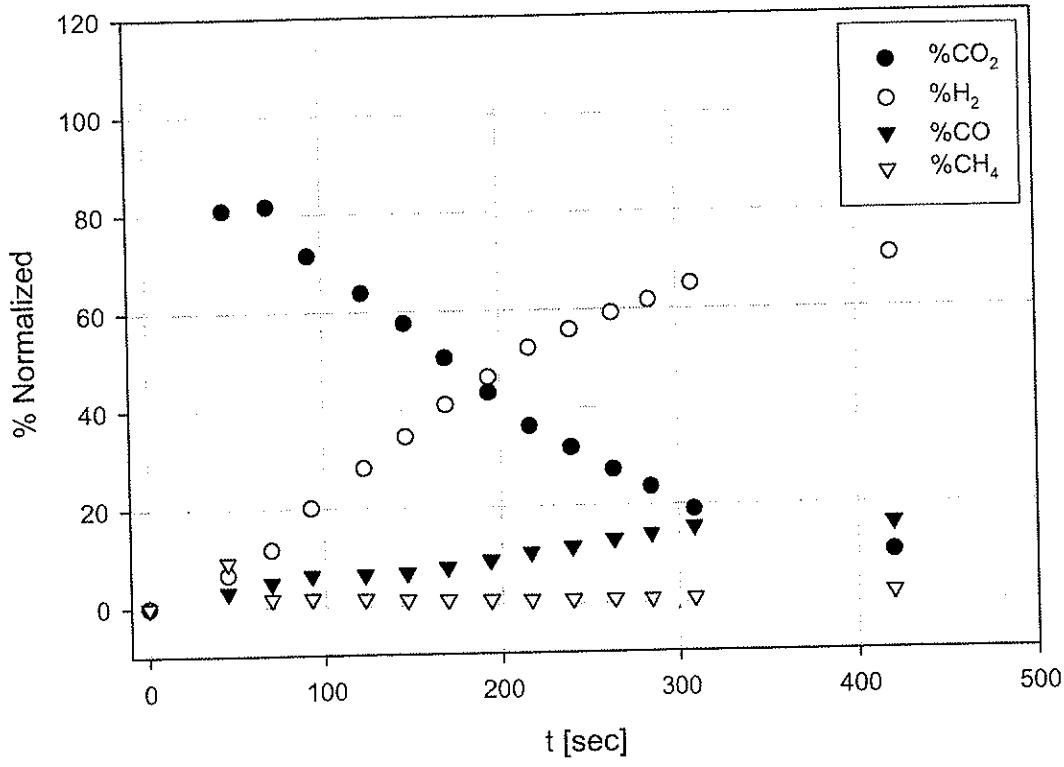

Figure 40 Reduction of NiONiAl with methane/steam (S/C)=2, T=800°C, 14th cycle

This apparent change in material properties will be discussed in connection with experiments using dry methane.

5.3 *Reduction of NiONiAl with methane*

In the following, the results of reduction of NiONiAl with dry methane will be presented.

5.3.1 Objective and overview

From experiments using a mixture of methane and steam as fuel, it is concluded that a typical reduction consists of three phases: direct fuel reduction (DFR) with NiO (initial stage), a transitional stage in which reforming reactions becomes dominant. Indications of material properties change have also been observed.

When dry methane is used, a combination of methane cracking (MC) and SMR are possible side-reactions. Reforming reactions are catalyzed by elementary nickel, so it is believed that the extent of reforming versus reduction will be dependent on the molar fraction of NiO remaining in the solid. The initial part of the reaction is that of main interest, and more precisely, determining a practical *operating point* ($y_{S,R}$) below which reforming-side reactions are limited. To investigate further a series of time-dependent reductions were carried out using dry methane as reactant.

A batch of NiONiAl (β=0.6) [0.2, > d_p > 0.02] mm, was weighed in (24.3 g) and used in the following experiments.

Reduction time-frame

From the amount of solid reactant present initially it can be estimated a minimum time of reaction to full solids conversion (y_S=0):

$$\tau_{min} = \frac{n^0_{NiO}}{4 \cdot \phi \cdot \dot{n}_{CH4}} \qquad (5.1)$$

Molar flowrate of reactant is estimated from ideal gas-law:

$$P_{CH4} \cdot \dot{V}_{CH4} = \dot{n}^0_{CH4} \cdot RT^0 \qquad (5.2)$$

With a methane flow-rate of 500 mln/min (0.000341 mol/s) at 1 atm, 298K and assuming constant fuel conversion (ϕ=1.0) the reduction has a minimum time-frame of 142 seconds.

At a total flowrate of 500 mln/min, it is observed (by MS) that responses in gas concentrations are 35-40 seconds 'delayed'. The volume of the reactor

from MFCs to the point of sample extraction is thus approximately 500*40/60 = 330 mln.

In cycle #1, it was attempted to use methane (500 mln/min). Since doubling the reactant feed rate (as compared to methane/steam experiments) effectively halves the reduction time-frame determined for methane/steam reduction, it was found that the number of samples that can be manually sampled during the operational window (60s) is too small to give a full picture of the exhaust gas concentration profiles during the course of the reaction.

To maintain the desired reactor flow regime, 250 ml/min methane + 250 mln/min nitrogen was used as reactant. It is assumed that nitrogen will serve as an inert volumetric addition, not affecting reaction rates significantly. This assumption is supported by previous measurements showing that feed concentration does not affect conversion significantly. The advantage is that results from methane/steam trials will be directly comparable with similar time-frames.

In Table 21, time on stream (TOS) is defined as the time period during which methane/nitrogen is fed to the reactor. Temperature is the furnace set-point and it should be noted that the temperature during reduction decreases as a result of the positive reduction enthalpy. For details on the temperature during reduction and oxidation it is referred to section 5.4.

Table 21 Overview of methane reduction with GC quantification

Cycle #	V (CH_4) [mln/min]	V(N_2) [mln/min]	TOS [s]	T [°C]
1	500	0	60	600
2	250	250	120	600
3	250	250	183	600
4	250	250	150	700
5	250	250	150	800
6	250	250	150	600

5.3.2 Effluent concentration profiles

In the following the effluent gas-concentration profiles obtained in reduction cycles 2-6 will be discussed.

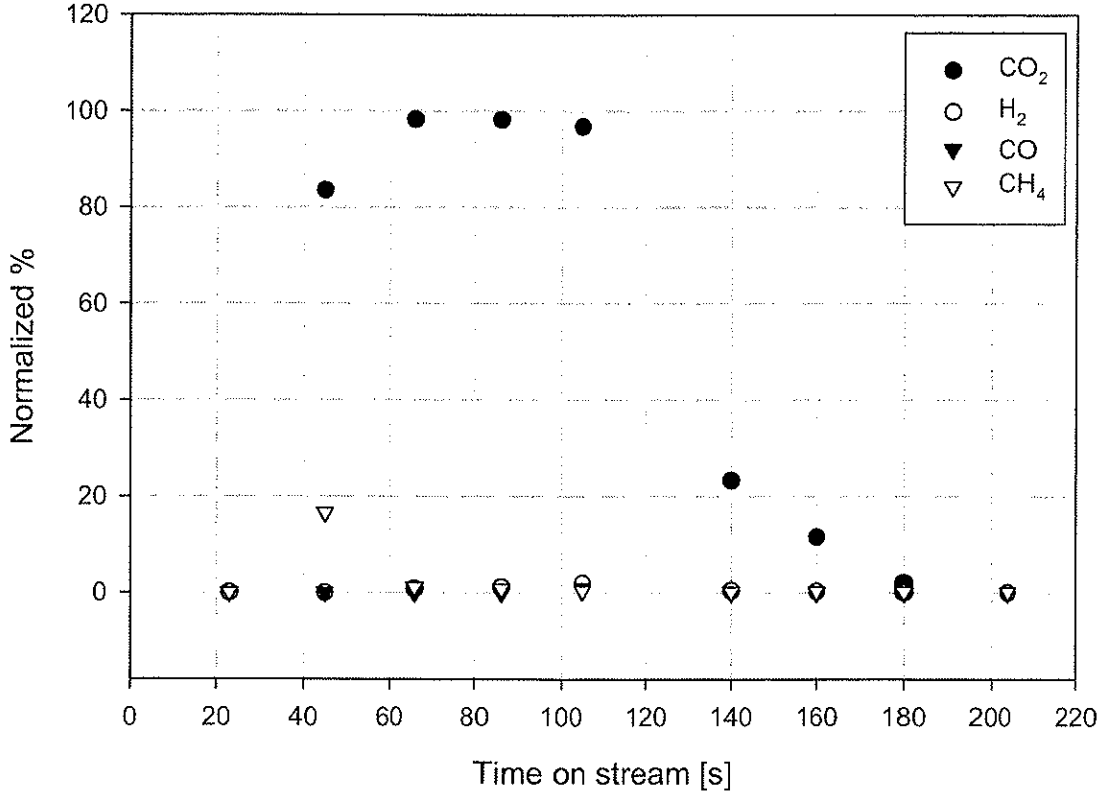

Figure 41 Reduction of NiONiAl with methane at 600°C, TOS=120s, cycle #2

Apart from a small peak of un-reacted methane during the initial stage, the above curve shows excellent characteristics of NiONiAl as an oxygen carrier, as CO_2-production is virtually quantitative throughout the period of methane feed. The methane peak is also observed in experiments with MS analysis and is probably related to poor fluidization caused by the interruption of gas flow when switching the supply valve.

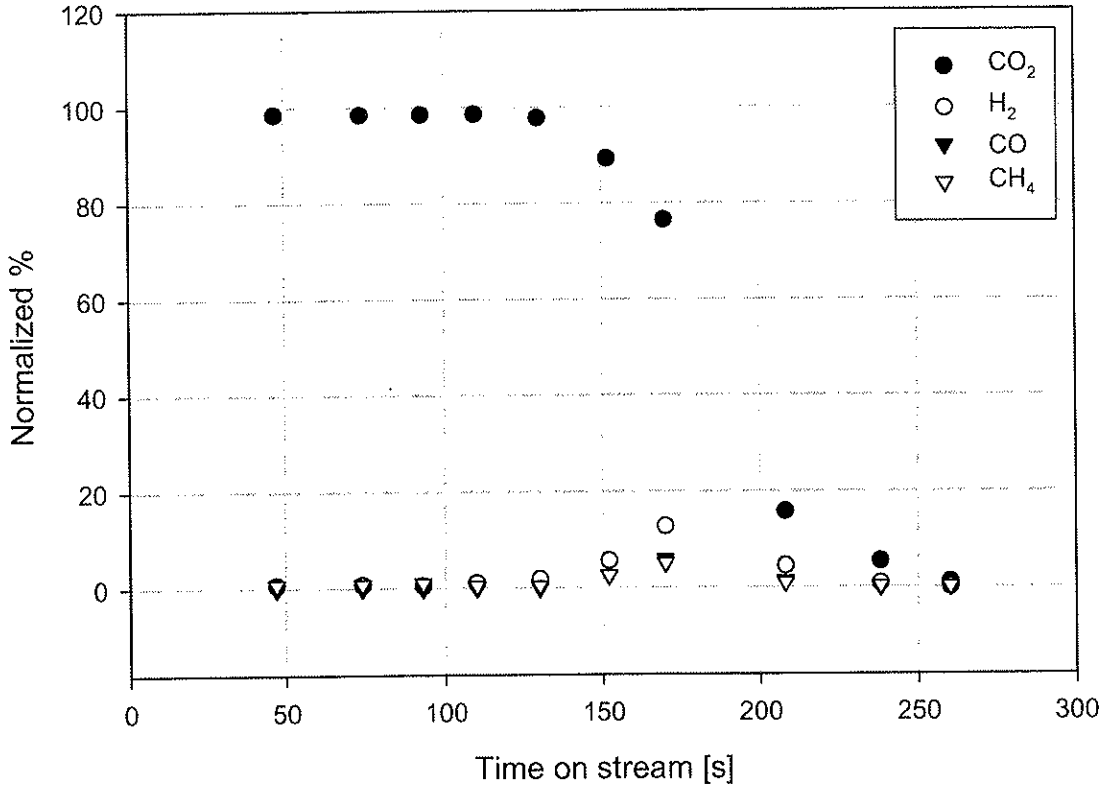

Figure 42 Reduction of NiONiAl with methane at 600°C, TOS=183s, cycle #3

Figure 42 resembles Figure 41 initially, with near ideal behavior as far as selectivity is concerned. In the above figure, TOS is 183 seconds, and effluent concentrations of hydrogen, carbon monoxide and methane starts to increase around 150 s. Increased concentrations of hydrogen and carbon monoxide, indicates that SMR and/or MC become more dominating at this point.

Whereas cycles #2 and #3 are only slightly different, there is a marked change in the material properties as observed in the effluent gas concentration profiles in the 4^{th} cycle (Figure 43).

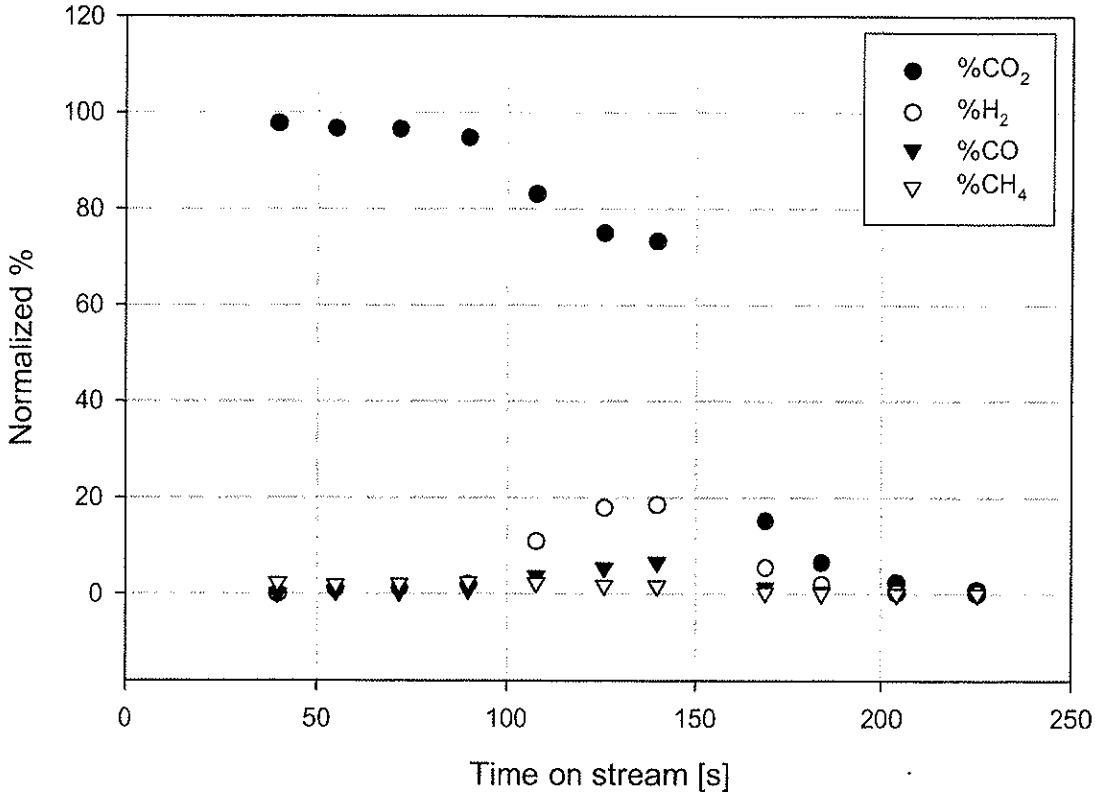

Figure 43 Reduction of NiONiAl with methane at 700°C, TOS 150s, cycle #4

At 700°C, hydrogen is generated in increasing amounts from 100 seconds onwards accompanied by an increase in CO and CH_4. Effluent hydrogen levels apparently stabilize at 20 % before methane shutoff (150s). Note that methane conversion during later stages before methane shutoff is higher than at 600°C. The period of pure DFR is significantly shorter than in cycles 2 & 3.

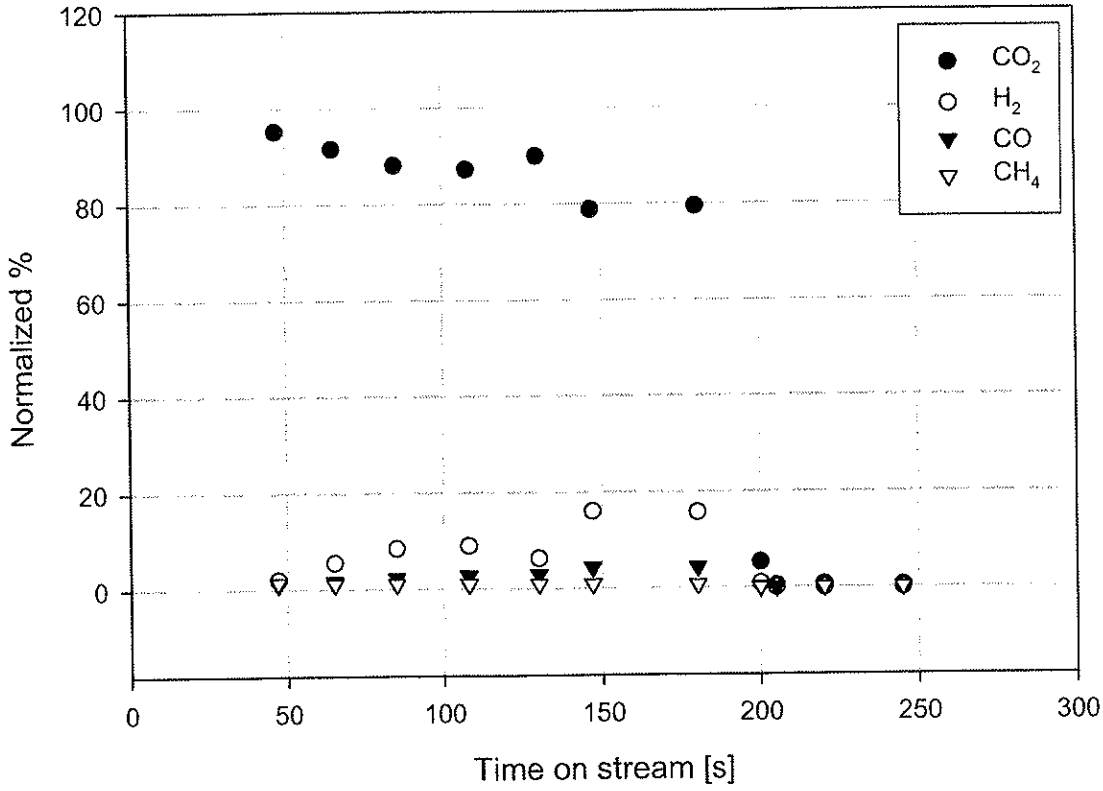

Figure 44 Reduction of NiONiAl with methane at 800°C, TOS 150s, cycle #5

The trend towards poorer selectivity observed in cycles 2-4 is also seen at 800°C. Significant amounts of hydrogen is observed from TOS=60 seconds onwards, stabilizing at 18% at TOS=150 seconds. Overall fuel conversion is around 0.98, similar to cycle 4 (700°C).

Note that sample #5 (TOS=130 s) breaks with the general trend during the course of the reaction and is related to an unsuccessful sampling and/or injection.

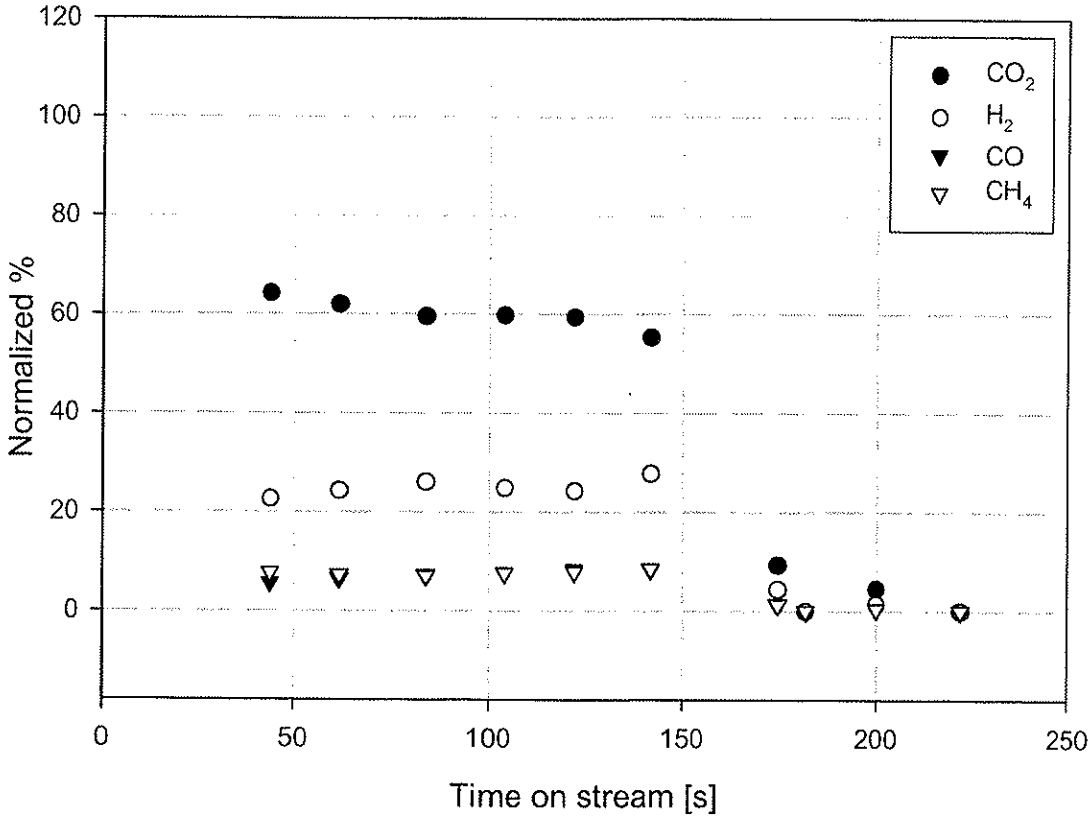

Figure 45 Reduction of NiONiAl with methane, 600°C, TOS=150s cycle #6

In the 6th cycle, effluent composition is relatively stable throughout the course of the reaction. Hence the material-properties appear to have stabilized, yielding effluent concentrations during the operational window of 60% CO_2, 22-25% H_2, 7-8% CO and 7-8% unconverted CH_4. Note that the conversion of methane is reduced to 0.92-0.93 as compared to cycles 2 & 3 where conversion was 0.98-1.0. It is likely that this is connected to the reduction selectivity, as a greater portion of the methane reacts via reforming reactions in which conversion is less than for DFR.

There is evidently a gradual deterioration in material selectivity towards DFR and consequent reduction in fuel conversion (ϕ) during the first 6 cycles of reduction and oxidation.

Table 22 Summary of results, cycle 2 - 6

#	T [°C]	%CO_2	%H_2	%CO	%CH_4	Comment
2	600	100	0	0	0	Near ideal behavior
3	600	95-90	0-15%	0-5	0-5	DFR dominates initially, gradual increase in H_2 from 120 s
4	700	95-75	5-20	0-5	0-2.5	Gradual increase in H_2 from 100 seconds onwards
5	800	95-80	5-18	0.5-6	2.5	Gradual increase in H_2 from 50 seconds onward
6	600	65-60	22-25	7-8	7-8	Stable effluent composition throughout

From near-ideal behavior in cycle 2, with no observable reforming products (S≈1) and high fuel conversion ($0.95 < \phi < 1.0$), selectivity has decreased significantly, producing a CO_2-rich (60-65%) effluent mixture containing reforming products; 22-25% H_2, 7-8% CO and 7-8% unconverted CH_4.

5.3.3 Estimation of solid molar fraction

In cycle 3, effluent composition is virtually constant, and the molar composition of the carrier at the point of transition towards reforming conditions (TOS≈130s) can be estimated using Eq. 2.27d and assumptions given in Table 23. The calculation is valid under the assumption that NiO reacts only with CH_4 in DFR.

$$y_A(t) = y_A^0 - \frac{1}{n_A^0}\frac{b}{a}\dot{n}_B^0 \cdot \int_{\tau 0}^{\tau 1} \phi_B(t)\,dt$$

Initial amount of nickel oxide is given by Eq. 2.33:

$$n_{NiO}^0 = \frac{m_b^0 \cdot \beta}{Mw(NiO)}$$

Table 23 Estimation of parameters used in solid molar fraction calculation in cycle 3 at TOS=130

Parameter	Value	Comment
ϕ	0.98	Estimated from average molar fraction of methane in effluent, cycle 3
S	≈1.0	Realistic approximation based on the absence of reforming products (H_2, CO)
m_b^0	23.1 g	Assuming that no significant amount of carrier has been entrained.
$\dot{n}_{CH4}^0$	0.000171 mol/s	Calculated from volumetric flowrate of methane and ideal gas law at 1 atm, 298 K, R=0.082 $dm^3 atm\ K^{-1}\ mol^{-1}$
y_S^0	1.0	Assuming that full re-oxidation is achieved
τ^0	0	Start time
τ^1	130 s	Methane shutoff
β	0.60	Predefined solid gross composition
a	¼	From stoichiometry
b	1	From stoichiometry

Substitution of the variables in Table 23 and integration of the (constant) fuel conversion function, simplifies the expression to:

$$y_{S,R}(130s) = 1 - \left(4 \frac{74.69(g/mol) \cdot 0.000171(mol/s)}{23.1(g) \cdot 0.6} \cdot 0.98 \right) \cdot [130 - 0](s)$$

$$y_{S,R}(130s) = 0.54$$

The above method is effectively a geometric consideration of areas. Based on this approximated result, it can be concluded that, in the best case, roughly 50% of the available oxygen in NiONiAl (60% NiO by mass) can be transferred by reduction of methane to carbon dioxide before competing reforming reactions become dominating. In a *continuous* reactor, being fed fully oxidized NiONiAl, with perfect solid mixing, the operating point, i.e. the average composition of the solids leaving the reduction reactor is equal to the above result, i.e. $y_{S,R} \approx 0.5$. It should be emphasized that this is only valid under the ideal conditions using relatively fresh oxygen carrier, as it is clear from cycles 4-6 that the performance of the carrier deteriorates with time and number of cycles.

Estimation of solid molar fraction in cycles 3-5 is significantly more problematic due to the gradual increase in hydrogen and other species related to reforming. Additionally, since the material apparently undergoes a change in selectivity during each cycle, such a calculation is of limited interest.

In cycle 6, solid composition at TOS=130s can be estimated similarly to cycle 3, since effluent composition remains essentially constant.

Table 24 Estimation of parameters used in solid molar fraction calculation in cycle 6 at TOS=130

Parameter	Value	Comment
ϕ	0.92	Estimated from average molar fraction of methane in effluent, cycle 6
S	0.90	Based on calculation in section 5.3.4
S_R	0.95	Based on calculation in section 5.3.4
m_b^0	23.1 g	Assuming that no significant amount of carrier has been entrained.
$\dot{n}_{CH4}^0$	0.000171 mol/s	Calculated from volumetric flowrate of methane and ideal gas law at 1 atm, 298 K, R=0.082 $dm^3 atm\ K^{-1}\ mol^{-1}$
y_S^0	1.0	Assuming that full re-oxidation is achieved
τ^0	0	Start time
τ^1	130 s	Methane shutoff
β	0.60	Predefined solid gross composition
a	¼	From stoichiometry
b	1	From stoichiometry

Overall selectivity is introduced into Eq. 2.27d by multiplication of the molar feed rate of methane:

$$y_A(t) = y_A^0 - \frac{1}{n_A^0}\frac{b}{a}\dot{n}_B^0 \cdot S \cdot \int_{\tau 0}^{\tau 1}\phi_B(t)\,dt \qquad (5.3)$$

Reforming selectivity (S_R) does not affect $y_{S,R}$ as it is assumed that solid reduction is only mediated by DFR. This introduces some uncertainty, as generated hydrogen is capable of reducing NiO as well. With the current data, it is not possible to address this issue quantitatively.

The calculation yields a molar composition of $y_{S,R} \approx 0.60$, which will be taken as the average solids molar composition for particles with a residence time of 130 seconds in reduction.

The material selectivity towards direct fuel reduction has thus decreased from cycle 3 to cycle 6, resulting in less available oxygen for reduction. In cycle 3 50% of the NiO is reduced whereas only 60% is reduced under similar conditions in cycle 6.

5.3.4 Estimation of selectivity

In the following, effluent data for cycle 6 is assumed to be representative of the long-term performance of NiONiAl in reduction with methane at atmospheric pressure and a reaction temperature of 600°C. This assumption is supported by the regenerability study (section 5.5).

It is evident that conversion of methane is split between DFR and competing side-reactions.

It is hypothesized that methane conversion in CLC using NiONiAl and dry methane is divided according to Figure 46:

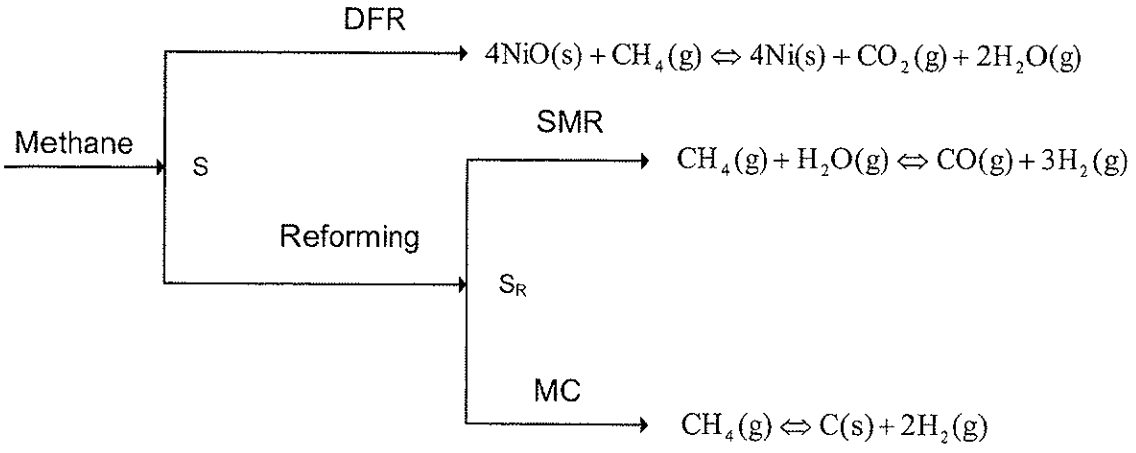

Figure 46 Reaction overview, with direct fuel reduction (DFR), steam methane reforming (SMR) and methane cracking (MC).

The rationale for this hypothesis is that the ratio of hydrogen to carbon monoxide in the effluent $y_{H2}/y_{CO} = 3.1$, - indicating that steam methane

reforming (SMR) is the predominant reforming reaction, i.e. S_R is close to unity.

Furthermore, CO_2 is observed during the initial stage of re-oxidation (section 5.4), indicating that coke is produced in minor amounts during reduction. Coke is believed to be produced either by methane cracking or by the Boudouard-reaction:

$$2CO(g) \Leftrightarrow C(s) + CO_2(g) \tag{5.4}$$

Since the latter involves conversion of 2 CO equivalents, it is believed that coking via the Boudouard would yield H_2/CO-ratios significantly below 3.

Overall selectivity (S) is defined as:

$$S = \frac{\dot{n}_i}{(\dot{n}_{DFR} + \dot{n}_{SMR} + \dot{n}_{MC})} \tag{5.5}$$

Reforming selectivity (S_R) is defined similarly:

$$S_R = \frac{\dot{n}_{SMR}}{\dot{n}_{MC} + \dot{n}_{SMR}} \tag{5.6}$$

A model of CLC based on molar balances was developed to investigate the impact of overall fuel conversion (ϕ), selectivity (S), reforming selectivity (S_R) and solids molar composition (y_S) on stream composition, required solid fluxes and coke formation. In this model, CH_4 is used as reducing agent while re-oxidation is mediated by dry air. Oxygen carrier is NiONiAl (60% NiO). Water is condensed and removed in a separate stream within the reduction reactor, making the calculated exhaust composition directly comparable to experimental values.

It should be noted that fuel conversion (ϕ) is defined as a *cumulative* term approximated from remaining methane concentration. Fuel conversion thus accounts for the less-than-100% conversion in *all reactions* involved. *Individual* conversion factors for DFR, SMR and MC are difficult to determine from the present experimental data.

The basis of the calculation is CH_4 and the balance equations for carbon can now be calculated yielding individual effluent molar fluxes and solid streams

by multiplying with stoichiometric factors. The mathematical framework is outlined in Table 25.

Table 25 Mathematical framework

Inlet	Calculation	Exit
Methane converted by DFR:	$\dot{n}_{CH4,DFR} = \dot{n}^{0}_{CH4} \cdot \phi \cdot S = \dot{n}_{CO2,DFR} = \frac{1}{2}\dot{n}_{H2O,DFR}$	Generated $CO_2 + H_2O$
Methane and H_2O converted by SMR:	$\dot{n}_{CH4,SMR} = \dot{n}^{0}_{CH4} \cdot \phi \cdot (1-S) \cdot S_R$ $\dot{n}_{CH4,SMR} = \dot{n}_{H2O,SMR} = \frac{1}{3}\dot{n}_{H2,SMR} = \dot{n}_{CO}$	Generated $H_2 + CO$
Methane converted by MC:	$\dot{n}_{CH4,MC} = \dot{n}^{0}_{CH4} \cdot \phi \cdot (1-S) \cdot (1-S_R)$ $\dot{n}_{CH4,MC} = \frac{1}{2} \cdot \dot{n}_{H2,MC} = \dot{n}_{C,MC}$	Generated H_2 and C
Unconverted methane:	$\dot{n}_{CH4,out} = \dot{n}^{0}_{CH4} \cdot (1-\phi)$	Remaining CH_4
-	$\dot{n}_{H2} = \dot{n}_{H2,SMR} + \dot{n}_{H2,MC}$	Total H_2 generated
-	$\dot{n}_{H2O} = \dot{n}_{H2O,DFR} - \dot{n}_{H2O,SMR}$	Total H_2O generated
-	$y_i = \frac{\dot{n}_i}{(\dot{n}_{CH4,out} + \dot{n}_{H2} + \dot{n}_{CO2} + \dot{n}_{CO})}$	Effluent molar fractions (dry basis)
Converted nickel oxide	$\dot{n}_{NiO,CONV} = 4 \cdot \dot{n}_{CH4,DFR}$	Generated nickel
Reduction solids influx	$\dot{m}_{NiONiAl,IN} = \frac{\dot{n}_{NiO,CONV}}{Mw(NiO) \cdot \Delta y_S \cdot \beta}$	Oxidation solids outflux
Oxidation solids influx	$\dot{m}_{NiONiAl,OUT} = \dot{m}_{NiONiAl,IN} - \frac{\dot{n}_{NiO,CONV}}{Mw(NiO)} + \frac{\dot{n}_{C,MC}}{Mw(C)}$	Reduction solids outflux
Selectivity	$S = \frac{\dot{n}_{CH4,DFR}}{\dot{n}_{CH4,DFR} + \dot{n}_{CH4,SMR} + \dot{n}_{C,MC}}$	-
Reforming selectivity	$S_R = \frac{\dot{n}_{CH4,SMR}}{\dot{n}_{CH4,SMR} + \dot{n}_{C,H4,MC}}$	-

The framework was implemented in Excel, and a parameter sensitivity calculation with regard to overall selectivity (S), reforming selectivity (S_R) , fuel conversion (ϕ) and operating point ($y_{S,R}$) was carried out.

Exhaust molar fraction (y_i) is now calculated on a dry basis for different levels of overall selectivity and reforming selectivity.

Table 26 Calculated effluent compositions

S	S_R	y_{CO2}	y_{H2}	y_{CH4}	y_{CO}	y_{H2}/y_{CO}
	0.95	0.711	0.188	0.065	0.036	5.3
0.95	*0.75*	0.549	0.379	0.050	0.022	17.5
	0.50	0.427	0.522	0.039	0.011	46.5
	0.95	0.610	0.267	0.059	0.064	4.1
0.90	*0.75*	0.492	0.420	0.048	0.041	10.2
	0.50	0.396	0.544	0.038	0.022	24.7
	0.95	0.526	0.332	0.054	0.088	3.8
0.85	*0.75*	0.440	0.456	0.045	0.058	7.8
	0.50	0.366	0.565	0.037	0.032	17.5

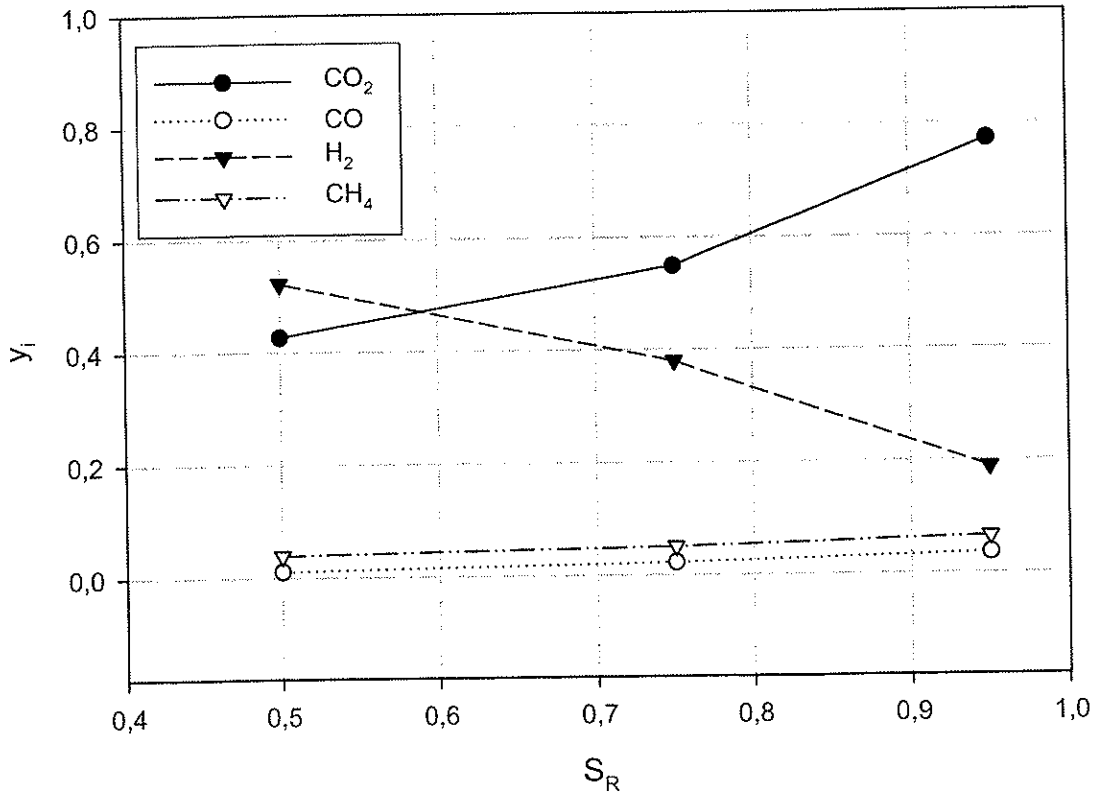

Figure 47 Calculated effluent composition y_i versus S_R; S=0.95

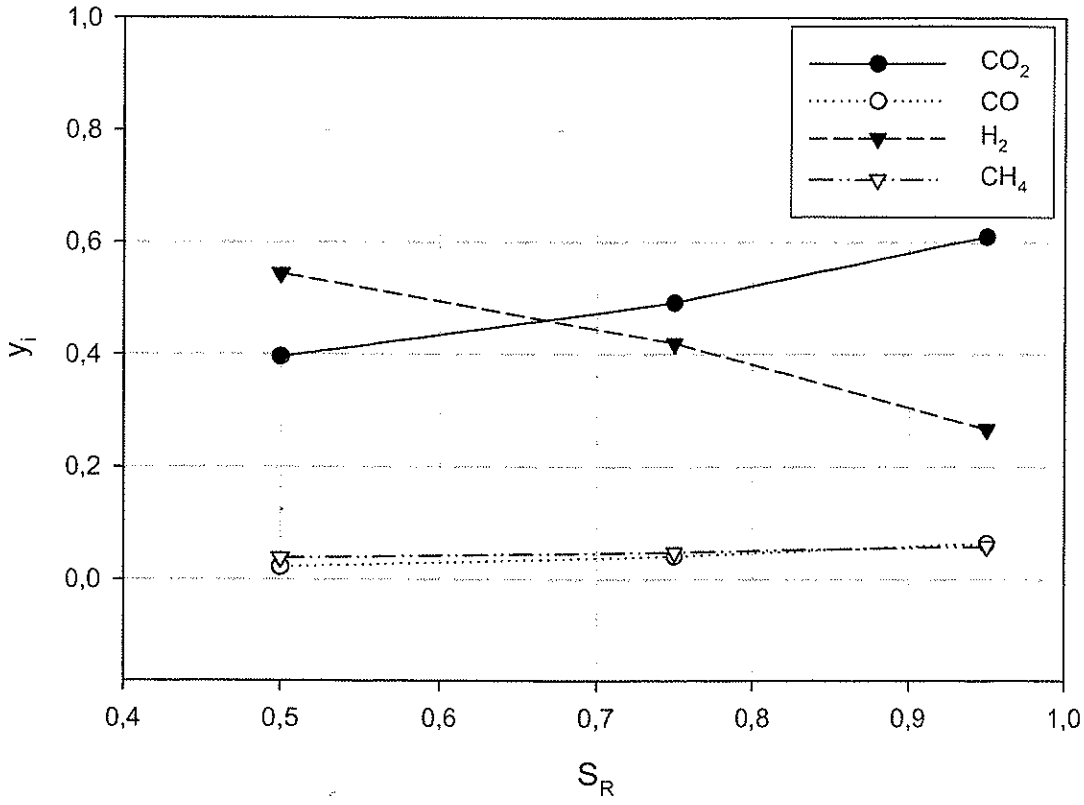

Figure 48 Calculated effluent composition, S=0.90

Note that calculated effluent compositions for S_R=0.95, closely match those obtained experimentally.

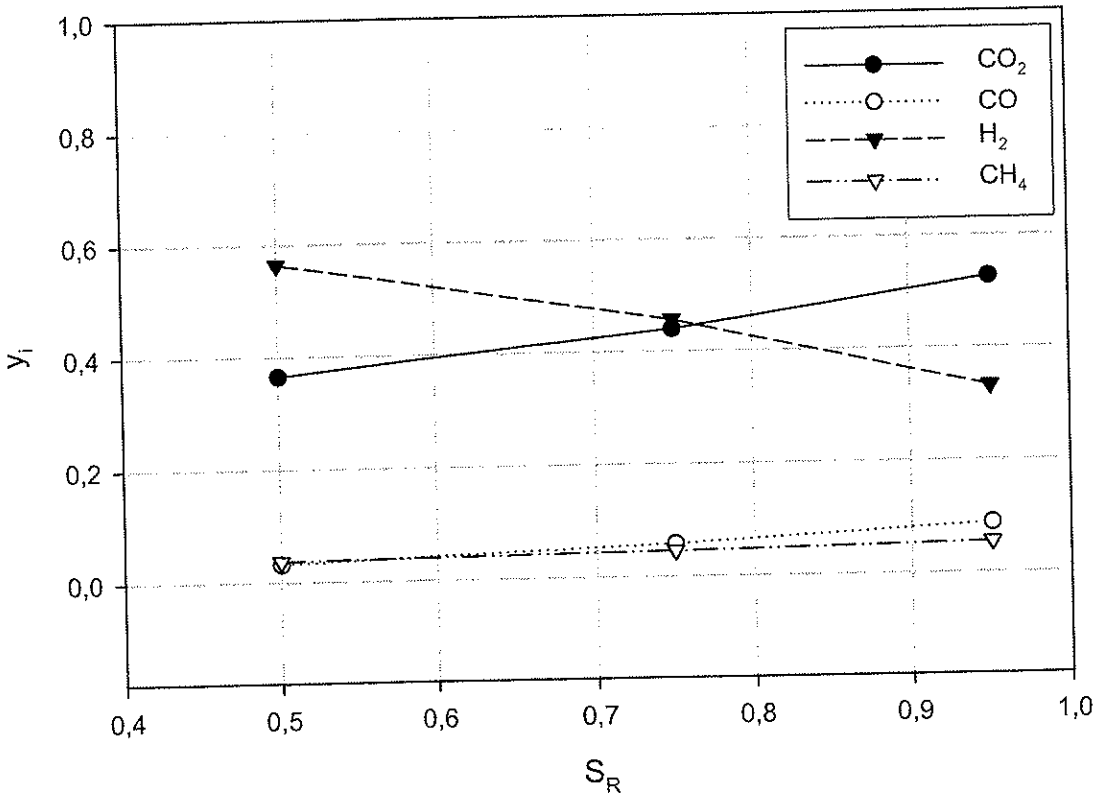

Figure 49 Calculated effluent composition, S=0.85

It can be seen that S is the overall governing factor for levels of hydrogen and CO, as well as the slopes of the curves, i.e. the sensitivity of composition y on S_R.

The combinations of S and Sr that give calculated effluent concentrations similar to those obtained experimentally in reduction with methane is (S=0.90, S_R=0.95).

Calculated values for H_2/CO-ratios are considerably higher that the observed 3.1. It is speculated that this is due to reduction of NiO by hydrogen. The extent of this competing reaction can not be accurately determined from the available data.

5.3.5 Solid mass flux estimation

Two fundamental approaches when determining the solid fluxes in CLC can be distinguished. Firstly, the fluxes can be determined on the basis of criteria in the heat balance of the reduction vessel, i.e. a certain amount of sensible heat needs to be transferred from the air reactor, to meet e.g. a temperature requirement in the reduction vessel. In this case, the composition of the solids as they leave reduction will be a variable quantity determined by the residence time and fuel feed rate at the design point. Alternatively, solid fluxes can be estimated from molar balances and stoichiometry.

For a given fuel feed rate, the necessary minimum influx of NiO to support the continuous conversion in the fuel reactor is given by reaction stoichiometry. Furthermore, the *difference in solid molar composition* (Δy_S) between the inlet and outlet streams, i.e. the fraction of NiO entering of the reduction reactor that is available for fuel reduction, is the overall governing factor for necessary total solids influx.

The necessary total solid influx is now found by correcting for the weight fraction of inert support in the solid. In Figure 50, reduction vessel solid influx as a function of Δy_S (assuming that $y_{S,OX}=1$) is calculated for NiONiAl ($\beta=0.6$) at different levels of overall selectivity, on the basis of 1.0 kg CH_4/s.

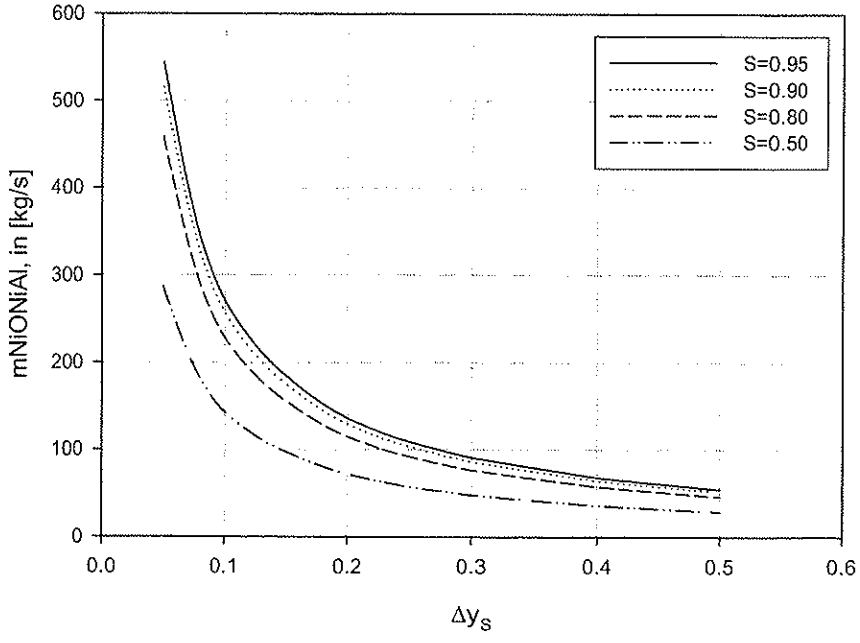

Figure 50 Calculated total solids influx pr kg methane feed, versus solid conversion difference

It can be seen that necessary solid influx increases dramatically for solid conversion differences below 0.2. The region above Δy_S=0.2 can be defined as the 'safe area' for CLC as the curves asymptotically approach the lowest theoretical mass flux, which is found for Δy_S=1.0. At this point, 100% of the oxygen in NiO is converted by oxidation of methane. This operating point can not be considered a realistic option, due to the previously mentioned tendency towards reforming at low NiO content. In section 5.3.3, long term Δy_S was estimated to 0.4 for particles with average residence time 130 s.

On the basis of 1 kg/s CH_4 necessary reduction solid influx in reduction is estimated according to the curve for S=0.90 at ≈68 kg NiONiAl.

Reduction outflux is dictated by the oxy-fuel nature of CLC, and found to be ≈64 kg reduced NiONiAl kg^{-1} methane, as 1 kg methane requires approximately 4 kg oxygen to be converted.

As expected, a decrease in selectivity has the effect of reducing the necessary solid influx, as less NiO is converted in DFR. Under the assumption that DFR is the only means by which NiO is converted, reforming selectivity, S_R, does not affect solid fluxes, apart from an increased solids outflux as a result of coking.

With reforming selectivity S_R=0.95, 2.3 kg/s CO_2 is generated in the reduction vessel while 0.037 kg/s coke is formed and transferred to the oxidation vessel where it is quantitatively converted to CO_2. The resulting emission of 0.13 kg /s CO_2 yields a CO_2 separation ratio of 94%, defined as the ratio of CO_2 in reduction exhaust to total CO_2 generated.

5.4 Study of regenerability

The batch of NiONiAl, previously subjected to 6 reduction/oxidation cycles in section 5.3, was repeatedly reduced and re-oxidized at a furnace set-point of 800°C, using methane and dry air as reactants. The exhaust concentrations of relevant species were monitored by on-line mass spectrometry. Bed temperature (2 cm above sinter) was also monitored during both reactions. A total of 25 cycles where carried out, in which each cycle consists of:

1) Time-controlled reduction with methane (TOS=150 s)

2) Reactor purge

3) Re-oxidation with dry air

4) Reactor purge.

Flowrates during the different part of the experimental cycle are given in Table 27.

Table 27 Flow data for reduction/oxidation cycle

	$V(CH_4)$ [mln/min]	**$V(N_2)$ [mln/min]**	**V(Air) [mln/min]**	**Time**
Reduction	250.0	250.0	0	t(red,start)-150 s
Reactor purge 1	0	500.0	0	2 min
Oxidation	0	0	500.0	12-13 min
Reactor purge 2	0	500.0	0	2 min

In order to find indications of changes in the chemical activity of the carrier as a result of repeated red/ox cycling, several parameters where defined based on representative MS-data and temperature measurements.

Temperature variables:

T_{Red}^{0}	Bed temperature at start of reduction [°C]
T_{Red}^{1}	Bed temperature at end of reduction (methane shutoff) [°C]
T_{Ox}^{0}	Bed temperature at start of oxidation [°C]
T_{Max}	Maximum bed temperature during oxidation [°C]

Time variables:

t_{Max}	Elapsed oxidation time at maximum bed temperature (T_{Max}) [s]
t_{O2}	Elapsed oxidation time when O_2 intensity starts to increase [s]
t_{Tot}	Elapsed oxidation time when O_2 intensity reaches a stable level (total oxidation time) [s]

In all cycles (except cycles 22&25), total reduction time is 150s. Cycles 22 & 25 are control experiments with reduction times of +/- 10% of the standard (i.e. 135 s and 165 s, respectively) to determine the sensitivity of the above parameters.

A representative chart of a typical reduction/oxidation cycle is given in Figure 51 which is a semi-logarithmic plot is of actual intensity versus time raw data for the relevant species (CH_4,CO_2, H_2 and O_2).

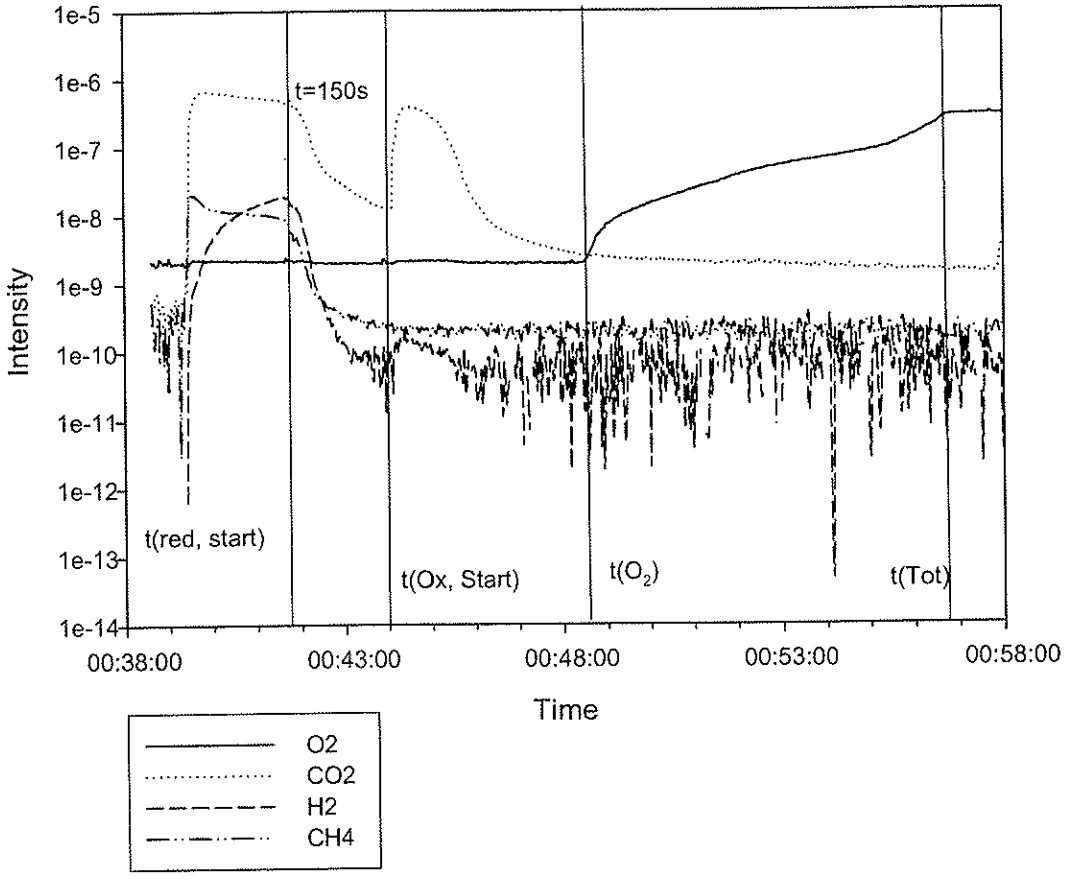

Figure 51 Representative intensity versus time chart, reduction/oxidation (cycle # 7)

The variations that can be seen for hydrogen and methane during the period of oxidation, is indicative of effluent concentrations at the detection limit, i.e. noise.

It should be noted that CO (M^+=28) was not monitored, since the oxidation air and inert bypass feed both contains N_2 (M^+=28) which would effectively mask the relatively small amounts of CO produced in reduction/oxidation. CO production in reduction using methane and reoxidation with air has been quantified in experiments with GC-analysis and found to be negligible.

General remarks

Reduction starts at t(red, start) and is characterized by near constant CO_2 production with some methane cracking and methane steam reforming (seen as H_2). Hydrogen production increases gradually during reduction, implying that reforming reactions are dependent on the availability of elementary nickel. At t=150 s methane supply is shut off, and the reactor is purged of any combustibles until t(Ox,start) when the supply valve is switched to feed dry air.

Oxidation is characterized by an initial phase when O_2 conversion is essentially 100% and any coke produced during reduction is oxidized to CO_2. The sharp increase in CO_2 is a useful reference point that marks the start of oxidation. It should be noted that full O_2 conversion is maintained for a period even after all coke is 'burned off', suggesting that reoxidation of nickel is quantitative initially. Oxygen concentration then starts to increase at time ($t(O_2)$) Subsequently, O_2 increases gradually (by a characteristic s-shaped curve) until a stable level is reached at time (t_{Tot}). It is assumed that a stable O_2 exhaust-concentration is indicative of a complete reoxidation of the material within the reactor.

Two control experiments where carried out in order to determine the sensitivity of the parameters towards changes in the chemical activity of the solid. In cycle 22, reduction time was set to 135s (-10%) while in cycle 25 reduction time was 165s (+10%).

Temperature data are unavailable for cycles 7 & 8.

Table 28 Regenerability overview, all temperatures in (°C), times in seconds

	REDUCTION			OXIDATION					
Cycle #	T_{Red}^{0}	T_{Red}^{1}	ΔT_{Red}	T_{Ox}^{0}	T_{Max}	ΔT_{Ox}	t_{Max}	$t(O_2)$	t(Tot)
7								271	741
8								274	759
9	785	694	-91	774	978	204	205	276	774
10	785	695	-90	775	981	206	196	266	765
11	786	695	-91	785	983	198	200	263	764
12	785	695	-90	770	985	215	205	272	765
13	786	695	-91	771	984	213	196	262	759
14	785	695	-90	772	987	215	207	263	765
15	786	694	-92	772	990	218	196	263	768
16	786	693	-93	772	992	220	196	266	768
17	786	692	-94	772	994	222	196	268	767
18	786	692	-94	772	994	222	203	266	765
19	786	692	-94	772	993	221	198	265	767
20	785	692	-93	772	992	220	197	260	761
21	785	690	-95	772	994	222	198	264	766
22	785	693	-92	772	993	221	195	249	630
23	785	689	-96	772	993	221	202	260	767
24	786	689	-97	772	993	221	198	257	758
25	785	690	-95	774	998	224	195	276	857
26	785	689	-96	772	995	223	199	257	784
27	786	689	-97	772	994	222	207	258	779
28	785	690	-95	772	993	221	201	250	781
29	785	689	-96	772	993	221	210	257	777
30	785	689	-96	774	992	218	203	256	780
31	786	689	-97	772	992	220	206	254	786
32	786	689	-97	772	991	219	210	249	779

In Figure 52, time to maximum bed temperature in oxidation (t(Max), time of full O_2 conversion ($t(O_2)$) and total re-oxidation time (t(Tot)), for each cycle are plotted.

In Figure 53, temperature increase/decrease in reduction and oxidation respectively are plotted for each cycle.

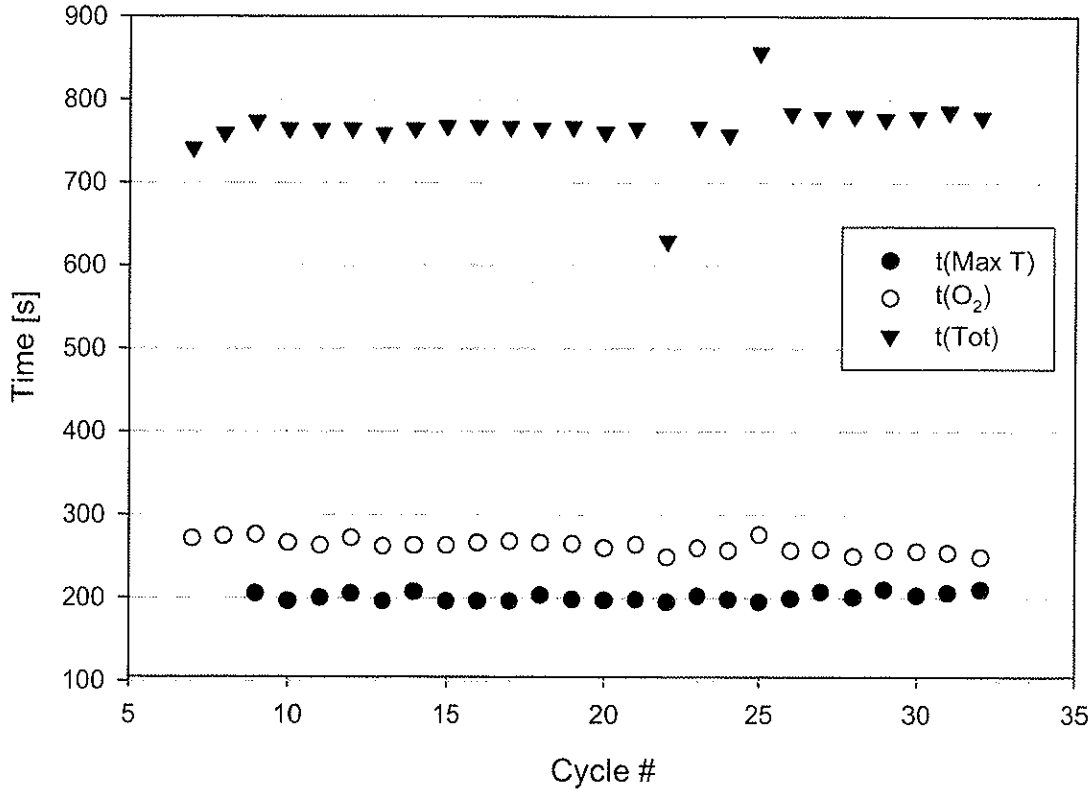

Figure 52 Oxidation time variables, cycle 22&25 are control experiments.

Control experiments of 10% shorter and longer reduction duration (cycle 22 & 25, respectively) are clear deviations from the average value for t(Tot), implying that the method is capable of detecting changes within this range of conversion.

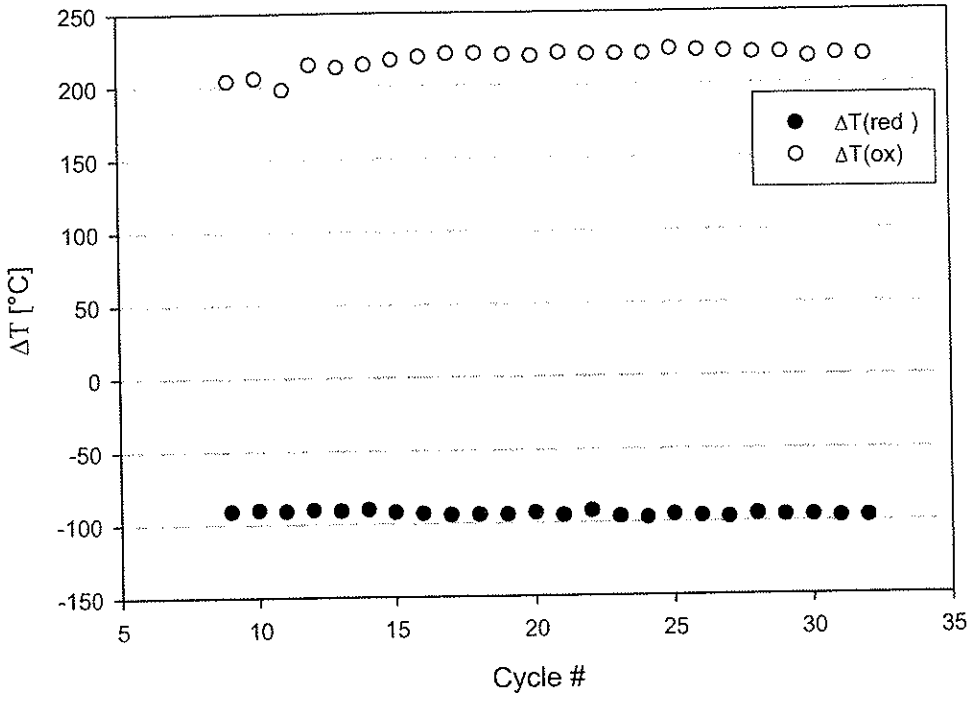

Figure 53 Temperature decrease/increase in reduction/oxidation respectively, cycle 20 & 23 are control experiments

A can be seen in Figure 52, the control experiments are characterized by a big impact on total oxidation time, and a slight impact on the time of full O_2 conversion. A 10% decrease in reduction time (cycle 22), gives a 4% decrease in t(O_2) and a comparatively larger effect is seen in t(Tot) which decreases with about 17%, as compared with average oxidation times for 150s reduction.

Similarly, 10% increase in reduction time (cycle 25), gives 6% increase in t(O_2) and 12% increase in t(Tot).

No significant changes can be seen in measured ΔT for reduction/oxidation for the control experiments, or in the time at which maximum bed temperature during oxidation is obtained. This indicates that these parameters cannot accurately be used to deduce changes in reactivity.

t(Tot) seems to be the best indicator of reactivity change, and interestingly, a slight change can be seen in the values for cycle 24 and onwards. Between

cycle 23 and 24 the reactor was idle overnight at 800°C with an inert flow of nitrogen (500ml/min). The slight shift of total reoxidation time from cycle 19 as compared to cycles 7-19 indicates that thermal stability of the carrier particles might be the most important factor regarding regenerability. It should also be noted that t(Tot) increases somewhat in cycle 7 & 8, until a relatively stable level is reached. This indicates that the gradual change in material properties that was observed in cycles 1-6, continues until cycle 9, after which the material appears to behave consistently.

From the MS-data (Figure 51), an estimation of the total amount of O_2 that has reacted during oxidation can be estimated by considering the different phases of re-oxidation. I.e. if one assumes full conversion (y_{O2}=0) from t=0 to t(O_2), and a *linear* increase in O_2 concentration until y_{O2}=0.21 in the period from t(O_2) to t(Tot), the amount of O_2 reacted becomes:

$$n_{O2} = n_{O2}^{0}\left(t_{O2} + \frac{(t_{Tot} - t_{O2})}{2}\right)$$

$$n_{O2} = y_{O2}^{0} \cdot \frac{P\dot{V}_{Air}}{RT^{0}}\left(t_{O2} + \frac{(t_{Tot} - t_{O2})}{2}\right)$$

$$n_{O2} = 7.162 \cdot 10^{-5}(\text{mol/s}) \cdot \left(266\text{s} + \frac{(765 - 266)\text{s}}{2}\right)$$

$$n_{O2} = 0.0369\,\text{mol}\,O_2$$

$$n_{Ni} = n_{O2} \cdot 2 = 0.0738\,\text{mol Ni}$$

In the above calculation, time-data for cycle 10 in Table 28 has been used, and coke oxidation is not considered. To check if the findings for fuel conversion and selectivity for cycle #6 at 600°C (Table 24) holds for cycle #10 at 800°C the amount of Nickel generated can be estimated:

$$n_{CH4,DFR} = \dot{n}_{CH4}^{0} \cdot \phi \cdot S \cdot t_R$$

$$n_{CH4,DFR} = 0.000171\,\text{mol/s} \cdot 0.92 \cdot 0.90 \cdot 150\text{s} = 0.0212\,\text{mol}\,CH_4$$

$$n_{Ni} = 4 \cdot n_{CH4,DFR} = 0.0848\,\text{mol Ni}$$

The findings for cycle# 6 (600°C) thus over-predicts the generated amount of nickel by ≈14% when compared to that which is estimated from MS-data for cycle#10 (800°C) when the material has apparently stabilized. This indicates that long term fuel conversion and/or selectivity is lower at 800°C than what was proposed for cycle #6 at 600°C. Another factor that might explain the

observed difference is that TOS is 150s in cycle#10, whereas it is 130s in cycle#6. The longer reduction time during regenerability experiments, will presumably result in lower average selectivity, since more nickel is present to catalyze reforming reactions during the final 20 seconds of reduction in Figure 51. Determining exactly what causes the difference is not possible with the present data, since effluent species have not been quantified by GC for cycle#10 onwards. It is speculated, however, that the biggest impact is for selectivity, which might be closer to 0.8 at 800°C for cycle#10 onwards.

5.5 *Oxidation of NiNiAl with air*

The re-oxidation of nickel represents the source of thermal energy within CLC. Measurements of the rate of oxidation at different temperatures is therefore of importance.

In order to investigate oxidation characteristics, NiONiAl (60% NiO by mass), m_b^0= 18.02 g, [0.2, > d_p > 0.02] mm, was first reduced with hydrogen until zero hydrogen conversion was observed (similar to Figure 38). It is assumed that near-complete reduction of NiO can be achieved in this way, but it is difficult to ascertain the exact value for $y_{S,R}$. Re-oxidation is then mediated by passing 500 mln/min dry air through the bed. The sequence was performed at 600, 700, 800 and 900°C, with MS-analysis of remaining O_2 in effluent.

Figure 54 is representative of the results and shows O_2 conversion versus time at 900°C.

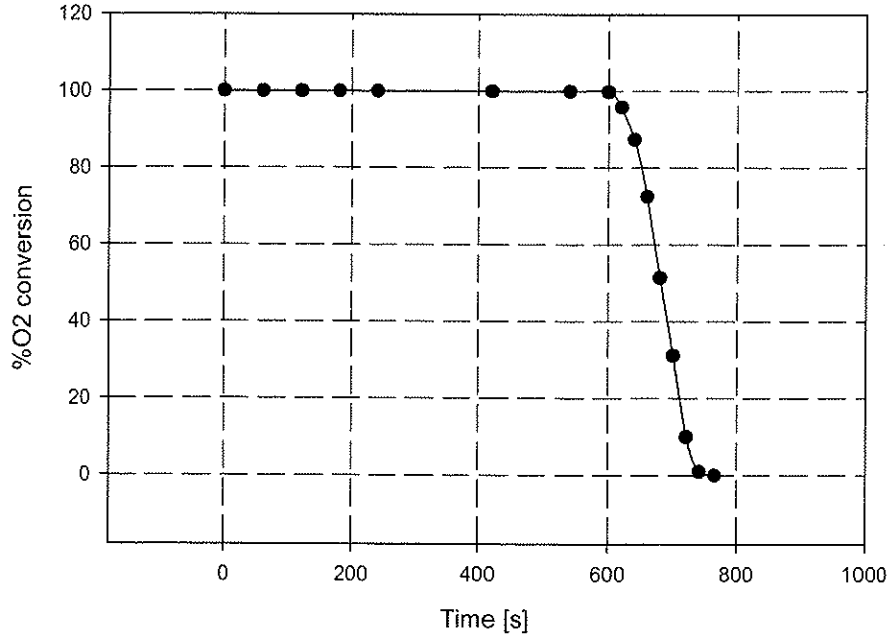

Figure 54 O_2 conversion in oxidation of NiONiAl (60%) at 900°C using dry air

The data clearly indicate that at 900°C re-oxidation generally is characterized by:

- Initial period of full O_2 conversion.
- Gradual decrease in O_2 conversion until full re-oxidation.

Note that the period of full O_2 conversion is significantly longer than in Figure 51 of the regenerability study, since the sample in the above figure is nearly completely reduced.

The temperature increase during a typical re-oxidation has been shown (section 5.4) to be 200-250°C with the current bed masses and reactant flow rates. This effectively limits furnace set-point for safe operation during oxidation to below 900°C as temperatures in excess of 1100°C could have adverse effects on the quartz reactor. All simulations of CLC have indicated that maximizing oxidation temperature is of critical importance (chapter 3) and should ideally be at least 1000°C.

Additionally, the most suitable configuration of the oxidation vessel in a continuous, moving bed CLC-unit has been assumed to be a transport reactor with high superficial velocity. The reactor at hand does not facilitate experiments with material transport.

As a result of these limitations, oxidation cannot be studied under conditions similar to those of an operational CLC-plant, with the present equipment.

The results that have been compiled on oxidation of nickel are encouraging nonetheless and point the way to further investigation (chapter 7). Even at relatively low (as compared to ideal) temperatures (600-900°C) in a bubbling fluidized bed, oxidation is found to be quantitative during the conversion of the bulk of the available nickel. Conversion of the least accessible nickel in the carrier is characterized by a gradual decrease in reactant conversion.

5.6 Reduction and oxidation of perovskite with methane-air

As a comparative study, a batch of perovskite ($La_{0.8}Sr_{0.2}Co_{0.2}Fe_{0.8}O_3$))synthesized by the procedure given in section 4.5.2, was subjected to reduction/oxidation using methane/steam and dry air, respectively. Initial bed mass, m_b^0=23.3 g, cut size [0.2< d_p < 0.09] mm. A water feed rate of 0.4 ml/min was used throughout, with variable methane flow of 250 mln/min, yielding a steam to carbon ratio S/C=2.

5.6.1 General characteristics

Inspection of Figure 55 and comparison with the results obtained from NiONiAl, provide strong indications that this perovskite will have difficulty competing with NiONiAl as an oxygen carrier in CLC.

A similar bed mass (23.3 g) yields a relatively small amount of CO_2, indicating that the perovskite has a very small amount of oxygen available for direct fuel reduction, as compared to NiONiAl..

Whereas CO_2 production remained on a high level for 150-200 seconds with the same feed rate of methane in experiments with NiONiAl, the all available oxygen is consumed within 20 seconds for this particular perovskite. The perovskite is found to be a poor catalyst for reforming as methane conversion effectively decreases to zero after reduction has been completed. Low levels of hydrogen indicate that carbon formation by methane pyrolysis is negligible with S/C=2. The re-oxidation of the material is seen to proceed with full O_2 conversion, until all solids are regenerated and effluent O_2 content abruptly returns to a stable level, indicating that no reaction takes place.

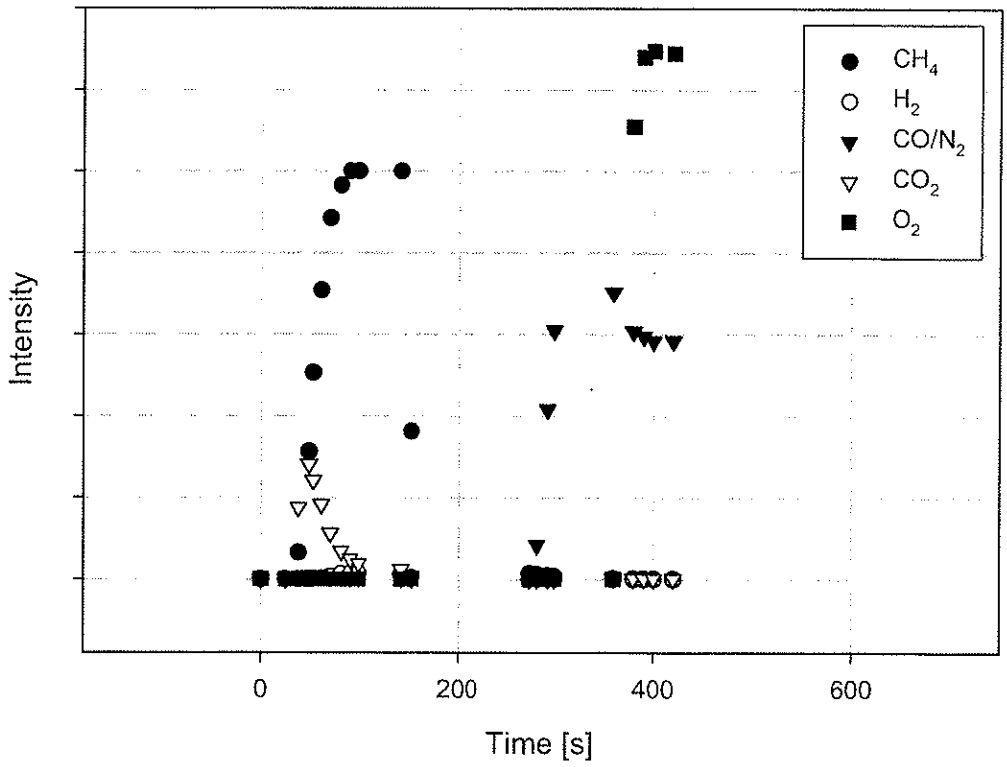

Figure 55 Reduction/oxidation of perovskite with methane/steam at 900°C, (S/C=2) and air/steam.

The abrupt return of O_2 level following the period of full O_2 conversion indicates that perovskites are more easily regenerated than NiONiAl.

5.6.2 Determination of delta

It has been observed that a steam carbon ration (S/C) of at least 1 is necessary to avoid coking.

Neglecting coking, the numerical value of δ can be found by estimating the number of O_2 equivalents that are consumed during reoxidation:

$$MeO_{3-\delta} + \delta/2\, O_2 \longrightarrow MeO_3 \qquad (5.7)$$

The number of oxygen equivalents that have been absorbed by the perovskite can be estimated by measuring the re-oxidation time (τ_{ox}), i.e. time under

which re-oxidation is quantitative, and multiplying with the air flowrate from the ideal gas law:

$$n_O = 2 \cdot \tau_{ox} \cdot \dot{n}_{O_2} = 2 \cdot \tau_{ox} \cdot \frac{0.21 \cdot \dot{V}_{Air}}{RT^0} \qquad (5.8)$$

Furthermore, the number of oxygen equivalents necessary for full reoxidation is related to δ, via the total number of oxygen equivalents and the stoichiometric coefficient for oxygen:

$$\frac{n_O}{\delta} = \frac{n_{O,Tot}}{3} \qquad (5.9)$$

This was carried out for the re-oxidations following short reduction periods, thus effectively eliminating coking.

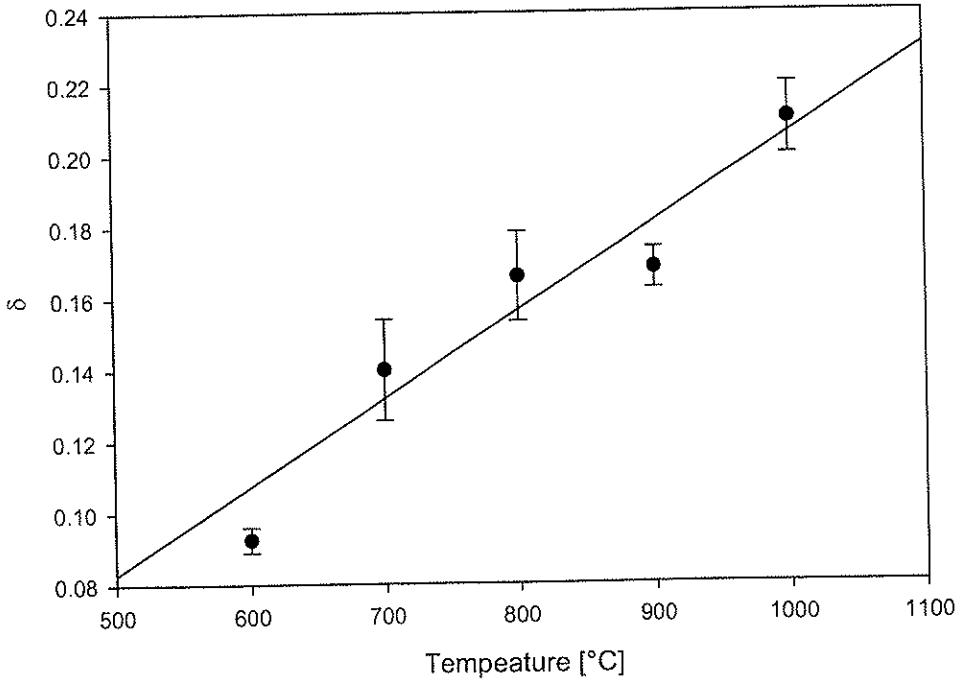

Figure 56 Average delta-values with error bars (standard deviation) versus furnace set point

The results appear to be consistent with unpublished data obtained in TGA experiments involving the same perovskite (personal reference, Yngve Larring).

Table 29 Estimation of delta

	Parallels				
T [°C]	**Exp #1**	**Exp #2**	**Exp #3**	**Exp #4**	**Average δ**
1000	0.22	0.20	0.21	-	0.21
900	0.17	0.16	0.17	0.173	0.169
800	0.18	0.164	0.17	0.15	0.167
700	0.12	0.14	0.15	0.15	0.146
600	0.09	0.095	-	-	0.09

Due to instabilities in the flow characteristics at the time, the MS data for some experiments is compromised.

It must be concluded that the precision of this method is not satisfactory and the results thereof should be regarded with considerable skepticism. More accurate methods should be used to accurately determine delta, but the results have value nonetheless as they clearly indicate of the main problem associated with the use of perovskites in a moving bed CLC-application: low available oxygen content relative to the total mass of carrier.

5.7 Miscellaneous experiments

Two supplementary experiments where carried out to provide additional data on structural and chemical changes as a result of repeated reduction/oxidation.

5.7.1 Scanning Electron Microscopy

A batch of 60% NiO on $NiAl_2O_4$, 0.09 <d_p<0.2 mm was prepared according to procedure given in chapter 4. From this batch two samples where obtained.

Sample 1: Taken from fresh batch of 60% NiO on $NiAl_2O_4$, 0.09 <d_p<0.2 mm

Sample 2: Collected from fluidized bed reactor after 14 completed reduction/oxidation cycles using methane/steam and air/steam at 800°C. To ensure full oxidization, dry air was fed to reactor

at 800°C for 1 hour before shutting down the rig and extracting the sample.

SEM images where obtained with the assistance Leiv Kolbeinsen and additional personnel from the Department of Materials Technology, NTNU, Norway.
Selected SEM images obtained from the samples are given in appendix D.

Whereas individual grains and crystal-facets are clearly visible in images of Sample 1, Sample 2 is characterized by a 'fused' structure with much less visible crystal-facets.

It is hypothesized that the observed change in material properties seen in experiments with dry methane and methane/steam is caused by sintering of individual grains, and possibly phase-separation producing a significant amount of elementary nickel, not readily re-oxidizable and capable of catalyzing steam reforming and methane pyrolysis throughout the course of the reaction.

5.7.2 X-ray diffraction analysis

Sample 1 & 2 in the previous section was also analyzed by XRD (by SINTEF personnel), to detect possible phase-changes as a result of repeated red/ox cycling.

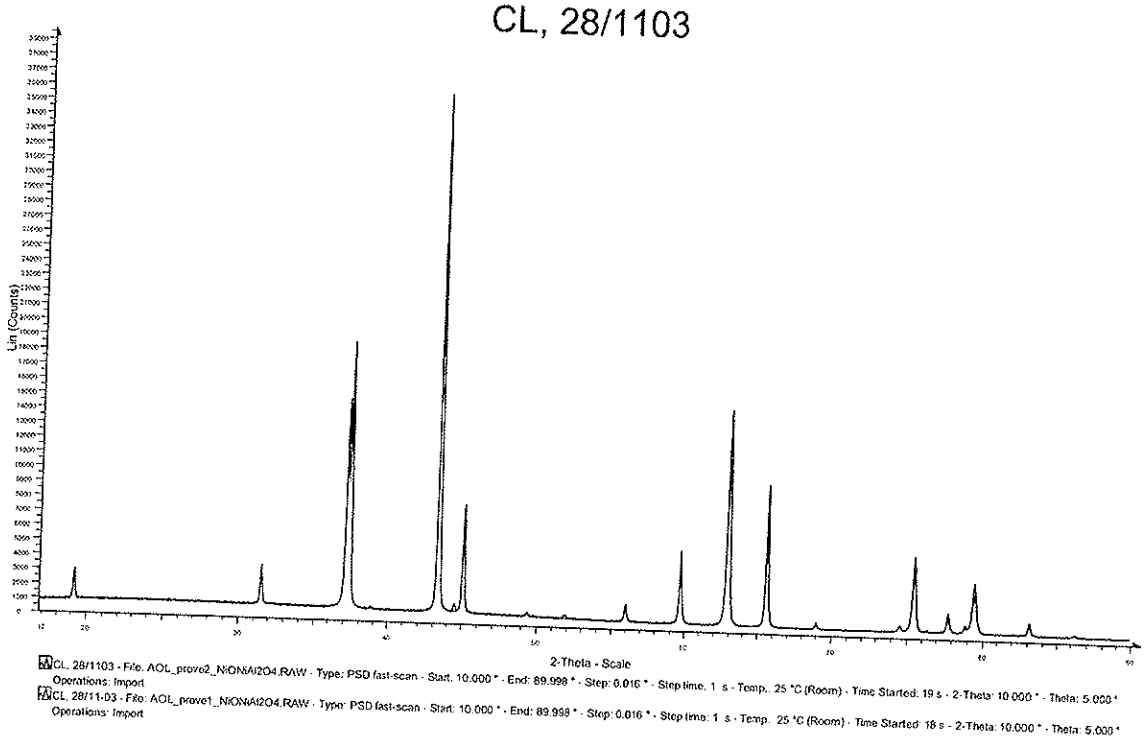

Figure 57 XRD-recording, sample 1 (red) & sample 2 (black)

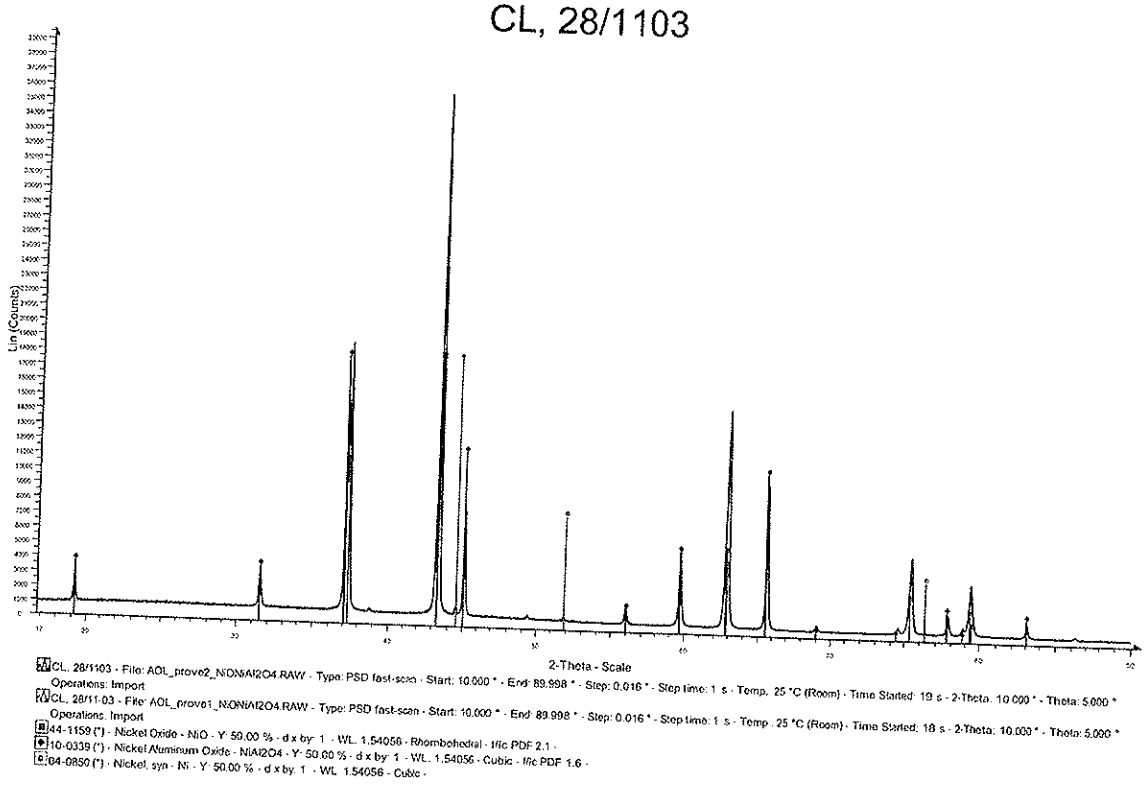

Figure 58 XRD-recording, peak matching

Correlation of signals with PDF database confirms the presence of nickel oxide (NiO) and spinel ($NiAl_2O_4$). Furthermore it can be concluded that samples are quite similar with regards to gross phase-composition, i.e. there are no major changes in phase distribution. In sample 2, however, signals (green) corresponding to elementary Nickel can be seen.

In can be concluded that repeated cycling of the material is accompanied by the formation of minor amounts of elementary nickel, not readily converted to nickel oxide upon re-oxidation.

This finding supports the observed decrease in material selectivity towards direct fuel reduction.

6 CONCLUSIONS

Chemical Looping Combustion has been investigated by means of process simulations and experimental work. Process simulations have focused on overall cycle efficiency of power cycles implementing CLC, and identification and quantification of important process parameters with regard to efficiency. The experimental work has focused on characterization of oxygen carriers, with determination of reactant- and solids conversion and durability.

Process simulations

CLC has promising thermodynamic potential as a power/heat generation concept. Main advantages are inherent CO_2 separation without the need for separation equipment, potentially high efficiencies and reduced irreversibilities as a result of reaction splitting. All cycles yield highly concentrated CO_2 and oxygen depleted air as product streams.

The CLC-related parameters that have the highest impact on cycle efficiency are found to be oxidation reactor inlet and outlet temperatures, operating pressure and extent of fuel conversion.

A combined gas turbine and steam turbine cycle with chemical looping combustion, using state-of-the art assumptions for unit operation properties and 1200 °C oxidation and reduction temperatures, has a net plant efficiency approaching 53%, including CO_2 compression to 100 bar. The cycle employs NiONiAl and natural gas.

CLC was also evaluated for use in a humid air turbine (HAT) concept, and found to have a net plant efficiency of 51%, including CO_2 compression. The cycle employs NiO on YSZ and methane.

The most likely short term candidate for implementation of CLC in a power/heat generating cycle is an atmospheric oxidation/reduction process with internal steam generation (ISG), where the steam is utilized in a conventional steam cycle. Cycle net plant efficiency is found to be around 41%, including CO_2 compression. The cycle employs NiONiAl, and natural gas.

Experimental work

The investigation of NiONiAl as an oxygen carrier in CLC, have concluded that a reduction reactor, using NiONiAl and dry methane, will be a partial reforming/solid-reduction reactor. At a reduction temperature of 600°C, an estimated 90% of the methane reacts via the desired pathway of direct fuel conversion (DFR) while the remainder of the fuel is converted in reforming reactions. Steam methane reforming (SMR) is the dominating reforming reaction but minor amounts of coke is also formed, presumably via methane cracking (MC). Long term reduction exhaust compositions on a dry basis have been measured at 60-65% CO_2, 22-25% H_2, 7-8% CO and 7-8% unconverted CH_4.

Coking can be avoided entirely, if a mixture of methane/steam is used as fuel. A steam to carbon ratio of 2 is required to suppress coking mechanisms. The experimental data indicates, however, that the addition of steam might further promote SMR by virtue of higher water vapor abundance. The added complexity and energy demands involved in using methane/steam as fuel should thus be weighed against a certain emission of CO_2.

The heat potential of CLC generally lies within regeneration of the reduced form of the oxide. Re-oxidation of nickel with dry air has been found to be initially rapid at 800°C, but having limited rates at high solid NiO-content ($y_S \rightarrow 1.0$). From a thermodynamic perspective, oxidation temperature should be maximized, and ideally be carried out at temperatures from 1000-1200°C. Oxidation reaction temperature was limited to below 1000°C due to reactor material specifications being exceeded by oxidation temperature increase. Hence, oxidation characteristics above 1000°C can not be firmly concluded upon.

On the basis of experimental data, necessary solid fluxes in a continuous CLC-plant have been estimated. Apart from overall fuel feed rate, solid fluxes are dependent on the attainable solid composition difference between oxidation and reduction vessels (Δy_S), overall reduction selectivity (S) and ratio of oxygen transferring component to total mass (β). When methane is used as fuel, required reduction influx is found to be ≈68 kg NiONiAl kg^{-1} CH_4. Oxidation reactor solids influx is estimated at ≈64 kg NiONiAl kg^{-1} CH_4. The calculation is based on the assumption that solid molar composition (y_S) is 0.6 at reduction exit, and 1.0 at reduction inlet, β=0.60 and S=0.90.

A methodology for investigation of long term durability of NiONiAl has been proposed. NiONiAl behaves initially as an ideal oxygen carrier, with

near quantitative conversion of fuel to carbon dioxide. During the first 6 cycles, however, material properties change significantly, resulting in reduced selectivity towards direct fuel conversion and higher tendency towards reforming. From the 6^{th} to the 32^{nd} red/ox cycle, little change in material selectivity is observed. It is hypothesized that the initial change in material properties is related to the formation of elementary nickel agglomerates separated from the spinel matrix, -in which the bulk of the nickel/nickel oxide is distributed. The agglomerates are not reactive towards oxidation, thus providing readily accessible catalytic sites from the beginning of batch reduction and onwards. This thesis is supported by scanning electron images and x-ray diffraction analyses, but further study is required to firmly conclude.

A Perovskite ($La_{0.8}Sr_{0.2}Co_{0.2}Fe_{0.8}O_{3-\delta}$) has been investigated as a potential oxygen carrier. The advantage of rapid and quantitative oxidation is found to be outweighed by severely limited relative oxygen capacity. Oxygen availability (δ) has been determined at different temperatures and found to be consistent with thermo-gravimetric experiments.

The results from methane reduction of NiONiAl indicate that complete conversion of fuel to CO_2 and water vapor is not feasible in a single gas-solid reaction vessel. This is due to the tendency of elementary nickel to catalyze reforming reactions, and herein lays the main disadvantage of nickel based carriers. However, reduction of NiONiAl with hydrogen has been shown to proceed with excellent reactant conversion at temperatures above 600°C, and this indicates that a dual reactor set-up could be a working solution to the problem. A second alternative is to utilize the properties of nickel as a reforming catalyst, and operate the fuel reactor as a steam methane reforming unit. These alternatives are elaborated further in the following chapter. Thirdly, it might be argued that nickel based materials are inherently unsuitable for CLC, by virtue of the catalyzing properties of nickel towards competing reactions. The focus of the research may thus be shifted towards metal oxides in which the reduced form of the oxide does *not* catalyze reforming reactions.

The principal question of CLC is whether a set of heterogeneous gas-solid reactions can effectively substitute conventional, homogenous fuel combustion. Since long-term mechanical and chemical integrity of oxygen carriers has not been investigated in the present work, it is still too early to conclude on the feasibility of CLC as a power generating concept. The present results does not rule out CLC as an alternative, however, and

considering the thermodynamic potential that has been observed, it would seem appropriate to continue exploring the concept.

7 FURTHER WORK

The present work points the way to further studies with regard to process simulations and experimental work.

7.1 Modeling and process simulation

1. Further investigation of CLC cycles, implementing experimental findings

Existing models of CLC should be refined to incorporate the essential experimental findings. This principally influences solid conversion and the composition of the reduction exhaust. Subsequent simulations should therefore focus on finding the best method to utilize the chemical energy present in hydrogen and carbon monoxide found in the exhaust of a CLC reduction reactor.

A dual-vessel fuel conversion stage might be a working solution, and should include a primary converter and a secondary countercurrent plug-flow reactor. The primary converter may be designed as a continuous stirred reactor, converting the bulk of the fuel to CO_2, H_2, CO, H_2O and CH_4. A secondary converter, ideally operated as a counter-current plug-flow reactor, is capable of handling the byproducts of the former reactor, converting H_2 to water vapor and elementary nickel, CO to CO_2 and H_2 via the water gas-shift reaction, and possibly the remaining fuel. Keeping in mind the results obtained in hydrogen reduction, introduction of fresh oxygen carrier (from the oxidation vessel) near the reactor exit should reduce secondary exhaust H_2 content to negligible levels.

As pointed out in the previous chapter, CLC might be employed as a method for co-producing hydrogen and heat/power. In such a set-up, the fuel reactor acts as a syngas production stage in which the catalyst is intermittently regenerated by oxidation with air. Provided that solid residence times in reduction are sufficient, NiONiAl with methane/steam has been demonstrated to yield a hydrogen-rich exhaust, closely resembling that associated with SMR equilibrium. Implementing a secondary water gas shift reactor, with subsequent CO_2 separation, the hydrogen thus produced can be utilized in the same way as for existing PCDC-schemes. The oxidation reactor can be

operated independently of the nature of the fuel reactor(s) and regenerates NiO exothermally, thus providing power or heat for internal process requirements or external recipients.

Another approach might involve a Solid Oxide Fuel Cell utilizing the CO_2-rich 'syngas' from a single CLC reduction stage. It can be argued, however, that the coupling of two immature technologies introduces excessive technical uncertainties, and that simpler methods should be investigated first.

A conventional afterburner could readily convert the remaining combustibles in the reduction exhaust emitted from a single CLC reduction vessel. However, the dilution of the already-produced CO_2 with nitrogen would seriously compromise the characteristic advantages of CLC with regard to CO_2 capture. Pure oxygen might be used, but implementation of an ASU would arguably increase complexity and reduce efficiencies significantly.

A 'reheat gas turbine cycle', should be investigated as a method to optimize oxidation exhaust temperature prior to expansion, if material constraints limit TIT to below 1000°C. Two schemes might be envisioned; applying post-oxidation exhaust heating, or so-called multi-stage CLC. In the former, secondary fuel is combusted prior to expansion, thus increasing TIT to 1300°C. The CO_2 formed in secondary heating will not be captured. In multi-stage CLC, oxidation exhaust is extracted from one stage of the turbine and subsequently re-heated in a second CLC unit before being injected in the next turbine. The scheme might include 2-3 CLC units, and has the added advantage that all CO_2 is captured.

2 Part load performance, control strategy and transient behavior

Following initial design-point simulations, off-design evaluation of CLC is the next logical step in the development of the concept. The study should include various load conditions and account for variations in the ambient temperature. As follow-ups to this, the control strategies and dynamic behavior of CLC should be explored.

3 Reactor system modeling

The reactors in CLC have been highly idealized in the present work. Realistic estimates of required solid fluxes are now available as a result of the experimental work. These findings should be included in a sophisticated reactor model for a dual vessel reactor system consisting of, e.g. a bubbling

fluidized bed and a CFB riser. Average residence times, pressure drops and internal solid recirculation in the riser should be the main focus of the investigation.

7.2 Experimental work

1 Pulse experiments for rapid screening of oxygen carriers

Firstly a large number of oxygen carriers on different supports should be synthesized. Among the most promising active components besides NiO are CuO and CoO. The most efficient way to validate potential oxygen carriers at an early stage is by TPX (Temperature Programmed Reduction/Oxidation). This instrument allows for rapid cycling of a small amount of carrier in a highly repeatable way with acceptable manual work. The investigation should include nickel oxide on different supports, to determine if other combinations of nickel oxide and an inert binder might yield a material with better long-term selectivity towards DFR.

2 Long term durability study of NiONiAl

Long term regenerability studies (>>100 cycles) in an alternating reduction/oxidation batch reactor should be carried out. Automated valves and computer assisted analysis (e.g. using Labview) should be applied to reduce the necessary amount of manual labor. The general methodology outlined in section 5.5 should be applied to monitor changes in reactivity.

3 High temperature data for oxidation in a CFB

As discussed in chapter 5, uncertainties still remain with regard to the estimation of oxidation rates under the conditions that have been assumed in simulations. Although not without practical problems, data on oxidation in a transport reactor at 1200°Cwould be highly valuable. A temperature resistant reactor operated at high superficial air velocity is necessary. Transported solids should be collected and recycled.

4 Experiments at elevated pressure

The effect of pressure on the reaction mechanisms found in reduction should be investigated. The existing rig at SINTEF Chemistry, Oslo (Rig-II) is

suitable with the prerequisite that suitable analytical equipment for quantification of exhaust is installed. Infrared spectrometry (IR) is a natural choice as far as analytical method is concerned.

5 Dual vessel CLC pilot plant

The ultimate test for CLC is a pressurized, small scale reactor system with solid circulation. Such a pilot plant is currently being operated at Chalmers, Gothenburg, Sweden, and the results thereof are awaited with considerable excitement.

8 REFERENCES

Journal articles directly related to chemical looping combustion (in chronological order)

Richter H.J., Knoche K., **1983,** *"Reversibility of Combustion processes"*, Efficiency and Costing – Second Law Analysis of Processes, ACS Symposium series 235, p. 71-85

Ishida M., Zheng D., Akehata T., **1987**, *"Evaluation of a chemical-looping-combustion power-generation system by graphic exergy analysis"*, Energy, vol. 12, p. 147-154

Harvey S. P., Richter H. J., **1994**, *"A high efficiency gas turbine power generation cycle with solid oxide fuel cell technology and chemical looping combustion"*, AES-vol33, Thermodynamics and the Design, Analysis and improvement of energy systems ASME, p. 65-76

Ishida M., Jin H., **1994a,** *"A novel combustor based on chemical-looping reactions and its reaction kinetics"*, Journal of Chemical Engineering of Japan, vol. 27, No. 3, p. 296-301

Ishida M., Jin H., **1994b**, *"A new advanced power-generation system using chemical-looping combustion"*, Energy, vol. 19, No. 4, p. 415-422

Anheden M., Nesholm A. S., Svedberg G., **1995**,*"Chemical-looping combustion - Efficient conversion of chemical energy in fuels into work"*, Intersociety Energy Conversion Engineering Conference, vol. 30, p. 75-81

Anheden M., Svedberg G., **1996**, *"Chemical-looping combustion in combination with integrated coal gasification"*, Intersociety Energy Conversion Engineering conference, vol. 31, p. 2045-50

Ishida M., Jin H., **1996**, *"A novel Chemical-Looping Combustor without NOx Formation"*, Research Notes, Industrial and Engineering Chemistry, vol. 35, p. 2469-2472

Ishida M., Jin H., Okamoto T., **1996**, *"A fundamental study of a new kind of medium material for chemical-looping combustion"*, Energy & Fuels, vol. 10, p. 923-963

Hatanaka T., Matsuda S., Hatano H., **1997**, *"A new-concept gas-solid combustion system "MERIT" for high combustion efficiency and low emissions"*, Proceedings of the 32nd Intersociety Energy Conversion Engineering Conference, p. 944-947

Ishida M., Jin H., **1997**, *"CO_2 recovery in a power plant with chemical looping combustion"*, Energy Conversion and Management, vol. 38, Suppl., p. 187-192

Anheden M., Svedberg G., **1998**, *"Exergy analysis of chemical-looping combustion systems"*, Energy conversion and management, vol. 39, no. 16-18, p. 1967-1980

Ishida M., Jin H., **1998**, *"CO_2 recovery without energy penalty: A novel Chemical Looping Combustion"*, The 2nd Int. Workshop on ZEPP ULG., Belgium, January

Ishida M., Jin H., Okamoto T., **1998a**, *"Development of a novel chemical-looping combustion: Synthesis of a looping material with a double metal oxide of CoO-NiO"*, Energy & Fuels, vol. 12, p. 1272-1277

Ishida M., Jin H., Okamoto T., **1998b**, *"Kinetic behavior of solid particle in chemical-looping combustion: Suppressing Carbon deposition in reduction"*, Energy & Fuels, vol. 12, p. 223-229

Ishida M., Jin H., **1999**, *"Greenhouse gas control by a novel combustion: No energy penalty and no CO_2 separation equipment"*, Greenhouse Gas Control Technologies, Proceedings of the 4th International conference on Greenhouse Gas Control Technologies, 30 Aug – 2 Sep 1998, Interlaken, Switzerland, p. 627-632

Jin H., Okamoto T., Ishida M., **1999**, *"Development of a novel chemical-looping combustion: Synthesis of a Solid looping material $NiO/NiAl_2O_4$"*, Industrial and Engineering Chemistry Research, vol. 38, p. 126-132

Jin H., Ishida M., **2000,** *"A novel gas turbine cycle with hydrogen-fueled chemical-looping combustion"*, International Journal of Hydrogen Energy, vol. 25, no 12, p 1209-1215

Brandvoll Ø., Bolland O., Vestøl S., **2001**, *"Chemical Looping Combustion-Fuel Energy Conversion with inherent CO_2 capture"*, paper published in the proceedings of The International Conference Power Generation And Sustainable Development, Liege, Belgium, 8-9 October

Jin H., Ishida M., **2001**, *"Reactivity study on a novel hydrogen fueled chemical-looping combustion"*, International Journal of Hydrogen Energy, vol. 26, p 889-894

Lyngfelt A., Leckner B., Mattisson T., **2001**, *"A fluidized-bed combustion process with inherent CO2 separation"*, Chemical Engineering Science, vol. 56, no. 10, Jun 12, 2001, p 3101-3113

Mattisson T., Lyngfelt A., Cho P., **2001**, *"The use of iron oxide as an oxygen carrier in chemical-looping combustion of methane with inherent separation of CO_2"*, Fuel, vol. 80, no. 13, p. 1953-1962

Ryu H.J., Bae D.H., Han K.H., Lee S.Y., Jin G.T., Choi J.H., **2001**, *"Oxidation and reduction characteristics of oxygen carrier particles and reaction kinetics by unreacted core model"*, Korean Journal of Chemical Engineering, vol. 18, no. 6, p. 831-837

Ishida M., Yamamoto M., Ohba T., **2002**, *"Experimental results of chemical-looping combustion with NiO/NiAl2O4 particle circulation at 1200°C"*, Energy Conversion and Management, vol. 43, p. 1469-1478

Jin H., Ishida M., **2002**, *"Reactivity study on natural-gas-fueled chemical-looping combustion by a fixed-bed reactor"*, Industrial and Engineering Chemistry Research, vol. 41, no. 16, Aug 7, p 4004-4007

Copeland R.J., Alptekin G., Cesario M., Gershanovich Y., **2002**, *"Sorbent energy transfer system (SETS) for CO2 separation with high efficiency"*, Presented on the 27th International Conference on Coal utilization & Fuel Systems, Clearwater, Florida, March 4-7

Gabbrielli R, Singh R., **2003**, *"Thermodynamic performance analysis of new gas turbine combined cycles with no emissions of carbon dioxide"*, Journal of Engineering for gas and Power and Power-Transactions of the ASME, vol. 125, no. 4, p. 940-946

Brandvoll Ø., Olsen N., Bolland O., **2003**,"*Chemical Looping Combustion – Reduction of nickel oxide/nickel aluminate with hydrogen*", Chemical Engineering Transactions, vol. 3, p 105-110

Johansson E., Lyngfelt A, Mattisson T., Johnsson F., **2003**, *"Gas leakage measurements in a cold model of an interconnected fluidized bed for chemical-looping combustion"*, Powder Technology 134, p. 210-217

Mattisson T., Järdnäs A., Lyngfelt A., **2003**, *"Reactivity of some metal oxides supported on alumina with alternating methane and oxygen-application for Chemical-Looping combustion"*, Energy & Fuels, v 17, p 643-651

Villa R., Cristiani C., Groppi G., Lietti L., Forzatti P., Cornaro U., Rossini S., **2003**, *"Ni based mixed oxide materials for CH4 oxidation under redox cycle conditions*", Journal of Molecular Catalysis A-Chemical, vol. 204, p. 637-646

Yu J., Corripio A.B., Harrison D.P., Copeland R.J., **2003,** *"Analysis of the Sorbent Energy Transfer System (SETS) for power generation and CO_2 capture"*, Advances in Environmental Research, vol. 7, p. 335-345

Adánez J., de Diego L.F., García-Labiano F., Gayán P., Abad A., Palacios J.M., **2004**, *"Selection of Oxygen Carriers for Chemical-Looping Combustion"*, Energy & Fuels, vol. 18, p. 371-377

de Diego L.F., García-Labiano F., Adánez J., Gayán P., Abad A., Corbella B.M., Palacios J.M., **2004**, *"Development of Cu-based oxygen carriers for chemical-looping combustion"*, Fuel, vol. 83, p. 1749-1757

Brandvoll Ø., Bolland O., **2004**, *"Inherent CO_2 Capture Using Chemical Looping Combustion in a Natural Gas Fired Power Cycle"*, Journal of Engineering for Gas Turbines and Power, vol. 126, p. 316-321

Cho P., Mattisson T., Lyngfelt A., **2004** *"Comparison of iron-, nickel-, copper- and manganese-based oxygen carriers for chemical-looping combustion"*, Fuel, vol. 83, p. 1215 -1225

Jin H., Ishida M., **2004**, *"A new type of coal gas fueled chemical-looping combustion"*, Fuel, vol. 83, p. 2411-2417

Lyngfelt A., Kronberger B., Adánez J., Morin J.-X., Hurst P., **2004**, *"The Grace Project. Development of oxygen carrier particles for Chemical-*

Looping Combustion. Design and operation of a 10kW Chemical-Looping Combustor", Presented at GHG7, Vancouver, Canada, 5-9 september 2004

Mattisson T., Johansson M., Lyngfelt A., **2004**, *"Multicycle Reduction and Oxidation of Different Types of Iron Oxide Particles- Application to Chemical-Looping Combustion"*, Energy & Fuels, vol. 18, p. 628-637

Naqvi R., Bolland O., Brandvoll O., Helle K., **2004**,*"Chemical Looping Combustion, Analysis of natural gas fired power cycle with inherent CO_2 capture"*, Paper submitted to ASME turbo expo 2004, 14-17 June, Vienna, Austria

Literature related to steam reforming

Lødeng R., De Chen, Jakobsen C.K., Holmen A., **2000**, *"A study of coke formation kinetics by a conventional and an oscillating microbalance on steam reforming catalysts"*, Studies in Surface Science and Catalysis, Vol. 130, p. 3639-3644

Hou K., Hughes R., **2001**, *"The kinetics of methane steam reforming over a Ni/α-Al_2O catalyst"*, Chemical Engineering Journal, Vol. 82, p. 311-328

General subjects

Ishida M., Wen C.Y., **1968**,*"Comparison of Kinetic and Diffusional Models for Solid-Gas Reactions"*, AiChe Journal, Vol. 14, No. 2, p. 311-317

Zheng D., Uchiyama Y., Ishida M., **1986**, *"Energy-utilization diagrams for two types of LNG power-generation systems"*, Energy, vol. 11, No. 6, p. 631-639

Trumble K.P., Rühle M., **1991**, *"The thermodynamics of spinel interphase formation at diffusion-bonded Ni/Al2O4 interfaces"*, Acta metal. mater. vol. 39, No. 8, p. 1915-1924

Jin H., Ishida M., **1993**, *"Graphical exergy analysis of complex cycles"*, Energy, vol. 18, no. 3, p. 615-625

Jin H., Ishida M., **1994**, *"Graphical exergy analysis of a new type of advanced cycle with saturated air"*, Heat Recovery Systems & CHP, vol. 14, No. 2, p. 105-116

Bolland O., Stadaas J.F., **1995,** *"Comparative evaluation of combined cycles and gas turbine systems with water injection, steam injection and recuperation"*, Journal of Engineering for Gas Turbines and Power, Vol. 117, p. 118-145

Gambini M., Vellini M., **2000**, *"CO_2 emission abatement from fossil fuel power plants by exhaust gas treatment"*, Proceedings of 2000 International Joint Power Generation Conference, Miami Beach, Florida, July 23-26, p. 453-463

Alfsen K.H., Kolshus H.H., Torvanger A., **2000**, *"Klimaendringer og klimapolitikk"*, CICERO (Center for International Climate and Environmental Research) Report

Griffin T., Bill A., Marion J.L., Nsakala N., **2002**, *"CO_2 Control Technologies. Alstom Power Approach"*, 6th International Conference on Greenhouse Gas Control Technologies, Paper L3-2, Kyoto, Japan

Rukes B., Taud R., **2002**, *"Status and perspectives of fossil power generation"*, Proceedings of ECOS 2002, July 3-5, Berlin

Anderson R., Brandt H., Doyle S., Pronske K., Viteri F., **2003**, *"Power generation with 100% carbon capture and sequestration"*, 2nd Annual Conference on Carbon Sequestration, Alexandria, VA., May 5-7

Bergstrøm T., **2003**,*"Simulation of metallurgical conversion of natural gas"*, Internal SINTEF report no. STF24F

Heitmer F., Jericha H., **2003**, *"Graz cycle-an optimized power plant concept for CO_2 retention"*, First Int. Conf. on Industrial GT Technologies, RTD Framework Programme of the European Union, Brussels, July 2003

Mathieu P., **2003**, *"Mitigation of CO_2 emissions using low and near zero CO_2 emission power plants"*, Clean Air , International Journal on Energy for a Clean Environment, vol. 4, p. 1-16

Jukkola G., Levasseur A., Turek D., Teigen B., Suresh J., Thibeault P., **2003**, *"Performance results with ALSTOM's circulating moving bed combustor"*, Proceedings of FBC2003, 17th Fluidized Bed Conference, p. 99-105

Shimomura, Y., **2003**, "The CO_2 wheel: a revolutionary approach to carbon dioxide capture", Modern Power Systems p.15-17

Monographs by year of publication

Perry R.H., Chilton C.H., Kirkpatrick S.D., *"Perry's Chemical Engineers' Handbook"*, McGraw-Hill book company Inc., **1963**

Szekely J., Themelis N.J., *"Rate phenomena in process metallurgy"*, John Wiley & Sons, **1971**

Szekely J., Evans J., Hong Y.S., "*Gas-solid Reactions*", Academic Press, **1976**

Weast R.C (editor), *"Handbook of Chemistry and Physics"*, CRC Press, 57th edition, **1976**

Barrow G.M., *"Physical chemistry"*, McGraw-Hill, 5th ed., **1988**

Brady J.E., "*General Chemistry*", John Wiley & Sons, **1990**

Doebelin E.O., *"Measurement systems – Application and Design"*, McGraw Hill, **1990**

Evans J.W., De Jonghe L.C., "*The Production of Inorganic materials*", Macmillian Publishing Company, **1991**

Kunii D., Levenspiel O., "*Fluidization Engineering*", Butterworth-Heinemann, **1991**

Silverstein R.M., Bassler G.C., Morrill T.C., *"Spectrometric Identification of Organic Compounds"*, John Wiley & sons, inc., 5th ed., **1991**

Pleym H., *"Miljøstudier"*, NKI Forlaget, **1992**

Mills A. F., "*Heat and Mass Transfer*", Richard D. Irwin Inc., **1995**

Griffiths J.F., Barnard J.A., *"Flame and combustion"*, 3rd ed., Chapman & Hall, **1995**

Barin I, "*Thermochemical data of pure substances*", 3rd ed., VCH Verlagsgesellschaft, **1995**

Kotas T.J, "*The exergy method of thermal plant analysis*", Krieger Publishing Company, **1995**

Olafsen A., *"Structure and Stability of Rare Earth Oxide Carbonates. Properties of Nd-based Ruddlesden-Popper Type Oxides"*, Doctoral thesis, Faculty of Mathematics and Natural Science, University of Oslo, **1999**.

Anheden M, *"Analysis of gas turbine systems for sustainable energy conversion"*, Doctoral thesis, Department of Chemical Engineering and Technology Energy Processes, Royal institute of Technology, Stockholm, Sweden, **2000**

Saravanamuttoo H.I.H., Rogers G.F.C., Cohen H., *"Gas turbine theory"*, 5th ed., Pearson education Ltd., **2001**

Victor D.G., *"The collapse of the Kyoto protocol and the struggle to slow global warming"*, Princeton University Press, **2001**

Personal references

Kari Anne Andreassen, Laboratory technician, SINTEF Materials and Chemistry, Oslo, Norway

Ivar M. Dahl, Scientist, SINTEF Materials and Chemistry, Oslo, Norway

Yngve Larring, Scientist, SINTEF Materials and Chemistry, Oslo, Norway

Anja Olafsen, Scientist, SINTEF Materials and Chemistry, Oslo, Norway

Appendix A COMPUTATIONAL ASSUMPTIONS

A1 Cycle calculations

Table 30 Computational assumptions (Part I)

	HAT	CC & ISG
Fuel	Methane	Natural gas
Composition [mol%]	CH_4(100)	N_2 (0.89), CO_2 (2.0), CH_4 (89.0), C_2H_6 (7.0), C_3H_8 (1.0), C_4H_{10} (0.1), C_5H_{12} (0.01)
LHV [MJ/kg]	50.2	46.503
Steam/Carbon ratio	0	2.0
X_R (reduction solid conversion)	0.1	0.3
X_O (oxidation solid conversion)	0.8	1.0
ϕ_{FUEL}	1.0	0.95-1.0
Reactors	CFB + BB	CFB + BB
ε_{red}	0.45	0.45
ε_{ox}	0.95	0.95
P_r	10-20	10-20
$\Delta P(red)$	1 bar	P_r * 5/100
$\Delta P(ox)$	1 bar	P_{ox} * 5/100
Ambient conditions	(ISO 3977-2:1997)	
Air composition (mole percent)	N_2(79), O_2(21)	N_2 (77.3), O_2 (20.74), CO_2 (0.03), H_2O (1.01), Ar (0.92)
T^0	15°C	15°C
P^0	1.01 bar	1.013 bar
H_R	60%	60%

Table 31 Computational assumptions (Part II)

	HAT	CC & ISG
HRSG		
HP	N/A	60 bar
LP	-	5 bar
Hot side ΔT	-	20°C
IP Temperature	-	260°C
Pinch (HP,IP)	-	10°C
Min. stack temp.		80°C
Steam cycle		
HP	N/A	160 bar
IP	-	30
HP temperature	-	560°C
Steam turbine adiabatic efficiency (HP,IP)	-	92, 92 %
Condenser pressure	-	0.04 bar
ΔT_{MAX}	-	10°C
CO_2 compression		
Polytropic efficiency (stage 1,2,3)	85, 80, 75 %	85, 80, 75 %
Heat exchanger ΔP (stage 1,2,3)	0.15, 1.5, 2.4 bar	0.15, 1.5, 2.4 bar
Cold utility outlet temp.	24°C	24°C
Adiabatic efficiency (pump)	75%	75%
Compressor intercooler exit temperature	30°C	30°C

A2 Equation of state

The PRK-equation of state is formulated as:

$$P = \frac{RT}{V-b} - \frac{a}{V(V+b)}$$

where coefficients *a* and *b* are functions of critical temperature and pressure:

$$a = 0.42748 \cdot \frac{R^2 T_C^2}{P_C}\left[1 + K \cdot \left(1 - T_R^{1/2}\right)\right]^2$$

$$b = 0.08664 \cdot \frac{RT_C}{P_C}$$

The constant *K* is calculated from the acentric factor, κ:

$$K = 0.48 + 1.57\kappa - 0.17\kappa^2$$

Another form that the SRK equation can take uses the compressibility factor (Z). This establishes a cubic equation of state:

$$Z^3 - Z^2 + (A - B - B^2)Z - AB = 0$$

$$A = \frac{Pa}{(RT)^2}$$

$$B = \frac{Pb}{RT}$$

Relevant properties for hydrocarbons found in natural gas (used as fuel in CC and ISG) are given Table 32.

Table 32 Thermodynamic properties for selected hydrocarbons

	Mw [g/mol]	κ	Tc [K]	P [bar]	Z_c
Methane	16.043	0.012	190.6	45.99	0.286
Ethane	30.070	0.100	305.3	48.72	0.279
Propane	44.097	0.152	369.8	42.48	0.276
n-Butane	58.123	0.200	425.1	37.96	0.274
n-Pentane	72.150	0.252	469.7	33.70	0.270
n-Hexane	86.177	0.301	507.6	30.25	0.266
n-Heptane	100.204	0.350	540.2	27.40	0.261

Appendix B EXPERIMENTAL DETAILS

B1 Reactor detail

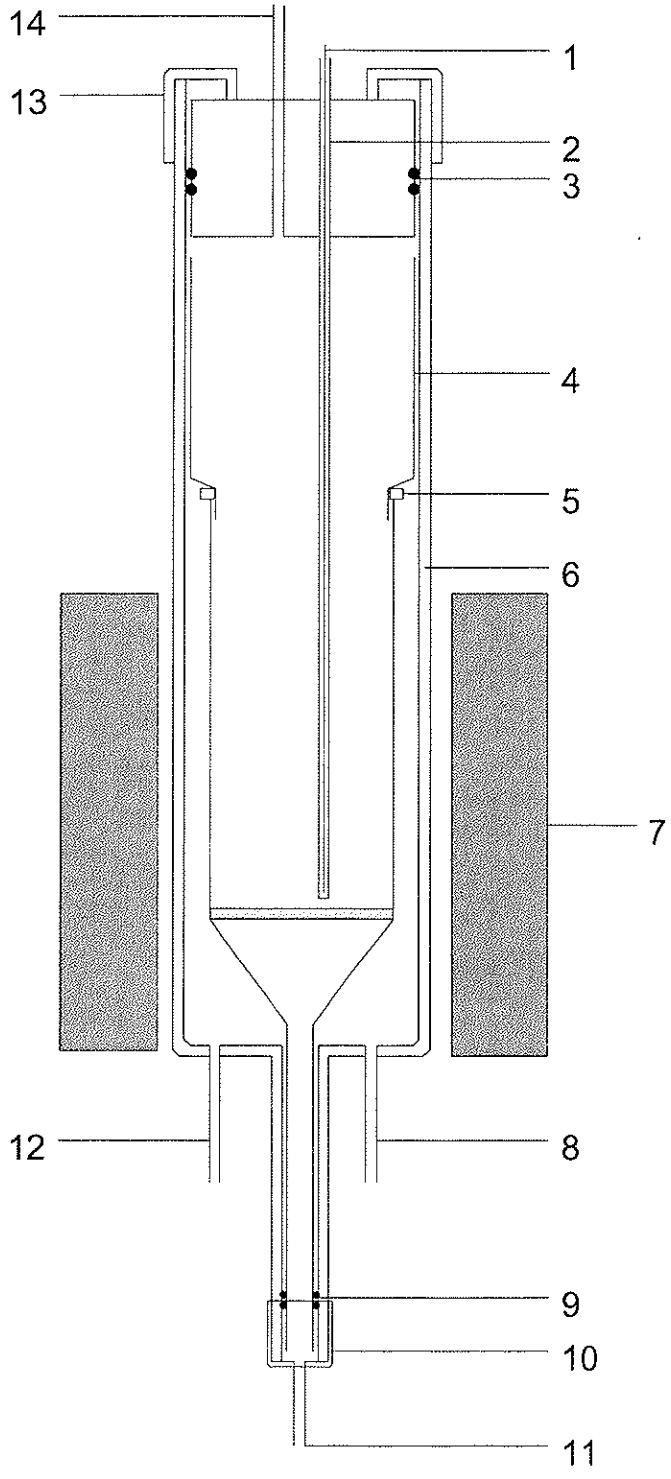

Figure 59 Reactor assembly schematic (not to scale)

B2 Specifications

Table 33 Reactor assembly specifications

No.	Description
1	Thermocouple N-type with NICROBEL A Class 1 mantel (TQ-0.5-R-1NICROBEL A-N-750-MM – *Teck Instrument AS*) and West Indicator (N8010Z2100/00 – *Teck Instrument AS*)
2	Thermocouple Well – welded at SINTEF in-house work shop (Hastelloy C276 OD: 1/16", ID:0.75 mm, length 70 cm – *Teknolab A/S*)
3	O-Rings (O22X3V80G700N; O9X1.5V80G700N; O11.1X1.6V80B027DK – *Busak+Shamban AS*)
4	Quarts Body Reactor with sinter (porosity = 1) - total length ≈ 85 cm (OD_1: 23-24 mm, ID_1: 20 mm, OD_2: 9 mm, ID_2: 7 mm – *Friedel Glassblåseri*). Indexes 1 and 2 referring to upper and lower parts of the reactor, respectively.
5	Spacer
6	Steel Body Reactor - total length ≈ 90 cm (THR-353-MA-33.7-4.15; THR-E-253MA-17.15-3.20 – *Avesta Polarit*)
7	Furnace System - Furnace - total furnace length ≈ 35 cm and Control Unit Box (in-house equipment at SINTEF); S-type thermocouples with alsint mantel (TK-6.0-R-1xALSINT-S-40 0-T-200-SM – *Teck Instrument AS*)
8	Metal-quartz interspace inlet, 1/8" SS-316 tubing
9	O-Rings (*Busak + Shamban AS*)
10	Threaded reactor end-cap (inlet)
11	Feed line, 1/8" SS-316 tubing
12	Metal-quartz interspace outlet, 1/8" SS-316 tubing
13	Threaded reactor end-cap (exit)
14	Effluent line, 1/8" SS-316 tubing

Table 34 Rig component specifications

Component	Description/specification	Supplier
Piping	1/8" SS 316	SVAFAS
Pressure gauges	Swagelok PGI-63B-BG16-LAQX-H Cajon Special	SVAFAS
Mass Flow Controllers	Standard MFCs from Bronkhorst (0-1000 mln/min), max pressure difference 20 bar	Flow-Teknikk AS
Back Pressure Regulator (BPR)	26-2362-24 TESCOM REG.	Teamtrade AS
Condenser	In-house equipment	Local workshop
Evaporator	In-house equipment	Local workshop
In-line filter	Swagelok – SS-2F-2	SVAFAS
Main supply valve	Whitey "43Z" Series Ball Valves 5-way	SVAFAS
DC-sources	0-200 Volts	
HPLC pump	In-house equipment	
Nafion dryer	In-house equipment	
Gases	Purity > 99.9 %	AGA

Appendix C INSTRUMENT SPECIFICATIONS

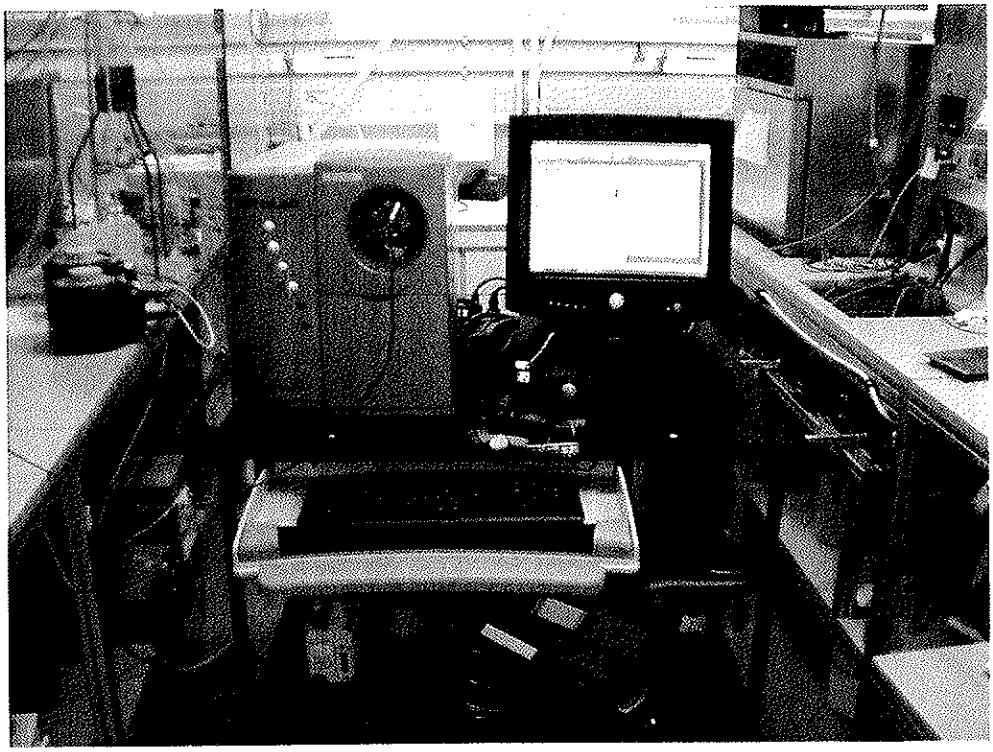

Figure 60 Prolab MS during analysis, heated inlet capillary seen in red

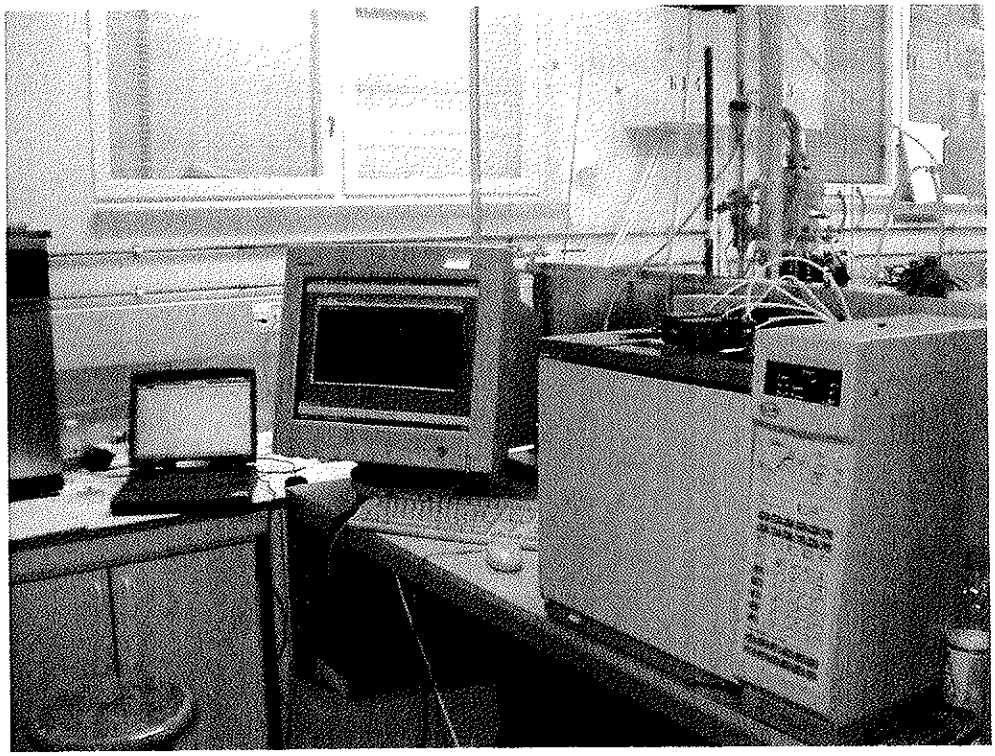

Figure 61 Agilent GC

Table 35 Mass spectrometer specifications

Manufacturer	ProLab
Type	Thermo Onix
Separator principle	Quadropole
Detector	Faraday/multiplier
Mass range	1-200, 1-300 amu
Sensitivity	5 E-4 A/mbar
Resolution	< 1 amu over the entire range
Min detectable	5 E-11 mbar (Faraday) 5 E-14 (Multiplier)
Max operating pressure	1 E-5 mbar (Faraday)
Nominal operating pressure	1 E-6 mbar (Multiplier)

The GC has a modular structure with three separate modules each containing a column designed for separation of specific species. This facilitates the detection and quantification of a wide variety of gases. The specifications of GC2 have not been made available to the author.

Table 36 Gas Chromatograph specifications

Manufacturer	Agilent (formerly MTI & Hewlett Packard)
Model	Agilent Micro-GC, 3 channels
Detector	Thermal Conductivity Detector (TCD)
Module 1	
Stationary phase	Molecular sieve 5Å zeolite
Length	10 m
Carrier gas	Argon
Analysis	Hydrogen and permanent gases
Module 2	
Stationary phase	Divinylbenzene-etylenglycol-dimethylacrylate polymer
Length	10 m
Carrier gas	Helium
Analysis	Polar hydrocarbons, nitriles/nitrous gases, alcohols/aldehydes, ethane/ethylene, sulphur-containing gases, oxygen in air, water (ppm)
Module 3	NOT IN USE

Appendix D MFC CALIBRATION

Mass flow controllers were calibrated using a digital universal flow meter. Actual flowrate ($\dot{V}$) was measured and plotted against MFC-controller readout (RD) providing linear correlations for the relevant species.

Table 37 MFC flow correlations for relevant gas species

Species	Correlation
Methane (MFC1)	$\dot{V}(CH_4) = 7.8 \cdot RD + 16.09$
Hydrogen (MFC1)	$\dot{V}(H_2) = 5.66 \cdot RD + 0.142$
Air (MFC1)	$\dot{V}(Air) = 10.36 \cdot RD + 11.51$
Nitrogen (MFC2)	$\dot{V}(N_2) = 11.56 \cdot RD + 87.85$
Argon (MFC2)	$\dot{V}(Ar) = 11.75 \cdot RD + 104.04$

MFC3 & MFC4 where not calibrated as the as the same setting was used in all experiments.

In Individual data points in are calculated on the basis of 3 parallel measurements. Solid lines correspond to the respective correlations in Table 37, and have been calculated with linear regression. All MFCs show excellent linearity for the species involved, across the flow range.

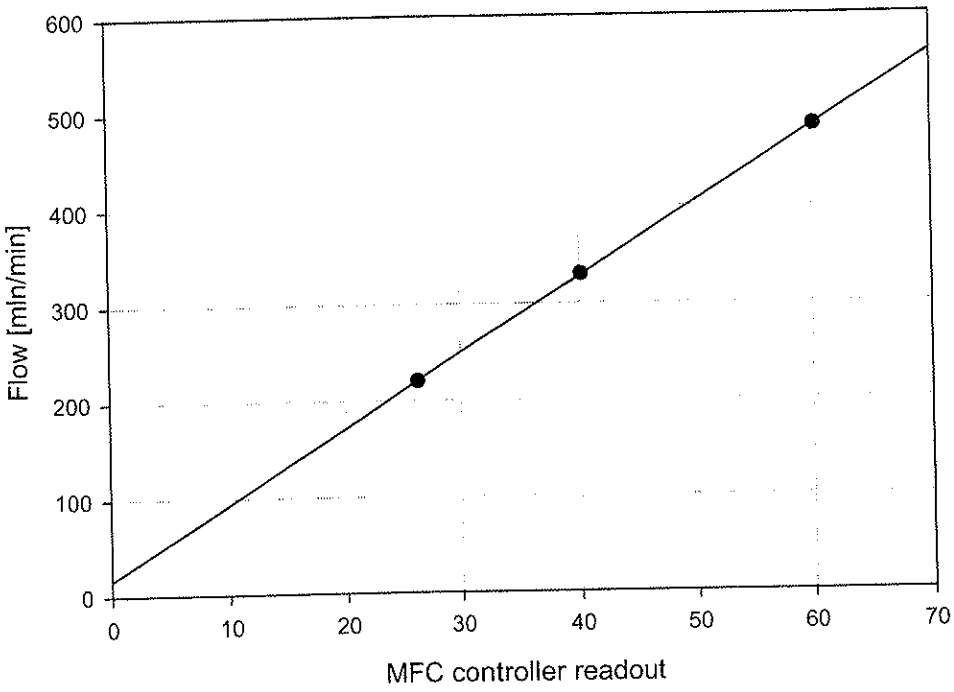

Figure 62 MFC1 calibration data, CH_4

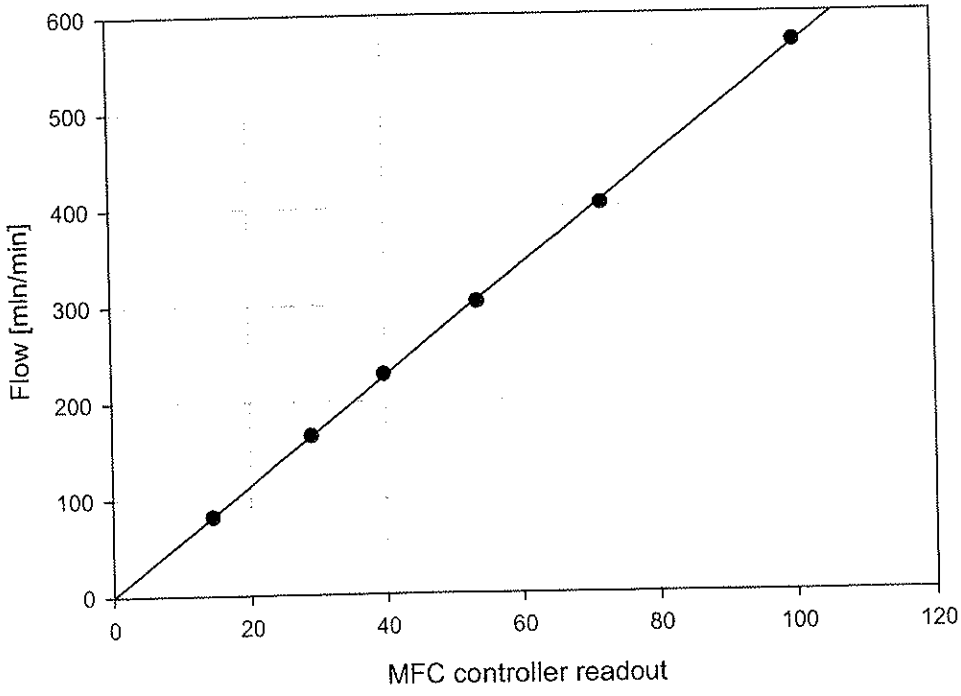

Figure 63 MFC1 calibration, H_2

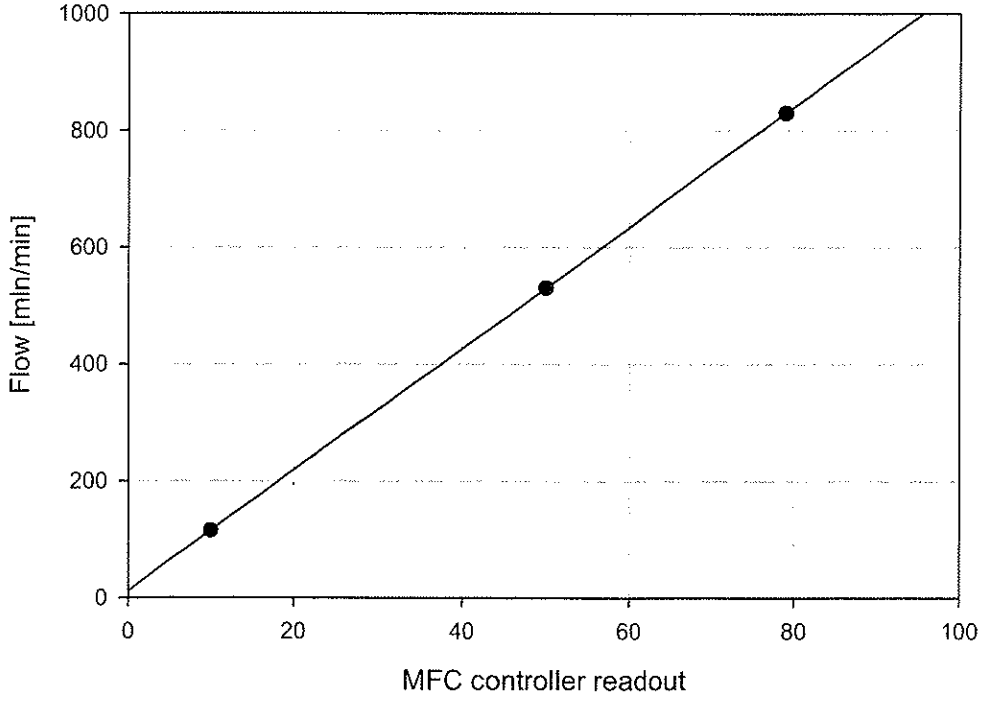

Figure 64 MFC1 calibration, Air

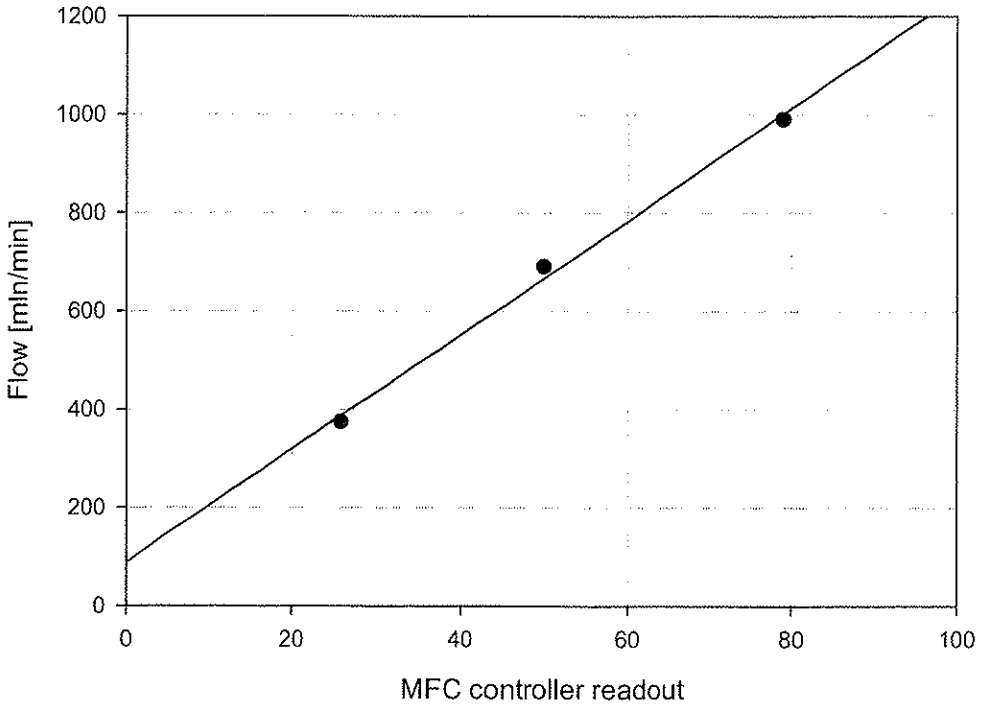

Figure 65 MFC2 calibration, N_2

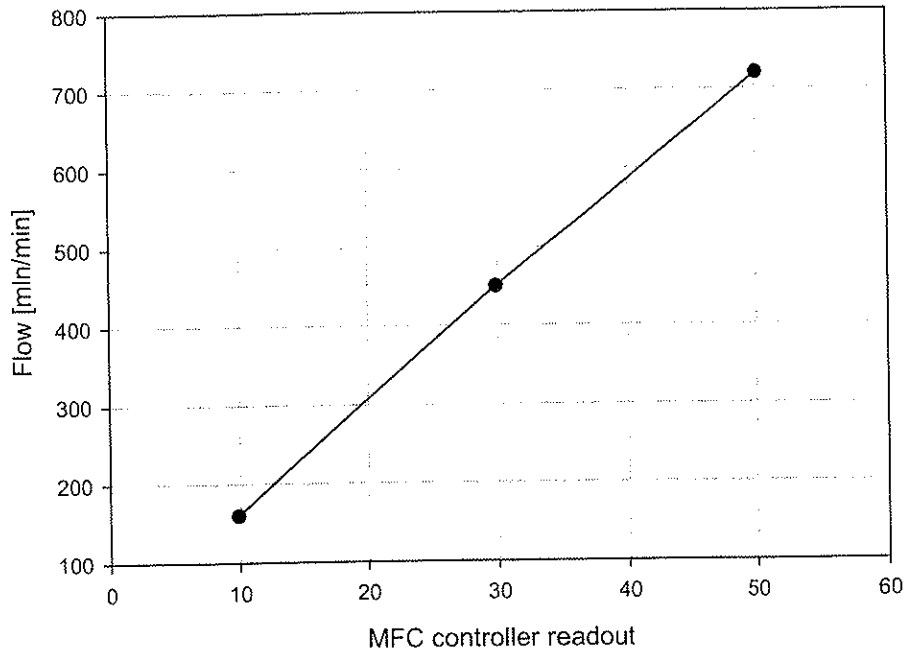

Figure 66 MFC2 calibration, Ar

Appendix E SEM IMAGES

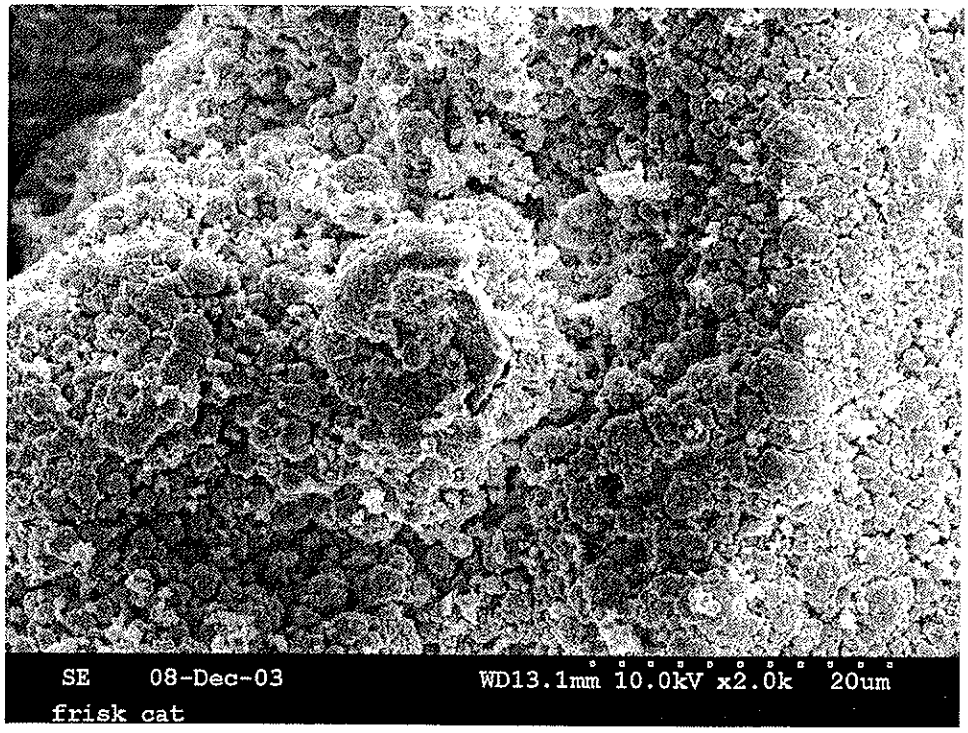

Figure 67 Sample 1, NiONiAl, magnification 2.000

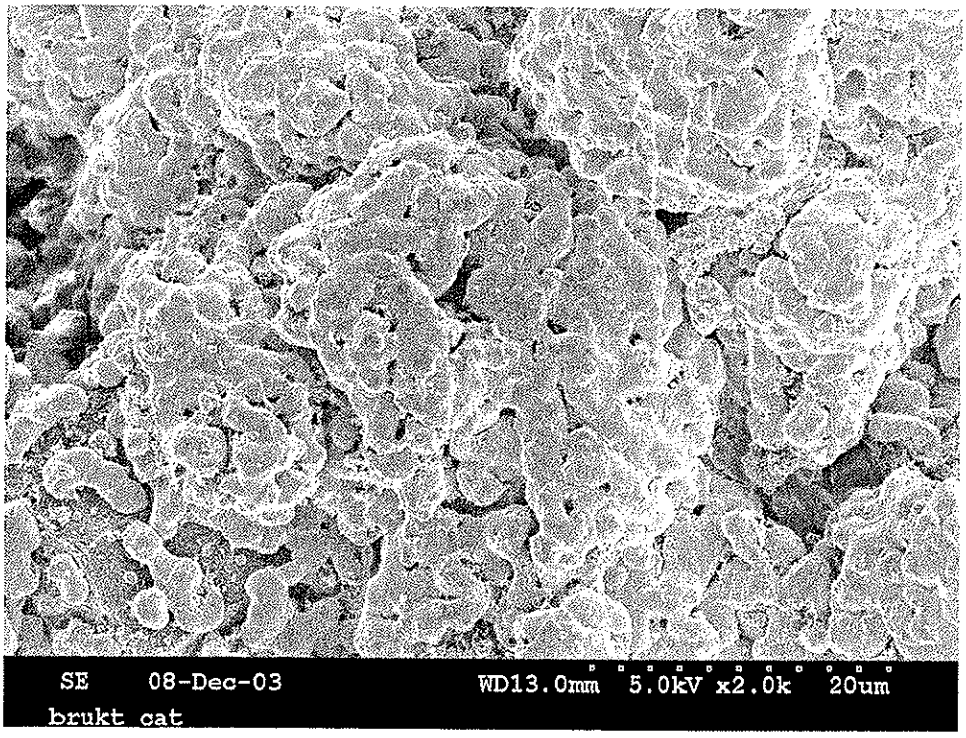

Figure 68 Sample 2, NiONiAl, magnification 2.000

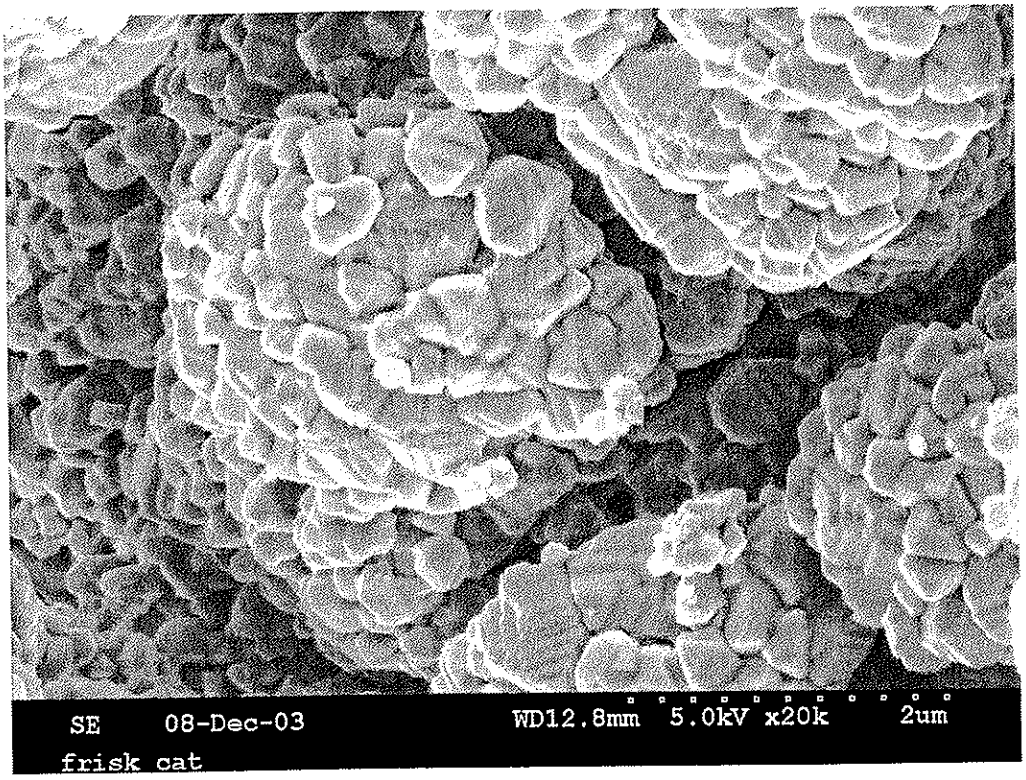

Figure 69 Sample 1, NiONiAl, magnification 20.000

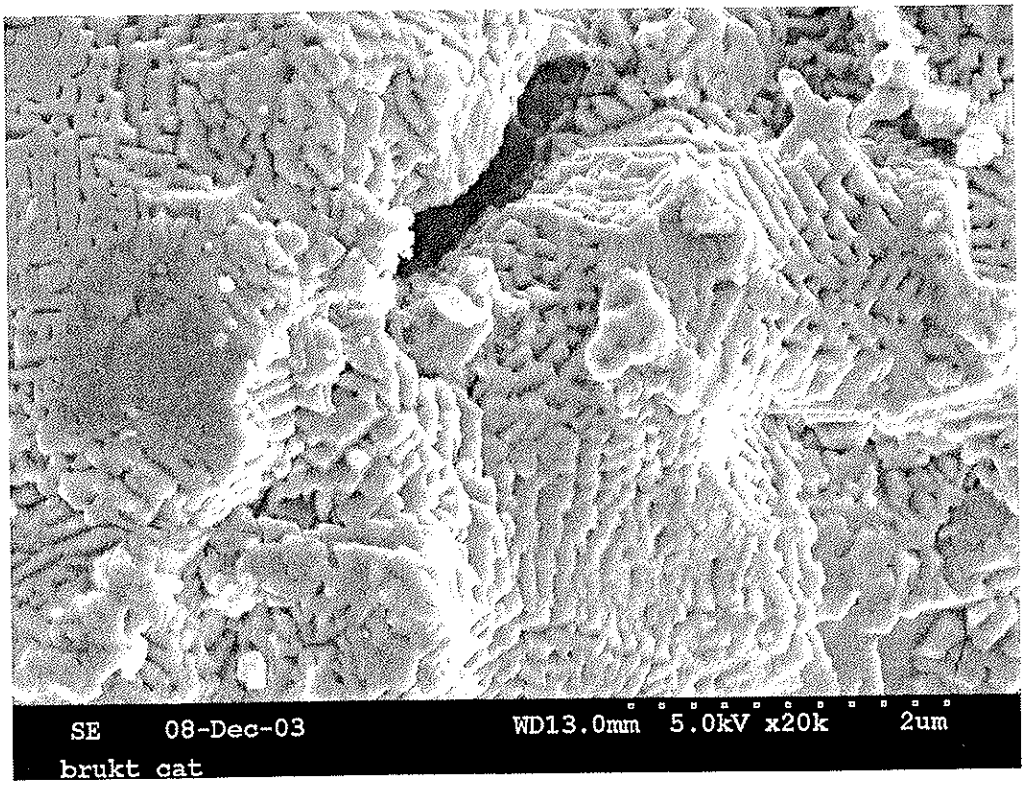

Figure 70 Sample 2, NiONiAl, magnification 20.000

Paper I

CHEMICAL LOOPING COMBUSTION – FUEL ENERGY CONVERSION WITH INHERENT CO_2 CAPTURE

Øyvind Brandvoll, Norwegian University of Science and Technology, N-7491 Trondheim, Norway,
Tel: +47 73593984 - Fax: +47 73598390 – E-mail: brand@maskin.ntnu.no
Olav Bolland, Norwegian University of Science and Technology, N-7491 Trondheim, Norway,
Tel: +47 73591604 - Fax: +47 73598390 – E-mail: olav.bolland@tev.ntnu.no
Sondre Vestøl, Norwegian University of Science and Technology, N-7491 Trondheim, Norway

INTRODUCTION

Originally proposed by Richter & Knoche[1] in 1983, the main idea of Chemical Looping Combustion (CLC) is to split combustion of natural gas into separate oxidation and reduction reactions by introducing a suitable metal oxide as an oxygen carrier to circulate between the two reactors, as indicated in Figure 1.

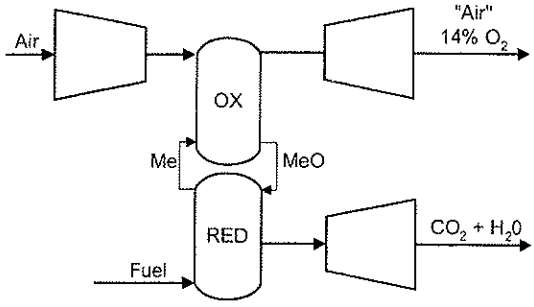

Figure 1 The Chemical Looping Combustion principle

The oxide is reduced to metal in the presence of hydrocarbons, and reformed by oxidation with air. The reaction for methane and a metal oxide can be formulated as follows:

$$Me + \tfrac{1}{2}O_2 \longrightarrow MeO \qquad (1)$$

$$CH_4 + 4MeO \longrightarrow CO_2 + 2H_2O + 4Me \qquad (2)$$

The oxidation is highly exothermic (ΔH_{OX}=-959 kJ/mol) and provides high temperature exhaust gas for power production (or as a heat source), and metal oxide which supply heat to the exhaust stream from the reduction reactor in a gas-solid heat exchange reactor, thus increasing the power generating potential of this exhaust, as well as supplying heat to the endothermic reduction reaction (ΔH_{RED}= 156 kJ/mol). CLC is a method for reducing the exergy loss associated with the highly irreversible combustion of a fuel. The advantage of inherent CO_2 separation without severe energy penalties has drawn increased attention in light of the current global warming debate. Formation of NO_X is also very low by virtue of the relatively low temperature conditions in the reactors. Current literature directly related to CLC is sparse. An overview of current CLC research is summarised in Table 1.

The bulk of the research has concentrated on reaction kinetics/oxygen carrier tests, reactor design and exergy analysis, whereas calculations regarding the power generating capabilities of a CLC process have not been investigated in detail.

PROCEDURE

This paper presents the results of a simulation of a CLC power plant. The simulations were performed in Matlab 5.0. The applied process schematic is shown in Figure 2. This is essentially similar to that proposed by Ishida et. al[2] (US Pat. 5,447,024).The model is made up from the mass and energy balances for the 6 main component types in the flowsheet: Turbine, compressor, pump, reactors, heat exchangers and condensers. Standard equations for compressor and turbine work, required pump power and heat exchange calculations have been used. The CLC system could be integrated in various power cycles. In the present study it was chosen to use the humid air turbine (HAT) principle. A humidifying tower is used to saturate the incoming air, before entering the oxidation reactor. Thermochemical data from Barin[3] are used throughout the calculation, and heat capacities for mixtures of gases have been estimated by assuming ideal-gas behaviour. Power requirements to circulate the oxygen carrier, besides reactor pressure drop, are considered negligible.

Key parameters employed in calculations on this system are the degree of oxidation (X) and the conversion factor or Gas Yield (γ_{red}):

$$X = 1 - \frac{m_{oxd} - m}{m_{oxd} - m_{red}} = \frac{m - m_{red}}{m_{oxd} - m_{red}} \qquad (3)$$

$$\gamma_{red} = \frac{P_{CO_2,out}}{P_{CH_4,out} + P_{CO_2,out} + P_{CO\,out}} \qquad (4)$$

X describes the state of the oxygen carrier at a given point in the process, and is defined as the fraction of the oxygen carrier material that is oxidised at a given time. γ_{red}, which has been used by some authors[4], is here assumed to be unity. The *conversion difference* ΔX per unit time between initial and current degree of oxidation of the carrier material, is also a measure of the reaction efficiency.

Table 1 Published work on CLC power generation systems

Authors	Studied area	Results
Ishida et. al.[2,5,6] Anheden[7]	Thermodynamics, exergy analysis	Reduced exergy loss compared to conventional combustion, as a result of reaction splitting
Mattison & Lyngfeldt [4]	Reaction characteristics of different types of ferrous (III) oxides	Reactions rates (red/ox) are sufficient for power generating applications
Ishida et. al.[8-15]	Oxygen carriers: reduction/oxidation rates, synthesis, mechanical properties, carbon deposition, kinetics	Several promising oxygen carriers have been investigated, reaction rates are sufficiently large
Lyngfeldt et. al.[16]	Reactor design and technical feasibility	Circulating fluidized bed concept discussed as a suitable reactor set up
Hatanaka et. al.[17]	Reaction kinetics	Reaction rates are sufficiently large

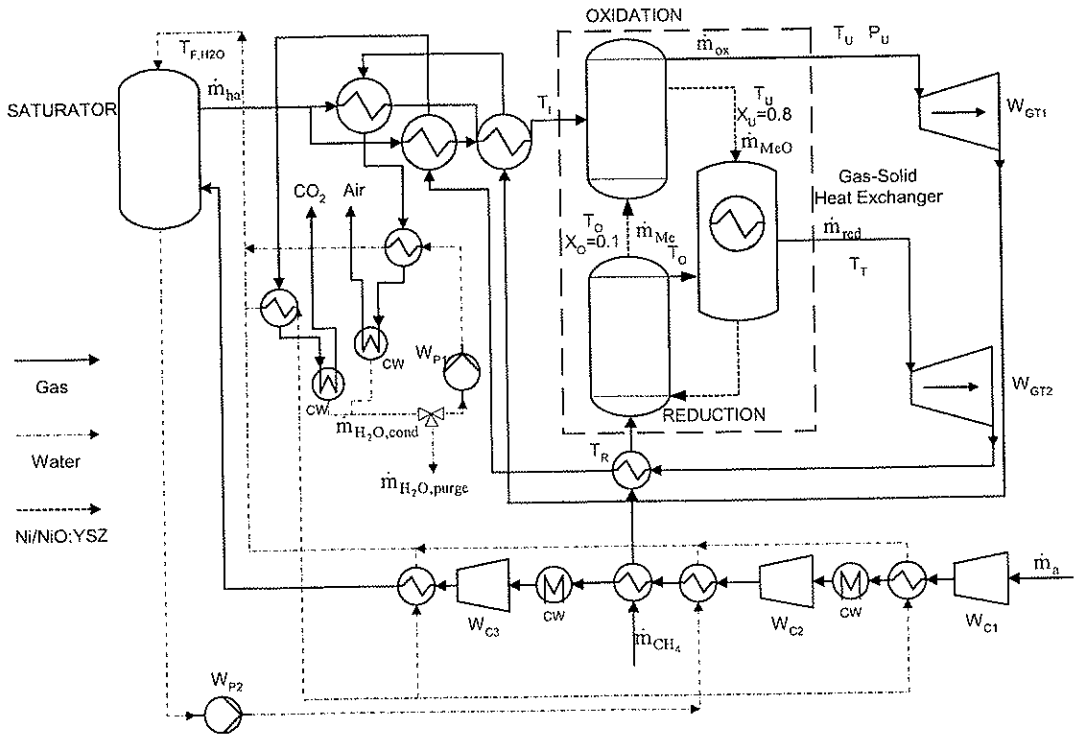

Figure 2 Process flowsheet. A gas turbine cycle with compressor intercooling and air humidification. The CLC system is shown within the dashed box.

Choice of Oxygen carrier

Based on previous experiments[8] NiO/YSZ on a 3:2 mass basis was selected as oxygen carrier. A number of promising oxygen carriers have been found, of which $NiO/NiAl_2O_4$ is perhaps the most interesting[14]. The main reason for not choosing the latter for this study is the lack of thermodynamic data. The degree of oxidation X_O is set to 0.1 at the oxidation reactor entrance, and $X_U = 0.8$ at the reduction reactor entrance. These values have been selected (instead of 0.0 and 1.0) in order to decrease the reactor volumes (and residence times) necessary for complete transformation of the material, whilst maintaining a relatively low mass-flow of oxygen carrier.

RESULTS AND DISCUSSION

Six process parameters that are believed to affect the overall efficiency (LHV) were identified: oxidation reactor air inlet temperature T_I, fuel inlet temperature T_R, oxidation reactor exhaust temperature T_U, primary reduction exhaust temperature T_O, were varied in turn, and their influence on important process parameters and ultimately on the overall efficiency was calculated. The basis of the simulation is a fuel consumption rate of 1.0 kg CH_4/s. Table 2 presents the main results in a highly compressed form. Variation of primary parameters is shown in italics, and gives rise to degrees of freedom in other process parameters, in addition to the primary sought effect on total efficiency.

Table 2 Summary of simulation results.

	PARAMETERS						Response
CASES #	T_I [°C]	T_R [°C]	T_U [°C]	T_T [°C]	T_O [°C]	P_U [Bar]	η_{TOT}
Base case	520	465	1200	900	560	20	55.3
1	*400-520*	465	1200	900	560	20	50.2-55.3
2	522-519	*375-465*	1200	900	548	20	55.2-55.3
3	349-519	465	*900-1200*	900	257	20	45.1-55.3
4	519-527	681	1200	*900-1200*	485-560	20	55.3-55.9
5	519	465	1200	900	*224-1067*	20	55.4-54.0
6	633-505	549	1200	900	573	*10-20*	54.6-55.3

1) Oxidation inlet temperature, T_I

The temperature of the air as it enters the oxidation reactor will affect the power production of W_{GT1}, as it determines the airflow rate through the process when reactor outlet temperature and heat exchanger duties are given. An increase in total efficiency is observed due to a proportionally larger turbine output gain as the airflow rate increases when going from T_I = 400-520°C, than the rise in required compressive work. T_I will also affect the water temperature in the humidifier, as more high temperature heat is available at low T_I. T_I is found to have significant impact on η_{TOT}, - about 5.1% over the temperature range. The upper limit for T_I is 519°C, due to ΔT_{min} requirements in the preheating exchangers. Based on this result, the following simulations use all available high temperature heat to increase T_I to optimise efficiency.

2) Fuel inlet temperature, T_R

With given outlet conditions and fuel flow, lowering the fuel inlet temperature allows more heat to be transferred in the air-preheaters thus allowing a further increase in T_I. The amount of fuel entering the system is much lower than the amount of air. Subsequently, the total energy influx to the reactors remains constant, and little effect is observed in η_{TOT}. A slight increase is observed, however. Maximum fuel inlet temperature, limited by ΔT_{MIN} requirements in the heat exchangers, is therefore chosen in the following simulations.

3) Oxidation reactor outlet temperature, T_U

Lowering the turbine inlet temperature T_U, immediately lowers the GT1 turbine power output. Turbine outlet temperature also decreases, and less energy is available for air preheating. On the other hand, the airflow can be increased, and the need for costly turbine- and reactor cooling might be eliminated. The increased airflow cancels the effect of the temperature decrease and the power output W_{GT1} remains constant, but the required compressor power increases significantly, as can be seen in Figure 3B. The power generating potential of GT1 is unaffected and a significant effect on total efficiency is thus observed.

4) Turbine GT2 inlet temperature, T_T

Increasing T_T is possible by increasing the mean residence time of the particles in the gas-solid heat exchanger, thus transferring more energy. Less energy is thus available when the oxygen carrier enters the oxidation reactor. Consequently the airflow must be reduced to maintain constant outlet conditions. Increased power in turbine GT2 comes at the cost of lowering the power in turbine GT1 and η_{TOT} is relatively unaffected. Economical considerations with regard to turbine GT2 imply that a low inlet temperature is desirable to avoid cooling of the turbine.

5) Reduction reactor outlet temperature, T_O

By increasing the carrier mass flow rate, while maintaining a constant volume in the gas-solid heat exchanger, the oxygen carrier will have a higher temperature as it enters the reduction reactor. This will lead to an increase in T_O. Additionally a change in X_U (after oxidation) and X_O (after reduction) is observed as the reactor volumes are considered to be constant and the mean residence times (τ_{ox}, τ_{red}) decreases. This leads to a slight change in the energy balance for the reduction reactor, the net result being a small decrease in efficiency. This observation is important because of the implication that T_O can be chosen to optimise the kinetics of the reduction reaction, without significant losses in efficiency.

6) Reactor pressure

Reduced pressure invariably leads to reduced power generation in both turbines, along with a reduction in required compressor work. The airflow rate will increase, however, and only a slight net effect is observed. When going from 10 to 20 bar, there is a slight increase in compressor work whilst W_{GT1} remains constant. η_{TOT} increases, however, due to the increased contribution from turbine GT2. The total efficiency rises slightly for pressures up to 20 bar, where the compressor work exceeds the increase in W_{GT2}. 20 bar therefore seems to be an optimal operating pressure for the reactor system.

In Figure 3A, T_I and T_U are plotted against total efficiency. Note that changing T_U also leads to a change in T_I due to the heat integration of the two streams. Figure 3B shows the effect on airflow rate when reducing T_U from 1200 to 900°C.

REACTOR SYSTEM

A key issue in CLC considerations is the type of reactor-system chosen. The concept of a *circulating fluidised bed* (CFB) has been proposed[16] and is believed to be the most promising set-up for successful long-term operation. The

basis for the simulation is a CFB (ε=0.95) for oxidation, and a fluidised bed (ε=0.45) for reduction. It is assumed that the oxygen carrier transport is gravity-driven in the reduction reactor. Key parameters are shown in Table 3. The flow of metal/metal oxide between the reactors is about 1.4-1.5 kg per MJ of net plant power output. The specific work (net plant power output per kg of air) is about 1/1.78=0.56 MJ/kg, which is somewhat higher (20-30%) than that of a gas turbine. The oxidation reactor volume is around 1.1 m^3/MW of net plant power output, which is below that of a conventional CFB combustion plant.

Table 3 Reactor key parameters (28 MW power output, 50 MW fuel lower heating value, $X_O = 0.1$, $X_U = 0.8$)

	kg/s	kg/MJ_{el}	kg/MJ_{LHV}
MeO	43.9	1.57	0.88
Me	39.3	1.40	0.79
Oxidation reactor airflow	49.8	1.78	1.0
	m^3	m^3/MW_{el}	kg/MW_{LHV}
Oxidation reactor (CFB)	31.2	1.11	155
Reduction reactor (FB)	3.3	0.12	141

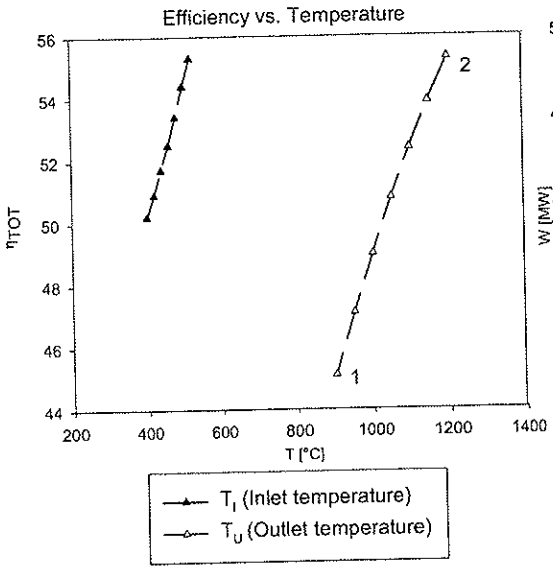

A) T - η diagram for T_I & T_U

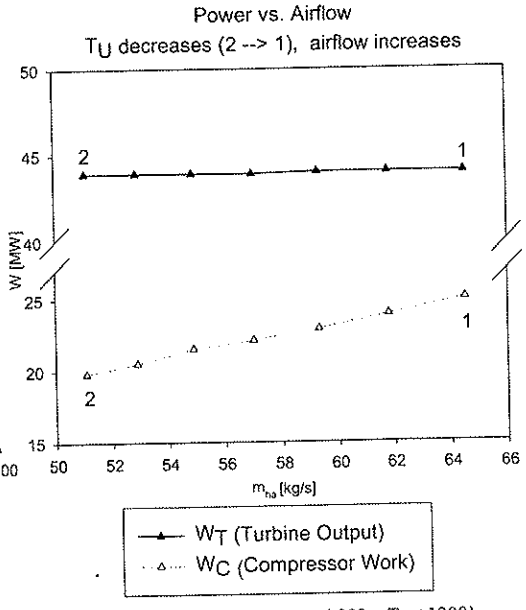

B) W – m_{ha} diagram, { 900 < T_U < 1200}

Figure 3

CONCLUSIONS

The oxidation reactor air inlet temperature (T_I) and the oxidation reactor exhaust temperature (T_U) have a significant impact on the overall efficiency. This can be attributed to the controlling effect of these parameters on the required airflow rate. An optimum efficiency of 55.9% has been found for T_I=527 °C, T_U=T_T=1200 °C, T_O=485 °C and $\dot{m}_a$ = 49.3 kg/s. The captured CO_2 is at atmospheric pressure. If taking into account the compression of CO_2 1-100 bar, the efficiency would be lowered by 2%-points, to about 54%. Crucial issues of oxygen carrier durability, chemical performance and mechanical properties have been highly idealized, and further research on the feasibility of CLC is needed. Whether or not the assumption of $\gamma_{red} \approx 1$ holds, is a crucial issue and remains to be determined experimentally. Results of previous studies on chemical kinetics are used directly in the simulations, under conditions quite different from the original study, and thus introduce uncertainties in the calculations, as successful long term operation of chemical looping systems of this particular type have yet to be demonstrated. The simulation points out a very promising potential of CLC as a power/heat generating method with inherent capture of CO_2. Simulations of this type will prove useful in designing CLC systems in the future when promising oxygen carriers have been investigated in more detail.

ACKNOWLEDGEMENTS

This study was funded by the Norwegian Research Council programme - Energy for the Future.

APPENDIX

A NOMENCLATURE

Symbols

ΔH_{rx}	heat of reaction	[kJ/kmol]
m	instantaneous mass of oxygen carrier	[kg]
$\dot{m}$	mass flow rate	[kg/s]
m_{oxd}	mass of oxygen carrier when 100% oxidized	[kg]
m_{red}	mass of oxygen carrier when 100% reduced	[kg]
P_i	partial pressure of component *i*	[bar]
T	temperature	[°C]

V	volume	[m^3]
W	work	[MW]
X	degree of oxidation	
y_i	molar fraction of component *i*	
ε	bed void	
γ_{red}	gas yield	
η	efficiency	
ρ	particle density	[kg/m^3]
τ	mean residence time	[s]

Abbreviations

a	Air
CFB	Circulating Fluidized Bed
CLC	Chemical Looping Combustion
ha	Humid air
LHV	Lower Heating Value
w	Water

B COMPUTATIONAL ASSUMPTIONS

Ambient air = 15°C, 1.013 bar, 60%RH
Cooling water temperature = 15°C
Ideal gas behaviour is assumed.

Saturator:
Water temperature at saturator water exit: $T_{wb} \approx 80°C$

Turbomachinery

Isentropic turbine efficiency:	$\eta_t = 0.885$
Isentropic compressor efficiency:	$\eta_c = 0.85$
Pump efficiency:	$\eta_P = 0.70$

Isothermal operation is assumed

Reactors:

Oxidation:	Reduction:
$V_O = 31.2\ m^3$	$V_R = 3.3\ m^3$
$X_U = 0.8$	$X_O = 0.1$
$\rho_U = 5000\ kg/m^3$	$\rho_O = 3.900\ kg/m^3$
$\tau_{ox} = 180$ s	$\tau_{red} = 180$ s
Heat loss: 1 MW	Heat loss: 0.1 MW
Pressure loss = 1 bar	Pressure loss = 2 bar including gas/solid heat exchanger

Heat exchangers:
Minimum temperature difference: $\Delta T_{MIN} = 10°C$
Pressure loss = 1-1.3%

Efficiency definition:

$$\eta = \frac{W_{NET}}{LHV}, \text{ where LHV} = 802.6 \text{ kJ/mol}$$

REFERENCES

1. Richter H.J., Knoche K., **1983**, *Reversibility of Combustion processes*, Efficiency and Costing – Second Law Analysis of Processes, ACS Symposium series 235, p. 71-85
2. Ishida M., Zheng D., Akehata T., **1987**, *Evaluation of a chemical-looping-combustion power-generation system by graphic exergy analysis*, Energy, vol. 12, p. 147-154
3. Barin I., **1995**, *Thermochemical data of pure substances*, 3rd ed., VCH Verlagsgesellschaft
4. Mattisson T., Lyngfelt A., Cho P., **2000**, *Possibility of using iron oxide as an oxygen carrier for combustion of methane with removal of CO_2 – application of chemical-looping combustion*, HTTP://www.entek.chalmers.se/~anly/co2/ghgt5.pdf.
5. Ishida M., Jin H., **1993**, *Graphical exergy analysis of complex cycles*, Energy, vol. 18, no. 3, p. 615-625
6. Ishida M., Jin H., **1994**, *A new advanced power-generation system using chemical-looping combustion*, Energy, vol. 19, No. 4, p. 415-422
7. Anheden M., **2000**, *Analysis of gas turbine systems for sustainable energy conversion*, Doctoral thesis, Department of Chemical Engineering and Technology Energy Processes, Royal institute of Technology, Stockholm, Sweden
8. Ishida M., Jin H., **1994a**, *A novel combustor based on chemical-looping reactions and its reaction kinetics*, Journal of Chemical Engineering of Japan, vol. 27, No. 3, p. 296-301
9. Ishida M., Jin H., **1996**, *A novel chemical-looping combustor without NO_x formation*, Research Notes, Industrial and Engineering Chemistry, vol. 35, p. 2469-2472
10. Ishida M., Jin H., Okamoto T., **1996**, *A fundamental study of a new kind of medium material for chemical-looping combustion*, Energy & Fuels, vol. 10, p. 923-963
11. Ishida M., Jin H., Okamoto T., **1998**, *Kinetic behavior of solid particle in chemical-looping combustion: Suppressing Carbon deposition in reduction*, Energy & Fuels, vol. 12, p. 223-229
12. Ishida M., Jin H., Okamoto T., **1998**, *Development of a novel chemical-looping combustion: Synthesis of a looping material with a double metal oxide of CoO-NiO*, Energy & Fuels, vol. 12, p. 1272-1277
13. Ishida M, Jin H., **1997**, *CO_2 recovery in a power plant with chemical looping combustion*, Energy Conversion and Management, vol. 38, Suppl., p. 187-192
14. Jin H., Okamoto T., Ishida M., **1999**, *Development of a Novel Chemical-Looping Combustion: Synthesis of a Solid Looping Material of $NiO/NiAl_2O_4$*, Ind. Eng. Chem. Res., vol. 3, 126-132
15. Ishida M., Jin H., **1998**, *Greenhouse gas control by a novel combustion: No energy penalty and no CO_2 separation equipment*, Greenhouse Gas Control Technologies, Proceedings of the 4th International conference on Greenhouse Gas Control Technologies, 30 Aug – 2 Sep 1998, Interlaken, Switzerland, p. 627-632
16. Lyngfelt A., Leckner B., Mattisson T., **2000**, *A fluidized-bed combustion process with inherent CO_2 separation*, submitted to Chem. Eng. Sci. for publication
17. Hatanaka T., Matsuda S., Hatano H., **1997**, *A new-concept gas-solid combustion system "MERIT" for high combustion efficiency and low emissions*, Proceedings of the 32nd Intersociety Energy Conversion Engineering Conference, p. 944-947

Paper II

Inherent CO_2 Capture Using Chemical Looping Combustion in a Natural Gas Fired Power Cycle

Ø. Brandvoll

O. Bolland

The Norwegian University of Science and Technology, N-7491 Trondheim, Norway

In this paper an alternative to the so-called "oxy-fuel" combustion for CO_2 capture is evaluated. "Chemical looping combustion" (CLC), is closely related to oxy-fuel combustion as the chemically bound oxygen reacts in a stoichiometric ratio with the fuel. In the CLC process the overall combustion reaction takes place in two reaction steps in two separate reactors. In the reduction reactor, the fuel is oxidized by the oxygen carrier, i.e., the metal oxide MeO. The metal oxide is reduced to a metal oxide with a lower oxidation number, Me, in the reaction with the fuel. In this manner, pure oxygen is supplied to the reaction with the fuel without using a traditional air separation plant, like cryogenic distillation of air. The paper presents a thermodynamic cycle analysis, where CLC is applied in a humid air turbine concept. Main parameters are identified, and these are varied to examine the influence on cycle efficiency. Results on cycle efficiency are presented and compared to other CO_2 capture options. Further, an evaluation of the oxygen carrier, metals/oxides, is presented. An exergy analysis is carried out in order to understand where losses occur, and to explain the difference between CLC and conventional combustion. The oxidation reactor air inlet temperature and the oxidation reactor exhaust temperature have a significant impact on the overall efficiency. This can be attributed to the controlling effect of these parameters on the required airflow rate. An optimum efficiency of 55.9% has been found for a given set of input parameters. Crucial issues of oxygen carrier durability, chemical performance, and mechanical properties have been idealized, and further research on the feasibility of CLC is needed. Whether or not the assumption 100% gas conversion holds, is a crucial issue and remains to be determined experimentally. Successful long-term operation of chemical looping systems of this particular type has not yet been demonstrated. The simulation points out a very promising potential of CLC as a power/heat generating method with inherent capture of CO_2. Exergy analysis show reduced irreversibilities for CLC compared to conventional combustion. Simulations of this type will prove useful in designing CLC systems in the future when promizing oxygen carriers have been investigated in more detail
.[DOI: 10.1115/1.1615251]

Introduction

Originally proposed by Richter and Knoche [1] in 1983, the main idea of chemical looping combustion (CLC) is to split combustion of natural gas into separate oxidation and reduction reactions by introducing a suitable metal oxide as an oxygen carrier to circulate between the two reactors, as indicated in Fig. 1.

The oxide is reduced to metal in the presence of hydrocarbons, and reformed by oxidation with air. The reaction for methane and a metal oxide can be formulated as follows:

$$\mathrm{Me} + \frac{1}{2}\mathrm{O_2} \rightarrow \mathrm{MeO} \tag{1}$$

$$\mathrm{CH_4} + 4\mathrm{MeO} \rightarrow \mathrm{CO_2} + 2\mathrm{H_2O} + 4\mathrm{Me}. \tag{2}$$

The oxidation is highly exothermic ($\Delta H_{OX} = -959$ kJ/mol) and provides high temperature exhaust gas for power production (or as a heat source), and metal oxide which supply heat to the exhaust stream from the reduction reactor in a gas-solid heat exchange reactor, thus increasing the power generating potential of this exhaust, as well as supplying heat to the endothermic reduction reaction ($\Delta H_{RED} = 156$ kJ/mol). CLC is a method for reducing the exergy loss associated with the highly irreversible combustion of a fuel. This reduction is, however, dependent upon the degree of conversion in the two reactors. The advantage of inherent CO_2 separation without severe energy penalties has drawn increased attention in light of the current global warming debate, [2]. Formation of NO_X is also very low by virtue of the relatively low temperature conditions in the reactors. Current literature directly related to CLC is sparse. An overview of current CLC research is summarized in Table 1.

Procedure

This paper presents the results of a simulation of a CLC power plant. The simulations were performed in Matlab 5.0. The applied

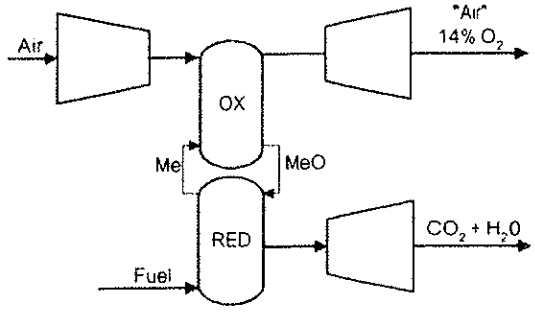

Fig. 1 The chemical looping combustion principle

Contributed by the International Gas Turbine Institute (IGTI) of THE AMERICAN SOCIETY OF MECHANICAL ENGINEERS for publication in the ASME JOURNAL OF ENGINEERING FOR GAS TURBINES AND POWER. Paper presented at the International Gas Turbine and Aeroengine Congress and Exhibition, Amsterdam, The Netherlands, June 3–6, 2002; Paper No. 2002-GT-30129. Manuscript received by IGTI, Dec. 2001, final revision, Mar. 2002. Associate Editor: E. Benvenuti.

Table 1 Published work on CLC power generation systems

Authors	Studied Area	Results
Ishida et al. [2,10,11]	Thermodynamics, exergy analysis	Reduced exergy loss compared to conventional combustion, as a result of reaction splitting
Anheden [9]		
Mattison and Lyngfeldt [5]	Reaction characteristics of different types of ferrous (III) oxides	Reactions rates (red/ox) are sufficient for power generating applications
Ishida et al. [6,7,12–17]	Oxygen carriers: reduction/oxidation rates, synthesis, mechanical properties, carbon deposition, kinetics	Several promising oxygen carriers have been investigated, reaction rates are sufficiently large
Lyngfeldt et al. [8]	Reactor design and technical feasibility	Circulating fluidized bed concept discussed as a suitable reactor set up
Hatanaka et al. [18]	Reaction kinetics	Reaction rates are sufficiently large

process schematic is shown in Fig. 2. This is essentially similar to that proposed by Ishida et al. [2]. The model is made up from the mass and energy balances for the six main component types in the flowsheet: turbine, compressor, pump, reactors, heat exchangers, and condensers. Standard equations for compressor and turbine work, required pump power and heat exchange calculations have been used. Turbine cooling efficiency penalty is not included in the present work. The heat losses in both reactors are set to 1% of the inlet stream enthalpies. The CLC system could be integrated in various power cycles. In the present study it was chosen to use the humid air turbine (HAT) principle. A humidifying tower is used to saturate the incoming air, before entering the oxidation reactor. Thermochemical data from Barin [3] and Kotas [4] are used throughout the calculation, and heat capacities for mixtures of gases have been estimated by assuming ideal-gas behavior. Power requirements to circulate the oxygen carrier, besides reactor pressure drop, are considered negligible.

Key parameters employed in calculations on this system are the degree of oxidation (X) and the conversion factor or Gas Yield (γ_{red}):

$$X = 1 - \frac{m_{oxd} - m}{m_{oxd} - m_{red}} = \frac{m - m_{red}}{m_{oxd} - m_{red}} \tag{3}$$

$$\gamma_{red} = \frac{P_{CO_2,out}}{P_{CH_4,out} + P_{CO_2,out} + P_{CO,out}}. \tag{4}$$

X describes the state of the oxygen carrier at a given point in the process, and is defined as the fraction of the oxygen carrier material that is oxidized at a given time. γ_{red}, which has been used by some authors, [5], is here assumed to be unity. The *conversion difference* ΔX per unit time between initial and current degree of oxidation of the carrier material, is also a measure of the reaction efficiency.

Choice of Oxygen Carrier. A number of promising oxygen carriers have been found, of which $NiO/NiAl_2O_4$ is perhaps the most interesting, [6]. Based on previous experiments; [7], and availability of thermodynamical data, NiO/YSZ on a 3:2 mass basis was selected as oxygen carrier. The degree of oxidation X_O

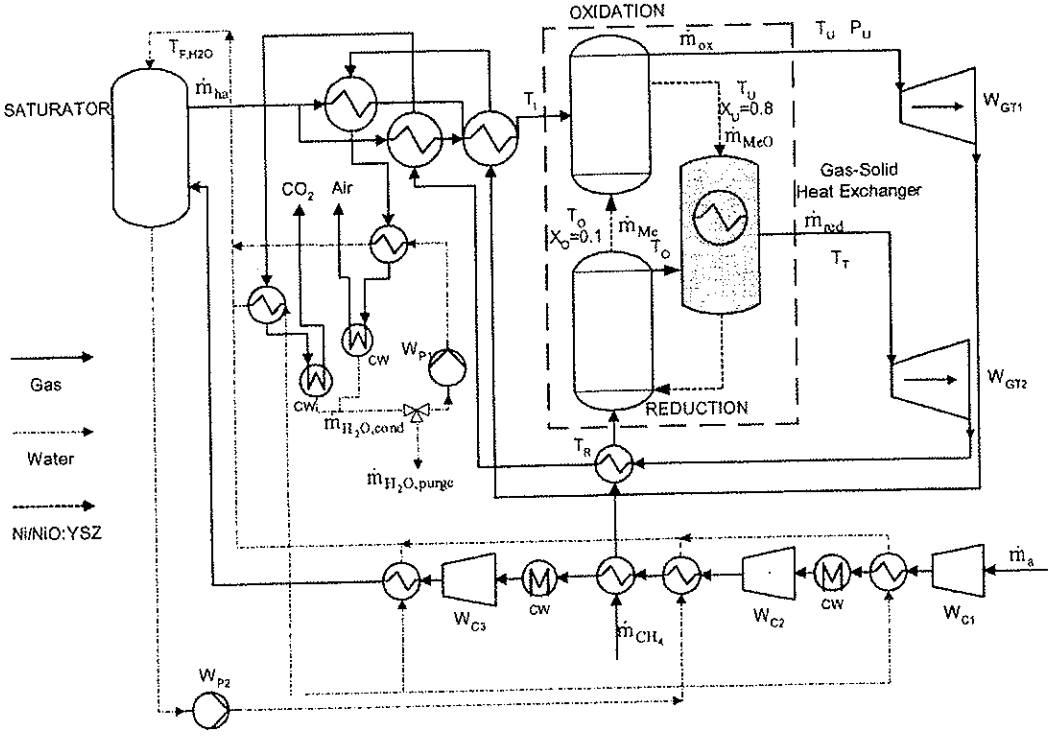

Fig. 2 Process flowsheet. A gas turbine with compressor intercooling and air saturation. The CLC system is shown within the dashed box.

Table 2 Summary of simulation results

Base Case	520	465	1200	900	560	20	55.3
	PARAMETERS						Response
CASES #	T_I[°C]	T_R[°C]	T_U[°C]	T_T[°C]	T_O[°C]	P_U[Bar]	η_{TOT}
1	*400–520*	465	1200	900	560	20	50.2–55.3
2	522–519	*375–465*	1200	900	548	20	55.2–55.3
3	349–519	465	*900–1200*	900	257	20	45.1–55.3
4	519–527	681	1200	*900–1200*	485–560	20	55.3–55.9
5	519	465	1200	900	*224–1067*	20	55.4–54.0
6	633–505	549	1200	900	573	*10–20*	54.6–55.3

is set to 0.1 at the oxidation reactor entrance, and $X_U = 0.8$ at the reduction reactor entrance. These values have been selected (instead of 0.0 and 1.0) in order to decrease the reactor volumes (and residence times) necessary for complete transformation of the material, while maintaining a relatively low mass-flow of the oxygen carrier.

Results and Discussion

Six process parameters that are believed to affect the overall efficiency were identified: oxidation reactor air inlet temperature T_I, fuel inlet temperature T_R, oxidation reactor exhaust temperature T_U, primary reduction exhaust temperature T_O, were varied in turn, and their influence on important process parameters and ultimately on the overall efficiency was calculated. The efficiency is defined as the ratio of net shaft power output (work of turbines minus work of compressors and pumps) to the lower heating value of CH_4. The basis of the simulation is a fuel consumption rate of 1.0 kg CH_4 /s. Table 2 presents the main results in a highly compressed form. Variation of primary parameters is shown in italics, and gives rise to degrees-of-freedom in other process parameters, in addition to the primary sought effect on total efficiency.

(1) Oxidation inlet temperature, T_I. The temperature of the air as it enters the oxidation reactor will affect the power production of W_{GT1}, as it determines the airflow rate through the process when reactor outlet temperature and heat exchanger duties are given. An increase in total efficiency is observed due to a proportionally larger turbine output gain as the airflow rate increases when going from $T_I = 400-520$°C, than the rise in required compressive work. T_I will also affect the water temperature in the saturator, as more high temperature heat is available at low T_I. T_I is found to have significant impact on η_{TOT},—about 5.1% over the temperature range. The temperature T_I is set as high as possible, limited by the ΔT_{min} requirements in the preheating exchangers. Based on this result, the following simulations use all available high-temperature heat to increase T_I to optimize efficiency.

(2) Fuel inlet temperature, T_R. With given outlet conditions and fuel flow, lowering the fuel inlet temperature allows more heat to be transferred in the air-preheaters thus allowing a further increase in T_I. The amount of fuel entering the system is much lower than the amount of air. Subsequently, the total energy influx to the reactors remains constant, and little effect is observed in η_{TOT}. A slight increase is observed, however. Maximum fuel inlet temperature, limited by ΔT_{MIN} requirements in the heat exchangers, is therefore chosen in the following simulations.

(3) Oxidation reactor outlet temperature, T_U. Lowering the turbine inlet temperature T_U, immediately lowers the GT1 turbine power output. Turbine outlet temperature also decreases, and less energy is available for air preheating. On the other hand, the airflow can be increased, and the need for costly turbine and reactor cooling might be eliminated. The increased airflow cancels the effect of the temperature decrease and the power output W_{GT1} remains constant, but the required compressor power increases significantly, as can be seen in Fig. 3(*b*). The power generating potential of GT1 is unaffected and a significant effect on total efficiency is thus observed.

(4) Turbine GT2 inlet temperature, T_T. Increasing T_T is possible by increasing the mean residence time of the particles in the gas-solid heat exchanger, thus transferring more energy. Less energy is thus available when the oxygen carrier enters the oxidation reactor. Consequently the airflow must be reduced to maintain constant outlet conditions. Increased power in turbine GT2 comes at the cost of lowering the power in turbine GT1 and η_{TOT} is relatively unaffected. Economical considerations with regard to turbine GT2 imply that a low inlet temperature is desirable to avoid cooling of the turbine.

(5) Reduction reactor outlet temperature, T_O. By increasing the carrier mass flow rate, while maintaining a constant volume in the gas-solid heat exchanger, the oxygen carrier will have a higher temperature as it enters the reduction reactor. This will lead to an increase in T_O. Additionally a change in X_U (after oxidation) and X_O (after reduction) is observed as the reactor volumes are considered to be constant and the mean residence times (τ_{ox}, τ_{red}) decreases. This leads to a slight change in the energy balance for the reduction reactor, the net result being a small decrease in efficiency. This observation is important because of the implication that T_O can be chosen to optimize the kinetics of the reduction reaction, without significant losses in efficiency.

(6) Reactor pressure. Reduced pressure invariably leads to reduced power generation in both turbines, along with a reduction in required compressor work. The airflow rate will increase, however, and only a slight net effect is observed. When going from 10 to 20 bars, there is a slight increase in compressor work while W_{GT1} remains constant. η_{TOT} increases, however, due to the increased contribution from turbine GT2. The total efficiency rises slightly for pressures up to 20 bar, where the increase in compressor work exceeds the increase in W_{GT2}. 20 bars therefore seem to be an optimal operating pressure for the reactor system.

In Fig. 3(*a*), T_I and T_U are plotted against total efficiency, assuming constant fuel input. Note that changing T_U also leads to a change in T_I due to the heat integration of the two streams. Figure 3(*b*) shows the effect on airflow rate when reducing T_U from 1200 to 900°C.

Reactor System

A key issue in CLC considerations is the type of reactor system chosen. The concept of a *circulating fluidized bed* (CFB) has been proposed, [8], and is believed to be the most promising setup for successful long-term operation. The basis for the simulation is a CFB ($\varepsilon = 0.95$) for oxidation, and a fluidized bed ($\varepsilon = 0.45$) for reduction. It is assumed that the oxygen carrier transport is gravity-driven in the reduction reactor. Key parameters are shown in Table 3. The flow of metal/metal oxide between the reactors is about 1.4–1.5 kg per MJ of net plant power output. The specific work (net plant power output per kg of air) is about 1/1.78=0.56 MJ/kg, which is somewhat higher (20–30%) than that of a gas turbine. The oxidation reactor volume is around 1.1 m^3/MW of net plant power output, which is below that of a conventional CFB combustion plant.

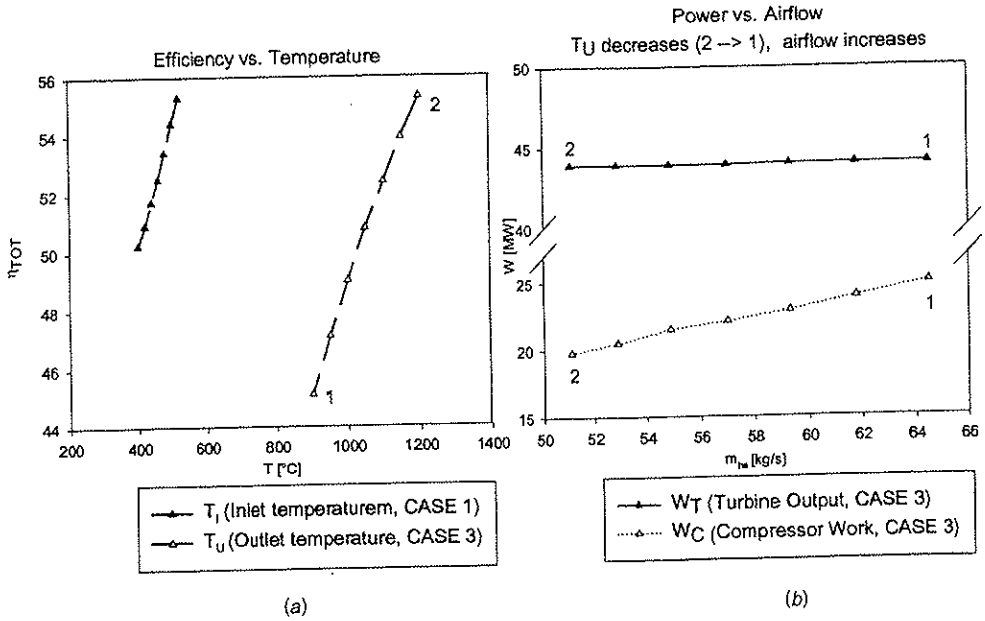

(a) (b)

Fig. 3 (a) $T-\eta$ diagram for T_I and T_U). (b) $W-m_{he}$ diagram, ($900<T_U$, 1200).

Table 3 Reactor key parameters (28 MW power output, 50 MW fuel lower heating value, X_O=0.1, X_U=0.8)

	kg/s	kg/MJ$_{el}$	kg/MJ$_{LHV}$
MeO	43.9	1.57	0.88
Me	39.3	1.40	0.79
Oxidation reactor airflow	49.8	1.78	1.0
	m^3	m^3/MW$_{el}$	kg/MW$_{LHV}$
Oxidation reactor (CFB)	31.2	1.11	155
Reduction reactor (FB)	3.3	0.12	141

Exergy Considerations

Thermodynamics states that the maximum amount of mechanical energy from transformation of a chemical compound is obtained when the conversion is reversible, i.e., occurs at a state of equilibrium. Due to material limitations in the combustor and turbine of a gas turbine, combustion is carried out at temperatures far below that of the equilibrium temperature associated with the oxidation of fuel with oxygen. The reaction is thus highly irreversible with considerable entropy generation. Exergy is also destroyed by irreversibilities in process components such as turbines and heat exchangers.

In order to compare CLC with conventional combustion with respect to irreversibilities, it is assumed that the process in Fig. 2 can either use CLC or have a conventional combustor within the dashed box shown in Fig. 2. The intention of this comparison is to show that the chemical conversion of fuel in CLC is done with reduced exergy loss compared to traditional combustion processes. The process would be the same with these two combustion systems, except that a conventional combustion system would have one hot pressurized gas stream to expand through a turbine, whereas for the CLC system there are two separate streams expanded through two separate turbines. It is for the exergy consideration assumed that the system outside the dashed box in Fig. 2 is the same so that the difference in irreversibilities for the whole process is related to the combustion block, see Fig. 4.

In the following it is assumed that the irreversibilities outside the reactor are similar in CLC and conventional combustion, although the proposed use of a CFB indicates a slightly higher pressure loss in the CLC combustion block.

Fundamentally, the exergy balance for a control volume at steady state can be formulated as follows:

$$E_D=\sum_{cv} E_Q-W_{cv}+\left(\sum_i \dot{m}_i e_i-\sum_e \dot{m}_e e_e\right) \tag{5}$$

where

$$\sum_{cv} E_Q=\sum_{cv}\left(1-\frac{T_0}{T_j}\right). \tag{6}$$

The first and second terms of Eq. (5) are exergy transfer associated with heat transfer and work. Adiabatic conditions are assumed and the work term is not considered since the control volume does not include the turbines. The specific exergy terms e_i and e_e for process streams at inlet (i) and exit (e) (n components), can be further decomposed into physical (e^P) and chemical (e^{CH}) exergy, assuming mechanical exergy to be negligible:

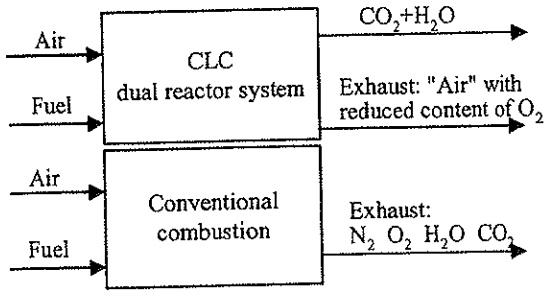

Fig. 4 Comparison of two combustion principles

Table 4 Exergy considerations (T,P)

	Exergy [kW]		
	e^P	e^{CH}	e^{TOT}
CLC:			
Fuel (T=681°C, 21 bar)	1,599	52,080	53,679
Air (527,21.3)	27,849	1,441	29,290
CO_2+H_2O (1200,19.4)	8,214	2,347	10,562
Exhaust (1200,20)	58,713	1,900	60,613
		$\dot{E}_D=11{,}789$	
		$1-\eta_{ex}=22.6\%$	
Conventional combustion:			
Fuel (681,21)	1,599	52,080	53,679
Air (527,21)	27,757	1,441	29,198
Exhaust (1200,20.5)	66,746	3,057	69,803
		$\dot{E}_D=13{,}074$	
		$1-\eta_{ex}=24.4\%$	

$$e^P=(h-h_0)-T_0(s-s_0) \tag{7}$$

$$e^{CH}=\sum_n y_n e_n^{CH}+\bar{R}T_0\sum_n y_n \ln y_n \tag{8}$$

The rate of exergy destruction in the reactor can thus be estimated from the difference in exergy content in the streams at the volume boundary. Exergetic efficiency is defined accordingly as

$$\eta_{ex}=1-\frac{E_D}{E_F}. \tag{9}$$

Using stream data from the simulation with the highest overall efficiency (case 4, 55.9%), an exergy balance for a control volume over the reactor section (indicated with a dashed box in Fig. 2) has been considered. For comparison, the same process streams are applicable in a conventional humid air gas turbine in order to estimate the difference in exergy loss associated with reaction splitting. The results are shown in Table 4 and are consistent with other studies, [2,9].

The exergy loss of CLC is about 2%—points less compared to conventional combustion. The reduced exergy loss in CLC becomes even more evident considering that a conventional combustion cycle will need a CO_2 separation unit.

Conclusions

The oxidation reactor air inlet temperature (T_I) and the oxidation reactor exhaust temperature (T_U) have a significant impact on the overall efficiency. This can be attributed to the controlling effect of these parameters on the required airflow rate. An optimum efficiency of 55.9% has been found for $T_I=527°C$, $T_U=T_T=1200°C$, $T_O=485°C$, and $\dot{m}_a=49.3$ kg/s. The captured CO_2 is at atmospheric pressure. If taking into account the compression of CO_2 1–100 bar, the efficiency would be lowered by 2% points, to about 54%. Crucial issues of oxygen carrier durability, chemical performance, and mechanical properties have been highly idealized, and further research on the feasibility of CLC is needed. Whether or not the assumption of $\gamma_{red}\sim 1$ holds, is a crucial issue and remains to be determined experimentally. Results of previous studies on chemical kinetics are used directly in the simulations, under conditions quite different from the original study, and thus introduce uncertainties in the calculations, as successful long-term operation of chemical looping systems of this particular type has not yet been demonstrated. The simulation points out a very promising potential of CLC as a power/heat generating method with inherent capture of CO_2. Exergy analysis show reduced irreversibilities for CLC compared to conventional combustion. Simulations of this type will prove useful in designing CLC systems in the future when promising oxygen carriers have been investigated in more detail.

Acknowledgments

This study was funded by the Norwegian Research Council program—Energy for the Future.

Nomenclature

- e^{CH} = specific chemical exergy (kJ/kg)
- e^P = specific physical exergy (kJ/kg)
- E_D = exergy destruction rate (kW)
- E_F = exergy supplied from fuel (kW)
- E_L = exergy loss (kW)
- E_Q = exergy transfer due to heat transfer (kW)
- h = specific enthalpy (kJ/kg)
- ΔH_{rx} = heat of reaction (kJ/kmol)
- m = instantaneous mass of oxygen carrier (kg)
- $\dot{m}$ = mass flow rate (kg/s)
- m_{oxd} = mass of oxygen carrier when 100% oxidized (kg)
- m_{red} = mass of oxygen carrier when 100% reduced (kg)
- P_i = partial pressure of component i (bar)
- $\bar{R}$ = gas constant (kJ/K kmol)
- s = entropy (kJ/kg K)
- T = temperature (°C)
- V = volume (m^3)
- W = work (MW)
- X = degree of oxidation
- y_i = molar fraction of component i
- Y = absolute humidity
- ε = bed void
- γ_{red} = gas yield
- η = efficiency
- ρ = particle density (kg/m^3)
- τ = mean residence time (s)

References

[1] Richter, H. J., and Knoche, K., 1983, "Reversibility of Combustion Processes," *Efficiency and Costing—Second Law Analysis of Processes* (ACS Symposium Series 235), ACS, Washington, DC, pp. 71–85.

[2] Ishida, M., and Jin, H., 1994, "A New Advanced Power-Generation System Using Chemical-Looping Combustion," Energy, **19**(4), pp. 415–422.

[3] Barin, I., 1995, *Thermochemical Data of Pure Substances*, 3rd Ed., VCH Verlagsgesellschaft.

[4] Kotas, T. J., 1995, *The Exergy Method of Thermal Plant Analysis*, Krieger, Melbourne, FL.

[5] Mattisson, T., Lyngfelt, A., and Cho, P., 2000, "Possibility of Using Iron Oxide as an Oxygen Carrier for Combustion of Methane With Removal of CO_2—Application of Chemical-Looping Combustion," HTTP://www.entek.chalmers.se/~anly/co2/ghgt5.pdf.

[6] Jin, H., Okamoto, T., and Ishida, M., 1999, "Development of a Novel Chemical-Looping Combustion: Synthesis of a Solid Looping Material of $NiO/NiAl_2O_4$," Ind. Eng. Chem. Res., **3**, pp. 126–132.

[7] Ishida, M., and Jin, H., 1994, "A Novel Combustor Based on Chemical-Looping Reactions and Its Reaction Kinetics," J. Chem. Eng. Jpn., **27**(3), pp. 296–301.

[8] Lyngfelt, A., Leckner, B., and Mattisson, T., 2000, "A Fluidized-Bed Combustion Process With Inherent CO_2 Separation," Chem. Eng. Sci., submitted for publication.

[9] Anheden, M., 2000, "Analysis of Gas Turbine Systems for Sustainable Energy Conversion," doctoral thesis, Department of Chemical Engineering and Technology Energy Processes, Royal institute of Technology, Stockholm, Sweden.

[10] Ishida, M., Zheng, D., and Akehata, T., 1987, "Evaluation of a Chemical-Looping-Combustion Power-Generation System by Graphic Exergy Analysis," Energy, **12**, pp. 147–154.

[11] Ishida, M., and Jin, H., 1993, "Graphical Exergy Analysis of Complex Cycles," Energy, **18**(3), pp. 615–625.

[12] Ishida, M., and Jin, H., 1996, "A Novel Chemical-Looping Combustor Without NO_x Formation," Research Notes, Ind. Eng. Chem., **35**, pp. 2469–2472.

[13] Ishida, M., Jin, H., and Okamoto, T., 1996, "A Fundamental Study of a New Kind of Medium Material for Chemical-Looping Combustion," Energy Fuels, **10**, pp. 923–963.

[14] Ishida, M., Jin, H., and Okamoto, T., 1998, "Kinetic Behavior of Solid Particle in Chemical-Looping Combustion: Suppressing Carbon Deposition in Reduction," Energy Fuels, **12**, pp. 223–229.

[15] Ishida, M., Jin, H., and Okamoto, T., 1998, "Development of a Novel Chemical-Looping Combustion: Synthesis of a Looping Material With a

Double Metal Oxide of CoO-NiO," Energy Fuels, 12, pp. 1272–1277.
[16] Ishida, M., and Jin, H., 1997, "CO_2 Recovery in a Power Plant With Chemical Looping Combustion," Energy Convers. Manage., 38, Suppl., pp. 187–192.
[17] Ishida, M., and Jin, H., 1998, "Greenhouse Gas Control by a Novel Combustion: No Energy Penalty and No CO_2 Separation Equipment," *Greenhouse Gas Control Technologies*, Proceedings of the 4th International conference on Greenhouse Gas Control Technologies, Aug. 30–Sept. 2, Interlaken, Switzerland, pp. 627–632.
[18] Hatanaka, T., Matsuda, S., and Hatano, H., 1997, "A New-Concept Gas-Solid Combustion System 'MERIT' for High Combustion Efficiency and Low Emissions," *Proceedings of the 32nd Intersociety Energy Conversion Engineering Conference*, pp. 944–947.